



UNIVERSITÀ DI PISA

Dipartimento di Ingegneria Civile e Industriale

CORSO DI LAUREA MAGISTRALE IN INGEGNERIA NUCLEARE

**Experimental investigation and simulation of
HLM/water interaction in LIFUS5/Mod2 facility
for supporting LFR safety analysis**

Relatori

Prof. Ing. Walter Ambrosini

Dott. Ing. Nicola Forgone

Dott. Ing. Alessandro Del Nevo

Dott. Ing. Alessio Pesetti

Candidato

Nicola Giannini

Anno Accademico 2013/2014

(This page has been intentionally left blank)

ABSTRACT

The present thesis work has been carried out during an internship at ENEA Brasimone Research Centre (Italy). The technical activity was conducted in the framework of LEADER project (European Lead-cooled advanced Demonstration Reactor), launched from EURATOM under the 7th Framework Programme. This work contributes to the research and development activities focused on safety of Gen. IV reactors employing as primary coolant Heavy Liquid Metal (HLM). For these reactors a pool-type configuration in which the steam generators are inside the reactor vessel is provided. Therefore, the interaction between the secondary side coolant (water) and the HLM (e.g. steam generator tube rupture) has to be considered as challenging safety issue in the design and also in the preliminary safety analysis of these reactor types. In this framework, the experimental separate effect facility LIFUS5/Mod2, installed at ENEA Research Center, was modified (i.e. top flange, test section and, partially the instrumentation and control system), installing a new test section having a geometry representatives of the tube bundle of ELSY steam generator. Tests were executed to study the interaction between LBE and water, with boundary and initial conditions relevant for the first seconds of the SGTR accident, as well as to demonstrate the reliability of computer codes in simulating the phenomena of interest.

The activity can be divided into two main parts: one experimental and the second based on code application. The former has been employed for supporting the preparation of LIFUS5/Mod2 facility, the assembling of LEADER test section, the documentation of the facility configuration and instrumentation, the execution of the preparatory (i.e. protective cap pressure tests) and commissioning (i.e. tests procedures and acquisition system) tests. The experimental work was completed with the design, execution, analysis and documentation of two tests, B1.1 and B1.2. These experiments provided pressure, temperature and strain trends versus time at an acquisition frequency up to 10 kHz, suitable for the analysis of interaction phenomena and the code validation. The pressure trends have been highlighted a remarkable damping of pressure wave propagation generated. This is caused by the impact with the tube bundle (that was not damaged) and also by the forced passage through the lateral surface of the test section. This observation is also supported by the strain gage signal trends.

The second part of the activity has been focused on the use of codes for supporting the experimental campaign, the design of experiments and for the experimental data analysis.

RELAP5/MOD3.3 has been used to perform the analysis of the facility water injection line and to simulate the conditions reached by water before the interaction phase for Test B1.1. This was aimed at improving the understanding of the experiments as well as to improve the SIMMER-III code post-test activity. Indeed, the new configuration of LIFUS5/Mod2 facility was modeled by SIMMER-III code. The simulation of the first test (B1.1) was carried out. The post-test was mainly based on the comparisons of the experimental and calculated pressure trends. The analysis has shown results excellent simulation of the first pressure peak resulting from the rupture of the injector. Instead, the increase in pressure due to the evaporation of water injected was slightly overestimated by the code, due to geometrical approximations of SIMMER-III model.

(This page has been intentionally left blank)

SOMMARIO

Il presente lavoro di tesi è stato effettuato durante uno stage presso il Centro di Ricerche ENEA di Brasimone (Italia). L'attività svolta è stata condotta nell'ambito del progetto LEADER (European Lead-cooled advanced Demonstration Reactor), lanciato da EURATOM nell'ambito del 7° Framework Programme. Questo lavoro contribuisce alle attività di ricerca e sviluppo, incentrate sulla sicurezza dei reattori di IV generazione che impiegano come refrigerante primario metalli liquidi. Per questi reattori è prevista una configurazione pool-type in cui i generatori di vapore sono all'interno del reattore. Pertanto l'interazione tra fluido refrigerante lato secondario (acqua) e lato primario (metallo liquido), per esempio a seguito di un incidente di SGTR, deve essere considerata come problematica rilevante per la sicurezza, sia nella fase di progettazione che nell'analisi preliminare di sicurezza. In questo ambito la facility LIFUS5/Mod2, presente al Centro Ricerche ENEA, è stata modificata installando una nuova sezione di prova con una geometria rappresentativa del fascio tubiero del generatore di vapore previsto per ELSY. I test sono stati eseguiti per studiare l'interazione tra LBE e acqua, con condizioni al contorno e iniziali rilevanti per i primi secondi di un ipotetico incidente di SGTR, nonché per validare e sviluppare l'affidabilità dei codici di simulazione.

L'attività può essere suddivisa in due parti principali: una sperimentale e una legata all'utilizzo di codici di simulazione. La prima prevede l'assemblaggio della nuova sezione di prova LEADER, la documentazione della configurazione finale della facility e della strumentazione implementata, e l'esecuzione di prove di preparazione (come i test per valutare le caratteristiche dell'iniettore) e di messa in servizio. Il lavoro sperimentale è stato completato con la caratterizzazione, l'esecuzione, l'analisi e la documentazione dei due test B1.1 e B1.2. Dall'analisi sono stati ricavati gli andamenti nel tempo di pressione, temperatura e deformazione con una frequenza di acquisizione elevata (fino a 10 kHz), necessaria per l'analisi del fenomeno di interazione. L'andamento della pressione ha evidenziato uno smorzamento subito dalle onde di pressione generate durante la loro propagazione. Questo è dovuto all'impatto con il fascio tubiero (non danneggiato durante le prove) ed al passaggio forzato attraverso la superficie laterale della test section che l'onda subisce durante la sua propagazione. Questa osservazione è supportata anche dagli andamenti della deformazione misurati tramite strain gauge.

La seconda parte della attività si è focalizzata sull'uso di codici di simulazione per supportare l'intera campagna sperimentale. RELAP5/MOD3.3 è stato utilizzato per

eseguire l'analisi della linea di iniezione e per simulare le condizioni raggiunte dall'acqua prima della rottura dell'iniettore nel primo test svolto (B1.1). I parametri così ottenuti sono stati utilizzati per modellare l'intera facility tramite il codice SIMMER-III al fine di simulare il primo test svolto (B1.1). L'analisi di post-test si è basata sul confronto degli andamenti di pressione sperimentali e calcolati. Dal confronto sono stati ottenuti risultati in accordo per quanto riguarda il primo picco di pressione a seguito della rottura dell'iniettore. L'aumento della pressione dovuto all'evaporazione dell'acqua iniettata, invece, è stato leggermente sovrastimato dal codice, a causa delle approssimazioni geometriche presenti all'interno del modello SIMMER-III sviluppato.

(This page has been intentionally left blank)

ACKNOWLEDGMENTS (RINGRAZIAMENTI)

Con questo lavoro si conclude un capitolo importante della mia vita. Una avventura cominciata poco più di 6 anni fa è arrivata al termine attraverso un percorso in cui difficoltà, delusioni e soddisfazioni si sono alternate di continuo. Non posso non ringraziare alcune persone che hanno partecipato a questa mia esperienza sostenendomi e facendomi crescere sia come persona che come figura professionale.

Ringrazio il Prof. Ing. Walter Ambrosini, il Dott. Ing. Nicola Forgiione e il Prof. Ing. Paolo Di Marco per i consigli, la disponibilità e la cordialità che mi hanno sempre mostrato durante tutta la mia carriera da studente.

Ringrazio Alessandro Del Nevo e Alessio Pesetti che mi hanno accolto, seguito e sopportato durante la mia permanenza al CR ENEA Brasimone con attenzione e dedizione.

Ringrazio tutti gli altri ragazzi che come vivevano e stanno ancora vivendo la loro avventura al CR ENEA Brasimone, Marica, Daniele Martelli, Daniele Mazzi, Gianluca, Emanuela, Eugenio, Ranieri (Raniers), Ahmed e Davide per gli aiuti che mi hanno fornito e per la loro voglia di fare gruppo e sentirsi una unica grande squadra.

Ringraziamento a parte va fatto al mio coinquilino e collegato d'ufficio Luca (Lo Scalets) con cui ho condiviso 5 mesi di questa grande esperienza. Con Luca ho condiviso tutto, problemi tecnici incontrati sul lavoro e problemi personali e si è rivelato un compagno d'avventura insostituibile.

Ringrazio tutti tecnici con cui ho lavorato Daniel, Massimo, Saverio, Stefano, Moreno, Claudio, Andrea Antonelli e soprattutto Andrea Neri con cui ho passato intere giornate in officina che tra risate e prese in giro mi hanno lasciato un bagaglio di competenze pratiche di cui farò tesoro.

Ringrazio con tutto il cuore i miei genitori Luca e Simona per avermi permesso di studiare, per aver sempre creduto in me e nelle mie potenzialità, spronandomi a non mollare mai e insegnandomi che nella vita se affronti le tue sfide dando il massimo non avrai mai rimpianti.

Ringrazio mio fratello Lorenzo con cui condivido ogni mio dubbio e incertezza da sempre. Lorenzo ha saputo darmi sostegno e ottimi consigli durante tutto la mia crescita e vedendo in me un modello da seguire mi ha spinto a dare sempre il meglio.

Ringrazio tutti i miei compagni di corso con cui ho passato 5 anni indimenticabili. Tra questi un ringraziamento particolare va a Alessandro (therealaleven) con cui ho sudato sui libri e con cui è nata un' amicizia che durerà in eterno e a Giacomo (Jack) e Matteo (Montels) con cui ho condiviso giorni indimenticabili sia fuori che dentro l'università.

Ringrazio il mio amico Lodovico (il Cook) che ha saputo starmi accanto nonostante si trovasse dall'altra parte del mondo a conferma che le vere amicizie non possiedono confini.

Infine ringrazio la mia ragazza Jessica che con il suo amore ha saputo rimanere al mio fianco in questi mesi permettendomi di affrontare questa avventura con serenità e impegno. Jessica è entrata nella mia vita da poco più di un anno e mezzo ma fin da subito si è rivelata quel tassello che mi mancava per sentirmi completo. Lei sa starmi accanto come nessuno è mai riuscito, colmando i miei momenti di sconforto con abbracci e sorrisi e facendomi trovare una forza che non pensavo di avere.

Di nuovo grazie di cuore a tutti voi.

(This page has been intentionally left blank)

CONTENTS

ABSTRACT	II
SOMMARIO.....	V
ACKNOWLEDGMENTS (RINGRAZIAMENTI).....	VIII
CONTENTS.....	XI
LIST OF FIGURES	XIV
TABLES.....	XIX
NOMENCLATURE.....	XXI
1 INTRODUCTORY REMARKS.....	2
1.1 Objective of the activity	4
1.2 Structure of the thesis	5
2 ITERATION BETWEEN FLUIDS IN LIQUID METAL REACTORS.....	8
2.1 Generality	8
2.2 Phenomenology	8
2.3 Theoretical models	12
2.3.1 Spontaneous nucleation model	12
2.3.2 Thermal detonation.....	16
2.4 SGTR phenomena	19
2.5 Experimental campaign	21
3 ELSY PROJECT	25
3.1 Overview of primary system	25
3.2 Description of the steam generator design	27
4 LIFUS5/MOD2 FACILITY DESCRIPTION	31

4.1	LIFUS5/Mod2 facility	31
4.2	THINS test section	41
4.3	LEADER test section and description of the assembling.....	43
4.4	Protective cap tests	60
5	LIFUS5/MOD2 WATER INJECTION LINE ANALYSIS	65
5.1	RELAP5/MOD3.3 analysis	66
5.1.1	Analysis based on injection line pressure.....	69
5.1.2	Void fraction analysis.....	76
5.1.3	Mass flow analysis	83
5.1.4	Summary of results.....	84
5.2	SIMMER-III analysis of Test A1.2_2	85
5.2.1	SIMMER-III code nodalization of LIFUS5/Mod2 facility	86
5.2.2	Analysis of Test A1.2_2	88
6	LEADER EXPERIMENTAL CAMPAIGN.....	91
6.1	Test B1.1.....	91
6.1.1	Test configuration.....	91
6.1.2	Execution of the test	95
6.1.3	Data analysis and interpretation	97
6.1.4	Relap5 simulation of water injection line.....	110
6.1.5	Post-test analysis of Test B1.1 by SIMMER-III code.....	111
6.2	Test B1.2.....	119
6.2.1	Test configuration.....	119
6.2.2	Execution of the test	119
6.2.3	Data analysis and interpretation	121
7	CONCLUSIONS	134
	REFERENCES	139

(This page has been intentionally left blank)

LIST OF FIGURES

<i>Figure 1.1 – lead cooled fast reactor</i>	3
<i>Figure 1.2 – thesis work scheme</i>	7
<i>Figure 2.1 – Contact modes between liquid metal-coolant or fuel-coolant</i>	9
<i>Figure 2.2 – spontaneous nucleation model</i>	14
<i>Figure 2.3 – a) Geometry and schematic pressure and velocity profiles of a 1-D explosion. b) Schematic shock adiabetic (solid curve, reacted material; dashed curve, not reacted material)</i>	16
<i>Figure 2.4 – liquid metal-water mixture</i>	20
<i>Figure 2.5 – facility for impingement study</i>	22
<i>Figure 2.6 – steam explosion map</i>	23
<i>Figure 2.7 – SETS facility</i>	24
<i>Figure 3.1 – ELSY layout</i>	25
<i>Figure 3.2 – ELSY steam generator</i>	27
<i>Figure 4.1 – LIFUS5/Mod2 facility</i>	32
<i>Figure 4.2 – Garlock Helicoflex gasket</i>	34
<i>Figure 4.3 – LIFUS5/Mod2 bolts used to close S1 flange</i>	34
<i>Figure 4.4 – sketch of S1 penetrations with instrumentation</i>	35
<i>Figure 4.5 – strain gages measurement point positions inside S1</i>	36
<i>Figure 4.6 – view of S1 flange penetrations</i>	37
<i>Figure 4.7 – injectors with protective caps</i>	38
<i>Figure 4.8 – sketch of water injection line</i>	39
<i>Figure 4.9 – view of S2 and level measurement system</i>	40
<i>Figure 4.10 – view of S3 dump tank</i>	40
<i>Figure 4.11 – detailed view of the TCs’ support structure</i>	41
<i>Figure 4.12 – S1 water injection system</i>	42
<i>Figure 4.13 – 3D view of LEADER test section</i>	43
<i>Figure 4.14 – test section flange (left) and S1 flange connections (right)</i>	44
<i>Figure 4.15 – layout of LEADER test section inside S1</i>	44
<i>Figure 4.16 – LEADER test section horizontal sketch with instrumentation</i>	46
<i>Figure 4.17 – view of thermocouples (left) and strain gages (center and right)</i>	51
<i>Figure 4.18 – pressure test of pressurized tubes</i>	52
<i>Figure 4.19 – tube bundle assembly of LEADER test section</i>	52

<i>Figure 4.20 – pressurization system assembly</i>	<i>53</i>
<i>Figure 4.21 – LBE level control system</i>	<i>54</i>
<i>Figure 4.22 – pipe connection between LEADER test section and KISTLER PT on S1 top flange</i>	<i>54</i>
<i>Figure 4.23 – S1-S3 connection assembly.....</i>	<i>55</i>
<i>Figure 4.24 – heating cables and thermocouples of control and regulation</i>	<i>56</i>
<i>Figure 4.25 – LIFUS5/MOD2 synoptic.....</i>	<i>58</i>
<i>Figure 4.26 – pressure time trend during the pressure test of LIFUS5/Mod2 facility with LEADER test section</i>	<i>59</i>
<i>Figure 4.27 – scheme of protective cap test section.....</i>	<i>60</i>
<i>Figure 4.28 – pressure time trends measured for Test 1.....</i>	<i>62</i>
<i>Figure 4.29 – pressure time trends measured for Test 2.....</i>	<i>62</i>
<i>Figure 4.30 – pressure time trends measured for Test 3.....</i>	<i>63</i>
<i>Figure 4.31 – pressure time trends measured for Test 4.....</i>	<i>63</i>
<i>Figure 4.32 – pressure time trends measured for Test 5.....</i>	<i>64</i>
<i>Figure 4.33 – pressure time trends measured for Test 6.....</i>	<i>64</i>
<i>Figure 5.1 – 3D view of water injection line connected with S1.....</i>	<i>65</i>
<i>Figure 5.2 – sketch of a part of LIFUS5/Mod2 facility with pressure transducer highlighted</i>	<i>67</i>
<i>Figure 5.3 – Water injection line nodalization</i>	<i>68</i>
<i>Figure 5.4 – pressure sensitivity analysis based on Table 5.2 for Test A1.2_1</i>	<i>71</i>
<i>Figure 5.5 – pressure sensitivity analysis based on Table 5.3 for Test A1.2_1</i>	<i>72</i>
<i>Figure 5.6 – pressure sensitivity analysis based on Table 5.2 for Test A1.2_2</i>	<i>74</i>
<i>Figure 5.7 – zoom of pressure sensitivity analysis based on Table 5.2 for Test A1.2_2 which highlights the breaking point of the cap.....</i>	<i>74</i>
<i>Figure 5.8 – comparison between the experimental pressure trend and the “case_q” for Test A1.2_1.....</i>	<i>75</i>
<i>Figure 5.9 – comparison between the experimental pressure trend and the “case_q” for Test A1.2_2.....</i>	<i>76</i>
<i>Figure 5.10 – void fraction in tube 225 for Test A1.2_2 in “case_q” configuration</i>	<i>78</i>
<i>Figure 5.11 –zoom of void fraction in tube 225 for Test A1.2_2 in “case_q” configuration</i>	<i>78</i>
<i>Figure 5.12 – void fraction in tube 227 for Test A1.2_2 in “case_q” configuration</i>	<i>79</i>

<i>Figure 5.13 – zoom of void fraction in tube 227 for Test A1.2_2 in “case_q” configuration</i>	79
<i>Figure 5.14 – void fraction in tube 238 for Test A1.2_2 in “case_q” configuration</i>	80
<i>Figure 5.15 – void fraction in tube 235 for Test A1.2_2 in “case_q” configuration</i>	80
<i>Figure 5.16 – zoom of void fraction in tube 235 0-1.7 s for Test A1.2_2 in “case_q” configuration</i>	81
<i>Figure 5.17 – void fraction/pressure trend of S1 and injection line of tube 225, 238, 235 compared for Test A1.2_2 in “case_q” configuration</i>	82
<i>Figure 5.18 – mass flow/pressure trend of S1 and injection line for Test A1.2_2 in “case_q” configuration</i>	83
<i>Figure 5.19 – operating principle of Coriolis flow meter</i>	84
<i>Figure 5.20 – SIMMER-III code structure</i>	85
<i>Figure 5.21 – LIFUS5/Mod2 modeling</i>	86
<i>Figure 5.22 – experimental pressure trends for Test A1.2_2 compared with the SIMMER-III one</i>	88
<i>Figure 5.23 – Test A1.2_2 situation at t=0.5 s</i>	89
<i>Figure 5.24 – mass flow rate RELAP5 vs SIMMER-III</i>	90
<i>Figure 6.1 – LIFUS5/Mod2 synoptic with heating cable highlighted</i>	94
<i>Figure 6.2 – condition of LIFUS5/Mod2 synoptic for Test B1.1</i>	96
<i>Figure 6.3 – Test B1.1 valves V4 and V14 position</i>	100
<i>Figure 6.4 – Test B1.1 pressure trends in injection line, S1 and S3</i>	101
<i>Figure 6.5 – Test B1.1 pressure and temperature trends in injection line</i>	101
<i>Figure 6.6 – Test B1.1 S2 level measurement and mass flow trends</i>	102
<i>Figure 6.7 – Test B1.1 pressure trends in S1 and S3</i>	102
<i>Figure 6.8 – Test B1.1 zoom of pressure peak in S1</i>	103
<i>Figure 6.9 – Test B1.1 temperature trends of the ranks and internal surface of LEADER test section</i>	105
<i>Figure 6.10 – Test B1.1 LEADER test section strain gauges strain trends</i>	107
<i>Figure 6.11 – Test B1.1 S1 internal surface temperature trends</i>	108
<i>Figure 6.12 – Test B1.1 S1 internal surface strain trends</i>	108
<i>Figure 6.13 – Test B1.1 S1 internal surface strain trends zoom</i>	109
<i>Figure 6.14 – RELAP5 input implementation for testing pressure increase in water injection line of LIFUS5/Mod2 facility in Test B1.1</i>	110

<i>Figure 6.15 – RELAP5 and experimental water injection line pressure trends in Test B1.1</i>	111
<i>Figure 6.16 – cap and can wall modeling</i>	112
<i>Figure 6.17 – LEADER test section modeling</i>	113
<i>Figure 6.18 – example of rank 3 simulation procedure</i>	113
<i>Figure 6.19 – LUFUS5/Mod2 with LEADER test section model</i>	114
<i>Figure 6.20 – Test B1.1 water injection line conditions before cap rupture</i>	115
<i>Figure 6.21 – Test B1.1 SIMMER-III/experimental pressure trends comparison</i>	116
<i>Figure 6.22 – measurement point in the code SIMMER-III</i>	117
<i>Figure 6.23 – Test B1.1 initial peak zoom</i>	118
<i>Figure 6.24 – situation at t=0.3 seconds</i>	118
<i>Figure 6.25 – situation at t=1.2 seconds</i>	118
<i>Figure 6.26 – Test B1.2 valves V4 and V14 position</i>	124
<i>Figure 6.27 – Test B1.2 pressure trends in injection line, S1 and S3</i>	125
<i>Figure 6.28 – Test B1.2 pressure and temperature trends in injection line</i>	125
<i>Figure 6.29 – Test B1.2 S2 level measurement and mass flow trends</i>	126
<i>Figure 6.30 – Test B1.2 pressure trends in S1 and S3</i>	126
<i>Figure 6.31 – Test B1.2 zoom of pressure peak in S1</i>	127
<i>Figure 6.32 – Test B1.2 temperature trends of the ranks and internal surface of LEADER test section</i>	129
<i>Figure.6.33 – Test B1.2 LEADER test section strain gauges strain trends</i>	131
<i>Figure 6.34 – Test B1.2 S1 internal surface temperature trends</i>	132
<i>Figure 6.35 – Test B1.2 S1 internal surface strain trends</i>	132
<i>Figure 6.36 – Test B1.2 S1 internal surface strain trends zoom</i>	133

(This page has been intentionally left blank)

TABLES

<i>Table 2.1 – different between FCI and CCI</i>	20
<i>Table 3.1 – ELSY functional parameters</i>	26
<i>Table 3.2 – ELSY SG spiral tubes features</i>	28
<i>Table 3.3 – ELSY SG functional parameters</i>	29
<i>Table 3.4 – ELSY SG safety devices</i>	30
<i>Table 4.1 – tank S1, S2 and S3 features</i>	33
<i>Table 4.2 – S1 penetrations with instrumentation</i>	35
<i>Table 4.3 – S1 flange penetrations</i>	37
<i>Table 4.4 – injector ruptured dimensions</i>	39
<i>Table 4.5 – identification and features of the tubes in the test section</i>	51
<i>Table 4.6 – data of protective cap tests</i>	61
<i>Table 5.1 – S2 and injection line data for Test A1.2_1</i>	69
<i>Table 5.2 – list of the parameters for the first attempts</i>	70
<i>Table 5.3 – list of the parameters for the second attempts</i>	71
<i>Table 5.4 – S2 and injection line data for Test A1.2_2</i>	73
<i>Table 5.5 – list of the parameters for the overall attempts</i>	75
<i>Table 6.1 – LEADER project tests matrix</i>	91
<i>Table 6.2 – Test B1.1 parameters</i>	93
<i>Table 6.3 – Test B1.2 parameters</i>	120

(This page has been intentionally left blank)

NOMENCLATURE

Acronyms

AA	Aluminum Association
ADSs	Accelerator Driven Systems
AFDM	Advanced Fluid Dynamics Model
ALFRED	Advanced Lead Fast Reactor European Demonstrator
ATWS	Anticipated Transients Without Scram
CAMP	Code Applications and Maintenance Program
CCI	Coolant-Coolant Interactions
CDA	core Damage Accident
CEA	Commissariat á L'Energie Atomique
CHF	Critical Heat Flux
CRADA	Cooperative Research and Development Agreement
CRIEPI	Central Research Institute of Electric Power Industry
DHR	Decay Heat Removal
ELSY	European Lead cooled System
ENEA	Agenzia nazionale per le nuove tecnologie, l'energia e lo sviluppo economico sostenibile
EOS	Equation Of State
EOT	End Of Transient
EURATOM	European Atomic Energy Community
FCI	Fuel Coolant Interaction
FZK	Forschungszentrum Karlsruhe
HLM	Heavy Liquid Metal
HLMFRs	Heavy Liquid Metal Fast Reactors
ICAP	International Code Assessment and Applications Program
IFA	interface area
INL	Idaho National Laboratory
IRUG	International RELAP5 Users Group
JNC	Japan nuclear Cycle Development Institute
KAERI	Korea Atomic Energy Research Institute
LANL	Los Alamos National laboratory

LBE	Lead Bismuthic Eutectic
LEADER	European Lead-cooled advanced Demonstration Reactor
LIFUS5	Lithium Fusion
LWR	Light Water Reactor
MYRRHA	Multipurpose Hybrid Research Reactor for High-tech Applications
ORNL	Oak Ridge National Laboratory
PHXs	Primary Heat exchangers
RELAP	Reactor Excursion and Leak Analysis Program
SGs	Steam Generators
SGTR	Steam Generator Tube Rupture
SSTAR	Small, sealed, transportable, autonomous
STSG	Single Tube Steam Generator
THINS	Thermal Hydraulics of Innovative Nuclear Systems

Greek letters

α	volumetric fraction
δ	thermal penetration length (m)
Γ	mass-transfer rate per unit volume (kg/s/m^3)
κ	thermal diffusivity ($\text{W/m}\cdot\text{K}$)
ρ	density (kg/m^3)
$\bar{\rho}$	macroscopic density (kg/m^3)
σ	surface tension (N/m)
τ	time constant (s)
ν	specific volume (m^3/kg)

Roman letters

c	heat capacity ($\text{J/kg}\cdot\text{K}$)
e	specific internal energy (J/kg)
g	gravity (m/s^2)
G	shock front velocity
H	heaviside unit function
K	momentum exchange function ($\text{kg/m}^3/\text{s}$)
k	thermal conductivity $\text{W}/(\text{m}\cdot\text{K})$

P	pressure (Pa)
Q	heat transfer rate (W/m^3)
r	radius (m)
T	Temperature ($^{\circ}\text{C}$)
v	Velocity (m/s)
V	absolute velocity of mixture (m/s)
W	reversible work (J)
w	collision frequency of the liquid's molecules (1/s)
U	internal energy of the mixture (J)

Subscripts

C	cold fluid or coolant
C	condensation
$crit$	critical
F	freezing
g	Gas or vapour
GL	Terms existing at interface between vapour and liquid velocity
H	hot fluid
HT	heat transfer
I	interface
M	energy components
M	melting
m	components of density
N	nuclear
q	velocity fields
S	structure
SN	Spontaneous nucleation
V	vaporization

(This page has been intentionally left blank)

1 Introductory remarks

The use of Lead or Lead-Bismuth Eutectic alloy (LBE is a eutectic alloy of lead (44.5%) and bismuth (55.5%)) as a coolant for nuclear reactors began in the early 1950s in Russia for military submarine propulsion. Russian navy has built 15 reactors including 3 land system reactors and one replacement reactor for submarines. These reactors were significantly lighter than typical water-cooled reactors and they had the advantage of being able to pass from the minimum power and noise to maximum power (very noisy) quickly. However in the following years, the technology of LWR has dominated the field of nuclear energy. Recently issues such as high activity waste management and proliferation of military nuclear weapons have led to reconsider lead technology as possible candidates for Gen. IV. This is due to some proprieties of lead as the high shielding power and the rapid solidification that occurs during a LOCA limiting the release.

The expected LFR for Gen. IV is a flexible fast neutron reactor which can use depleted uranium or thorium fuel matrices and which can burn actinides from LWR fuel. Liquid metal (Pb or Pb-Bi eutectic) cooling is at low pressure by natural convection (at least for decay heat removal) [1-5]. Fuel is metal or nitride, with full actinide recycle from regional or central reprocessing plants. A wide range of unit sizes is envisaged, from factory-built "battery" with 15-20 year life for small grids or developing countries, to modular 300-400 MWe units and large single plants of 1400 MWe. Operating temperature of 550°C is readily achievable, but 800°C is envisaged with advanced materials to provide lead corrosion resistance at high temperatures: this would enable thermochemical hydrogen production. A two-stage development program leading to industrial deployment is expected: by 2025 for reactors operating with relatively low temperature and power density, and by 2035 for more advanced higher-temperature designs. In Figure 1.1 is shown a sketch of a lead cooled fast reactor scheduled for the generation IV.

Now in Russia the project BREST, Russian acronym for Lead-cooled fast reactor, and the project SVBR, Russian acronym for fast reactor cooled by lead-bismuth are developed. In particular BREST-300 is designed as multi-purpose reactor, for the production of electricity, the burning and the production of plutonium, the production of radioisotopes for medical and industrial use and the transmutation of fission products and long-lived actinides generated in the exercise of reactor. At the same time a considerable number of other research projects in support of LFR technology have been activated in other countries.

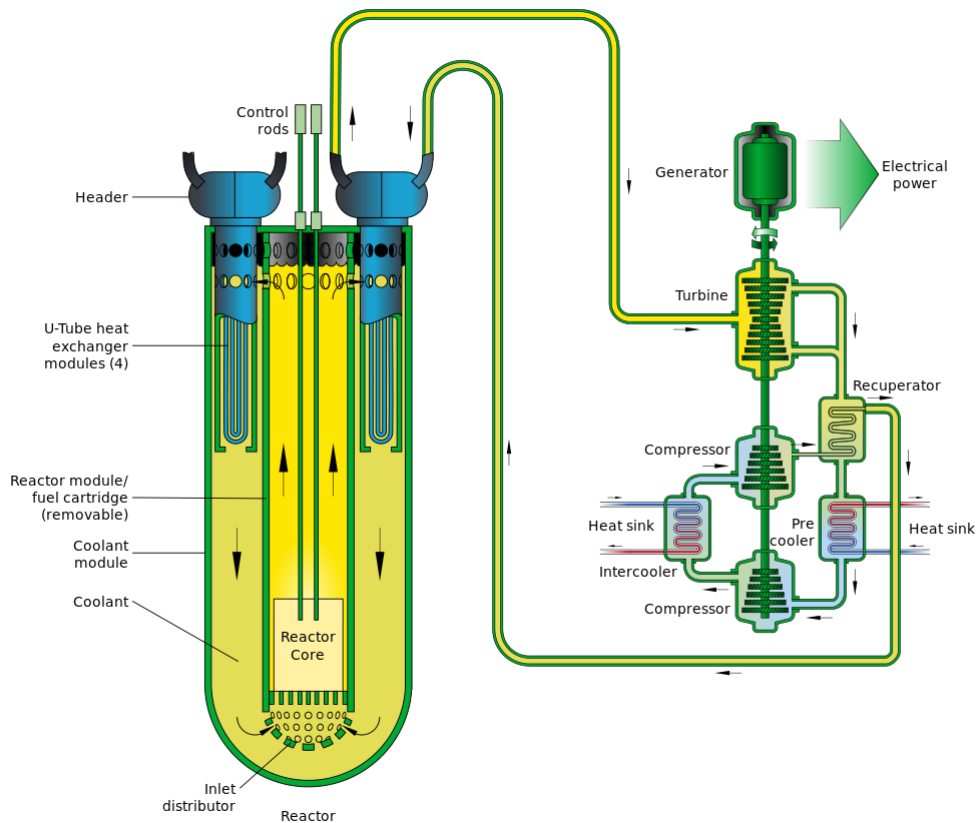


Figure 1.1 – lead cooled fast reactor

Since several years, the Belgian Nuclear Research Centre, SCK•CEN, is working to MYRRHA project. It is a fast spectrum research reactor, designed as an Accelerator Driven System (ADS), which can operate in critical and sub-critical ways. The accelerator provides the high-energy protons that are used in the spallation target to create neutrons, which in turn feed the subcritical core. In the current design of MYRRHA, the accelerator must be able to provide a proton beam with energy of 600 MeV and an average beam current of 3.2 mA. The core is composed by a mixed fuel plutonium-uranium oxide (MOX) and it is cooled by a lead-bismuth alloy.

The project SSTAR consists in a demonstrator small size reactor designed in the United States, with a fast neutron spectrum, to create systems that can also be connected in networks of limited extension, such as those are found in the countries in the developing, or at least to meet the needs of isolated or restricted communities. The project includes a reactor that works in natural circulation cooled with lead, with a power of 20 MWe (45 MWt).

In Europe EURATOM, European Atomic Energy Community, under the 6th Framework launched the ELSY project. The aim of this project was to study the construction of a fast

neutron spectrum reactor, cooled by lead, with a power of 600 MWe, that fulfilled the safety requirements of the Generation IV. This project also aimed at the reduction of radioactive waste through burning inside the reactor core. The ELSY project was completed in 2010 and EURATOM, under the 7th Framework Programme, launched the LEADER project (European Lead-cooled advanced Demonstration Reactor). The purpose of this project is the design of the ELFR (European Lead-cooled Fast Reactor): 16 European Organizations are involved in the project, including ANSALDO and ENEA. It was decided to define the configuration of a demonstrator plant ALFRED (Advanced Lead Fast Reactor European Demonstrator) that is basically conceived as a pool reactor with a thermal power of 300 MWt (125 MWe), cooled with lead. In normal operation, the coolant circulates through eight primary pumps, each placed inside a steam generator that is immersed in the pool around the core. The choice of lead, as expected in some projects as ALFRED, ELSY and SSTAR, even if until now LBE has been used, is connected with some favourable proprieties of this coolant [6]. Indeed lead, as LBE, produces radioactive polonium due to transmutation by neutron capture but in this case polonium has an activity less than that produced by LBE. Furthermore it has recently been highlighted that during the solidification, pure lead undergoes an expansion minor compared to LBE. This aspect is relevant for the safety of the structures (i.e. pipes) in case of freezing of lead due to an accident[4]. In addition, pure lead is cheaper and available. For these reasons lead is considered a possible alternative coolant for LFR technology.

1.1 Objective of the activity

The research centre ENEA Brasimone is involved into the task 6.4 of LEADER project. The activity is connected with the evaluation of safety of ELFR. In particular, the main objective is to investigate and assess the pressure waves caused by the SGTR event, besides to generation of experimental data for the development and validation of codes. Therefore an experimental campaign has been designed as set up.

The expected outcomes of the tests are:

- the generation of detailed and reliable experimental data;
- the improvement of the knowledge of physical behaviour and of understanding of the phenomenon;
- the investigation of the dynamic effects of energy release on the structures;
- the enlargement of the database for code validation.

The activity of the present master thesis is carried out in this framework, and it has the following objectives:

- the participation to the design and the assembling of the new LEADER experimental test section;
- the planning of tests, the definition of procedures, the set-up of initial and boundary conditions of tests;
- the participation in the execution of experiments;
- the generation and the analysis of detailed and reliable experimental data;
- the enlargement of the database for code validation;
- the acquisition of skills in using simulation codes such as RELAP5 and SIMMER-III codes;
- the simulation and preliminary assessment of the first test (B1.1) by SIMMER-III code.

Additional goals and experiences achieved are:

- the possibility to perform an internship at the ENEA Experimental Centre of Brasimone; and
- the acquisition of practical skills related to welding procedures, to pressure fittings, to gaskets and to measurement instrumentation thanks the participation in the preparation and operation of the experimental facility.

1.2 Structure of the thesis

The present thesis is divided into 5 main sections, besides the introductory remarks (section 1), an and the conclusive remarks (section 7). Figure 1.2 depicts the activity performed.

Section 2 presents a literature review of the interaction phenomenon between liquid metal and water. Selected and relevant recent experimental campaigns are mentioned. Section 3 gives a description of ELSY project, with details about ELSY steam generator design. Section 4 describes the planning, the construction and the assembly of the LEADER test section. Section 5 presents the analysis devoted to the characterization of the water injection line performed by means of RELAP/5MOD3.3. This study provides additional information for setting up SIMMER-III code post-test simulations. Section six reports the

analysis of the two experimental tests (B1.1 and B1.2) carried out on the LIFUS5/Mod2 facility. The main experimental time trends of the test are presented, analysed and discussed. Then, the modeling of the LIFUS5/Mod2 facility by SIMMER-III code is reported to introduce the post-test analysis of the first experiment and the independent assessment activity.

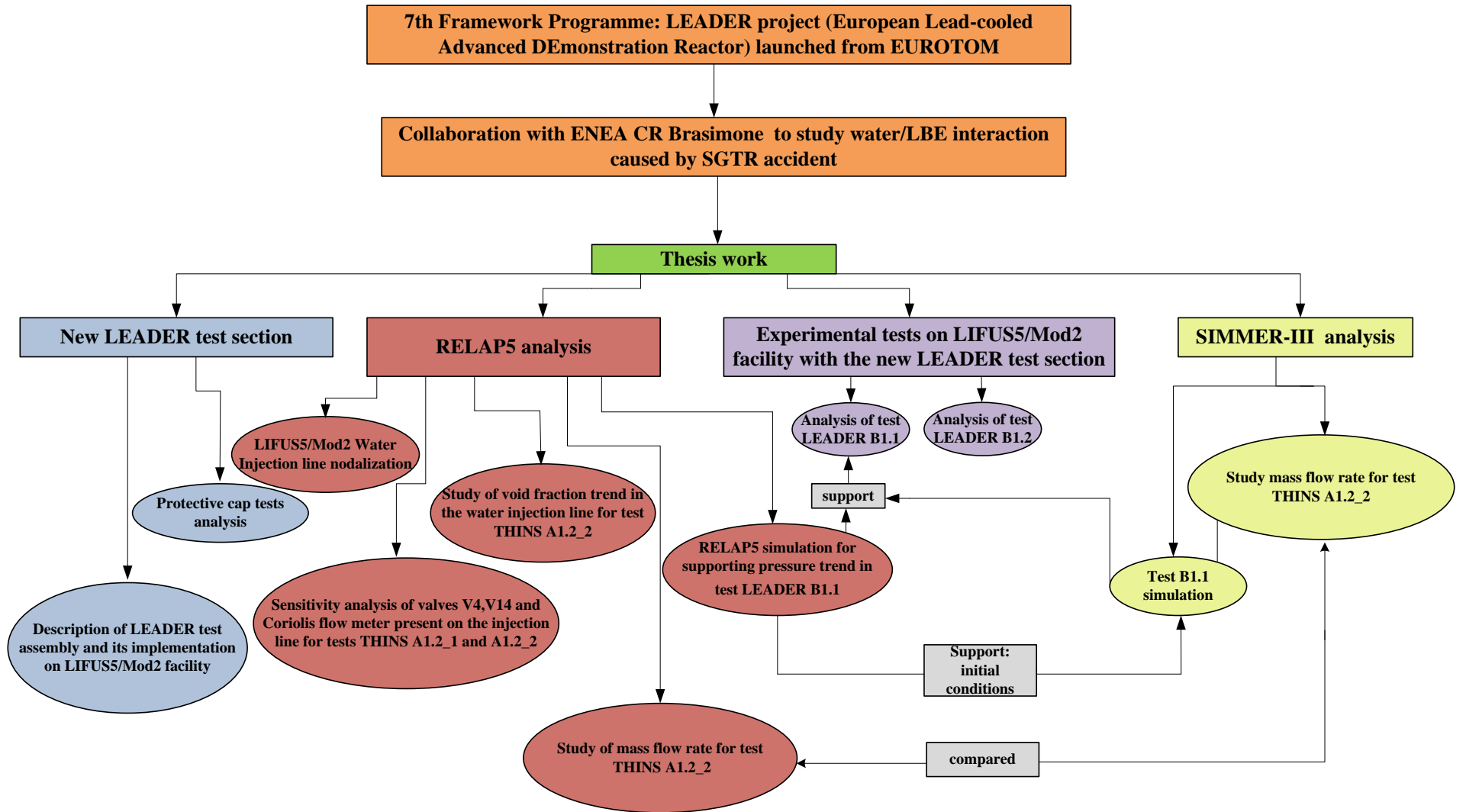


Figure 1.2 – thesis work scheme

2 Iteration between fluids in liquid metal reactors

2.1 Generality

In the frame of studies concerning liquid metal cooled reactor systems, the analysis of the so called “liquid metal-coolant interaction” is one of the most important concerns.

Generally speaking an amount of highly pressurized vapour is produced when a hot liquid comes into contact with a colder and volatile one. In this situation the hot liquid transfers its internal energy to the colder one. The heat transfer rate is correlated to the liquids fragmentation which drastically influences the interfacial area between the two liquids. The temperature and the pressure of the colder fluid increases and it expands affecting the surroundings. Moreover, if, the heat transfer between the two fluids is so fast that the timescale for heat transfer is shorter than the timescale for pressure relief, a vapour explosion can occur. As a consequence, the related formation of shock waves and/or the production of missiles during the expansion of coolant vapour can damage the surrounding structures. It is worth pointing out that the evolution of the interaction towards an explosive event (called vapour or steam explosion) are strictly depending on the masses and the densities of the involved materials. Regarding the field of nuclear applications the problem of the interaction between fuel and coolant fluid is historically in relation to an hypothetical core melt in conditions of serious malfunction. If a sufficient amount of molten fuel comes in contact with the refrigerant a steam explosion can occur. More recently, following the interest for fast reactors and in particular for reactors HMLRs and ADSs (Accelerator Driven Systems) the problem of interaction coolant-fuel, even if in a different scenario, is raised again. In fact, in case of a SGTR (steam generator tube rupture) accident, there is the possibility that the liquid metal comes into contact with the coolant of the secondary loop (often water) which removes heat from the primary loop. This kind of interaction is defined as CCI (Coolant-Coolant Interactions) and it has been studied within the ELSY, THINS, LEADER and MAXSIMA projects, which are European contributions supporting the development of fast nuclear power plant cooled by liquid lead.

2.2 Phenomenology

The formation of a large amount quantity of steam originates from the contact between two different fluids at different temperatures and densities may occur in three different geometric configurations (see Figure 2.1).

These are:

- a. dispersion of hot liquid fluid into cold liquid pool;
- b. dispersion of cold liquid droplets into a hot liquid pool;
- c. stratification between two fluids.

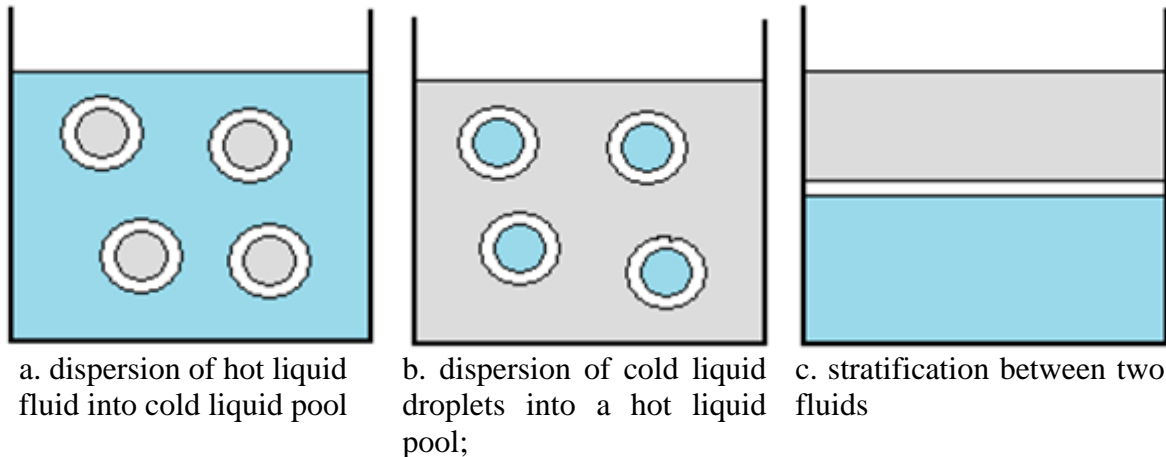


Figure 2.1 – Contact modes between liquid metal-coolant or fuel-coolant

The occurrence of one of the three cases depends on the application, such as reactor type or experiments. In the frame of nuclear reactor technology, we can have:

- The first type of configuration (Case a in Figure 2.1) can be framed a scenario resulting in an accident of core melt in a LWR, in which the molten fuel penetrates in contact with the coolant water of the primary circuit in the form of jets. This is the most common situation that might occur in LWR [17] following a Core Damage Accident (CDA).
- The second configuration (Case b in Figure 2.1) is an accidental scenario resulting in the rupture of a tube of the steam generator of a LMFR [18][19]. A jet of high pressure water protrudes from the secondary circuit and enters in the primary pool, consisting of liquid metal at very high temperature. In scientific literature this type of interaction is called "Coolant Coolant-Interaction" (CCI).
- The third configuration (case c. in Figure 2.1) might also occur in reactors if the hot dense phase reaches the bottom of the vessel and spreads out without freezing. In this situation there are two stratified liquid layers, separated by a vapour film.

The initial conditions, like temperature, pressure wave speed, presence of incondensable gas etc. affect the outcome of the iteration [15]. In particular, as mentioned above, in the case in which the time scale for the transfer of thermal energy from the liquid metal to the coolant proves to be less than the time scale of the propagation of pressure waves in the system, the interaction takes explosive characteristics. In this case, the rapid increase in pressure causes the formation of shock waves that propagate in the mixture undisturbed at a speed greater than the speed of sound in local thermodynamic conditions. The propagation of the shock waves formed will result in further fragmentation of the liquid metal and, consequently, the increase of the heat exchange surface and the production of high pressure steam which, in a second phase, expanding, will tend to get back into conditions equilibrium. The reaction will end when the internal energy of the liquid metal will be entirely converted into kinetic energy of the mixture. On the other hand, if the rate of heat transfer results to be less than the speed of pressure waves propagation, the development of the characteristic for a steam explosion phenomena do not occur. However, also the danger of this type of interaction should not be underestimated, because of the amount of high pressure steam produced and the consequent possibility of pressurization of the surrounding structures.

From the observation of the phenomena during several experiments, the steam explosion can be subdivided into four main phases [13][14]:

- I. Premixing,
- II. Triggering,
- III. Propagation,
- IV. Expansion.

Although the details of these four stages may vary in relation to the geometric configuration, each of them is always present during the explosion.

- I. Premixing: In this phase, as soon as the two liquids come in contact, a large heat transfer from the melt to water produces a vapour film around the melt droplets. Therefore at this point there are three liquid phases such as molten fuel or heavy liquid metal, liquid coolant and vapour. The timescale of the pre-mixing phase is in the range of few tenths of seconds to several seconds and the length scale is a relatively coarse one, yielding pre-fragmented melt droplets in the range of few millimeters to centimeters. The most vigorous steam

explosions are obtained in the case of large quantities of already pre-fragmented melt into contact with water and mixing them under limited void.

Several studies have highlighted the dependence of fragmentation from jet entry velocity and therefore on the Weber number [14], that represent the measure of the relative importance of the fluid's inertia compared to its surface tension, which provides a threshold (generally $We > 12$) for establishing fragmentation. In fact, owing to fluid acceleration, the consequent relative velocity between two fluids causes the deformation and the breakup of the particles.

- II. Triggering: during this phase we arrived to local fine fragmentation of one of the two fluid and this conduced to an enhanced of heat transfer and an increase of pressurization. In the specific triggering may produce destabilization of the vapour film, allowing liquid-liquid contacts through the collapse of the film itself. Therefore, this may lead to fragmentation and explosion. Through experiments it was observed that, in addition to speed, the pressure of the environment around the mixture of the fluids plays an important role, because it can suppress vapour explosion when the vapour film density increases [15]. Moreover, the coolant temperature and the respective subcooling can increase or decrease the risk of vapour explosion, because steam explosion becomes more likely with a higher subcooling.
- III. Propagation: The pressurization induced by the trigger destabilizes the surrounding vapour film, leading to a further fine fragmentation of the surrounding melt. The debris produced by such fine fragmentation processes is in a size range of 100 μm . Due to the larger melt surface area, the heat transfer rates strongly increase.
- IV. Expansion: During the expansion phase vapor expands and converts thermal energy into mechanical work. The conversion ratio of this phenomenon is very wide and varies from few percent to 50%.

2.3 Theoretical models

To explain the overall behaviour of the steam explosion, actually we have two theories [21]:

- The first, proposed by Fauske, is based on the spontaneous nucleation to determine the set of conditions necessary for the development of a steam explosion on a large scale.
- The second, proposed by the Board and Hall, and known as the theory of thermal detonation, focuses on the propagation of the explosion caused by hydrodynamic fragmentation, behind the shock wave.

2.3.1 Spontaneous nucleation model

The spontaneous nucleation theory studies the mechanism by which there is the formation of a nucleation center of critical dimensions as result of the fluctuation of the density in a liquid or in a pre-existing interface liquid-vapor or liquid-gas. To understand this theory it is necessary to recall some basic concepts. Firstly the interface temperature of two semi-infinite masses of liquid, which are located at different initial temperature is given by:

$$T_I = \frac{T_H \left(\frac{k}{\kappa} \right)_H + T_C \left(\frac{k}{\kappa} \right)_C}{\left(\frac{k}{\kappa} \right)_H + \left(\frac{k}{\kappa} \right)_C} \quad (2.1)$$

Where:

- k is the thermal conductivity
- κ the thermal diffusivity
- H indicates hot fluid
- C indicates cold fluid

Further, according to the kinetic theory of fluids, fluctuations of energy of the molecules can lead to the formation of vapor bubbles in a liquid bulb and, consequently, one can have the occurrence of spontaneous nucleation.

This can occur in the moment in which there is the formation of a nucleus of steam with a radius greater than or equal to the value of the critical radius.

The critical radius can be derived by Place equation that describes the capillary pressure difference sustained across the interface between two static fluids:

$$r_{crit} = \frac{2\sigma}{P_g - P_C} \quad (2.2)$$

Where:

- P_g is the vapor pressure of the nucleus
- P_C is the liquid pressure corresponding to saturation temperature
- σ is the surface tension

A bubble with internal pressure equal to P_g is, in general, unstable and if its radius is less than the critical radius collapses, while if it is above grows. The reversible work necessary to trigger nucleation and therefore required to form the spherical core of the vapor bubble in the liquid, is

$$W = 4\pi r_{crit}^2 \sigma - \frac{4}{3}\pi r_{crit}^3 (P_C - P_g) \quad (2.3)$$

where the first term represents the energy loss due to surface tension σ and the second term represents the energy gained in creating a new volume.

Finally, the rate of nucleation per unit time and volume is given by

$$J = wNe \left(-\frac{W_{eq}}{K_B T} \right) \quad (2.4)$$

Where:

- N is a constant whose value is 10^{22} cm^{-3} (approximately equal to the number of molecules per unit volume)
- w is the collision frequency of the liquid's molecules ($\sim 10^{10} \text{ s}^{-1}$)
- $W_{eq}/K_B T$, which is called Gibbs number, represents the ratio between the energy required for nucleation and the molecule's kinetic energy due to the thermal motion.

The nucleation rate is particularly sensitive to variations in temperature and above its specific value (equal to 10^{10}s^{-1}), there is the formation of a high number of bubbles so as to form the homogeneous nucleation. The temperature at which this happens is called precisely homogeneous nucleation temperature. Beyond a certain value of the nucleation rate depending on temperature, the number of bubbles formed is so high to destabilize the metastable liquid state. As the interface temperature T_I (individuated in case a in Figure 2.2) approaches the spontaneous nucleation temperature T_{SN} (see case b in Figure 2.2), the bubble nucleation rate increases exponentially, at the point at which vapor production occurs at explosive rates. In particular, the vapour explosion is expected if T_I is larger than T_{SN} .

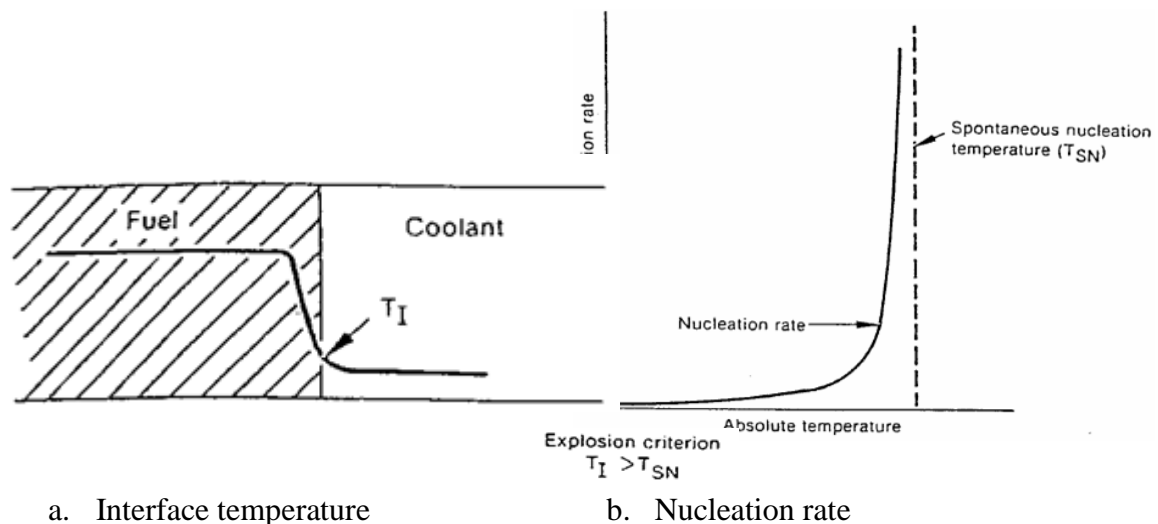


Figure 2.2 – spontaneous nucleation model

Therefore to have steam explosion must meet the following criteria:

- the onset of stable film boiling, so that the film of vapor separates the two liquids and permits mixing without excessive energy transfer;
- the occurrence of a direct contact between two liquids due to the collapse of the film of vapour;
- that at the moment of contact, the interface temperature exceeds the temperature of spontaneous nucleation causing rapid fragmentation and mixing of hot and cold liquids in a very short time;
- the presence of "inertial constraints", acts to support the shock wave for the time required by the explosion in a large scale.

When the nucleation process takes place at the interface between two liquids, the work needed for the bubble formation decreases together with the surface wetting properties. The value of the spontaneous nucleation temperature it is then influenced:

- for a surface completely wetted by a fluid the rate of spontaneous nucleation coincides with the rate of homogeneous nucleation and consequently the spontaneous nucleation temperature is equal to that of homogeneous nucleation;
- for an area not wetted by a fluid the temperature of spontaneous nucleation coincides with the saturation temperature;
- for a surface partially wet the spontaneous nucleation temperature is between the saturation temperature and the temperature of homogeneous nucleation.

Fluids like water and LBE have weak wetting properties and consequently the spontaneous nucleation temperature is very close to the homogeneous nucleation temperature that for water is about 583 K [15].

The achievement of all these conditions to get an explosion is difficult. This constitutes a limitation of this theory, which has been criticized in the light of some experimental results.

The main objections to this theory are related to the following aspects:

- The lack of information on the quantities of liquid metal coolant and you need to be involved in the process;
- The possibility of having steam explosion despite not having an interface temperature higher than the temperature of spontaneous nucleation, as occurred in the experiments conducted at low temperature. A possible explanation for this discrepancy, which is not universally accepted, is that in these cases the spontaneous nucleation temperature is altered by changes in the wettability characteristics of the surface related to the dynamics of the phenomenon;
- As observed in some experimental studies, the trigger spontaneous explosion is inhibited by a high pressure environment. This model are unable to consider this effect;
- The lack of consideration of the effects of solidification of liquids.

2.3.2 Thermal detonation

The theory of thermal detonation is inspired by experimental observations that the steam explosion can be maneuvered by fragmentation and mixing determined by the shock wave propagation. This model refers to the typical mechanisms of a chemical monodimensional detonation that are applied at the case of a planar shock front in propagation through the coarse mixing region between liquid metal and the coolant. The propagation of the shock wave causes a rapid fragmentation of the metal behind the front collision, due to the relative speed which induces instability phenomena. This mechanism of fragmentation is fundamentally different from that seen in the previous model and the two models are considered complementary: in particular, the concept of spontaneous nucleation describes the mechanism that produces the explosion, while the hydrodynamic fragmentation represents the dominant phenomenon once that the explosion has determined a front of explosion almost stationary. The model suggests that, in a system sufficiently extended or with appropriate inertial constraints, the explosion of steam may come to detonate when is available a sufficient ignition energy. Consider a one-dimensional system containing water and particles of liquid metal covered by a film of steam (see Figure 2.3 case a).

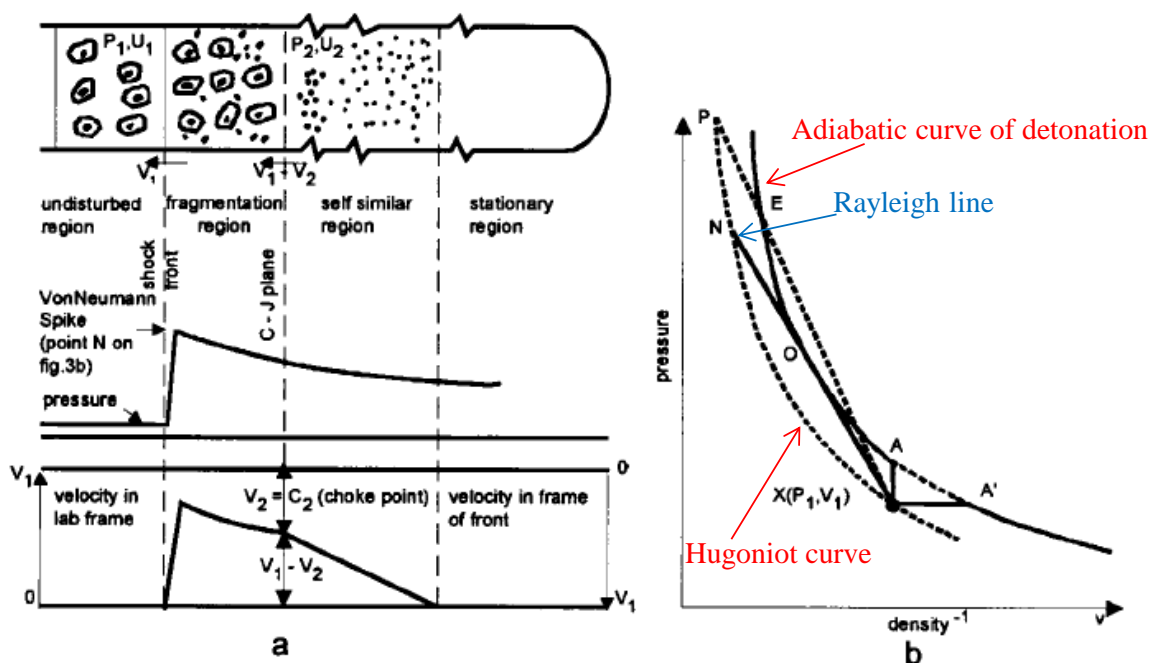


Figure 2.3 – a) Geometry and schematic pressure and velocity profiles of a 1-D explosion.
 b) Schematic shock adiabat (solid curve, reacted material; dashed curve, not reacted material)

Referring to the shock wave which propagates from right to left, we can write the balance equations. The balance equations of mass, momentum and energy for the homogeneous mixture of water, steam and liquid metal, written for a volume of small thickness at the turn of the wave front, are:

$$\rho_1 V_1 = \rho_2 V_2 = G \quad (2.5)$$

$$P_1 + \rho_1 V_1^2 = P_2 + \rho_2 V_2^2 \quad (2.6)$$

$$U_2 - U_1 = \frac{1}{2}(P_1 + P_2)(v_1 - v_2) \quad (2.7)$$

Where:

- ρ is the density
- V is the absolute velocity
- $U(p, v)$ is the internal energy of the mixture
- 1 is the material before the shock front that has not still reacted
- 2 is the material that as reacted completely

In the case of 1D steady-state detonation, Eq.(2.7) gives all the possible states of detonation and is called “Adiabatic curve of detonation” or “Crussard curve” (Figure 2.3b, thick curve). It must be pointed out that in case the jump conditions would be applied just through the shock front and not in the zones behind and in front of the shock front as mentioned before, the subscript 2 corresponds to the adiabatic compression of the reactants without any taking into account their reactions. Thus, in this case Eq.(2.7) would give all the possible states after a shock in an inert medium.

These states are located on the shock adiabatic or Hugoniot curve (Figure 2.3 b, dashed curve). From equation (2.5) and (2.6) it is possible find:

$$G = \left[\frac{(p_2 - p_1)}{(v_1 - v_2)} \right]^{\frac{1}{2}} \quad (2.8)$$

This equation determines the shock front velocity that is given by the slope of the line of the possible states of detonation (Rayleigh line), passing through the pole $X(p_1, v_1)$.

It was demonstrated [22] that the only possible stable steady state is obtained when the Rayleigh line is tangent to the adiabatic curve of detonation (point O In Figure 2.3 b). A steady-state chemical detonation can be described as in the following. The pressure of a shock wave going through the inert material increases up to the so called ‘Von Neumann spike’ (point N in Figure 2.3 b). Then, chemical reactions start, the fluid behind the shock front begins to expand and the pressure falls more or less rapidly, depending on the reaction rate, until the O point called the Chapman-Jouguet point. The liquid metal–coolant analogy is based on the hypothesis that fragmentation and mixing are due to shock wave propagation. Board [23] described the metastable premixture as the non-reacted material in which a shock wave propagates, increasing pressure up to the Von Neumann point for a chemical detonation. This pressure wave makes vapor film collapse and, owing to the density difference, induces large relative velocities between the fuel drops and the surrounding liquid. These velocity differences allow fine fragmentation and rapid heat transfer. This occurs in the fragmentation region which corresponds to the reaction zone for an explosive. Then, if the energy release is large enough to sustain the shock propagation, a steady state may be reached.

The concept of thermal detonation is a considerable contribution to the modeling of explosions of steam and gives a complete picture of the phenomenon; However, even in this model were raised some objections summarized below:

- The thermal detonation does not consider the effects of different amounts of mass between the various components of the mixture that give different speeds.
- Were raised doubts about the role of geometry that can affect the development of a detonation stationary wave.
- There are objective difficulties in extending the theory of monophasic chemical detonation to multiphase thermal detonation; in particular the theory of detonation thermal is based on the approximation of a front collision thin while shock waves in two-phase flow are not thin.
- Hydrodynamics fragmentation, in agreement with the mechanism of "stripping" of the layer at the interface, cannot take place so quickly as to support the thermal detonation, due to the reduction of the relative speed. So the heat detonation cannot be accurately assessed without quantitative information on the hydrodynamic fragmentation.

Despite these criticisms, the experiments showed that the explosion produces a shock wave similar to that of chemical detonation, thus supporting the theory. It is important to emphasize the fact that this model is macroscopic and therefore cannot explain the microscopic mechanisms such as fragmentation, ignition and heat transfer. It was necessary, therefore, the development of specific models for the mixing, fragmentation, ignition and propagation of the explosion and its expansion. The models related to these phases, however, have limitations regarding the assumptions, simplifications adopted, their range of validity and their applicability to real situations.

2.4 SGTR phenomena

The steam generator of a LMFR represents the component that transfers of energy between a liquid metal at high temperature and a fluid, constituted by steam at a lower temperature and high pressure takes place. The thermodynamic conditions of the primary and the secondary working fluids varies depending on the operating conditions of the system design. In principle, the liquid metal of the primary system has a temperature in a range of about 400-550°C, at pressure close to atmospheric. The secondary fluid (water) has pressure and temperatures which depend from the thermodynamic conditions of plant design.

In case of ELSY design, the pressure is 180 bar and the temperature ranges from 330 to 450°C. If a steam generator pipe break occurs, a jet of water is injected in the pool of molten lead because the high pressure difference between primary and secondary systems. The phenomena expected are postulated analogous to those occurring in the case of a severe accident in a LWR (i.e. FCI). Nevertheless, despite the similarities, the two events have significant differences. Compared to a scenario of FCI, Dinh [24] has highlighted these differences, as summarized in Table 2.1.

<u>FCI</u> (<i>Severe Accident</i>)	<u>CCI</u> (<i>Steam Generator Tube Rupture</i>)
jet of molten metal injected into a pool of coolant less dense	less dense jet of coolant injected into a pool of molten metal
Presence of drops of liquid metal at high temperature, separated by a continuous film of vapor from the liquid refrigerant	Presence of refrigerant less dense in the liquid phase in the form of drops in the liquid metal separated from the latter by a layer of vapor

Available energy dependent on the amount of heat given by molten liquid metal	Available energy limited by the amount of coolant (upper limit)
dominant radioactive heat exchange in the process of mixing	Heat exchange prevailing for film boiling

Table 2.1 – different between FCI and CCI

The multiphase phenomena, expected in the primary system of a LMFBRs following the SGTR event can be divided into four phases.

- The first phase starts from the tube break and the consequent injection of water in primary system. The flow rate (choked) of water injected from the tube is relevant, and drives the depressurization of the secondary loop and the formation of pressure waves in the primary system.
- The second phase is characterized by the formation of a region of steam, in correspondence of the area in which it is localized the rupture. The subsequent formation of steam and its expansion cause the mixing of the liquid metal. In particular, during the injection of the mixture of water and steam into the liquid metal, different types of hydrodynamic instabilities at the interface of the two fluids may occur. These instabilities cause further breakage of the jet of water and steam and consequently a formation of a flow regime characterized by water drops dispersed into the liquid metal and separated by a layer of steam (see Figure 2.4). The evaporation of the drops leads to the development and growth of a large vapor bubble in correspondence of the break.

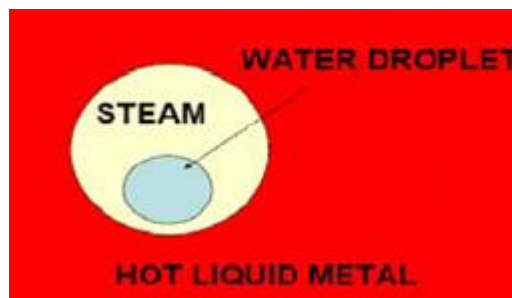


Figure 2.4 – liquid metal-water mixture

- The third phase involves the triggering of a CCI phenomenon, by means of contact between the two fluids in liquid phase, with the possible occurrence of steam explosion. Indeed, due to the expansion of the vapor bubble and, in correspondence of its critical dimension, the interface instability may cause its rupture, with

subsequent penetration of the liquid metal into the region of steam up to the contact with the drop of liquid. Its consequent fragmentation into smaller droplets increases the surface area and therefore the heat exchange and the rate of evaporation. This progression of the phenomenology is not frequent in case of SGTR postulated event. Indeed, an alternative phenomenology is more probable. The liquid phase of water undergoes to an effective fragmentation because the different pressure between primary and secondary systems, and the bubbles formed have a radius of about 1 mm. Bubbles having this size are relatively stable and the evaporation of the liquid phase is completed inside the steam coating. The amplitude of the bubbles increases, and the coalescence with the other causes the formation of a relatively large bubble. During the formation of these larger bubbles, the liquid drops evaporate almost completely. Therefore, when the critical size is reached and the liquid metal penetrates through the steam only a slight amount of liquid phase water coolant is available for the interaction.

- The last phase consists in the entrainment of the vapor bubbles finely dispersed into liquid metal and in the drag of these bubble into the reactor primary system.

Besides the possible occurrence of steam explosion, the SGTR postulated accident leads to formation of pressure waves and primary system pressurization which may impact the surrounding structures. Thus a comprehensive study of the phenomena are needed to evaluate the safety features of Generation IV LMFBRs.

2.5 Experimental campaign

The interaction between refrigerant and liquid metals has acquired an important role in the field of safety studies for nuclear reactors after TMI accident [25]. Several experimental campaigns were carried out to analyse the basic mechanisms.

Experimental programs were conducted worldwide, such as JAERI (Japan), FZK (Germany), CEA (France), KAERI (Korea), LANL (USA), ENEA (Italy) and universities.

Among these:

- HEADLIGHT and Krotos, [26] provided information on the production of hydrogen due to the processes of oxidation during the step of mixing in the interaction UO₂/ZrO₂ and
- THINA [26] started to study the phenomenology and the physics of the interaction between a molten mixture of aluminium, iron and sodium.

Recent studies were carried out in Japan at the Central Research Institute of Electric Power Industry (CRIEPI) in collaboration with KAERI. The goal of these campaigns is the development of "maps" for the definition of the conditions for steam explosions, in order to determine the conditions of safety LBE-water interaction [15].

One experimental campaign addressed the so-called "impingement". It is the study of liquid metal-water interaction when a drop of water falls into a bath of molten alloy. A layout of the facility utilized is reported in Figure 2.5. "Maps" were derived (Figure 2.6) from the analysis of experiments conducted with different initial and boundary conditions (i.e. different pressures and temperatures).

The following conclusions were achieved:

- criterion which establishes the occurrence of the explosion of steam, at atmospheric pressure, in this configuration, is summarized in: $T_{SN} < T_I < T_{crit}$;
- the steam explosions seem to take place when the water is sufficiently subcooled and when the contact temperature is greater than the spontaneous nucleation temperature;
- decreasing the subcooling of drops of water also decreases the intensity of the explosion.

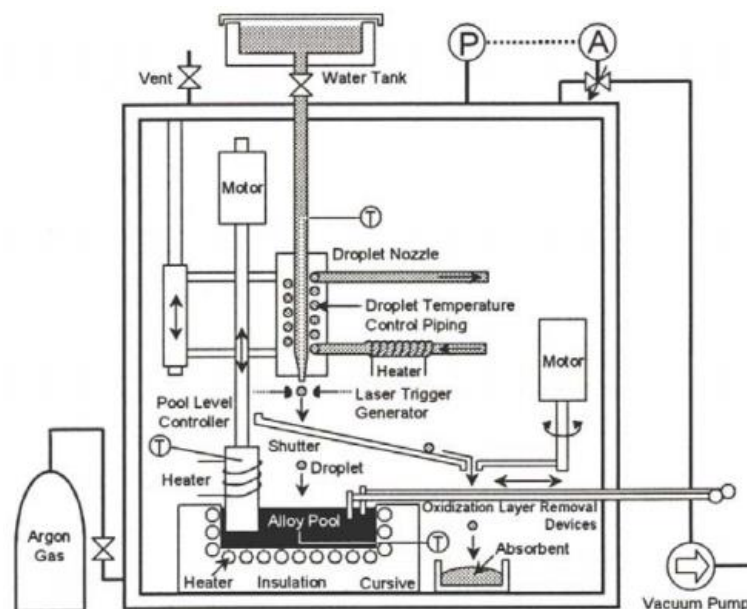


Figure 2.5 – facility for impingement study

As part of the prevention of explosions of steam, both conventional aluminum foundry industry and nuclear industry, have collaborated for developed a research program and

experimentation, called the CRADA [28], which involved, for several years, Oak Ridge National Laboratory (ORNL) and the Aluminum Association (AA).

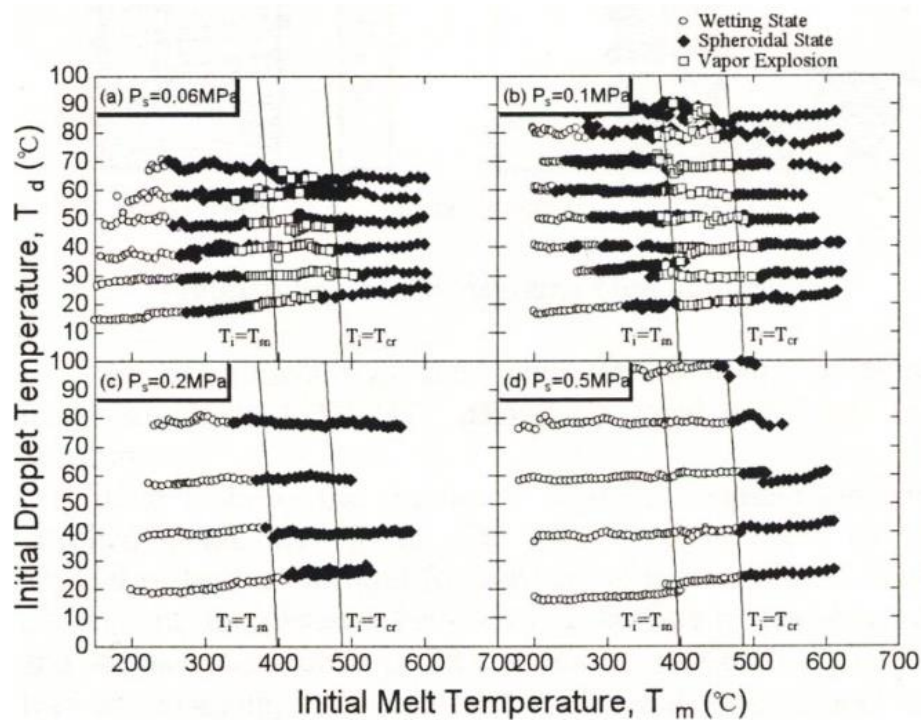


Figure 2.6 – steam explosion map

The research program has been focused on the role of non-condensable gases in the explosion. Two major categories of experiments were carried out: experiments on various types of surface coatings that can cause non-condensable gases and experiments injection of non-condensable gases from an external source. This plan called for the construction of experimental apparatus for the study of ignition of the explosion (SETS Facilities see Figure 2.7).

For the first category through various tests it is seen that the organic coatings produce a significant amount of incondensable during the attack by the molten metal and thus can avoid shock explosives during the boiling of the steam film of the trapped particle.

For the second category of experiments the results obtained showed that, under certain conditions in which the injected gas is mixed with the steam, the incondensable bring the transition temperature of the film boiling and nucleate boiling at lower levels, stabilize the film of steam and cause a significant delay of the transition. If the flow rate of injection of incondensable gases is high, they violently destroy the film of vapor and turbulence that is created can accelerate the transition to the regime of nucleate boiling. Experiments carried out with the tin to 700°C and water at 40°C have further confirmed the importance of the

incondensable: in fact the tin is a material that does not create a protective layer of oxide such as aluminum and which is extremely reactive with water. It is seen that without injection of incondensable is a violent fragmentation of the metal, while with their injection there is a shutdown of the interaction.

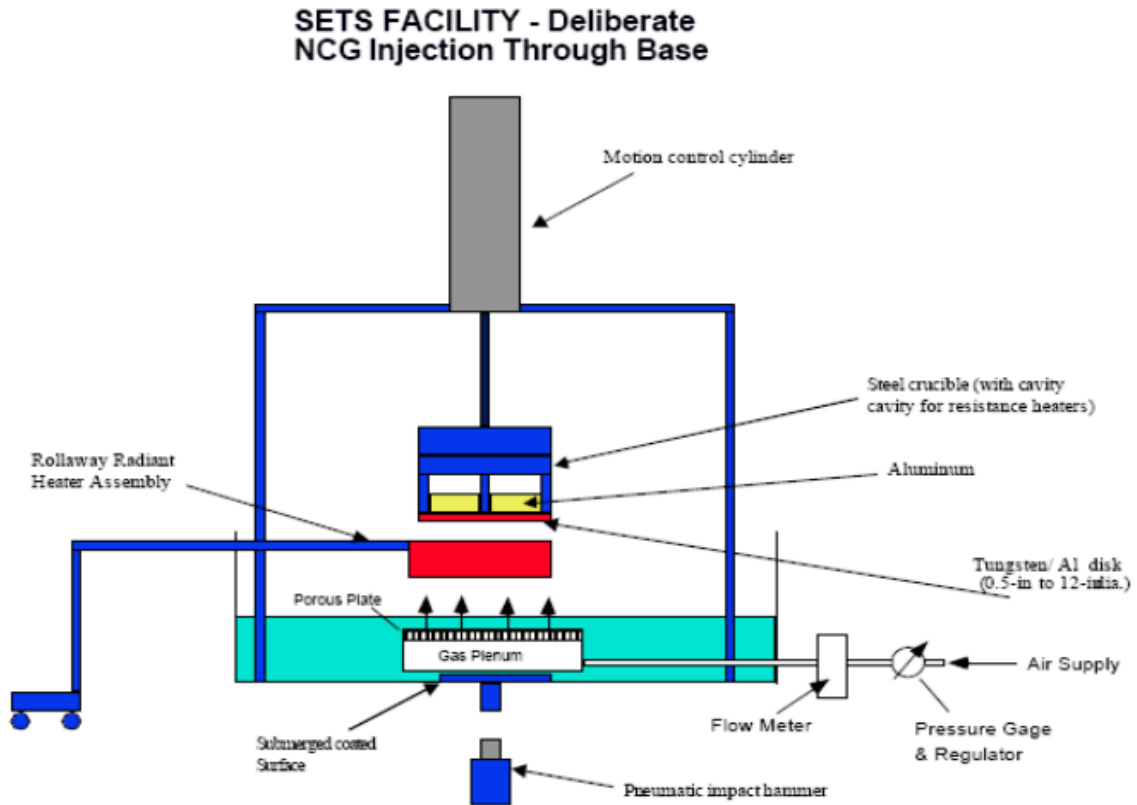


Figure 2.7 – SETS facility

An experimental campaign has been carried out at the ENEA Research Centre in Brasimone (Italy) with the aim to study the phenomenology of the water-LBE interaction. In this purpose, the LIFUS5 facility has been chosen for its ductility in working under different operating conditions. The facility was originally studied interactions lead-lithium-water and subsequently lead-bismuth-water, in the frame of THINS project [29][30]. The collected data were compared with those simulated by the code SIMMER-III to validate the code itself. The numerical results have shown an agreement with the experimental data, in terms of pressure trends in the reaction vessel [14][31]. Currently the LIFUS5/Mod2 facility is still involved in R&D activities aimed at investigating the interaction between lead-bismuth and water. In LEADER project focus is given to the consequences of the SGTR accident scenario on the surrounding structures. Detailed description of this activity is within the scope of the present thesis and discussed in the sections 4.

3 ELSY project

The ELSY project developed in the 6th Framework Programme of EURATOM has proposed and carried out a preliminary design of a competitive and safe fast critical reactor using simple engineered features, whilst fully complying with the Generation IV goals of sustainability, economics, safety, proliferation resistance and physical protection [9].

3.1 Overview of primary system

The thermal cycle selected has core inlet temperature equal to 400°C, in order to have sufficient margin above the lead freezing point and to avoid excessive embrittlement of structural material in fast neutron flux, and a mean core outlet temperature equal to 480°C, to mitigate corrosion, and to take advantages in term of creep and reduced thermal shocks in transient conditions [10]. In Figure 3.1 a layout of ELSY is reported and functional parameters are listed in Table 3.1.

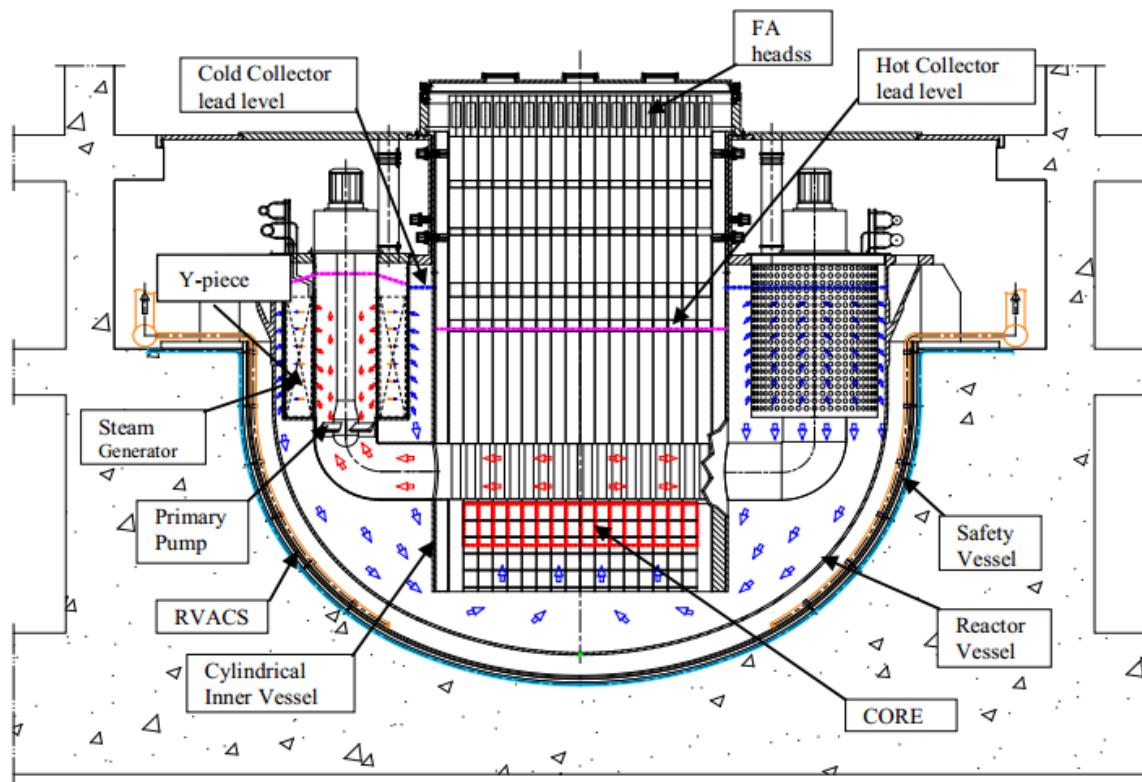


Figure 3.1 – ELSY layout

The drawback of such a thermal cycle is the need to increase the coolant flow rate which impacts on the primary system dimensions. This is due to the low lead velocities that can be achieved (< 2 m/s) in order to reduce corrosion and erosion phenomena. Additionally

the use of a coolant with very high density combined with large primary system, makes the mechanical design challenging with respect to mechanical loads, particularly to seismic loads. Based on the above mentioned considerations, a large effort has been made to design an innovative primary system as compact as possible. The result is a reactor with very short vessel (~ 9 m high), whose feasibility is confirmed by the preliminary mechanical analyses. This result, together with the elimination of the intermediate loop, opens the way to the feasibility of a competitive LFR. The adoption of a pool-type reactor configuration and, most importantly, the installation of a new-design, short-height steam generator (SG) with integrated mechanical pump are the main provisions to achieve the goal of compact design required to counter precisely the seismic loads.

Parameter	ELSY
Power, MWth	1500
Primary coolant	Lead
Primary coolant circulation (at power)	Forced
Core inlet temperature (°C)	400
Core outlet temperature (°C)	480
Fuel	MOX
Peak cladding temperature (°C)	550
Fuel pin diameter (mm)	10.5
Active core dimension Height/equivalent diameter (m)	0.9/4.32
Power conversion system working fluid	water-superheated steam at 180 bar, 450 °C
Primary/secondary heat transfer system	Eight Pb-to.H2O SGs
Fuel column height. (mm)	900
N° fuel assembly (FA)	162
FA geometry	Open square
FA pitch (mm)	294
N° fuel pins/FA	428
Fuel pins pitch (at 20°C) (mm)	19.9 square
Fuel pins outer diameter (mm)	10.5
Enrichment (%wHM)	14.54-17.63-20.61 Pu, three radial zones

Table 3.1 – ELSY functional parameters

Current design addresses the issue of material compatibility (i.e. corrosion) in lead through a protection technology based on a controlled dissolved oxygen approach. The technical risk associated with the corrosive behavior of lead does not readily permit assurance of the

ability to achieve the decades-long lifetime of the high-temperature components normally required for nuclear application. The only possible outcome of this issue has been so far the demonstration of the possibility to remove all the primary system components immersed in lead and their replacement with spare components.

Peculiar, innovative solution of ELSY is the cylindrical inner vessel of circular cross section, provided with ducts branching out from its lower part, each duct feeding hot lead to one SG. The cylindrical inner vessel provides also for the lateral restraint of the core and thanks to advanced technology solutions it is not connected to a core support plate. In general, the core support plate constitutes a critical component because it is exposed to fast neutron flux, it is not easy to replace and its in-service inspection and repair results prohibitive. The simple cylindrical inner vessel can be supported in the upper part by the roof and is removable for replacement in case of need.

3.2 Description of the steam generator design

The innovative SG conceived for ELSY (see Figure 3.2) offers several advantages in term of reactor cost, safety and reactor operability and simplicity of the lead flow path.

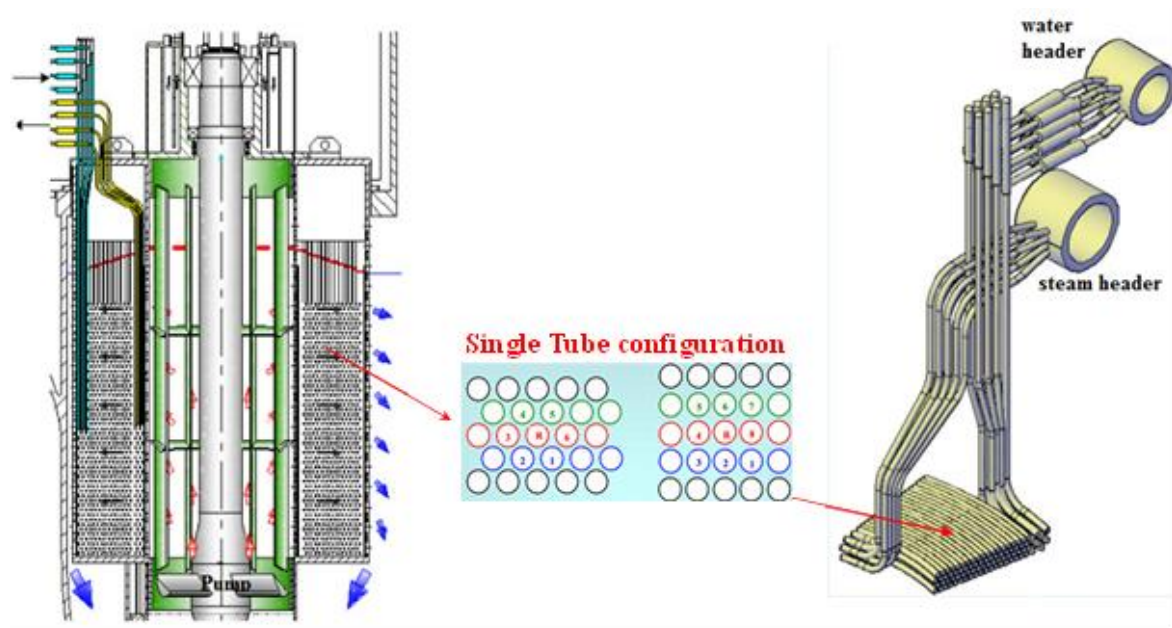


Figure 3.2 – ELSY steam generator

The SG tube bundle is composed of a stack of spiral-wound tubes (see Table 3.2 for more details) arranged in the bottom-closed, annular space formed by the perforated outer and inner shells of the SG. The inlet and outlet ends of each tube are connected to the feed water header and steam header, respectively, both arranged above the reactor roof. The tube spirals (one spiral for each tube), are arranged equally spaced one above the other.

This disposition gives the name to this type of steam generator, called STSG (Single Tube Steam Generator). Hot lead flows radially through the perforated inner shell and, once past the tube spirals, through the outer shell. There is no window, as a primary coolant inlet port and consequently there is no typical constraint of the classical design to locate deep enough the bottom edge of the window to cope with the case of a leaking reactor vessel. In fact, the shell perforations extend below the accidental coolant free level and ensure adequate flow rate for core cooling.

Parameter	ELSY SG spiral tubes
Inner diameter of the SG inner shell (mm)	1120
External diameter of the SG inner shell (mm)	1220
Inner diameter of the SG companion shell (mm)	1230
External diameter of the SG companion shell (mm)	1240
Porosity of the inner shell %	30
Inner diameter of the outer companion shell (mm)	2420
External diameter of the outer companion shell (mm)	2430
Inner diameter of the SG outer shell (mm)	2440
External diameter of the SG outer shell (mm)	2540
Porosity of the outer shells %	15
Number of tubes	218
length of tubes (m)	55
Outer diameter of the tubes (mm)	22.22
Thickness of tubes (mm)	2.5
Radial pitch (mm)	24
Axial pitch (mm)	24
Height (coils only) (mm)	2620

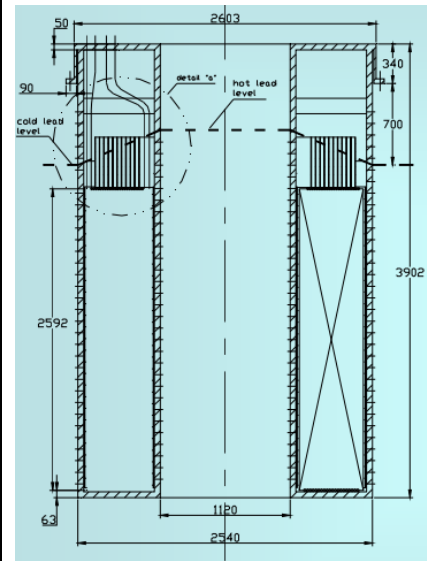


Table 3.2 – ELSY SG spiral tubes features

Consequently, the SG unit can be positioned at a higher level in the downcomer and the reactor vessel shortened accordingly. Main ELSY SG functional parameters are reported in Table 3.3. The installation of SGs inside the reactor vessel is a major challenge of a LFR design which includes the need of a sensitive and reliable leak detection system and of a reliable depressurization and isolation system. In ELSY, attention has been given to mitigation of consequences related to SG tube rupture, in order to reduce the risk of pressurization of the primary boundary. In this way, innovative provisions have been

conceived, which make the primary system more tolerant of the SG tube rupture event. Some of these aspects [11] are reported in Table 3.4.

Coaxial with the SG, a pump impeller is installed at an immersion depth of few meters, ensuring a realistic net positive suction head. Consequently, a short pump shaft is enough to connect the pump impeller to the pump motor located on the reactor roof. It is also implemented a decay heat removal (DHR) system that works injecting water from a storage water into the steam generator [12].

Despite all the mentioned precautions, the SGTR accidental scenario needs to be deeply studied, because the phenomena arising from the interaction between the two fluids is a relevant safety issue. Moreover, mastering of phenomena involved in the interaction is questionable and simulation capability is still limited. At ENEA CR Brasimone the test section implemented on the LIFUS5/Mod2 facility aims to simulate a sector of the spiral tube bundle between two spacer grids of the ELSY steam generator. Purpose of the experimental campaign, within the LEADER project, is to simulate a SGTR event in relevant configuration for ELSY reactor and derive useful data to validate calculation codes as explained in the following.

Parameter	ELSY SG
Lead temperature at SG inlet (°C)	480
Lead temperature at SG outlet (°C)	400
Steam generator feedwater temperature (°C)	335
Steam temperature at SG outlet (°C)	450
Water pressure at SG inlet (MPa)	19
Steam generator outlet pressure (MPa)	18
Steam Generator Power (MW)	1388
Water flow (kg/s)	115
Cycle efficiency %	43.05

Table 3.3 – ELSY SG functional parameters

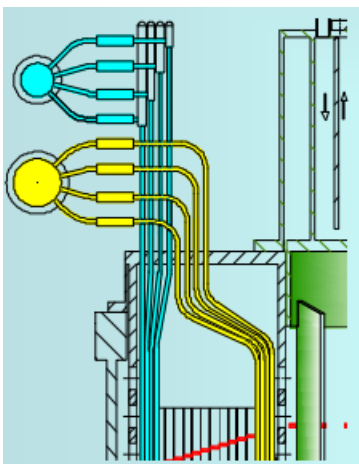
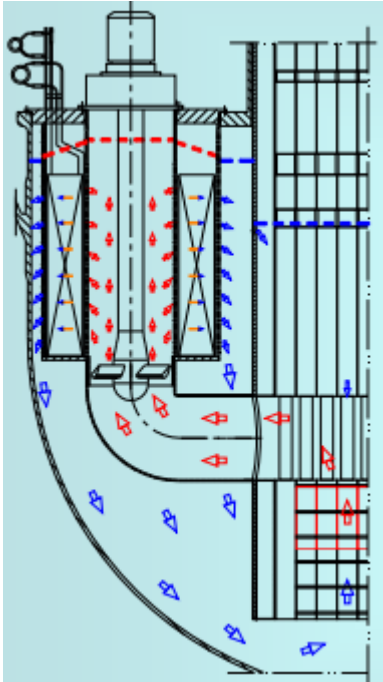
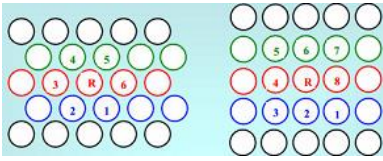
ELSY SG safety devices	
 <p>A schematic diagram showing a bundle of tubes extending from a reactor vessel. The tubes are connected to external manifolds for feed water (yellow) and steam (blue). Check valves and excess flow valves are shown at the connection points. A red dashed line indicates a potential leak path.</p>	<ul style="list-style-type: none"> • Feed water and steam manifolds are installed outside the reactor vessel to avoid the risk of catastrophic primary system pressurization. • On each tube of the bundle a check valve close to the steam header and an excess flow valve close to the feed water header are installed. In case of SGTR the water-steam leak is timely blocked (to be confirmed in term of feasibility).
 <p>A cross-sectional diagram of a tube bundle inside a reactor vessel. Red arrows indicate steam flow upwards, and blue arrows indicate water flow downwards. The bundle is bottom-closed. A red dashed line shows a steam leak near the lead-free level.</p>	<ul style="list-style-type: none"> • The tube bundle of the STSG is positioned up in the reactor vessel. In case of SGTR steam leaks near the lead free level reducing lead displacement. • The casing of tube bundle is bottom-closed. In case of SGTR no downward steam jet is possible and therefore it is extremely unlikely that bubbles can be entrained into the core. • The tube bundle of the SG is made of long tubes (high water-side pressure loss). Superheated or supercritical steam can be generated. In case of SGTR the water-steam leak rate is limited. • The SG tube bundle is positioned at higher level than the core. Lead natural circulation is therefore possible in case of decay heat removal by the water-steam loops.
 <p>A top-down view of a tube bundle layout. It shows two rows of tubes. The left row has tubes numbered 1 to 6, with a red 'R' in the center. The right row has tubes numbered 1 to 8, with a red 'R' in the center. Green and blue circles represent different tube types.</p>	<ul style="list-style-type: none"> • In ELSY SG each tube is surrounded by only two tubes, the former above (green) and the latter below (blue). In case of SGTR, the ruptured tube of the spiral-tube bundle can damage at most two other tubes.

Table 3.4 – ELSY SG safety devices

4 LIFUS5/Mod2 facility description

LIFUS5/Mod2 is an experimental facility installed at ENEA CR Brasimone. It is designed to be operated with different heavy liquid metals like Lithium-Lead alloy, Lead-Bismuth eutectic alloy and pure lead. Currently, the facility is employed in LEADER project, to investigate the LBE-water interaction following the simulation of a SGTR event. The main objective is to investigate and to assess the damping of pressure waves by SGTR event, besides the generation of experimental data for the development and validation of codes to support the design and the safety analysis of innovative HLM reactors. In connection with these goals, the expected outcomes of the tests are:

- the generation of detailed and reliable experimental data;
- the improvement of the knowledge of physical behavior and of understanding of the phenomenon;
- the investigation of the dynamic effects of energy release on the structures;
- the enlargement of the database for code validation.

4.1 LIFUS5/Mod2 facility

The main parts characterizing LIFUS5/Mod2 facility are shown in Figure 4.1. Four main components can be identified:

- main vessel S1 where LBE-water interaction occurs;
- S2 vessel where demineralized water is contained, it is injected in S1, simulating the SGTR event, by means of a pressurized gas cylinder connected to the top of S2;
- S3 vessel is a security volume connected with S1 to avoid an excessive increase of pressure during the test;
- S4 is the storage tank of LBE.

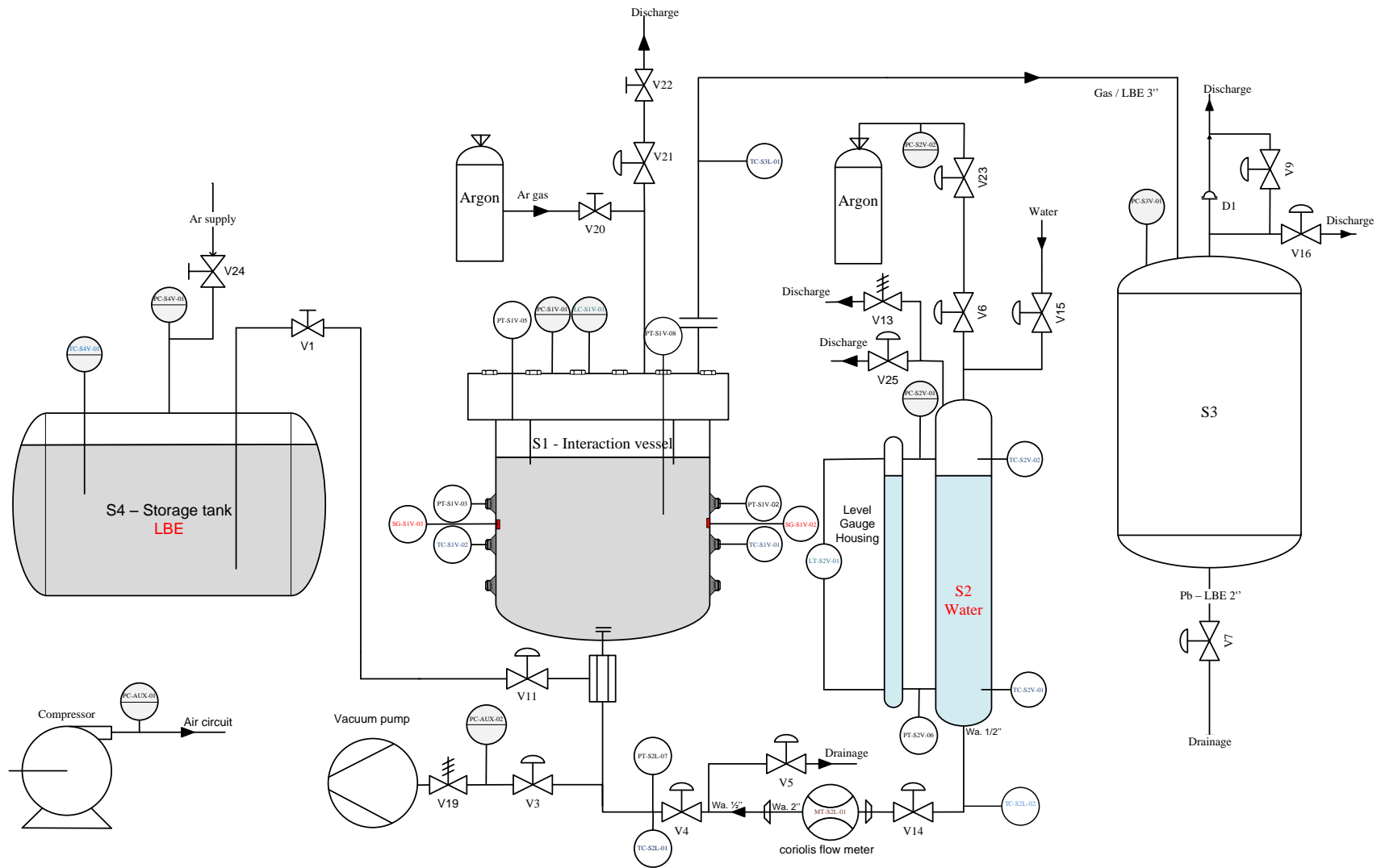


Figure 4.1 – LIFUS5/Mod2 facility

The main features of S1, S2 and S3 are shown in Table 4.1.

Component		
S1	Volume [m ³]	0.1
	Inner diameter [m]	0.42
	Height [m]	1.085
	Design pressure [bar]	200
	Design temperature [°C]	500
	Material	AISI 316
S2	Volume [m ³]	0.015
	Inner diameter	4 inch sch. 160
	Design pressure [bar]	200
	Design temperature [°C]	350
	Material	AISI 316
S3	Volume [m ³]	2
	Inner diameter [m]	1
	Design pressure [bar]	10
	Design temperature [°C]	400
	Material	AISI 316

Table 4.1 – tank S1, S2 and S3 features

The main vessel S1 is about 100 liters, and it is partially filled with LBE during the tests. It is closed by the top flange sealed with a Garlock HELICOFLEX gasket HN200. The sealing principle of the Helicoflex family [34] of seals is based upon the plastic deformation of a jacket of greater ductility than the flange materials. This occurs between the sealing face of a flange and an elastic core composed of a close-wound helical spring. The spring is selected to have a specific compression resistance. During compression, the resulting specific pressure forces the jacket to yield and fill the flange imperfections while ensuring positive contact with the flange sealing faces as shown in Figure 4.2. Each coil of the helical spring acts independently and allows the seal to conform to surface irregularities on the flange surface.

Considering LIFUS5/Mod2, the compression force is given by 20 bolts that are subjected to a tightening torque of about 170 Kgm. One bolt is about 580 mm long and its diameter is 45 mm as show in Figure 4.3. Internally, S1 can be divided into an upper cylindrical part

and a lower hemispherical part. The main diameter is 420 mm and the overall height is 780 mm. The cylindrical shell of S1 has penetrations allowing the passage of the instrumentation.

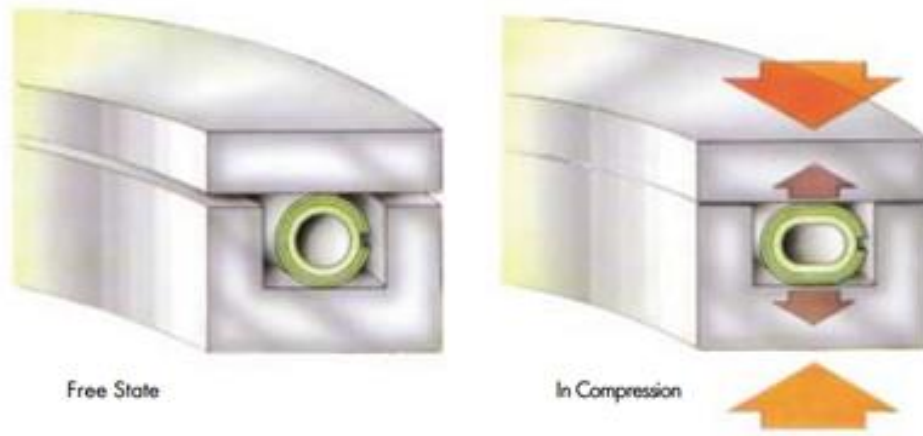


Figure 4.2 – Garlock Helicoflex gasket

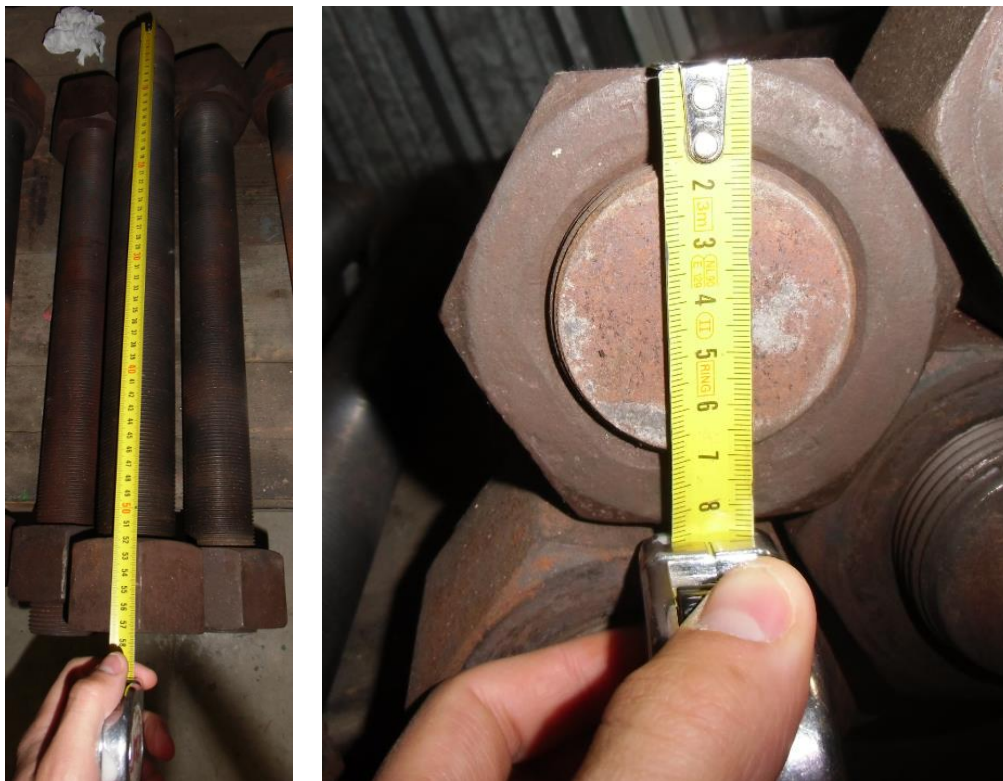


Figure 4.3 – LIFUS5/Mod2 bolts used to close S1 flange

These consist of four meters fast pressure transducers (PTs), two thermocouples (TCs) and six strain gages (SGs), five of which set on the inner S1 surface and one on the outside. The penetration positions are listed Table 4.2 and shown in Figure 4.4. It is important to highlight that the measurement points of the strain gages does not coincide with the relative penetrations. The correct measuring points are shown in Figure 4.5.

Position of the penetration	0° (South)	90°	180°	270°
UPPER RADIAL penetration 360mm from S1 flange	Pressure transducer PT-S1V-04	Pressure transducer PT-S1V-02	Strain gage SG-S1V-05 (B795)	Pressure transducer PT-S1V-03
MIDDLE RADIAL penetration 490mm from S1 flange	Temperature transducer TC-S1V-02	Strain gage SG-S1V-03 (B792)	Temperature transducer TC-S1V-01	Closed
LOWER RADIAL penetration 650mm from S1 flange	Strain gage SG-S1V-02 (B787)	Strain gages SG-S1V-04 (B790)	Pressure transducer PT-S1V-01	Strain gage SG-S1V-01 (B794)

Table 4.2 – S1 penetrations with instrumentation

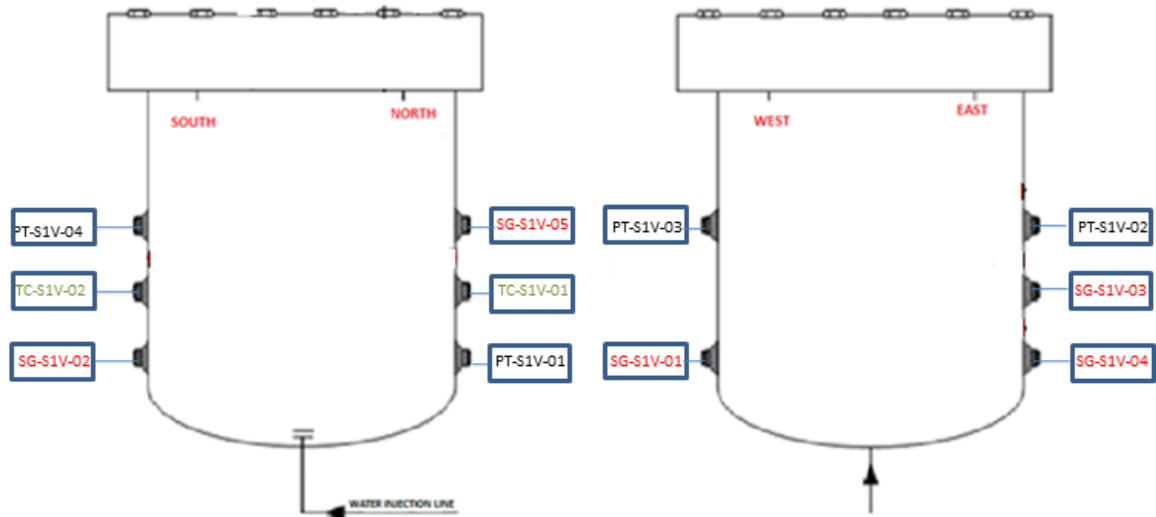


Figure 4.4 – sketch of S1 penetrations with instrumentation

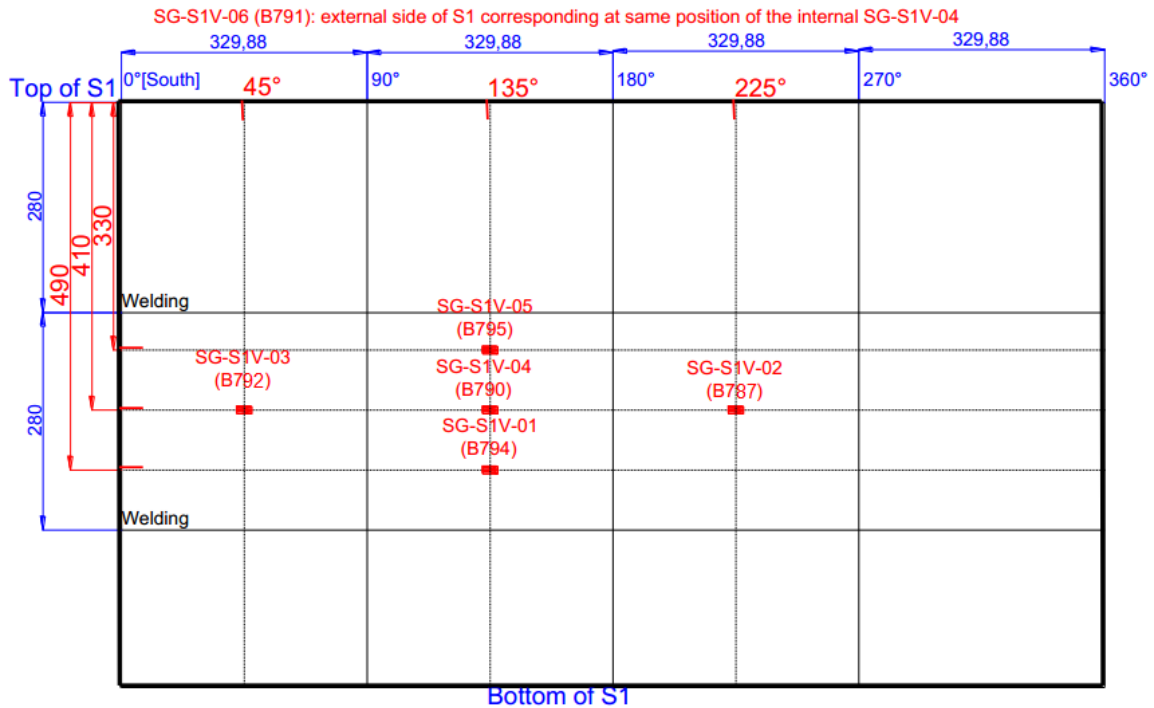


Figure 4.5 – strain gages measurement point positions inside S1.

Some other penetrations are implemented on the top flange of S1. In particular there are:

- a three-inch vent pipe that connects S1 to S3;
- a gooseneck tube through which thermocouples and strain gages wiring mounted on the test section exit from S1. This form of the pipe allows to seal it, pouring a small amount of molten lead into the tube, that goes to solidify on the first bend of the gooseneck;
- two 3/8" tubes on which KISTLER pressure transducers are positioned, one that measures the pressure in the S1 dome and one connected to the test section by 1/4" tube;
- an absolute pressure transducer connected to a 1/2" tube;
- one 1/2" penetration is used for inerting operation of S1;
- two 1/4" penetrations are implemented to pressurize components of the test section (see section 4.3).

A list of these penetrations is reported Table 4.3 and their position is shown in Figure 4.6.

It is important to highlight that compared to the previous THINS [33] experimental campaign, conducted on the LIFUS5/Mod2 facility, LEADER fast pressure transducers (PTs) acquire data at 10 KHz instead of 1 KHz. Such a decision aims to measure with

higher resolution the pressure peaks occurring in S1 at the time of the injector opening and LBE-water interaction start.

Pos.	No.	DN	Utilization
A	1	3"	Connection to S3
B	1	1"	Thermocouples and strain gages wiring passage
C	1	½" swagelok	Gas line cylinder for inerting operations
D	1	½" swagelok	Absolute pressure transducer. Safety valve (PC-S1V-01)
E	1	3/8"	KISTLER Pressure Gage on top flange, linked to the test section (PT-S1V-08)
F	1	3/8"	KISTLER Pressure Gage on top flange (PT-S1V-05)
G	1	¼"swagelok	Tube pressure line
H	1	¼"swagelok	Tube pressure line

Table 4.3 – S1 flange penetrations



Figure 4.6 – view of S1 flange penetrations

The water injection system enters the bottom of the vessel S1 in central position. The injection is carried out about 300 mm above the lower part of S1. The injector orifice is covered by a protective cap, which is broken by the pressure of the water jet at the beginning of the injection phase.

Therefore, the system shall be substituted at the end of each test. LEADER experiments provide a broken pressure of 180 bar, which is the design pressure for the secondary side of ELSY steam generator. To ensure that the cap rupture occurs at the scheduled pressure, a notch is executed by the ENEA workshop (see Figure 4.7). Tests were carried out to calibrate the deep of the notch and, consequently, the value of the resisting section. More details on test procedure and results are shown in section 4.4.

The tests will be performed adopting an injection orifice having different diameters, ranging from 4 to 13 mm (see Table 4.4). The upper limiting size is the water pipe diameter, because the orifice is at the end of the water injection line, based on a ½” sch 80 pipeline.

The maximum injection during the test is about 60% of the reference mass flow rate of the ELSY SG tube.



Figure 4.7 – injectors with protective caps

The sketch of water injection line is shown in Figure 4.8. The water injection line connects the tank S2 with the interaction vessel S1 and the vacuum pump line. In the middle a discharge valve is installed (V5), for draining the water at the end of the tests, and for removing steam formation during the conditioning heating phase. The water flows from S2 towards the valve V14, then the Coriolis flowmeter (in Figure 4.8 indicated with a letter C inside a red bounding) and finally through valve V4, before it enters in S1.

The water line is also connected with the vacuum pump. Valve V3 is placed between the vacuum pump and the vessel S1. Before the injection occurs, the vacuum pump is activated to remove air from the injection line

Test #	Section [%]	Section [mm ²]	Radius [mm]
B1	10.00	13.64	2.08
B2	50.00	68.22	4.66
B3	100.00	136.44	6.60

Table 4.4 – injector ruptured dimensions

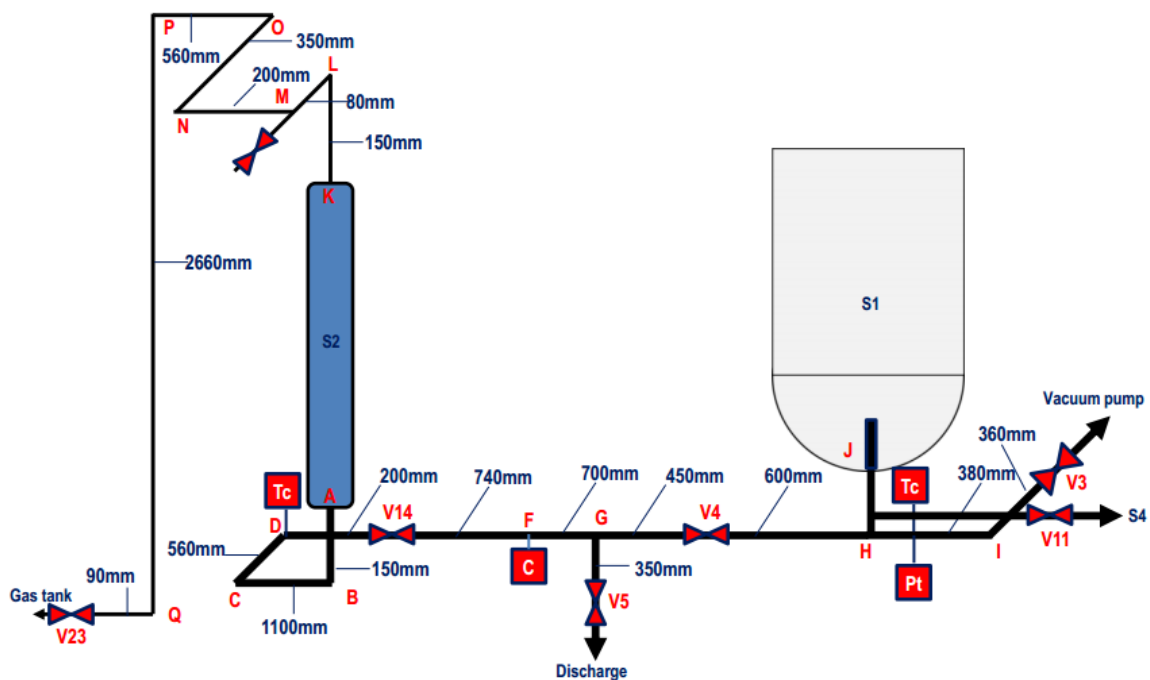


Figure 4.8 – sketch of water injection line

The water tank S2 is a 4 inch sch. 160 pipe, closed at the edges with proper welded plugs. It has a volume of 15 liters (plus those in the level meter). It is connected on the top with the gas line, which is used for setting and keeping the pressure of the water according with the test specifications. The water tank S2 is connected by means of two lateral flanges on a magnetic level measurement device. The connections are: one, on the upper part of S2, where a moisture of argon and vapor phase are present, and the other, on the lower part. A photo of the overall system comprising S2 and level measurement device, is shown in Figure 4.9.

The dump tank S3 is part of LIFUS5/Mod2 facility. It is connected by means of a 3” line to the top flange of S1. The S3 volume is equal to 2 m³ and the design pressure is 10 bar. It

represents a safety volume used to collect the vapour and the gas generated by the interaction between LBE and water. A photo of S3 is shown Figure 4.10.

When the facility is at rest, the LBE is stored in the liquid metal storage tank (S4), which is connected at the bottom of the main vessel S1, using the same penetration of the water injection system.



Figure 4.9 – view of S2 and level measurement system



Figure 4.10 – view of S3 dump tank

4.2 THINS test section

The THINS test section is configured in order to have an axial-symmetric geometry. This configuration was design to reduce, as far as possible, the perturbations due to structures inside the reaction vessel during the injection. The test section consists in a support frame, where 68 thermocouples are installed. The frame, welded on the old S1 top flange, has an overall length of 590 mm. The thermocouples, fastened to such a support structure, are immersed into the LBE melt. The structure has four horizontal cruciform levels supporting thermocouples. The lower cruciform support, Level 1, is the nearest to the injection orifice. At level 1, the diagonal frames are cut in the center, thus the central thermocouple is not installed (Figure 4.11). This choice is done to avoid the water jet impinging on the frames. The second level, above, presents the frame supporting thermocouples that reaches the axis of symmetry of the structure, see blue circle in Figure 4.11. Therefore, it constitutes an obstacle that fragments the water jet flowing upwards. The thermocouple set in the center of the horizontal support structure is coaxial with the reaction tank S1 and the injection orifice. Each one of the four horizontal branches constituting the cruciform support, called level, hosts four thermocouples. The thermocouples nearest to the central one are considered belonging to the first ring, the outer ones instead, are considered belonging to the fourth ring.

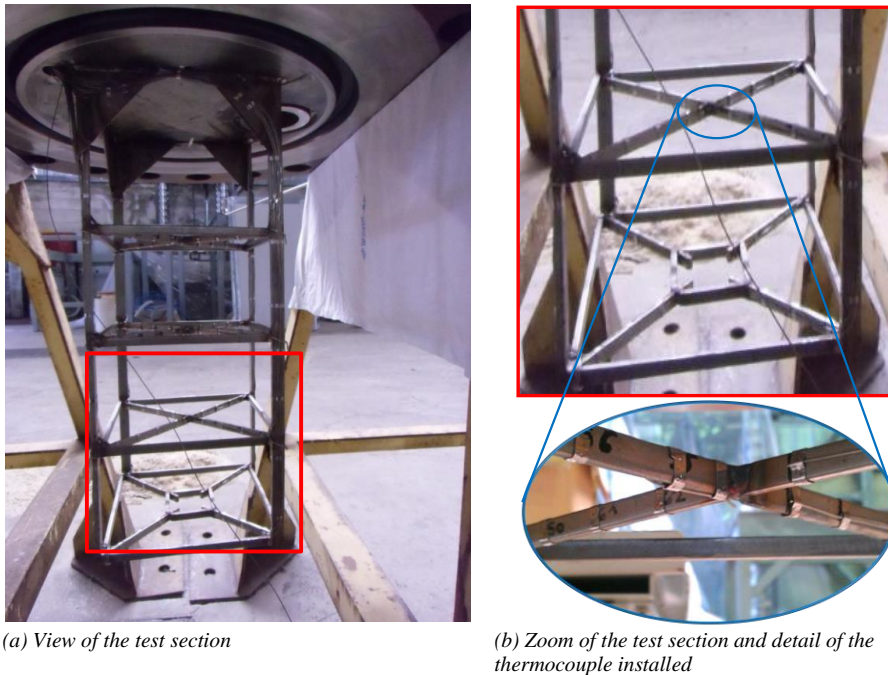


Figure 4.11 – detailed view of the TCs' support structure

The water injection nozzle enters in the bottom of the vessel S1 in central position (see Figure 4.12 (a)). The injection is carried out about 120 mm above the internal lower edge of the vessel. The injector orifice is covered by a protective cap (see Figure 4.12 (b)), which is broken by the pressure of the water jet at the beginning of the injection phase. Therefore, the system shall be substituted at the end of each test. The injection nozzle has a diameter equal to 4 mm. It is installed at the end of the water injection line based on a ½” sch 80 pipeline.

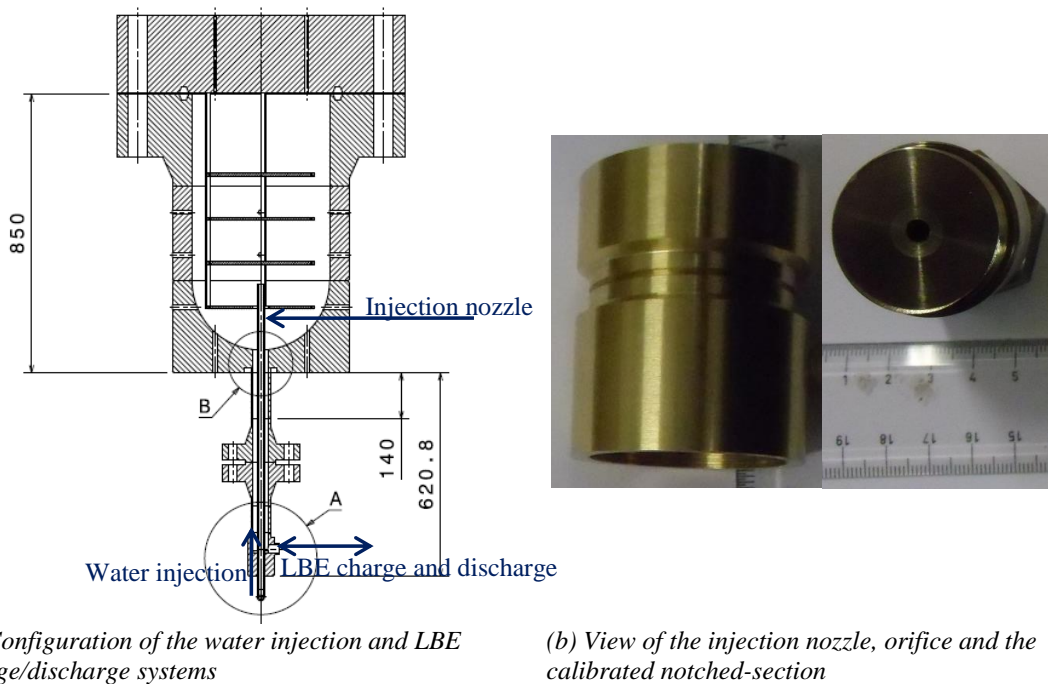


Figure 4.12 – S1 water injection system

Besides the 68 low time constant thermocouples (TC), 5 fast pressure transducers, one on the top of the vessel and four on the vessel wall at different elevations, and 6 high temperature strain gauges, five on the internal wall of S1 at different heights and one outside the vessel in correspondence with the central internal strain gauge, are implemented. 2 fast pressure transducers, placed on the top of the water tank and on the water injection line downstream the last valve V4; and 3 thermocouples, one in the gas zone of the water tank, the second in the water side of S2 and the third downstream the injection valve, are installed in the water injection system (S2).

The safety volume S3 is disconnected.

4.3 LEADER test section and description of the assembling

The LEADER test section shown in Figure 4.13 is placed vertically inside the vessel S1. This orientation is more favourable because the vertical axis is the longest. The test section is connected with the top flange of S1 and can be removed for maintenance, if needed. This connection is obtained through four screws on the top of the test section flange connected with other four screws positioned on the top flange of S1, by means of four long nuts. The screws of the test section flange are shown on the left side of Figure 4.14, instead on the right side of the same figure four screws and high nuts connected to the flange of S1 are shown.

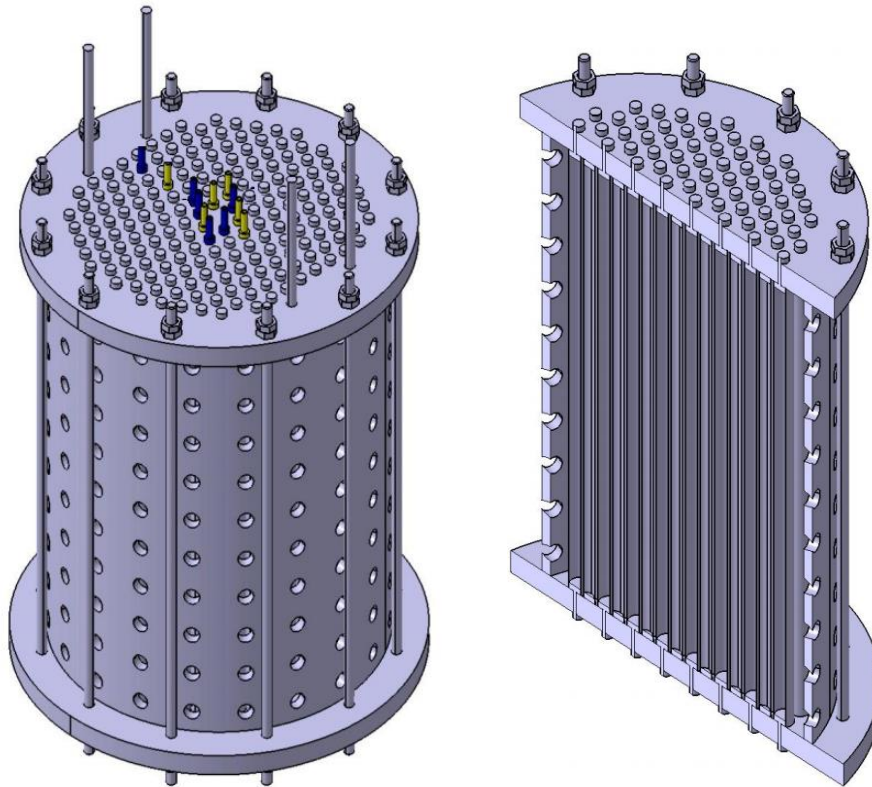


Figure 4.13 – 3D view of LEADER test section.

LEADER test section has a cylindrical shape characterized by an height of 400 mm. The thickness of the two closing flanges is 20 mm each. The radius of the test section is 155 mm, as shown in Figure 4.15. The test section is inserted inside S1, at 570 mm of distance from the bottom of the S1 top flange. The injection tube penetrates into the test section from its bottom flange for about 100 mm. The levels A and B, shown in the same figure, identify two planes at which thermocouples are placed.

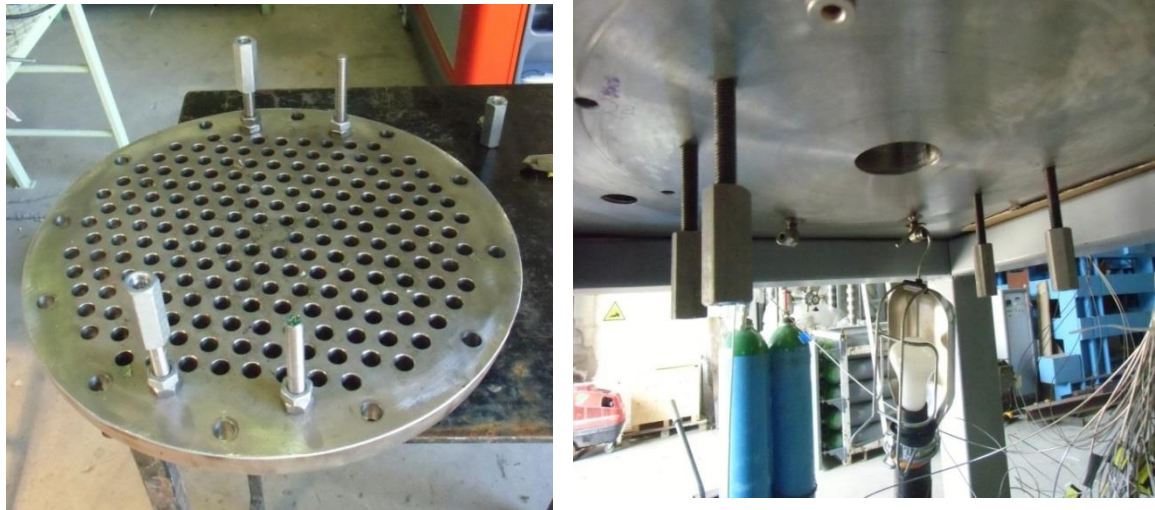


Figure 4.14 – test section flange (left) and S1 flange connections (right)

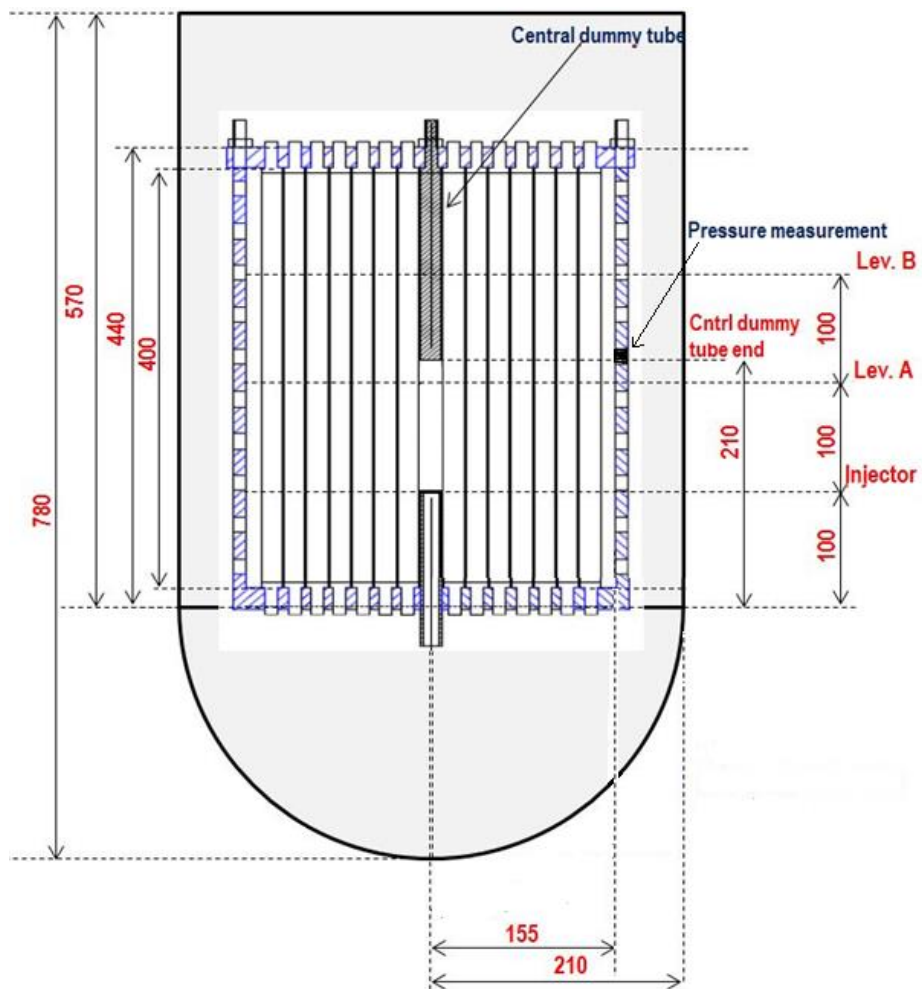


Figure 4.15 – layout of LEADER test section inside S1

The test section is composed by a bundle of 188 tubes, having external diameter equal to 18 mm and pitch of 19.8 mm, coherently with the geometrical parameters of the STSG (Single Tube Steam Generator) design of ELSY reactor [35] (see section 3). The arrangement of the tubes in the test section is scaled with respect to ELSY configuration according with the following rationale: 1) the area between the tubes is reduced of 60% in order to preserve the velocity of the fluid; 2) the length of the tubes is 400 mm, which corresponds to the distance between two consecutive grids of the ELSY bundle, corrected on the basis of the tube diameter scale; 3) the thickness of the tubes is reduced to 1 mm in order to have larger mechanical effect during the injection.

The tubes deformation is measured online by means of high temperature strain gages. The tubes are surrounded by a cylindrical shell having 200 holes of 15 mm of diameter. This provides a porosity of 30% that is coherent to the ELSY configuration, in which a pressure drop of about 0.05 bar is expected [36].

The tube bundle is composed by three different types of tubes:

- 12 tubes pressurized at 180 bar during the test execution. This is the value at which water in ELSY steam generator works;
- 128 holed dummy tubes that during the test are filled by LBE;
- 48 closed dummy tubes, containing air at atmospheric pressure and ambient temperature.

The first part of the test section assembly activity concerns the positioning of 70 thermocouples and 7 strain gages. Specifically, regarding the thermocouples there are:

- 20 thermocouples with a diameter of 0.5 mm that are installed on the central tubes;
- 50 thermocouples that have a diameter of 1 mm.

For what concern the strain gages, there are:

- 2 strain gages that are installed on the central tubes respectively on North and South directions;
- 3 strain gages are positioned in radial direction (East), to study the effect of the pressure wave propagation from the center to the outer region of the bundle;
- 2 strain gages are set on the outer surface of the perforated cylindrical shell, at North and East directions, respectively.

The sketch of the horizontal section of S1 and test section, highlighting the disposition of the tube types, thermocouples and strain gages, is shown in Figure 4.16. The thermocouples are placed axially at two different levels A and B (see Figure 4.15). The strain gages are located at level A.

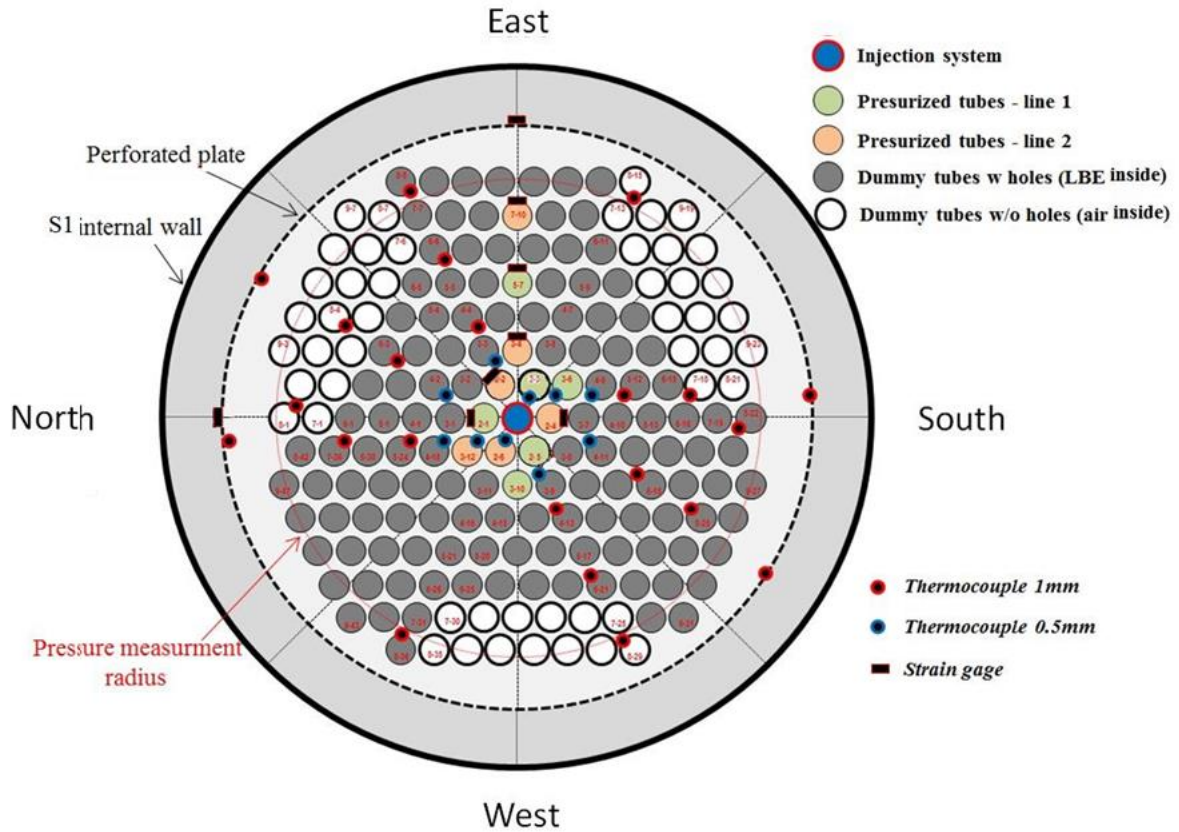


Figure 4.16 – LEADER test section horizontal sketch with instrumentation

The thermocouples are attached on the tubes, facing towards the center of the test section in order to be invested directly by the jet of steam during the water injection. The strain gages are welded on tubes facing outward, in order to work in tensile conditions during the propagation of the pressure waves. The strain gage set on the tube 202 (rank 2 position 2, north-east direction) showed malfunctions during the commissioning. Therefore, its measurement capability could be affected by errors.

The complete list of the tubes, the information of their locations and the number of measurements are reported in Table 4.5.

#	Rank	Tube	ID tube	Tube type	Measurement installed	No. of measurments
1	1	1	1-1	Injector	--	0
2	2	1	2-1	Pressurized line 1	Strain gage	1
3	2	2	2-2	Pressurized line 2	Strain gage	1
4	2	3	2-3	Pressurized line 1	TC 0.5mm	2
5	2	4	2-4	Pressurized line 2	Strain gage	1
6	2	5	2-5	Pressurized line 1	--	0
7	2	6	2-6	Pressurized line 2	TC 0.5mm	2
8	3	1	3-1	Dummy open	--	0
9	3	2	3-2	Dummy open	--	0
10	3	3	3-3	Dummy open	TC 0.5mm	2
11	3	4	3-4	Pressurized line 2	Strain gage	1
12	3	5	3-5	Dummy open	--	0
13	3	6	3-6	Pressurized line 1	TC 0.5mm	2
14	3	7	3-7	Dummy open	--	0
15	3	8	3-8	Dummy open	--	0
16	3	9	3-9	Dummy open	TC 0.5mm	2
17	3	10	3-10	Pressurized line 1	--	0
18	3	11	3-11	Dummy open	--	0
19	3	12	3-12	Pressurized line 2	TC 0.5mm	2
20	4	1	4-1	Dummy open	--	0
21	4	2	4-2	Dummy open	TC 0.5mm	2
22	4	3	4-3	Dummy open	--	0
23	4	4	4-4	Dummy open	TC 1mm	2
24	4	5	4-5	Dummy open	--	0
25	4	6	4-6	Dummy open	--	0
26	4	7	4-7	Dummy open	--	0
27	4	8	4-8	Dummy open	--	0
28	4	9	4-9	Dummy open	TC 0.5mm	2
29	4	10	4-10	Dummy open	--	0
30	4	11	4-11	Dummy open	TC 0.5mm	2
31	4	12	4-12	Dummy open	--	0
32	4	13	4-13	Dummy open	TC 1mm	2
33	4	14	4-14	Dummy open	--	0
34	4	15	4-15	Dummy open	--	0
35	4	16	4-16	Dummy open	--	0
36	4	17	4-17	Dummy open	--	0
37	4	18	4-18	Dummy open	TC 0.5mm	2
38	5	1	5-1	Dummy open	--	0
39	5	2	5-2	Dummy open	--	0
40	5	3	5-3	Dummy open	--	0
41	5	4	5-4	Dummy open	--	0
42	5	5	5-5	Dummy open	--	0
43	5	6	5-6	Dummy open	--	0
44	5	7	5-7	Pressurized line 1	Strain gage	1

#	Rank	Tube	ID tube	Tube type	Measurement installed	No. of measurments
45	5	8	5-8	Dummy open	--	0
46	5	9	5-9	Dummy open	--	0
47	5	10	5-10	Dummy open	--	0
48	5	11	5-11	Dummy open	--	0
49	5	12	5-12	Dummy open	TC 1mm	2
50	5	13	5-13	Dummy open	--	0
51	5	14	5-14	Dummy open	--	0
52	5	15	5-15	Dummy open	--	0
53	5	16	5-16	Dummy open	--	0
54	5	17	5-17	Dummy open	--	0
55	5	18	5-18	Dummy open	--	0
56	5	19	5-19	Dummy open	--	0
57	5	20	5-20	Dummy open	--	0
58	5	21	5-21	Dummy open	--	0
59	5	22	5-22	Dummy open	--	0
60	5	23	5-23	Dummy open	--	0
61	5	24	5-24	Dummy open	TC 1mm	2
62	6	1	6-1	Dummy open	--	0
63	6	2	6-2	Dummy open	--	0
64	6	3	6-3	Dummy open	TC 1mm	2
65	6	4	6-4	Dummy open	--	0
66	6	5	6-5	Dummy open	--	0
67	6	6	6-6	Dummy open	TC 1mm	2
68	6	7	6-7	Dummy open	--	0
69	6	8	6-8	Dummy open	--	0
70	6	9	6-9	Dummy open	--	0
71	6	10	6-10	Dummy open	--	0
72	6	11	6-11	Dummy open	--	0
73	6	12	6-12	Dummy open	--	0
74	6	13	6-13	Dummy open	--	0
75	6	14	6-14	Dummy open	--	0
76	6	15	6-15	Dummy open	--	0
77	6	16	6-16	Dummy open	--	0
78	6	17	6-17	Dummy open	--	0
79	6	18	6-18	Dummy open	TC 1mm	2
80	6	19	6-19	Dummy open	--	0
81	6	20	6-20	Dummy open	--	0
82	6	21	6-21	Dummy open	TC 1mm	2
83	6	22	6-22	Dummy open	--	0
84	6	23	6-23	Dummy open	--	0
85	6	24	6-24	Dummy open	--	0
86	6	25	6-25	Dummy open	--	0
87	6	26	6-26	Dummy open	--	0
88	6	27	6-27	Dummy open	--	0

#	Rank	Tube	ID tube	Tube type	Measurement installed	No. of measurments
89	6	28	6-28	Dummy open	--	0
90	6	29	6-29	Dummy open	--	0
91	6	30	6-30	Dummy open	--	0
92	7	1	7-1	Closed (air inside)	--	0
93	7	2	7-2	Closed (air inside)	--	0
94	7	3	7-3	Closed (air inside)	--	0
95	7	4	7-4	Closed (air inside)	--	0
96	7	5	7-5	Closed (air inside)	--	0
97	7	6	7-6	Closed (air inside)	--	0
98	7	7	7-7	Dummy open	--	0
99	7	8	7-8	Dummy open	--	0
100	7	9	7-9	Dummy open	--	0
101	7	10	7-10	Pressurized line 2	Strain gage	1
102	7	11	7-11	Dummy open	--	0
103	7	12	7-12	Dummy open	--	0
104	7	13	7-13	Closed (air inside)	--	0
105	7	14	7-14	Closed (air inside)	--	0
106	7	15	7-15	Closed (air inside)	--	0
107	7	16	7-16	Closed (air inside)	--	0
108	7	17	7-17	Closed (air inside)	--	0
109	7	18	7-18	Closed (air inside)	TC 1mm	2
110	7	19	7-19	Dummy open	--	0
111	7	20	7-20	Dummy open	--	0
112	7	21	7-21	Dummy open	--	0
113	7	22	7-22	Dummy open	--	0
114	7	23	7-23	Dummy open	--	0
115	7	24	7-24	Dummy open	--	0
116	7	25	7-25	Closed (air inside)	--	0
117	7	26	7-26	Closed (air inside)	--	0
118	7	27	7-27	Closed (air inside)	--	0
119	7	28	7-28	Closed (air inside)	--	0
120	7	29	7-29	Closed (air inside)	--	0
121	7	30	7-30	Closed (air inside)	--	0
122	7	31	7-31	Dummy open	--	0
123	7	32	7-32	Dummy open	--	0
124	7	33	7-33	Dummy open	--	0
125	7	34	7-34	Dummy open	--	0
126	7	35	7-35	Dummy open	--	0
127	7	36	7-36	Dummy open	TC 1mm	2
128	8	1	8-1	Closed (air inside)	TC 1mm	2
129	8	2	8-2	Closed (air inside)	--	0
130	8	3	8-3	Closed (air inside)	--	0
131	8	4	8-4	Closed (air inside)	TC 1mm	2
132	8	5	8-5	Closed (air inside)	--	0

#	Rank	Tube	ID tube	Tube type	Measurement installed	No. of measurments
133	8	6	8-6	Closed (air inside)	--	0
134	8	7	8-7	Closed (air inside)	--	0
135	8	8	8-8	Dummy open	TC 1mm	2
136	8	9	8-9	Dummy open	--	0
137	8	10	8-10	Dummy open	--	0
138	8	11	8-11	Dummy open	--	0
139	8	12	8-12	Dummy open	--	0
140	8	13	8-13	Dummy open	--	0
141	8	14	8-14	Dummy open	--	0
142	8	15	8-15	Closed (air inside)	TC 1mm	2
143	8	16	8-16	Closed (air inside)	--	0
144	8	17	8-17	Closed (air inside)	--	0
145	8	18	8-18	Closed (air inside)	--	0
146	8	19	8-19	Closed (air inside)	--	0
147	8	20	8-20	Closed (air inside)	--	0
148	8	21	8-21	Closed (air inside)	--	0
149	8	22	8-22	Dummy open	TC 1mm	2
150	8	23	8-23	Dummy open	--	0
151	8	24	8-24	Dummy open	--	0
152	8	25	8-25	Dummy open	TC 1mm	2
153	8	26	8-26	Dummy open	--	0
154	8	27	8-27	Dummy open	--	0
155	8	28	8-28	Dummy open	--	0
156	8	29	8-29	Closed (air inside)	TC 1mm -	2
157	8	30	8-30	Closed (air inside)	--	0
158	8	31	8-31	Closed (air inside)	--	0
159	8	32	8-32	Closed (air inside)	--	0
160	8	33	8-33	Closed (air inside)	--	0
161	8	34	8-34	Closed (air inside)	--	0
162	8	35	8-35	Closed (air inside)	--	0
163	8	36	8-36	Dummy open	TC 1mm	2
164	8	37	8-37	Dummy open	--	0
165	8	38	8-38	Dummy open	--	0
166	8	39	8-39	Dummy open	--	0
167	8	40	8-40	Dummy open	--	0
168	8	41	8-41	Dummy open	--	0
169	8	42	8-42	Dummy open	--	0
170	9	3	9-3	Closed (air inside)	--	0
171	9	4	9-4	Closed (air inside)	--	0
172	9	5	9-5	Closed (air inside)	--	0
173	9	6	9-6	Closed (air inside)	--	0
174	9	7	9-7	Closed (air inside)	--	0
175	9	19	9-19	Closed (air inside)	--	0
176	9	20	9-20	Closed (air inside)	--	0

#	Rank	Tube	ID tube	Tube type	Measurement installed	No. of measurments
177	9	21	9-21	Closed (air inside)	--	0
178	9	22	9-22	Closed (air inside)	--	0
179	9	23	9-23	Closed (air inside)	--	0
180	9	27	9-27	Dummy open	--	0
181	9	28	9-28	Dummy open	--	0
182	9	29	9-29	Dummy open	--	0
183	9	30	9-30	Dummy open	--	0
184	9	31	9-31	Dummy open	--	0
185	9	43	9-43	Dummy open	--	0
186	9	44	9-44	Dummy open	--	0
187	9	45	9-45	Dummy open	--	0
188	9	46	9-46	Dummy open	--	0
189	9	47	9-47	Dummy open	--	0

Table 4.5 – identification and features of the tubes in the test section

Views of two thermocouples with their fixing system at two different levels (A and B) and a strain gages are shown in Figure 4.17.



Figure 4.17 – view of thermocouples (left) and strain gages (center and right)

Before the thermocouples and strain gages have been installed on the tubes and perforated plate, the twelve pressurized tubes (green and orange tubes in Figure 4.16) are tested one by one with pressurized argon at 180 bar (Figure 4.18).

The test section is assembled inserting each tube in the holes of the lower flange. They are kept in vertical position with the aid of a grid, to facilitate the positioning of the test section top flange. A sequence of pictures showing the assembling phases (Figure 4.19).

When the test section is closed, the collectors are assembled. They are aimed at pressurizing the 12 tubes of the test section, with two separate lines. At the beginning of each test, this system pressurizes at 180 bar two set of six tubes, highlighted respectively in orange and green in Figure 4.16. Figure 4.20 shows different phases during the assembling.



Figure 4.18 – pressure test of pressurized tubes

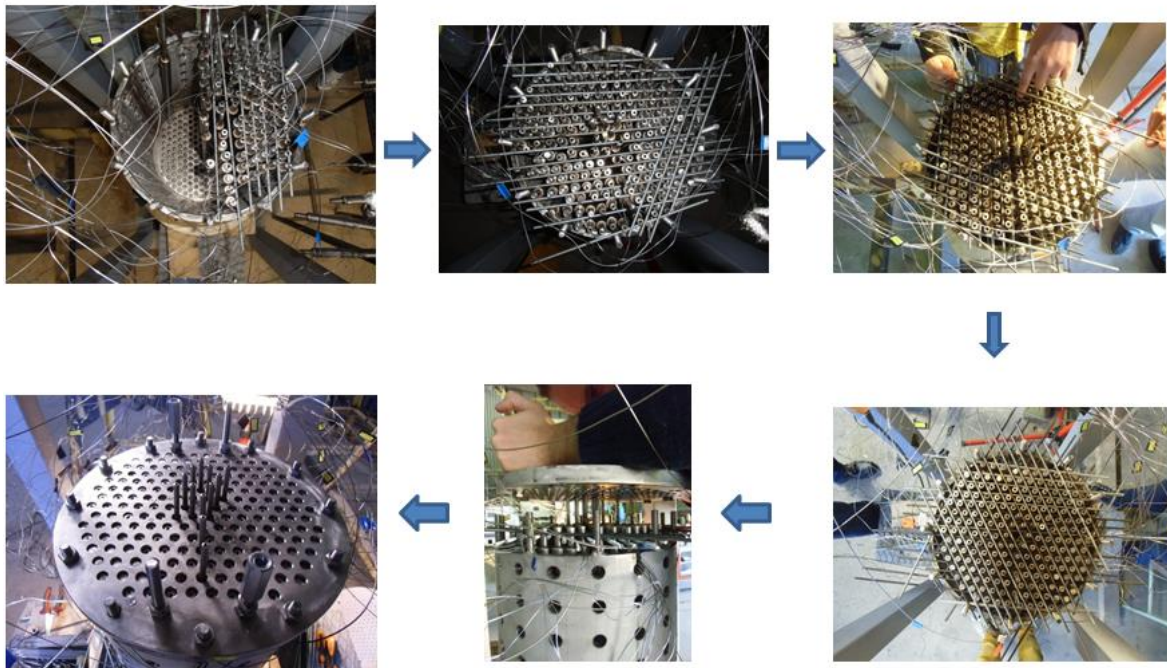


Figure 4.19 – tube bundle assembly of LEADER test section

Eight thermocouples are used to provide information of LBE level during the filling phase of the reaction tank S1. Six out of eight are fixed on a vertical plate welded to the top flange of the test section. The remaining two are welded in a lower position on the perforate shell. Thanks the control system of the facility it is possible to monitor the level

of LBE based on the temperature signal and stop the filling when the level defined in the specifications of the test is reached. A photo of the LBE level control system, emphasising the position of the welded thermocouples, is shown in Figure 4.21.

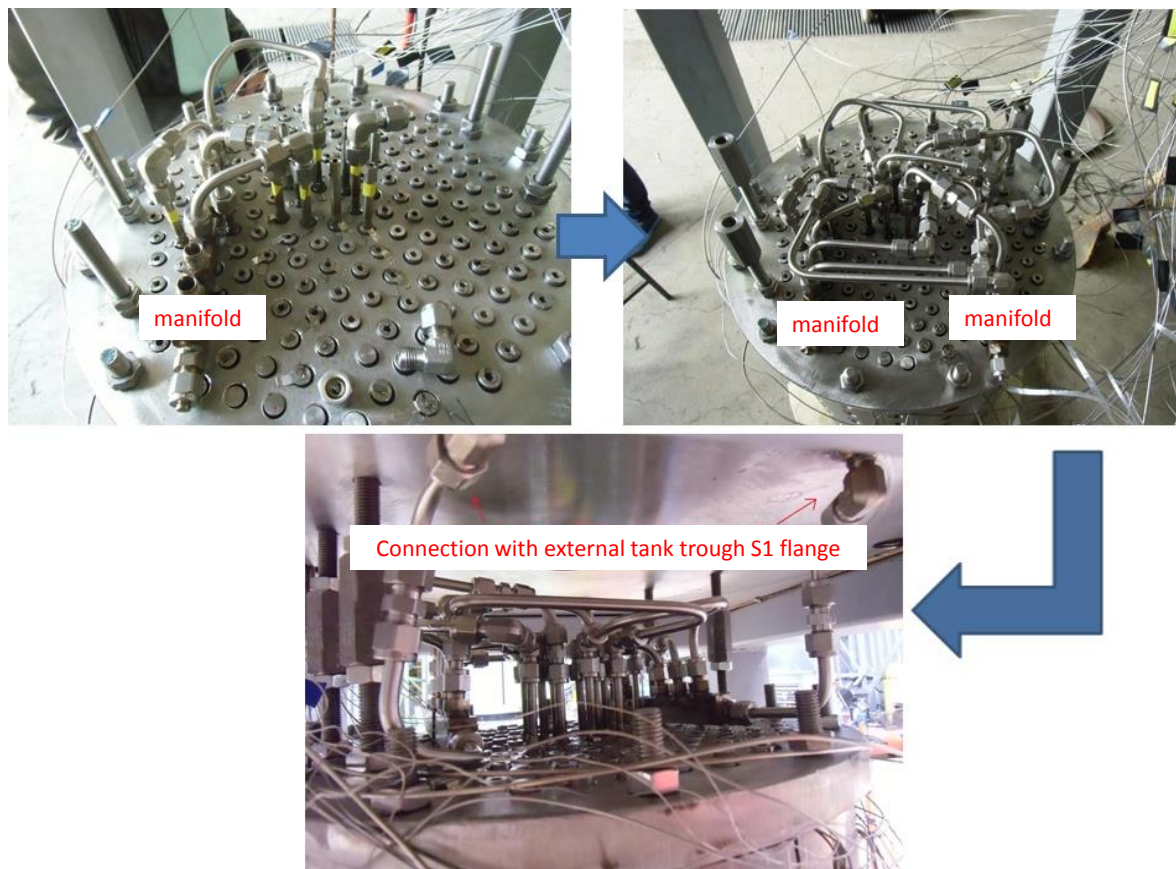


Figure 4.20 – pressurization system assembly

$\frac{1}{4}$ " tube (see Figure 4.22) is used to connects the internal of the test section with fast pressure transducer installed on the S1 top flange (PT-S1V-08), through penetration E indicated in Figure 4.6. This tube goes inside the test section, passing through one hole of the perforated cylindrical shell at 210 mm from the bottom of the test section, until it almost get in contact with the tubes inside the test section.

Then, the LEADER test section is inserted inside S1, thus closing the reaction vessel. 3" hole is available on the top flange. Through this S1 and S3 are connected with a 3" pipeline. The welding of the pipeline are controlled with penetrating liquids, at any welding pass to test the seal. Details are available in Figure 4.23.

Heating wires are installed on S1 top flange and on the connecting pipe with S3. Besides these exception, the heating system of LIFUS5/Mod2 was maintained, as it was designed for the THINS project configuration [33]. Insulation was replaced on the top flange of S1, top of S3 vessel and the connecting pipe

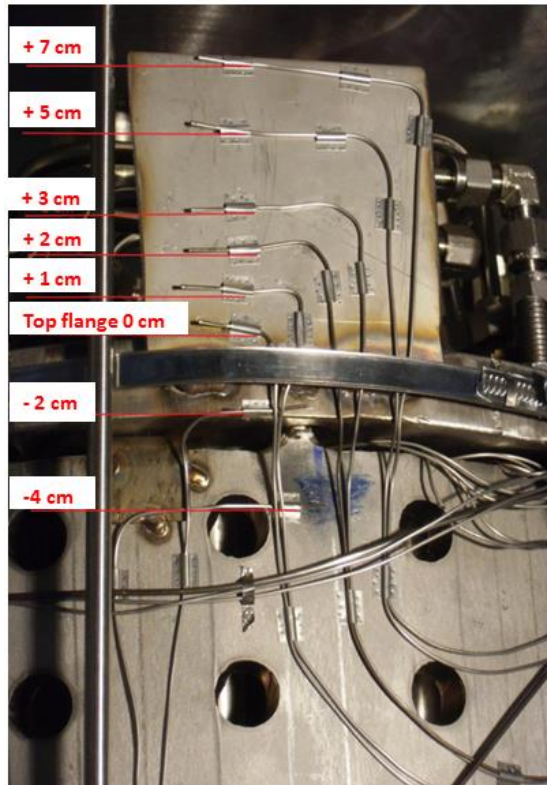


Figure 4.21 – LBE level control system



Figure 4.22 – pipe connection between LEADER test section and KISTLER PT on S1 top flange

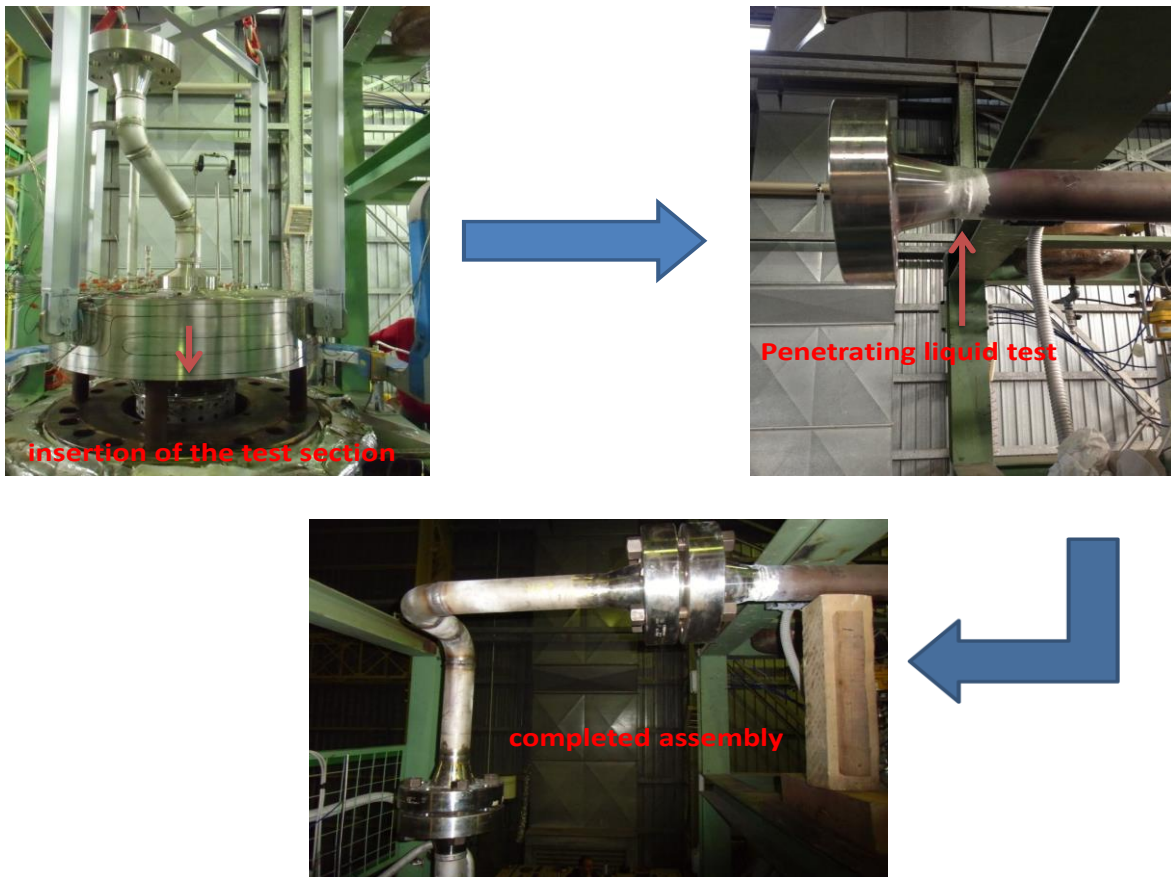


Figure 4.23 – S1-S3 connection assembly

To monitor and regulate the temperature of the heating wires thermocouples are set:

- on the heating cables to control and preserve their integrity;
- on structural components near heating cables to regulate their temperatures.

An example of heating cable and TCs is shown in Figure 4.24.

LIFUS5/Mod2 DACS (Data Acquisition and Control System) is realized using National Instruments hardware and software. Exception is the acquisition of the strain gages signals, which are processed by a dedicated hardware and software.

All acquired data from acquisition, control and regulation systems, are available to the operator via graphical interface (synoptic). Most of the graphical interfaces were developed in the frame of the THINS activities [33]. Modifications related the new test section is implemented for the LEADER experimental campaign (Figure 4.25). This displays the values measured by the thermocouples set on two different levels of the test section (A and B) and on S1 wall, pressure transducers connected to S1 and the test section and strain gages implemented on the tube bundle, test section perforated plate and S1 shell. The regulation system of the LBE level in S1 is also available.

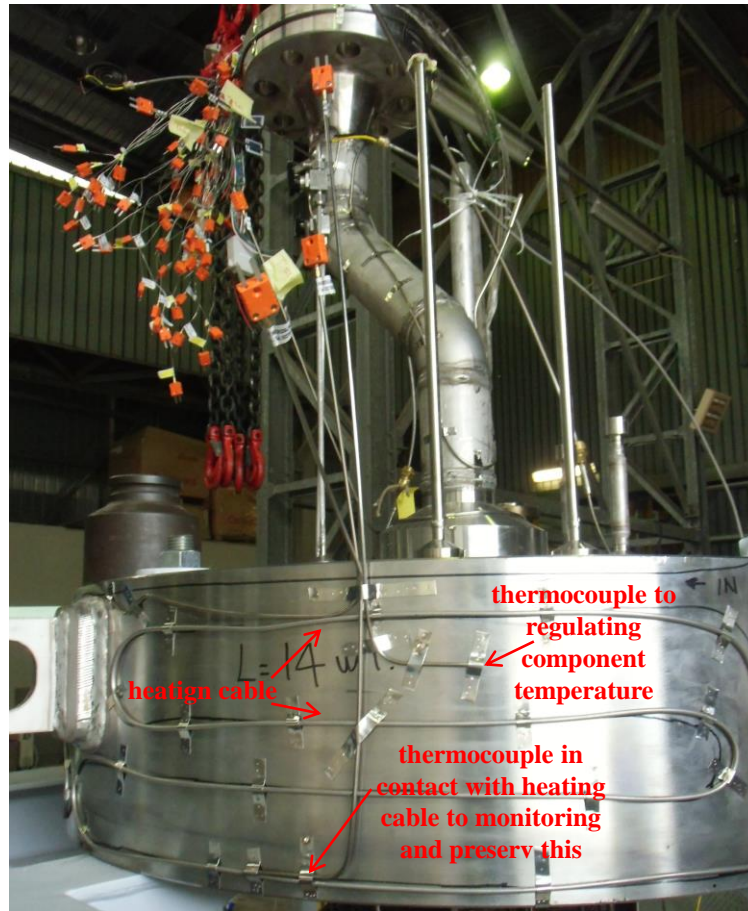


Figure 4.24 – heating cables and thermocouples of control and regulation

Commissioning tests have been done before the test executions, as hereafter mentioned.

- I. Pressure test. The vessels S1, S2 and the injection line are pressurized at about 120 bar. The pressure is monitored for about 1 hour in order to check the seal of the top flange of S1 and the connections in the pipeline. The test is done with S3 disconnected, thanks to a closure flange above the S1 top flange. Figure 4.26 shows the evolution of the pressure measured with the absolute pressure transducer installed on the top flange of S1. The measured leaking rate is 1 bar/h. This is acceptable considering that the acquisition of the test lasts about 30 seconds.
- II. Functionality test. This commissioning test has the twofold objective of checking the injection procedure, as well as the instrumentation and the data acquisition and control systems. The reaction tank S1 is filled by water. S1 dome is operated at atmospheric pressure because the discharge valve of S3 is opened. The water in S1 and S2 is heated up to 50 and 150°C, respectively. The injection line is filled with water until the valve V4 (set as injection valve) at the same thermodynamic conditions of the system S2. During the first part of the commissioning test focus is

given on correct behavior of the heating wires and their control system. Once the temperature set points are reached, the injection procedure starts. The test involves the following verifications.

- Operation vacuum pump installed in the injection line, to remove the non-condensable gas before the test execution.
- Water injection procedure carried out with the water in S2 set at 20 bar and 150°C, with the valve V4 set as injection valve and time for the injection equal to 2 seconds. The injection is executed with the injector without the protective cap.
- Instrumentation installed in the facility both for control and acquisition functions.
- Functions of the synoptic of the plant, to ensure the correct control of the plant parameter during the test conditioning.
- Data acquisition performances, thus demonstrating that hardware and software have the capability to withstand the maximum acquisition frequency defined in the test specifications (10 kHz).
- Design of protective cap and the resistant section (see below, section 4.4)

Commissioning test were successfully fulfilled and the facility was ready to be operated for the LEADER experimental campaign.

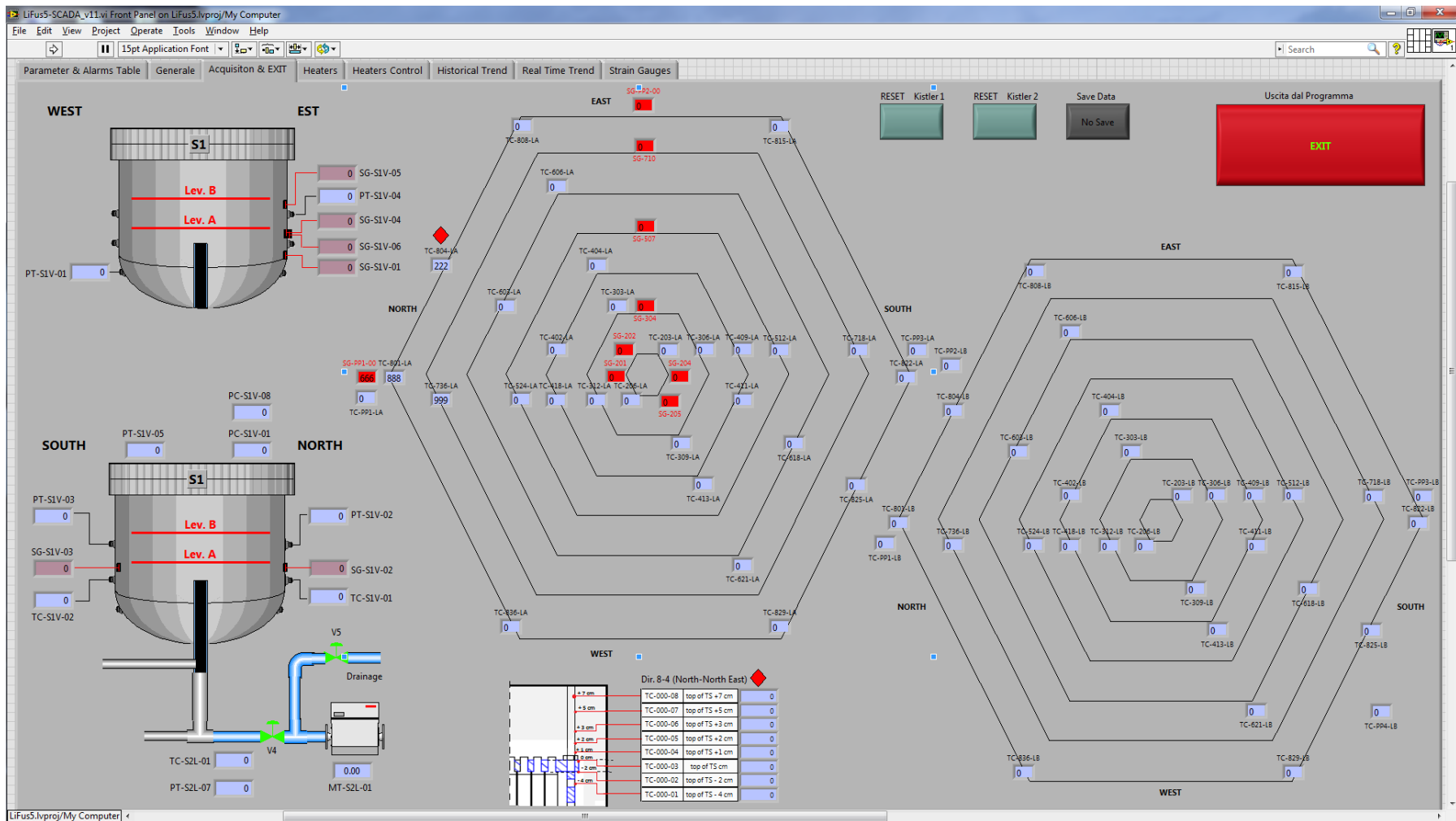


Figure 4.25 – LIFUS5/MOD2 synoptic



Figure 4.26 – pressure time trend during the pressure test of LIFUS5/Mod2 facility with LEADER test section

4.4 Protective cap tests

A simplified scheme of the system employed for testing the protective cap of the injector is shown in Figure 4.27. The purpose of the experimental investigation is to determine the notch value of the injector cap, and consequently the value of the resistant section, which is broken at the pressure of 180 bar.

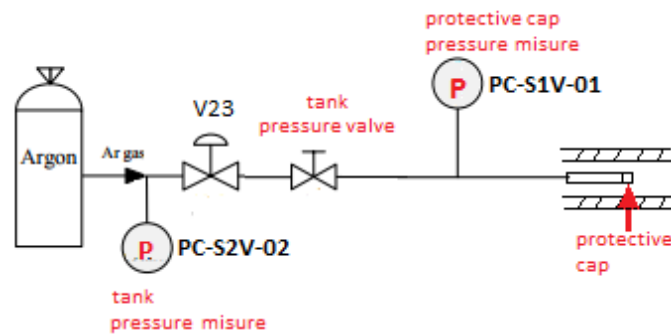


Figure 4.27 – scheme of protective cap test section

The tests involve a tank of argon connected to the injector device through a ¼” tube. Two valves are installed: V23 regulated to limit the pressurization rate of the line and the “tank pressure valve” operated manually. Two absolute pressure transducers are employed: the former is positioned upstream valve V23, named PC-S2V-02, measuring the tank pressure, and the latter PC-S1V-01, downstream V23, measures the protective cap pressure. Six tests are performed having different values of the notch depth. The results are shown in Figs. 4.28-4.33. The test procedure is carried out as follows. The test start with the “tank pressure valve” closed. Thus, PC-S2V-02 measures the tank pressure and PC-S1V-01 measures approximately atmospheric pressure (region A-B in Figure 4.29). After the manual opening of the “tank pressure valve”, PC-S2V-02 measures a rapid pressure decrease due to the gas flowing towards the injector device. Simultaneously, PC-S1V-01 shows a pressure increase, up to the pressure equalization (region B-C in in Figure 4.29). When the two pressures are equal (point C), they might increase until the pressure of the gas tank is reached in all system or the protective cap rupture occurs (point D), causing the sharp decrease of pressure end the end of the test (point E). The relevant initial and boundary conditions of the test are reported with the results in Table 4.6. All tests follow the trend discussed except test 1, in Figure 4.28. This test is executed with a slow manual opening of the valve and therefore the pressure transducer PC-S2V-02 does not measure any pressure change until the rupture occurred. According with the achieved results, it is set a resistant thickness of the notch equal to 1 mm.

#	Data	ID cap	No. Cap	Orifice [mm]	D_int_pip e (operator) [mm]	D_ext_notch (operator) [mm]	D_ext_pipe (measured) [mm]	notch_depth (measured) [mm]	D_ext_notch (measured) [mm]	Thickness [mm]	P rupture (operator) [bar]
1	22/01/2014	--	--	--	13	14	--	--	--	0.5	98.6
2	27/01/2014	PM 00414[1]	1	4	13	14.95	16	0.51-0.53	14.94-14.98	0.975	136.2
3	30/01/2014	--	2	--	13	15	--	--	--	1	156.9
4	11/02/2014	PM 01314[1]	3	4	13	15.1	16	0.44-0.45	15.10-15.12	1.05	174.6
5	08/04/2014	PM 08314[1]	4	4	13	15.1	16	0.45-0.46	15.08-15.10	1.05	186
6	16/04/2014	--	8	8.9	13	15	--	--	--	1	147.6

Table 4.6 – data of protective cap tests

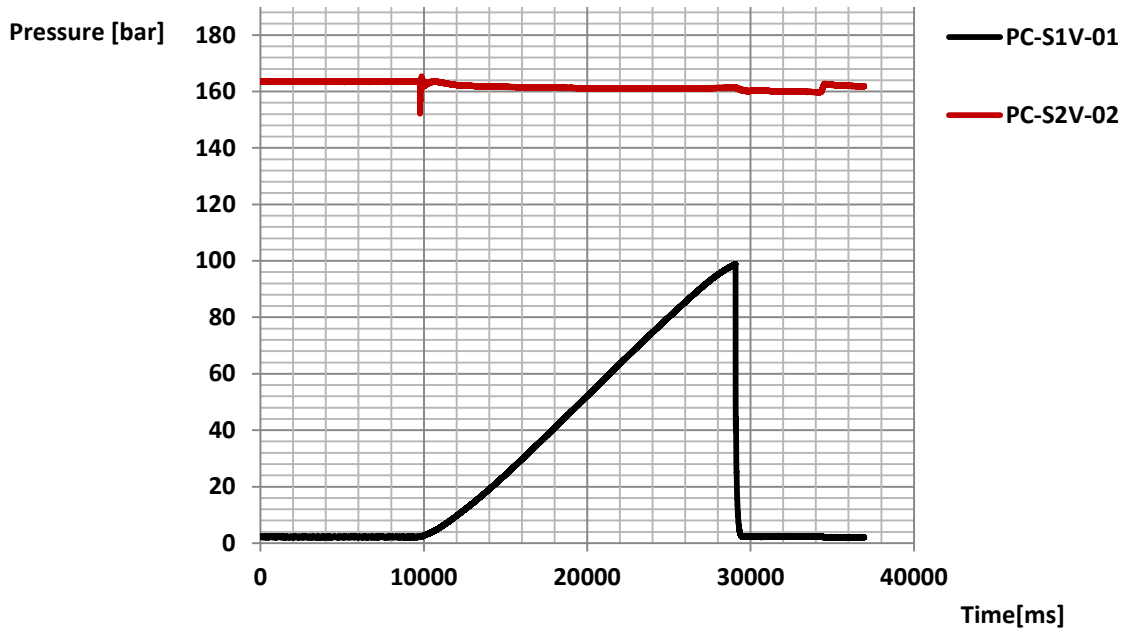


Figure 4.28 – pressure time trends measured for Test 1

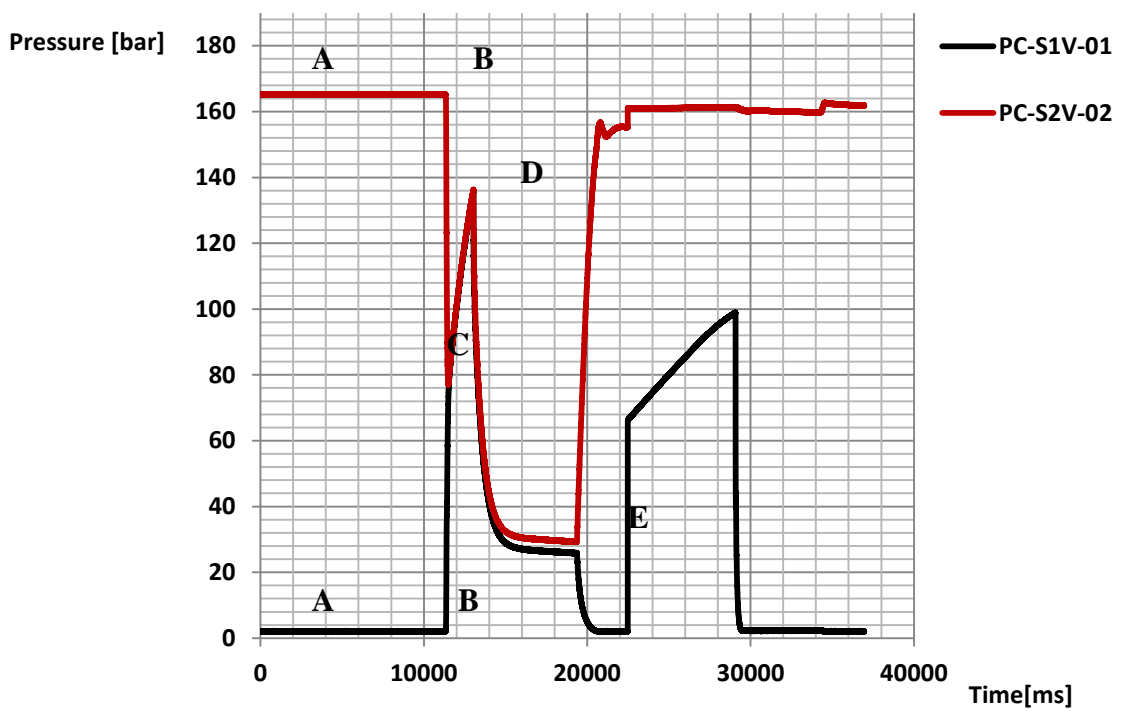


Figure 4.29 – pressure time trends measured for Test 2

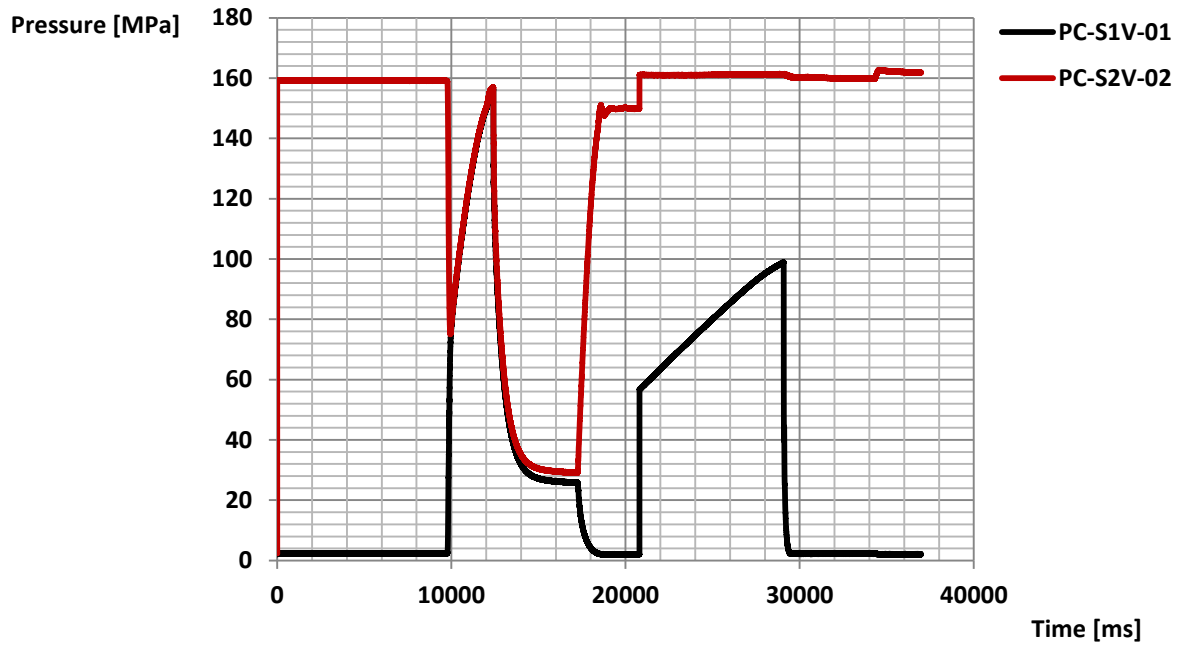


Figure 4.30 – pressure time trends measured for Test 3

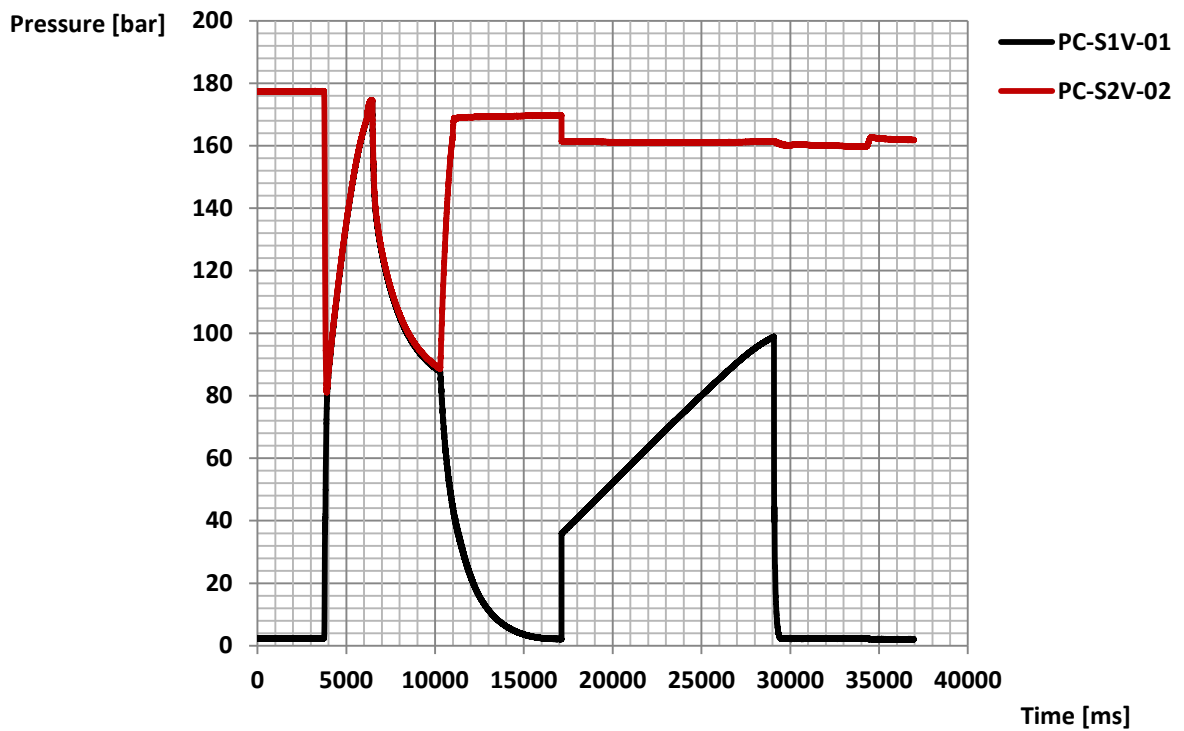


Figure 4.31 – pressure time trends measured for Test 4

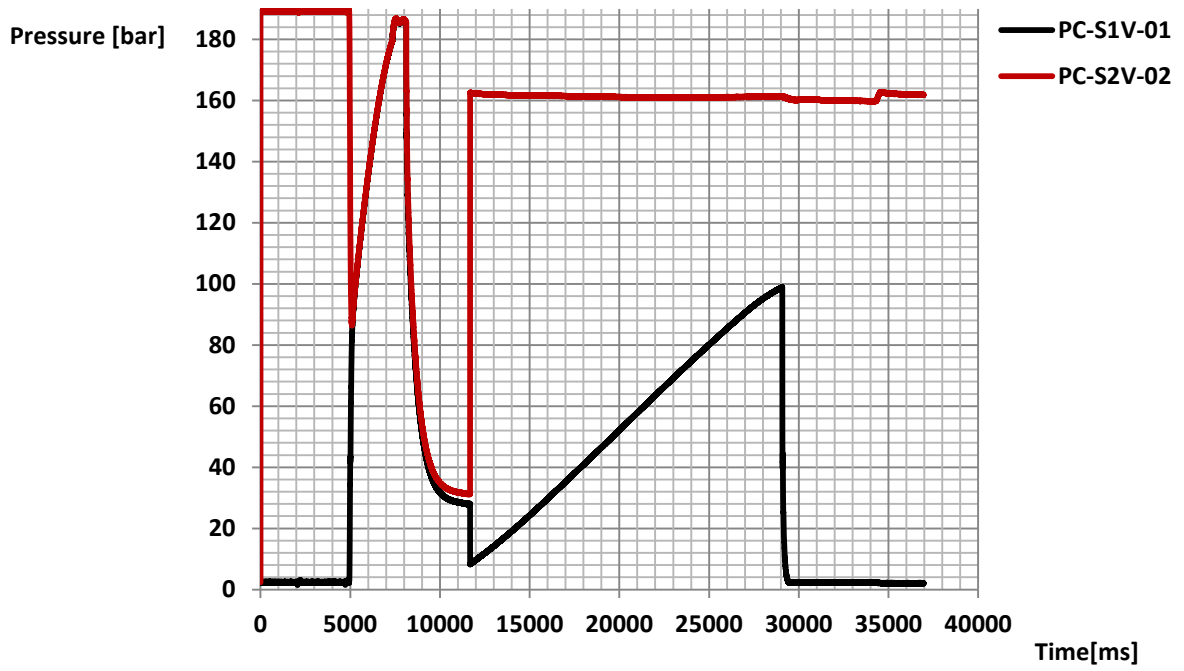


Figure 4.32 – pressure time trends measured for Test 5

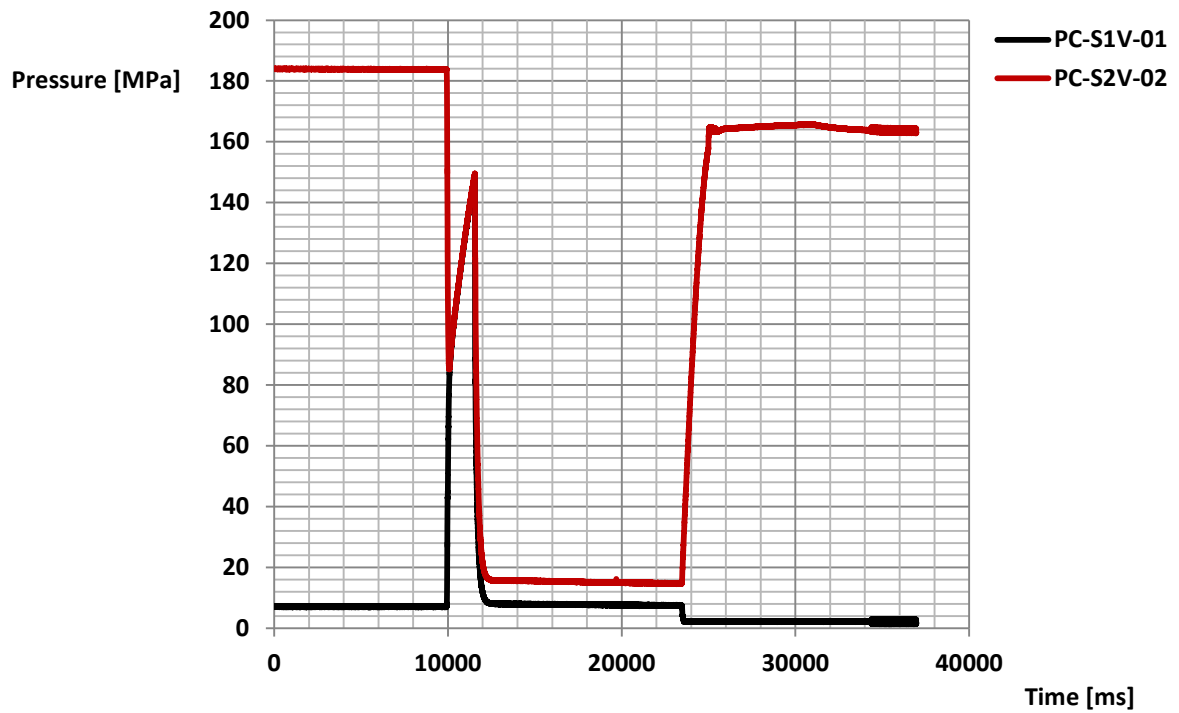


Figure 4.33 – pressure time trends measured for Test 6

5 LIFUS5/Mod2 water injection line analysis

The objective of the activity is to investigate the behavior the water injection line during injection (see Figure 5.1). The layout of the pipeline is described in section 4, together with the overall description of the facility. The analysis is performed with RELAP5/MOD3.3 code, through a set of sensitivity analyses aimed at characterizing the form loss coefficients of valves and of the Coriolis flow meter; and with SIMMER-III, investigating how the lesson learned impacts on the post-test analysis of LIFUS5 experiments. The tests selected are the tests A1.2_1 and A1.2_2 executed in the framework of THINS project.

Hereafter the following activities are described:

- Description of the RELAP5 code nodalization modeling the water injection line;
- Characterization of the injection line by RELAP5 code, through a set of calculations based on the Test A1.2_1;
- Assessment of the nodalization using the data of the Test A1.2_2;
- Simulation of the Test A1.2_2 by SIMMER-III, to qualify the modeling of the water system and injection line, which will be used for the post-test analysis of LEADER experiments.

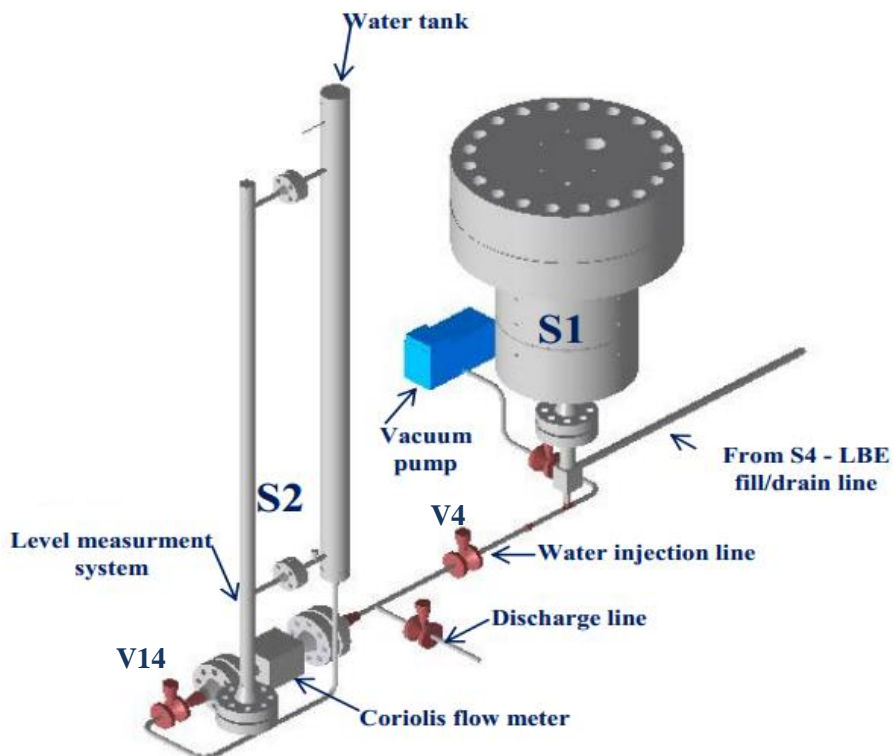


Figure 5.1 – 3D view of water injection line connected with S1

5.1 RELAP5/MOD3.3 analysis

RELAP5/MOD3 [38] is a generic code that is used for simulating the behavior of a nuclear power plant in normal operating conditions, anticipated operational occurrence, and accidental conditions. It is based on one-dimensional, non-homogeneous and non-equilibrium hydrodynamic model for the steam and liquid phases.

The code is used to simulate the water injection line. A layout of LIFUF5/Mod2 facility with the instrumentation is shown in Figure 5.2 and a sketch of the nodalization developed is shown in Figure 5.3. LIFUS5 water injection line is modeled with RELAP5 through the following components:

- 129 sub-volumes representing the hydraulic volumes of the pipeline;
- 10 single junctions that join the components;
- 3 motor valves, two representing the valve V14 and V4 installed in the plant and one simulating the injection cap;
- 2 time dependent volumes aimed at imposing the boundary conditions of the test, i.e. pressure versus time in S1 and in the gas line connected at top of S2.

The structure of the input includes the following parts:

- Time Step Control and the total time duration of the transient. The duration of the transient is equal to 110 s and it is divided into three parts:
 1. at 100 seconds, the stationary ends and the opening of the injection valve V14 happens;
 2. from 100s to 102s, pressure increases in injection line, rupture of the cap occurs and the interaction phenomena happens. The closing of the valve V4 itself, that stops the injection, is also included in this phase;
 3. The final part ends at 110 seconds and it delivers a phase of equalization after the interaction.
- Trips, which are used to identify the occurrence of an event through a boolean value, i.e. to actuate valves during the transient.
- Hydrodynamic Components defining the system geometry where the fluid is placed and the initial conditions. The dimension of the hydrodynamic volumes was set between 9 and 14 cm, according with the constraints of the system geometry.

- Control variables and material properties.

Boundary conditions are set by imposing pressure trends in the Argon line connected with S2 (TMDPVOL-100 in Figure 5.3), and in S1 (TMDPVOL-240 in Figure 5.3). These are based on the experimental data of THINS tests A1.2_1 and A1.2_2 [41] [31]. The main parameters of the tests are reported in Table 5.1 and in Table 5.4. In particular, the following experimental data are considered (highlighted by the dot line in blue Figure 5.2):

- pressure transducer PC-S2V-01, in S2;
- pressure transducer PT-S1V-03, in S1, which is selected because it measured the maximum pressure peak during the test.

A set of code calculations is defined to correlate the effect of selected parameters, i.e. form loss coefficients of valves and the Coriolis flow meter, and opening/closure time of injection valve, on the pressure versus time trend of water injection line. The code results are then compared with the experimental data recorded during the test, see below.

LIFUS5/Mod2

THINS configuration 2012

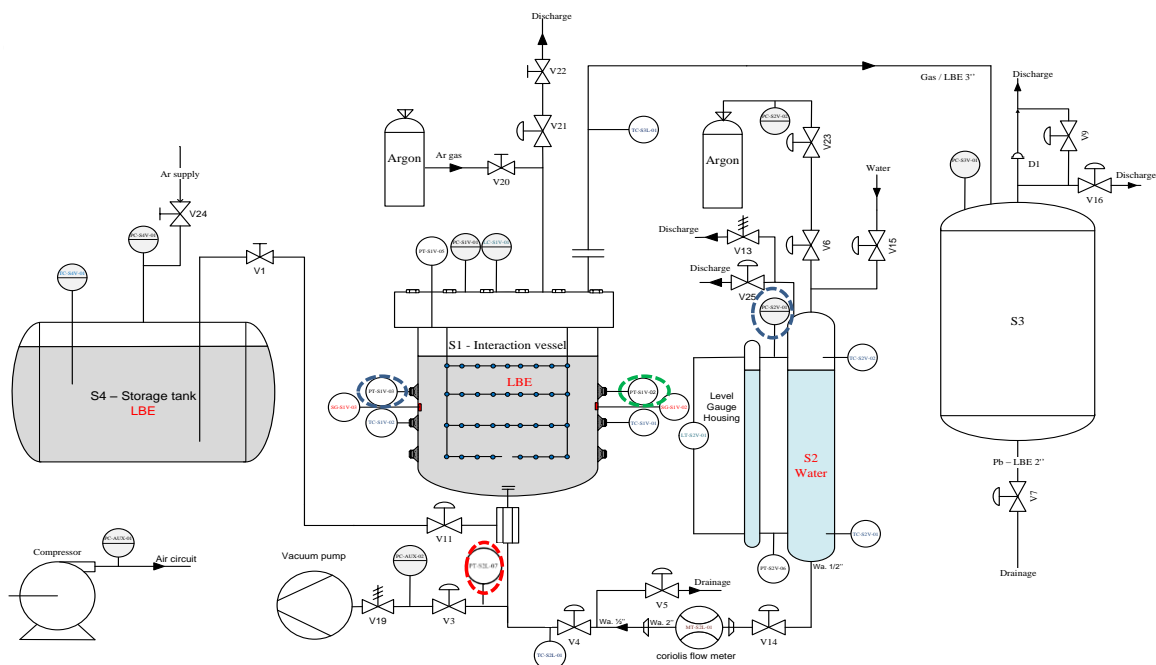


Figure 5.2 – sketch of a part of LIFUS5/Mod2 facility with pressure transducer highlighted

WATER INJECTION LINE LIFUS-5/Mod2 NODALIZATION

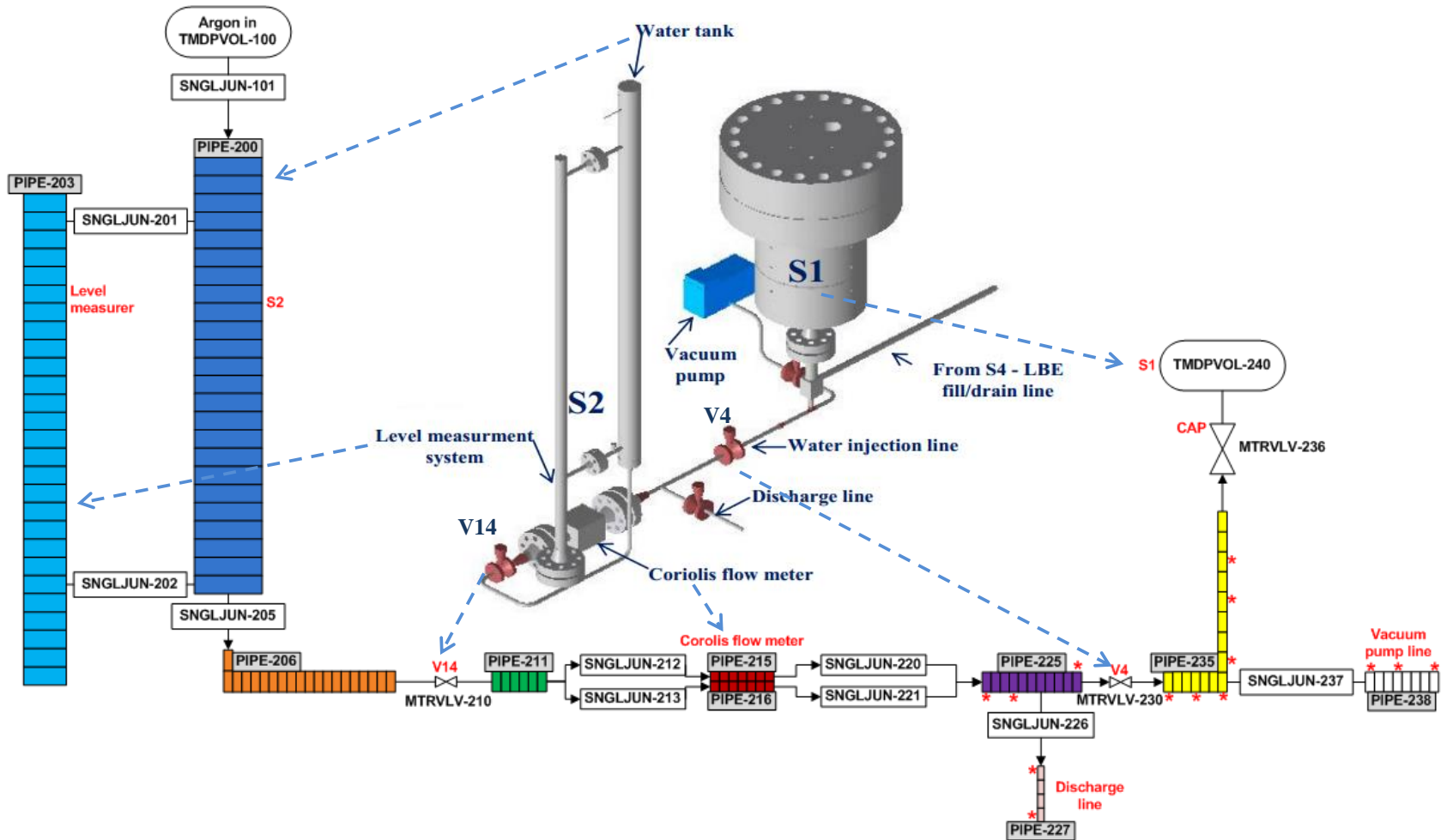


Figure 5.3 – Water injection line nodalization

5.1.1 Analysis based on injection line pressure

The analysis is based on the experimental data of THINS tests A1.2_1 and A1.2_2. Considering the Test A1.2_1 (Table 5.1), a reference code RUN (case_a in Table 5.2) is carried out. Based on the code results, a set of calculations is defined by changing one input parameter (in red in Table 5.2). Reference physical quantity for this analysis is the pressure in the injection line PT-S2L-07 (highlighted in red in Figure 5.2). The RELAP5/MOD3.3 control volume 238-02 (see Figure 5.3) correspond with the position of the pressure transducer.

The results, based on the Table 5.2, are shown in Figure 5.4. Experimental pressure trend increases at the opening of the V14 valve. At 250 milliseconds, a first peak (about 15 bar) is observed. It identifies the reaching of the bursting pressure of the injection cap. The achievement of the experimental breaking pressure value calculated by RELAP5 is anticipated of 100 ms in almost all code RUN. Then, the pressure trend continues to increase until the value in S1 is equal to the value in the injection line, at about 3 seconds from the beginning of the transient.

Parameter	ID	Unit	Design	Actual	Note
SYSTEM S2					
P in gas line @ SoT	PC-S2V-02	bar	--	41.1	--
P @ SoT	PC-S2V-01	bar	40	40.5	--
T @ SoT	TC-S2V-01	°C	240	240.7	--
LVL @ SoT	LT-S2V-01	mm	--	1207	--
Min. P during injection	PT-S2V-06	bar	--	36.2	--
P @ EoT	PC-S2V-01	bar	40	41.5	--
T @ EoT	TC-S2V-01	°C	240	239.5	--
LVL @ EoT	LT-S2V-01	mm	--	874	--
Mass of water injected	--	g	--	--	Estimated 420 g
Charged water vol.	--	l	--	8	--
Water vol. discharged	--	l	--	7.0	After the test execution
INJECTION SYSTEM					
Injection valve	--	--	--	V14	--
Injection time	--	s	--	3	Set points: 3s or $P_{S2}-P_{S1} < 0$ bar
Inject. Valve closure effective	--	ms	--	--	--
Injection valve fully closed	--	ms	--	2993	V4 closure on pressure signal
P @ injector cap rupture		bar	--	15.7	PT-S2L-07 data
Time of injector cap rupture		ms	--	124	--
Injector nozzle orifice		mm	4	4	--
Injection Nozzle ID	--	--	--	PM 01113[4]	
Injector penetration	--	mm	120	120	--

Table 5.1 – S2 and injection line data for Test A1.2_1

#	T vlv opening [s]	K [V4],[V14]	K [Coriolis]	A Coriolis [m ²]
a	0.25	7	0.5	9.06613e-05
b	1	7	0.5	9.06613e-05
c	0.1	7	0.5	9.06613e-05
d	0.25	1	0.5	9.06613e-05
e	0.25	70	0.5	9.06613e-05
f	0.25	7	5	9.06613e-05
g	0.25	7	10	9.06613e-05
h	0.25	7	0.5	9.06613e-04
i	0.25	7	0.5	9.06613e-06

Table 5.2 – list of the parameters for the first attempts

It should be noted that the present comparison consider the pressure trends from 0 up to 2993 milliseconds. Indeed, after, the LBE drops in the injection line. This cannot be simulated by RELAP5, which cannot simulate the presence of two working fluids.

Figure 5.4 shows as most of the results tend to overestimate the pressure trend and how the “case_e” is the most faithful to the experimental data. This an extreme case (K valves = 70) and provides the information that the overall pressure drop of the line is greater than it was postulated in the reference case. The solution is to increase of the pressure drops across the valves and the Coriolis flow meter.

Moreover, it should be noted that the experimental trend is enclosed almost entirely between two curves:

- “case_i” in Figure 5.4: case with the tubes area of the Coriolis reduced by an order of magnitude;
- “case_g” in Figure 5.4: case with the K of Coriolis equal to 10.

Further code RUN are therefore carried out (see Table 5.3) based on the information above. The result of these are in Figure 5.5. The best combination chosen as the most likely is that reported in Table 5.3 as “case_l”, with K of the valves and Coriolis equal to 10 and area of the Coriolis halved compared to the reference value.

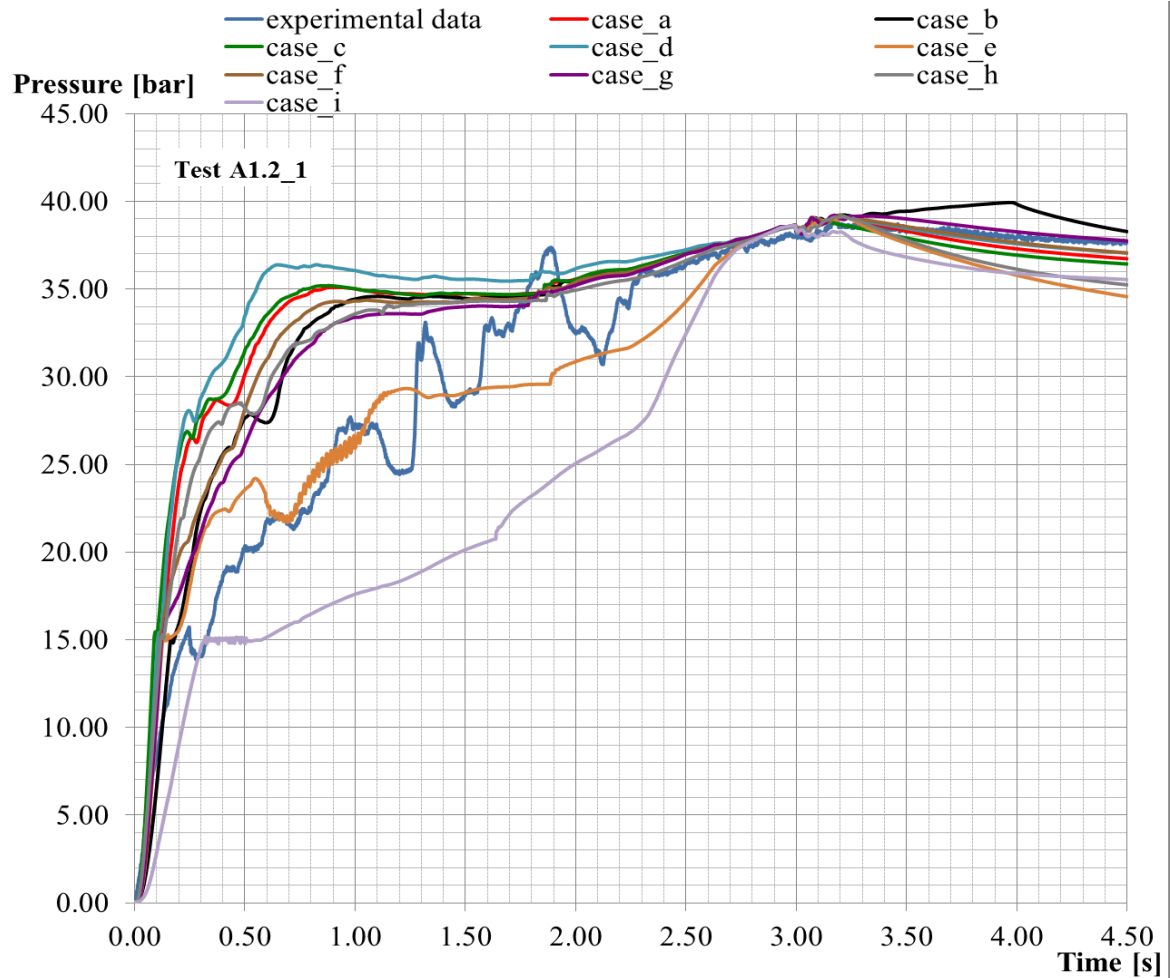


Figure 5.4 – pressure sensitivity analysis based on Table 5.2 for Test A1.2_1

#	T vlv opening [s]	K [V4],[V14]	K [Coriolis]	A [Coriolis]
j	0.25	10	10	9.07e-05
k	0.25	20	10	9.07e-05
l	0.25	10	10	4.53e-05

Table 5.3 – list of the parameters for the second attempts

Based on this analysis the test THINS A1.2_2 [31] is considered. Relevant parameters of Test A1.2_2 for the system S2 and the injection line are listed in Table 5.4. Boundary and initial conditions of RELAP5/ MOD3.3 input are modified accordingly with the new test. Among these, the injection valve is also modified because it is the valve V4 instead of the V14 (see Figure 5.1).

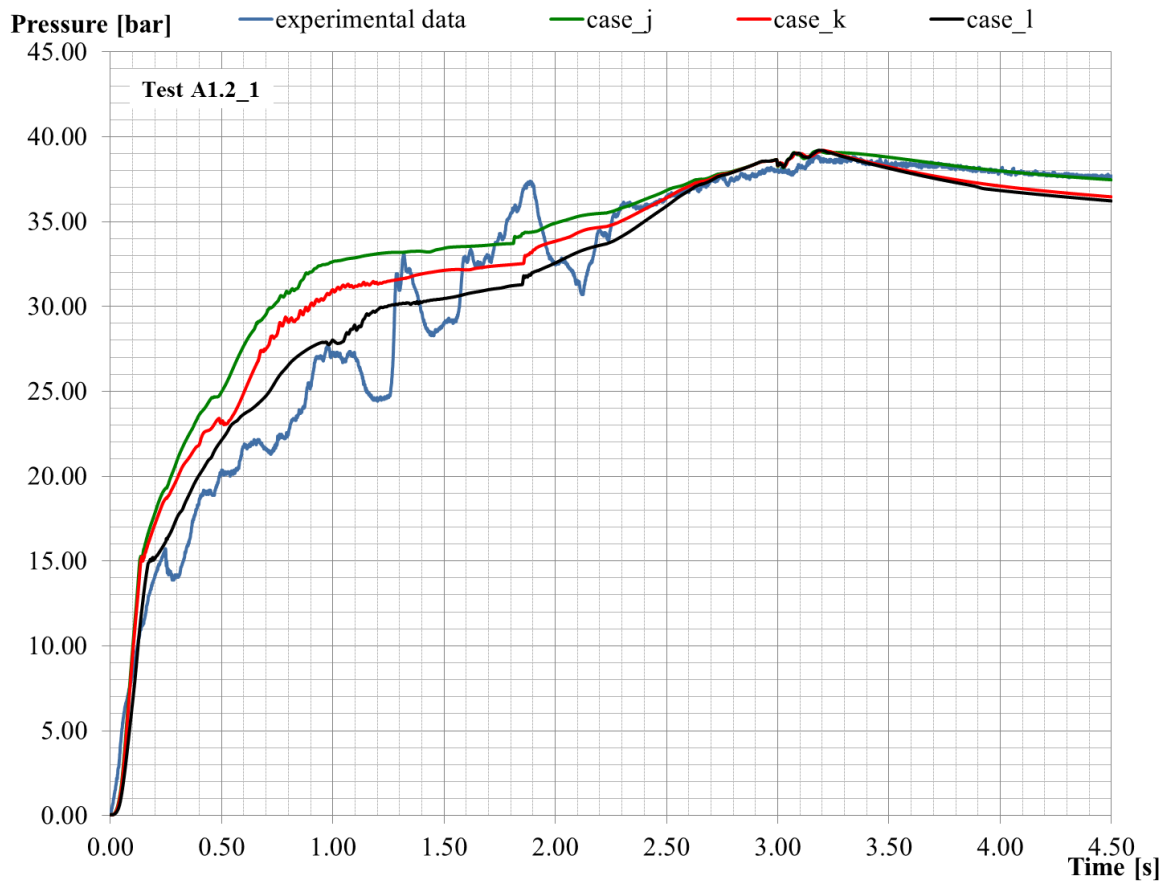


Figure 5.5 – pressure sensitivity analysis based on Table 5.3 for Test A1.2_1

The reference experimental pressure in S1 is recorded by the pressure transducer PT-S1V-02 (highlighted in green in Figure 5.2), selected with the same criterion exposed for the Test A1.2_1. The first set of calculations performed in based on the same rationale already discussed (Test A1.2_1) and reported in Table 5.2.

The experimental pressure trend (see Figure 5.6) increases at the opening of the valve V4. In this case the distance between the valve and the injection device is shorter. Thus, the volume under vacuum is lower and the time between the injection valve opening and the cap rupture is faster (approximately 37 ms, see Figure 5.7). From Figure 5.7, it is also possible to note that most of the result obtained with RELAP5 reach the value of breakage of the cap with an acceptable accuracy with the exception of “case_c”.

Then, the pressure trend continues to increase until the pressure value in S1 and in the injection line are equalized, at about 2 seconds from the beginning of the transient. The comparison with the experimental trend is applicable up to 2565 milliseconds, for the same reasons of case A1.2_1.

Parameter	ID	Unit	Design	Actual	Note
SYSTEM S2					
P in gas line @ SoT	PC-S2V-02	bar	--	44.4	--
P @ SoT	PC-S2V-01	bar	40	43.8	--
T @ SoT	TC-S2V-01	°C	240	242.7	--
LVL @ SoT	LT-S2V-01	mm	--	938	--
Min. P during injection	PT-S2V-06	bar	--	40.7	--
P @ EoT	PC-S2V-01	bar	40	42.7	--
T @ EoT	TC-S2V-01	°C	240	398.3	--
LVL @ EoT	LT-S2V-01	mm	--	848	--
Mass of water injected	--	g	--	439	--
Charged water vol.	--	l	--	8	--
Water vol. discharged	--	l	--	7.0	After the test execution
INJECTION SYSTEM					
Injection valve	--	--	--	V4	--
Injection time	--	s	--	2	Set points: 3s or $P_{S2}-P_{S1} < 0$ bar
Inject. Valve closure effective	--	ms	--	--	--
Injection valve fully closed	--	ms	--	2565	V4 closure on pressure signal
P @ injector cap rupture		bar	--	15.8	PT-S2L-07 data
Time of injector cap rupture		ms	--	34	--
Injector nozzle orifice		mm	4	4	--
Injection Nozzle ID	--	--	--	PM 01313[6]	
Injector penetration	--	mm	120	120	--

Table 5.4 – S2 and injection line data for Test A1.2_2

Figure 5.6 shows that “case_e” and “i” underestimate the pressure trend because pressure drops are overestimated. Conversely, the “case_d” overestimates the pressure trend because the opposite reason. The other cases are highlight a good agreement. Considering the input parameters and the knowledge of the facility layout and components, it may be concluded that some of the “acceptable” simulations can be disregarded because unrealistic. Further tests, summarized in Table 5.5, have been carried out to optimize the simulations of both tests (i.e. tests A1.2_1 and A1.2_2).

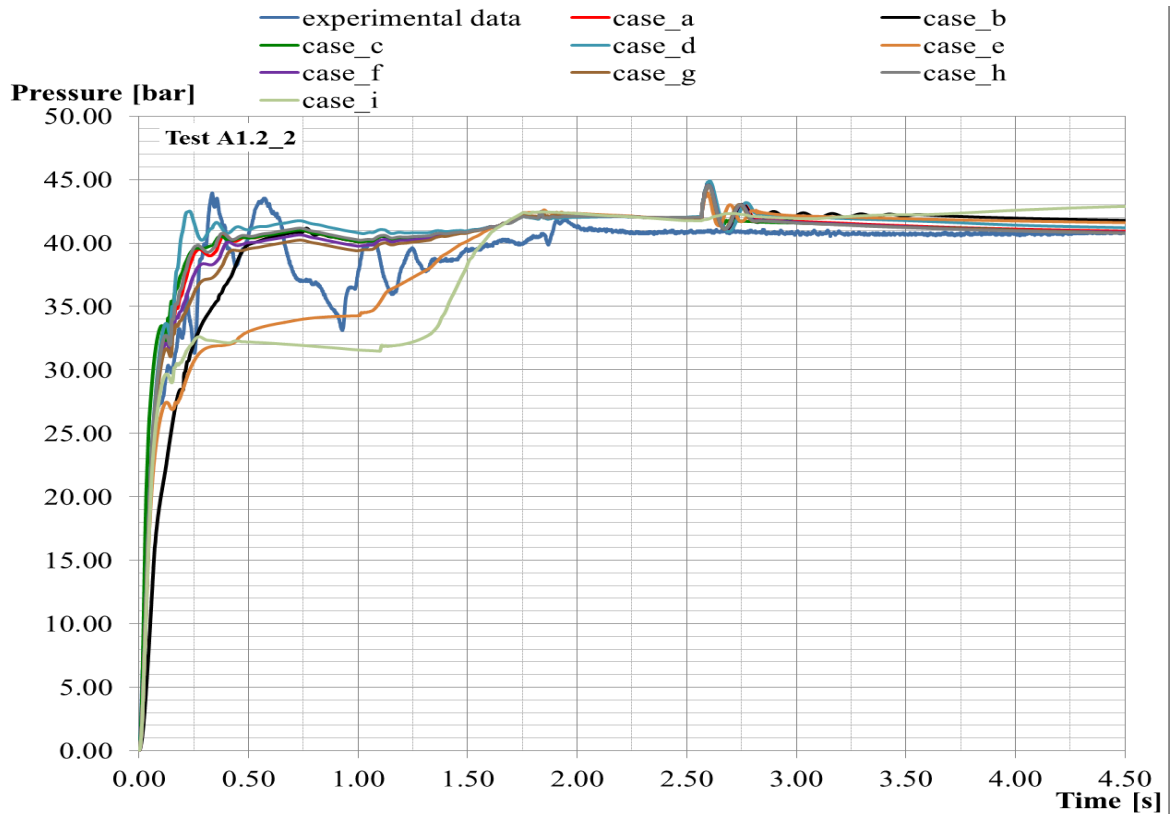


Figure 5.6 – pressure sensitivity analysis based on Table 5.2 for Test A1.2_2

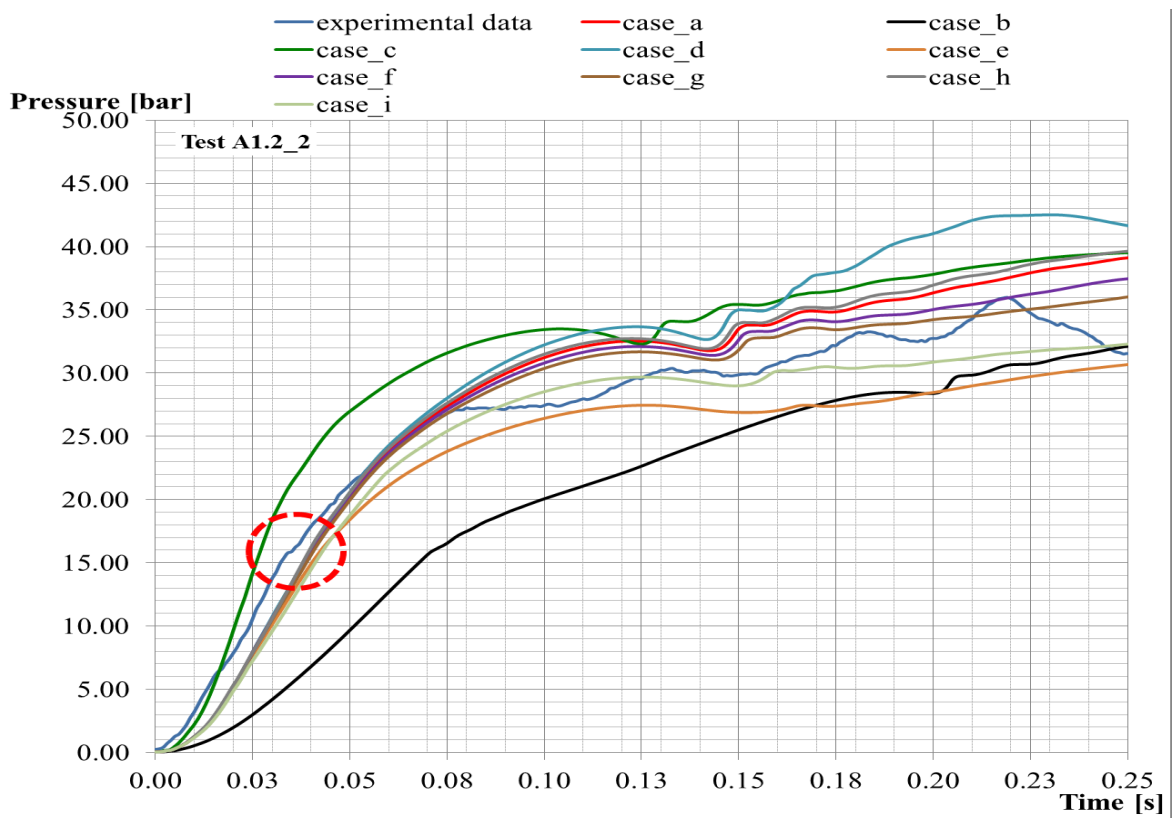


Figure 5.7 – zoom of pressure sensitivity analysis based on Table 5.2 for Test A1.2_2 which highlights the breaking point of the cap

#	T vlv opening [s]	K [V4],[V14]	K [Coriolis]	A [Coriolis]
m	0.25	7	0.5	4.53e-05
n	0.25	7	1	4.53e-05
o	0.25	7	2	4.53e-05
p	0.25	10	1	4.53e-05
q	0.25	10	2.5	4.53e-05

Table 5.5 – list of the parameters for the overall attempts

Best results are achieved for the “case_q”, where:

- the opening time of the valves is equal to 0.25 s;
- K of the valve is 10;
- K of Coriolis is 2.5;
- the area of single Coriolis tube is equal to $4.53e-05 \text{ m}^2$.

The comparisons between the experimental data and RELAP5 results for the tests are reported in Figure 5.8 and 5.9, respectively. The trends obtained by the simulation has relevance up to the instant of injection valve closure, respectively 2.99 seconds for Test A1.2_1 and 2.56 seconds for Test A1.2_2.

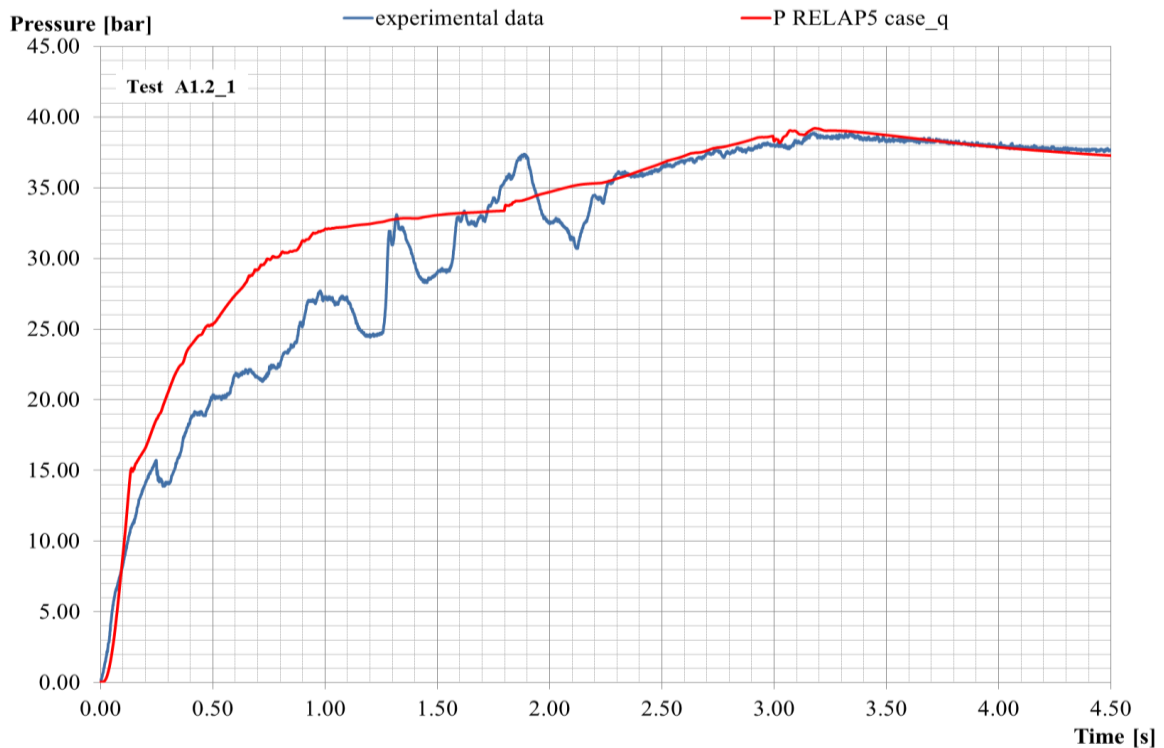


Figure 5.8 – comparison between the experimental pressure trend and the “case_q” for Test A1.2_1

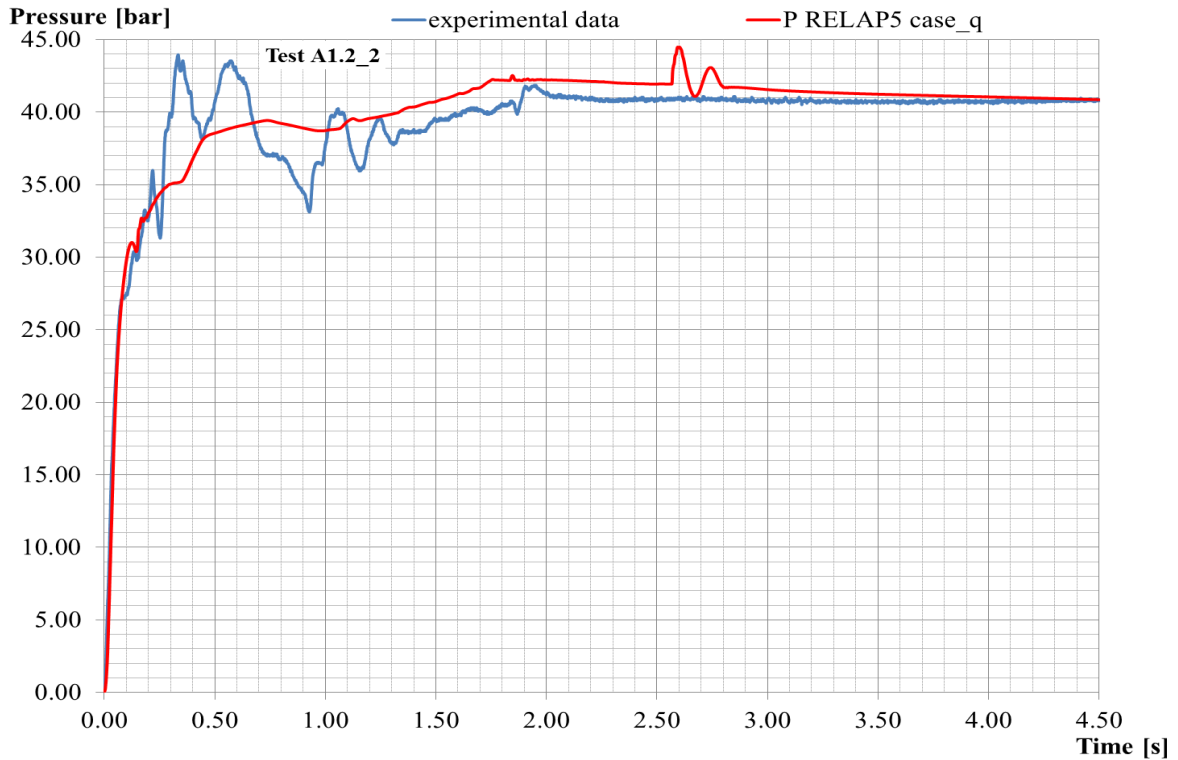


Figure 5.9 – comparison between the experimental pressure trend and the “case_q” for Test A1.2_2

5.1.2 Void fraction analysis

Purpose of this analysis is to investigate the void fraction in the injection line to verify the occurrence and formation of two-phase mixture. This study improves the understanding of the pressure evolution in S1, because the amount of mass inject is affected by the quality.

Test A1.2_2 is considered, because the injection is performed with valve V4 as planned for LEADER tests. Void fraction trends presented below are calculated in the RELAP5 control volumes highlighted with a red asterisk Figure 5.3

The results are hereafter discussed.

- Tube 225 (see Figure 5.11) is analyzed at both ends and at central volumes. This tube is located upstream of the injection valve V4 and, until the time of injection, is full of water. When the valve opens, void fraction occurs. In particular the value of void fraction decreases with the distance from the injection valve. The maximum in the component is about 10^{-2} and becomes zero in 0.4 seconds. The code does not predict the formation of void upstream this REALP5 component. Further

discussion on results and in particular on the origin of the void peaks calculated at about 1.75 seconds from the starting of transient is discussed below.

- Tube 227 (see Figure 5.13) is analyzed at both ends. The small increase of the void fraction (maximum 10^{-4}) is recorded only after about 35 ms, corresponding to the instant of the cap rupture. The result can be explained by assuming that at the time of rupture of the cap, a small amount of water in the tube is sucked by mean of the sudden pressure difference, which is generated downstream, creating a very small vacuum volume into the tube end. After the void fraction starts to decrease in all volumes, because the steam formed tends to exit from the tube itself to follow the main flow of water in the tube 225. During this phase, however, the vapor formed at the end of the tube (227-04), cross all other volumes, before reaching the injection line. Indeed, after an initial reduction in all volumes, the void fraction begins to rise slowly in volume from 227-01, due to the steam coming from the previous volumes, while it continues to fall in 227-04.
- Tube 238 (see Figure 5.14) is analyzed at both ends and at central volume. The sub-volumes of the component are empty at beginning of the transient. Then, when the valve is opened, the void fraction decreases starting from the farthest sub-volume (238-08), because the injection device is still closed. The void fraction in the node 238-01 reaches the value zero only for a while and, then, rises again due rupture of the cap.
- Tube 235 (see Figure 5.15) is analyzed in different volumes. Water before fills completely the horizontal volumes (235-01, 235-04, 235-07) and then the vertical ones, starting from about 0.75 seconds. It is interesting to note, Figure 5.16, that the void fraction of these tubes increases with different speeds. Indeed, the lowest volume close to the connection with the 238-01 increases with greater speed, and reaches the highest value of the void.

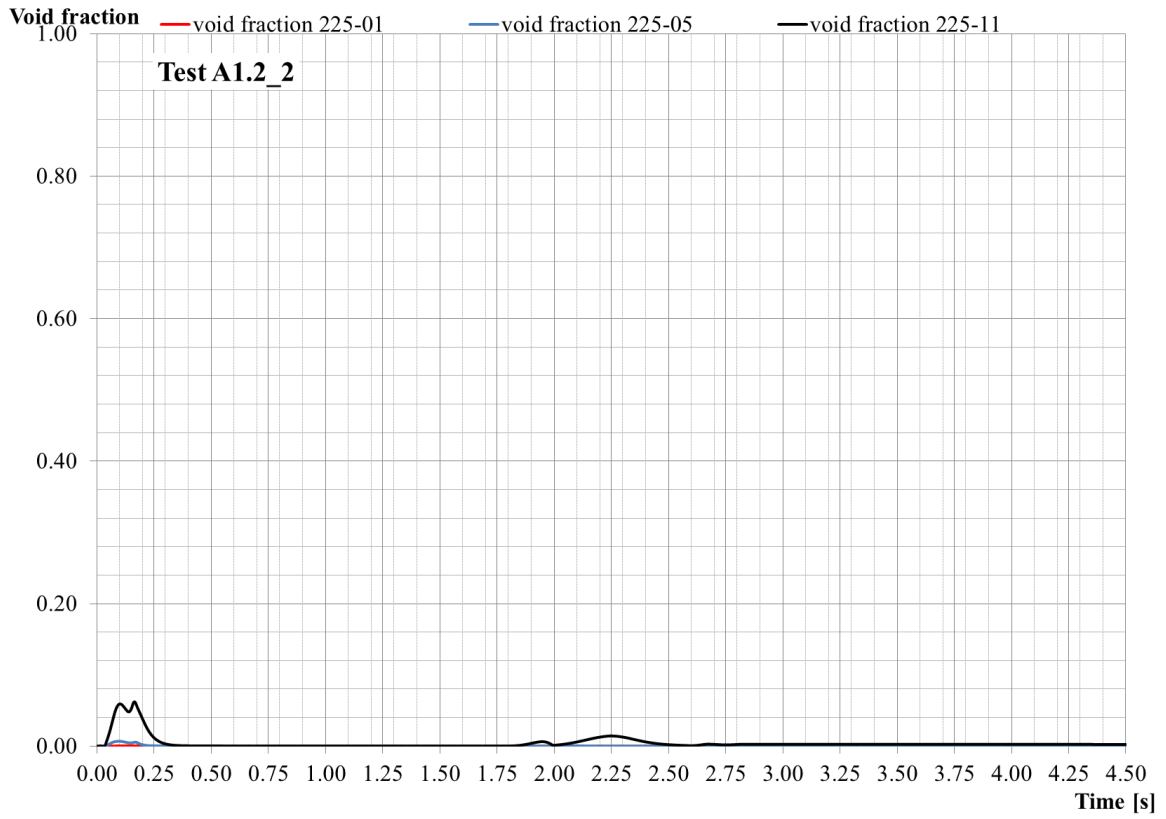


Figure 5.10 – void fraction in tube 225 for Test A1.2_2 in “case_q” configuration

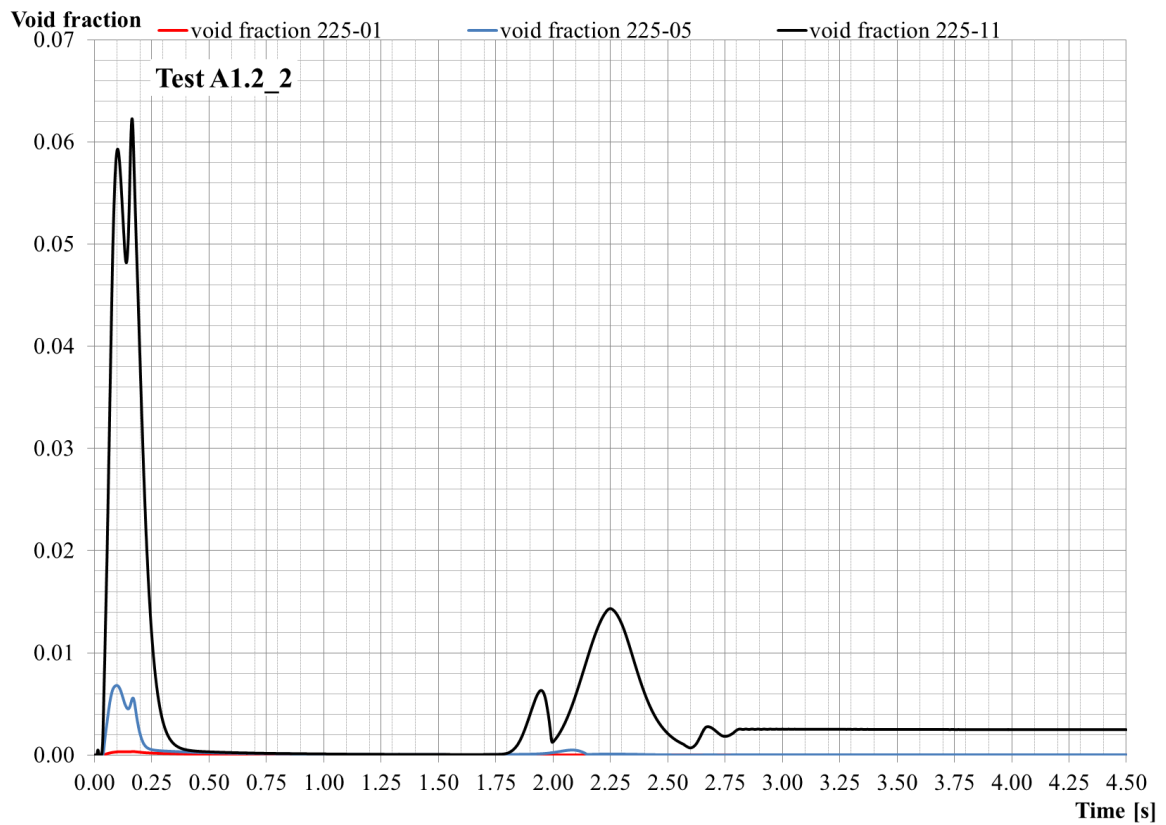


Figure 5.11 – zoom of void fraction in tube 225 for Test A1.2_2 in “case_q” configuration

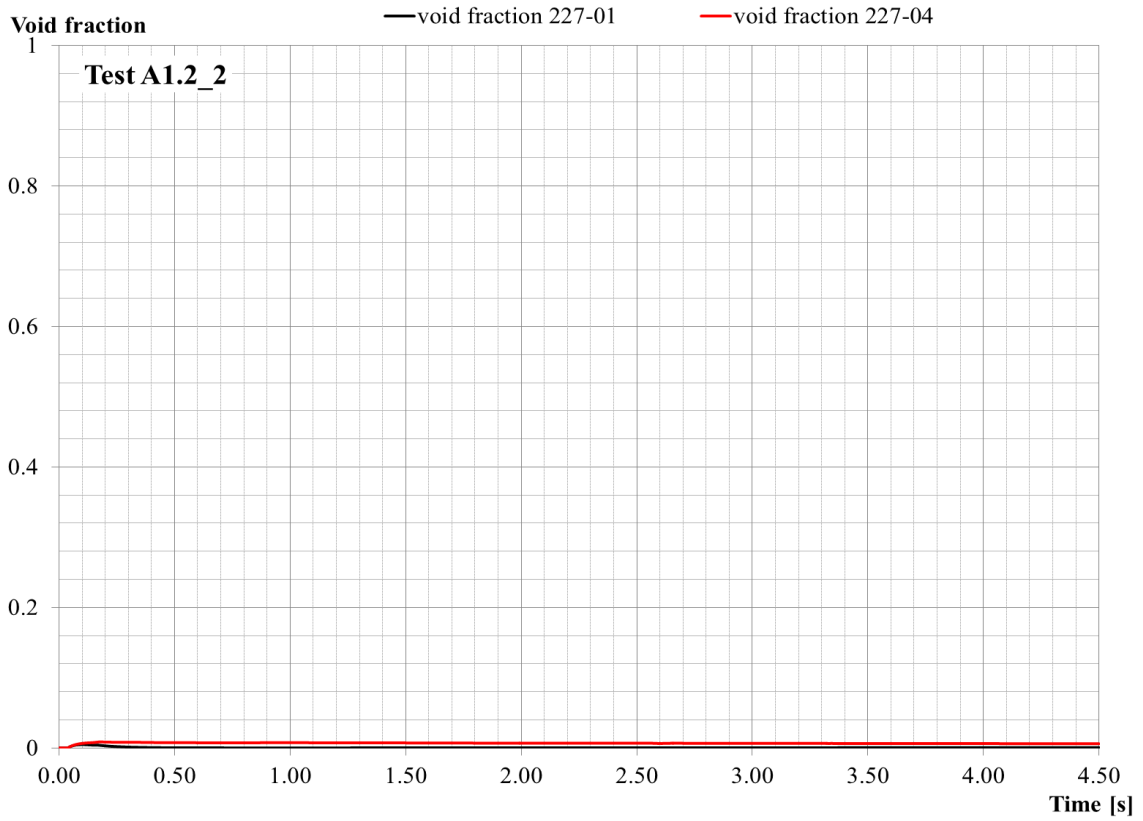


Figure 5.12 – void fraction in tube 227 for Test A1.2_2 in “case_q” configuration

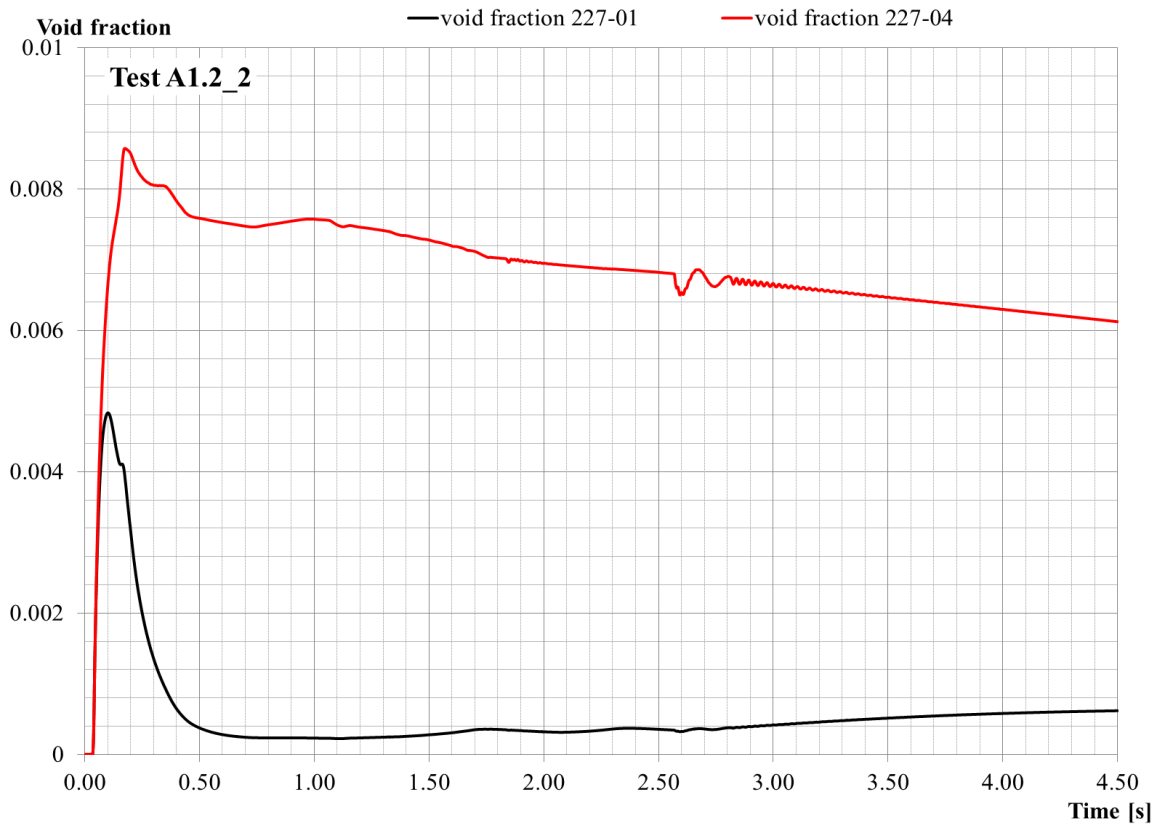


Figure 5.13 – zoom of void fraction in tube 227 for Test A1.2_2 in “case_q” configuration

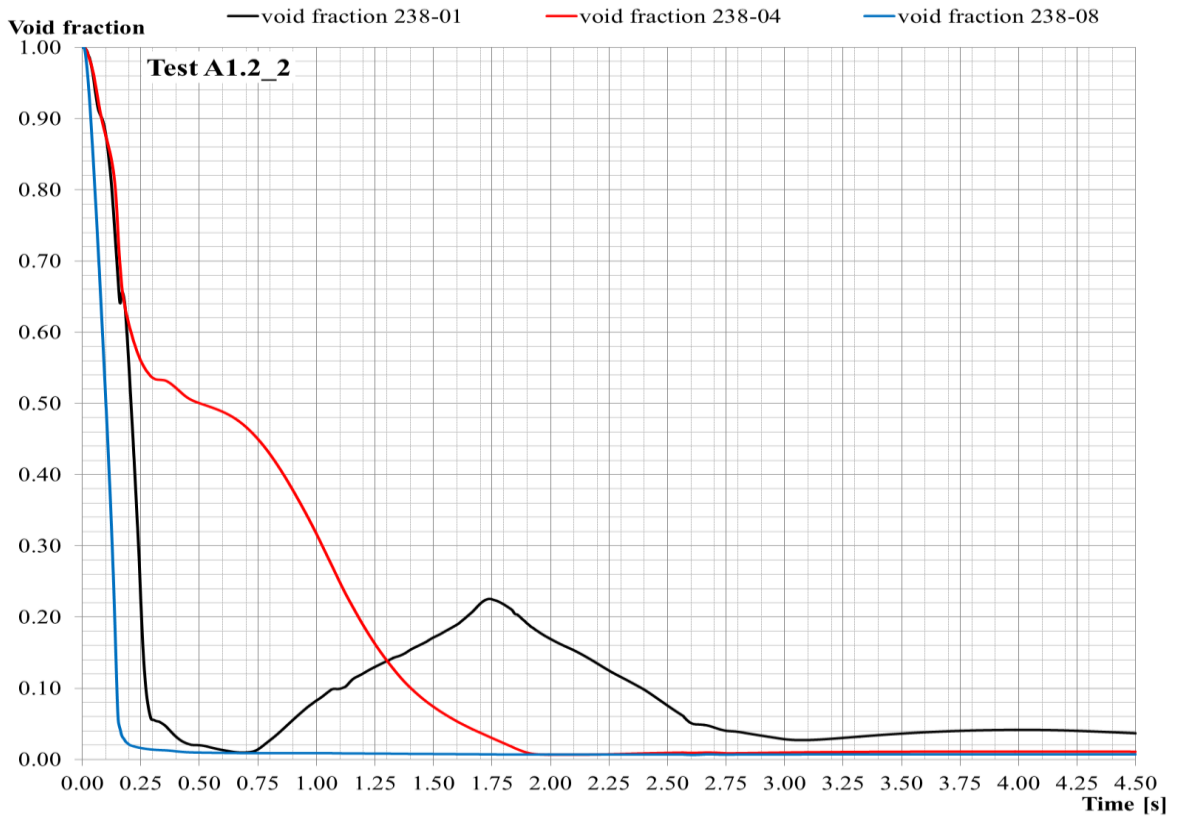


Figure 5.14 – void fraction in tube 238 for Test A1.2_2 in “case_q” configuration

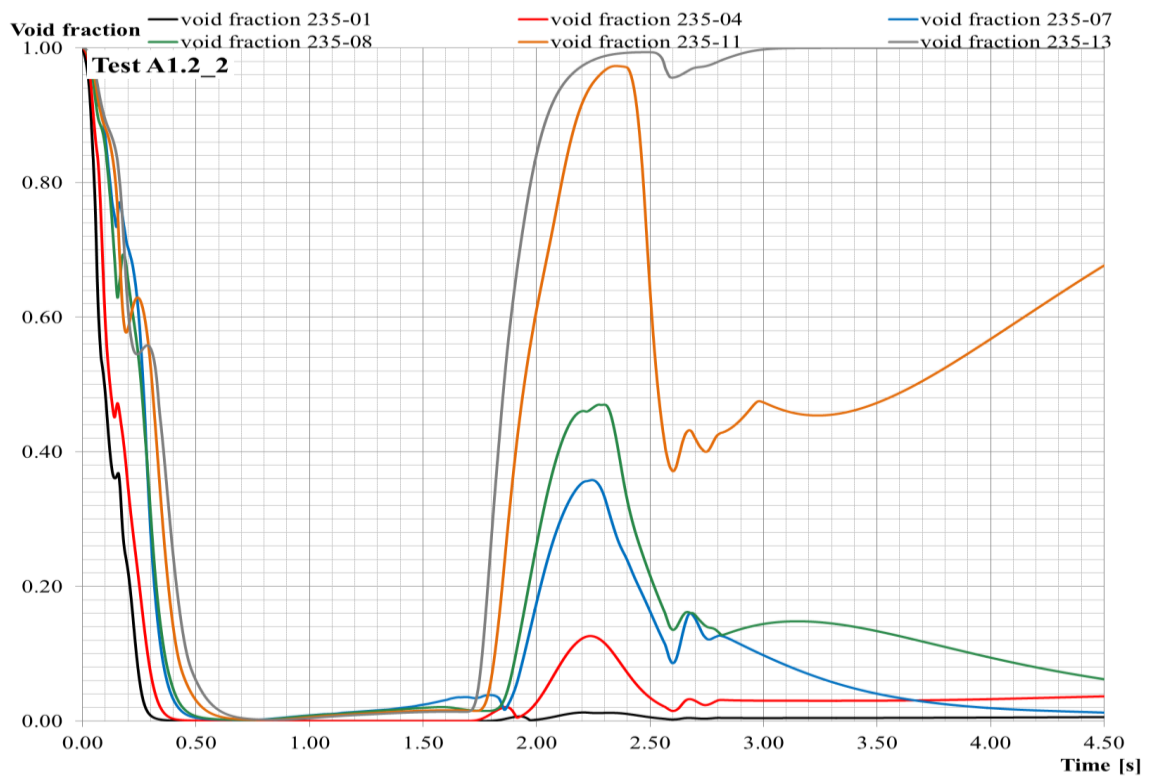


Figure 5.15 – void fraction in tube 235 for Test A1.2_2 in “case_q” configuration

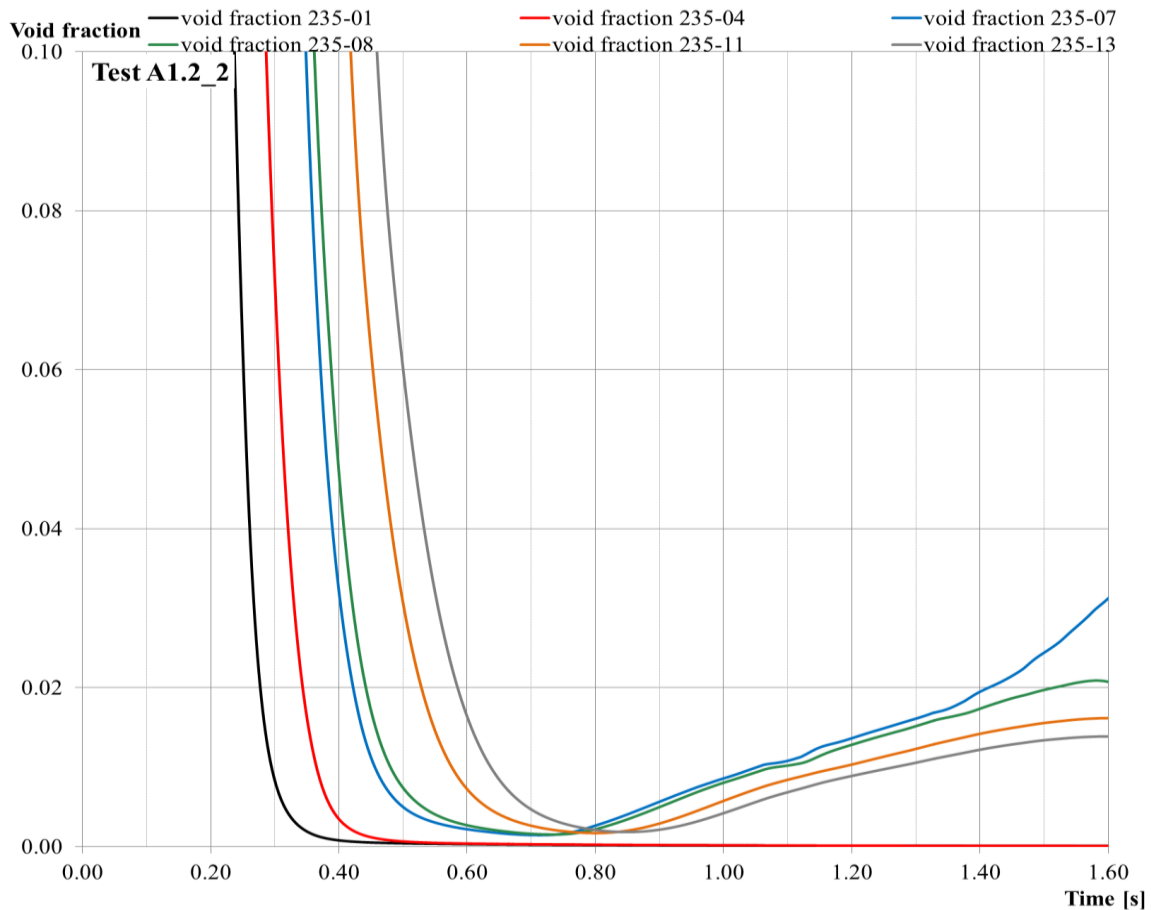


Figure 5.16 – zoom of void fraction in tube 235 0-1.7 s for Test A1.2_2 in “case_q” configuration

Regarding the void fraction analysis of Test A1.2_2, it should be noted that the pressure peak calculated at 1.75 seconds is connected with the time at which the code results becomes not anymore significant for the analysis (see Figure 5.17). Indeed, at this time the pressure of S1 exceeds the pressure of the injection line, calculated with parameters of “case_q” (pressure in S1 is imposed in REALP5 simulation). Therefore, in the code simulation, at this time non-condensable gas filling the REALP5 TIME DEPENDENT VOLUME to impose the pressure enters in the injection line.

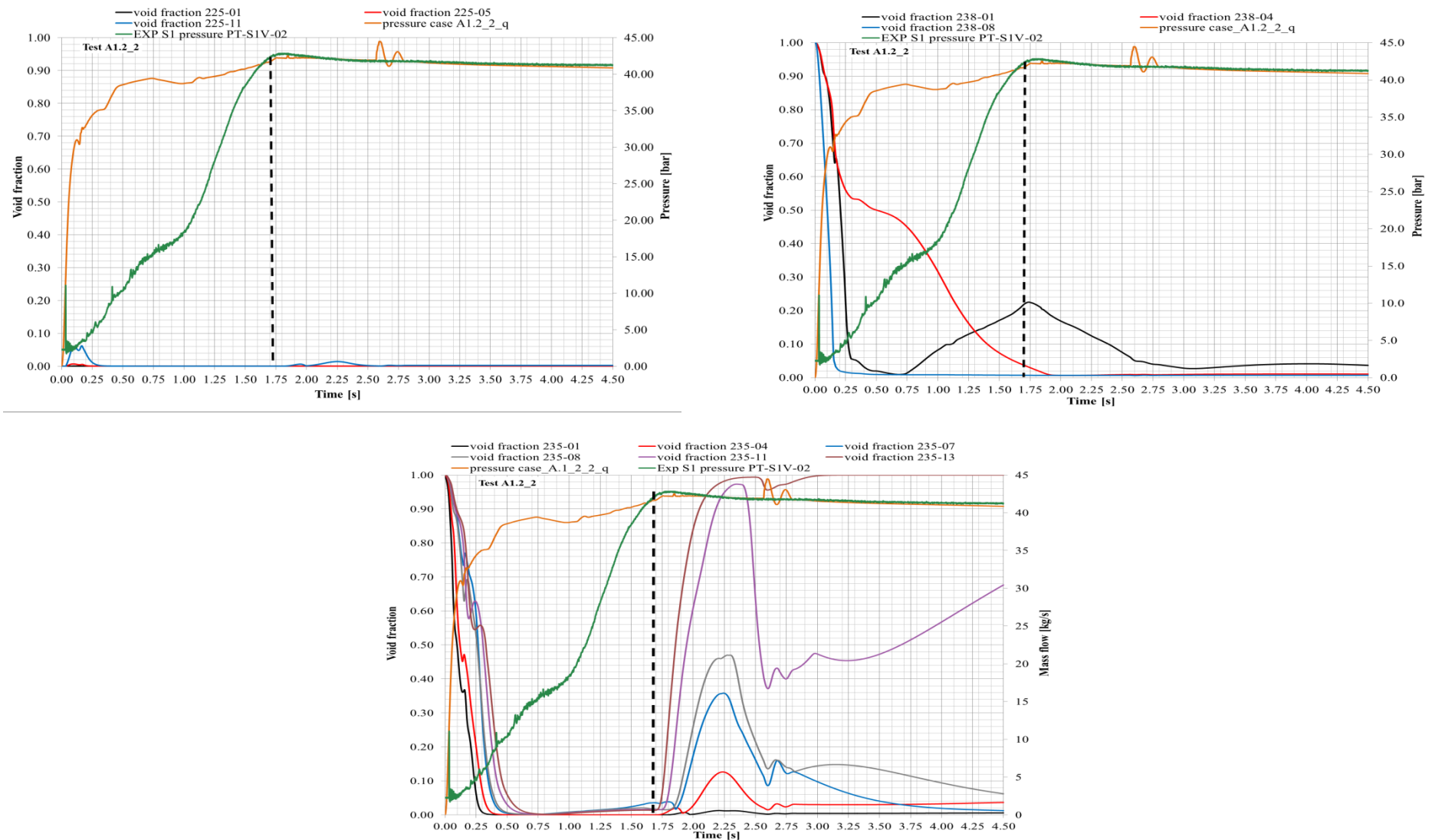


Figure 5.17 – void fraction/pressure trend of S1 and injection line of tube 225, 238, 235 compared for Test A1.2_2 in “case_q” configuration

5.1.3 Mass flow analysis

The mass flow rate calculated by RELAP5/MOD3.3 (“case_q”) is compared with the experimental measure (Figure 5.18). The Test A1.2_2 is considered as reference for the analysis.

The calculated mass flow rate rises fast from 0 kg/s, when the valve V4 is opened. At the time of rupture of the cap, identified from the pressure peak of about 11 bar in S1, the calculated mass flow rate decreases and, then, settles at 0.5 kg/s for about half a second. In this phase, the pressure in S1 rises with a slope approximately constant. After 1 second, the pressure trend in S1 increases faster, passing in half a second from 20 to 40 bar. This affects the mass flow, that begins to decrease rapidly up to reverse flow occurrence, when the pressure in S1 is larger than in the water injection line. This is identified by the dashed black vertical line in the graph, which represent the end of validity of code results as explained in section 5.1.2.

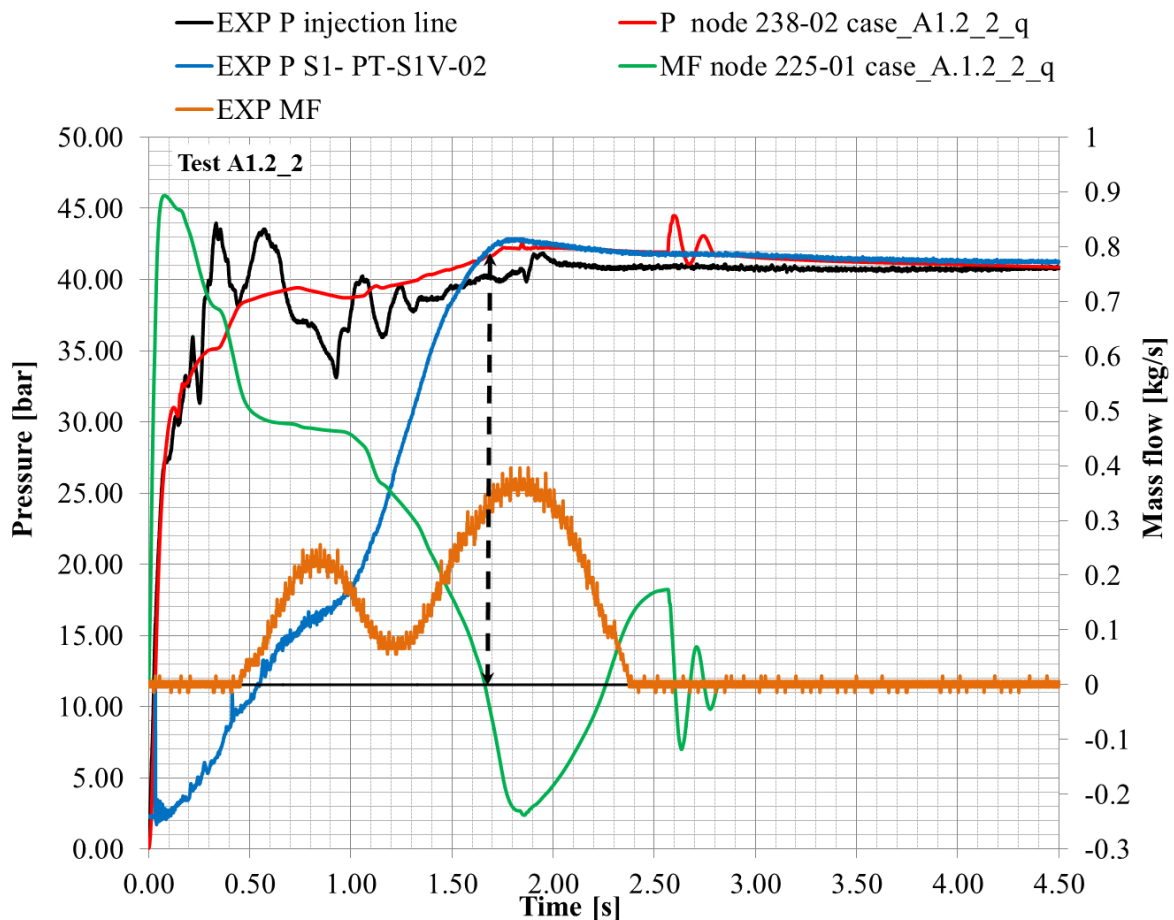


Figure 5.18 – mass flow/pressure trend of S1 and injection line for Test A1.2_2 in “case_q” configuration

The comparison with the experimental flow rate obtained by the Coriolis flow meter shows very large difference. For the first 0.5 seconds the mass flow measured by the Coriolis is equal to zero when the pressure already increases in S1. This means that the water filling the injection line, has broken the cap and it is entering in S1. This delay of Coriolis in detecting the mass flow, is probably due to the lag of the instrument. The experiment has a total duration of about 3 seconds in which the flow passes from zero to about 1.2 kg/s and then return to zero when the valve is closed.

The Coriolis flow meter is composed of two small tubes, which channel the flow from the main pipe and then region in the outlet pipe (see Figure 5.19). The mass flow is measured, by means of the vibrations of these small tubes due to the passage of water. It might be possible, considering the velocity of the transient, that the vibrations of the Coriolis reach a stable value near the end of the transient, reducing the measurement recorded.

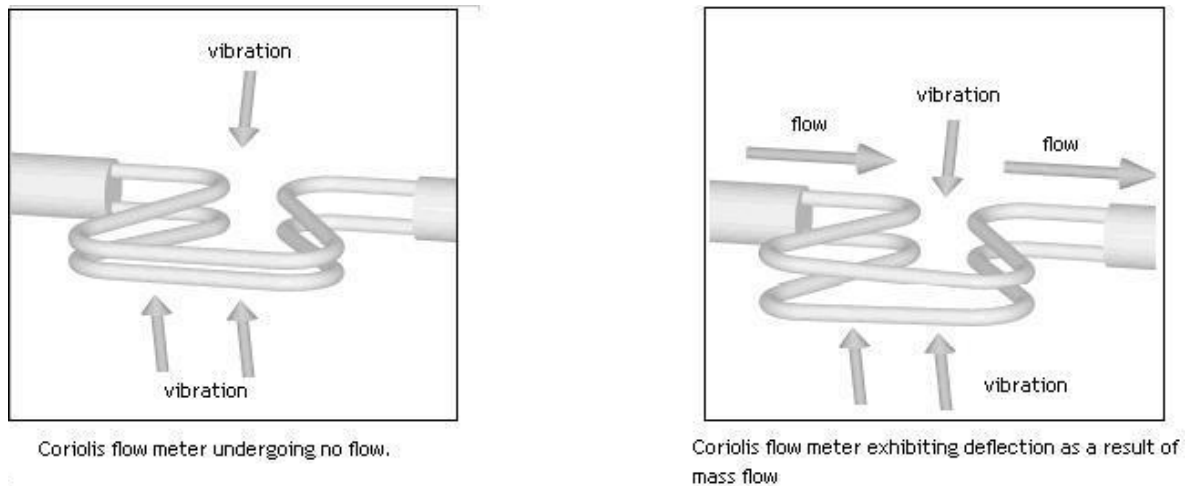


Figure 5.19 – operating principle of Coriolis flow meter

5.1.4 Summary of results

The analysis performed has the objectives to support the post-test analysis by SIMMER-III improving the reliability of the nodalization and to complement the experimental data of LIFUS5/Mod2 tests. The following main achievements from the analysis apply.

- Qualification of the nodalization by RELAP5 has been carried out using the Test A1.2_1 and post-test simulation of Test A1.2_2 confirms the reliability of the model.
- RELAP5 results confirm the improved quality of the experimental data achieved when the valve V4 is used as injection valve. Indeed, this reduces the

evaporation during the injection, improving the simulation of a SGTR accident and enhancing the amplitude of pressure waves and the pressure increase rate in S1.

- This model can be apply for improve the understanding of LEADER experiments (B series).
- RELAP5 simulations demonstrate the difficulties of the Coriolis flow meter in measuring the mass flow rate during the injection. Anyway it may support the evaluation of the integral mass flow rate.
- RELAP5 can be used as support code for SIMMER-III simulation, as discussed in next section.

5.2 SIMMER-III analysis of Test A1.2_2

SIMMER-III code is applied on the basis of the conclusions achieved with RELAP5/MOD3.3. In particular, the goal is to improve the simulation of LIFUS5/Mod2 facility tests. SIMMER-III is a code developed by LANL between 1974 and 1986 as the first practical tool of its kind [39], and has been used in many experimental and reactor analyses to preform DBA and BDBA accident analyses, including severe accident [40]. It is a two-dimensional (2-D), multi-velocity-field, multi-phase, multicomponent, Eulerian, fluid-dynamics code coupled with a fuel-pin model and a space-time and energy-dependent neutron kinetics model. The conceptual overall framework of the code is shown in Figure 5.20.

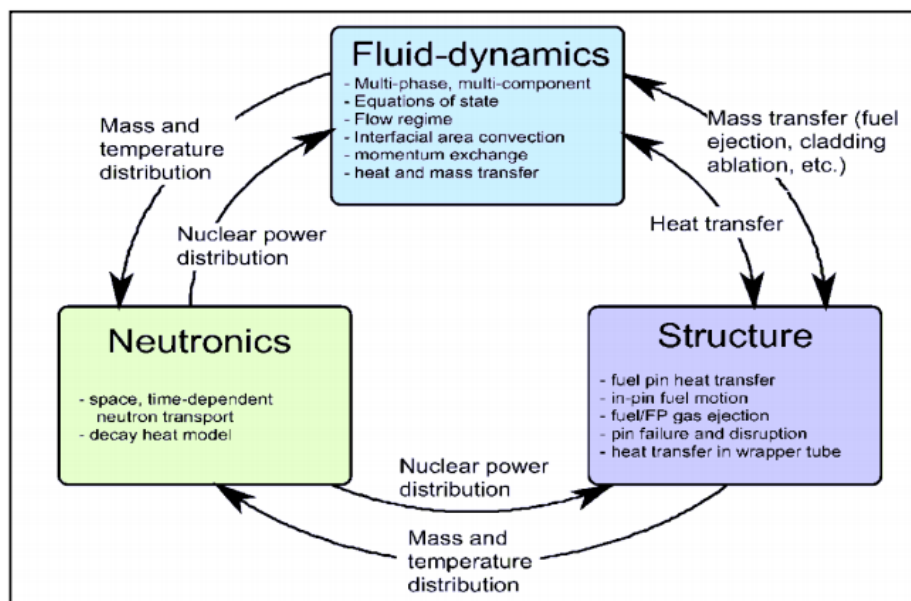


Figure 5.20 – SIMMER-III code structure

The code consists of three components: a fluid-dynamics model, a structure model and a neutronics model. The fluid-dynamic portion, which constitutes about two thirds of the code, is interfaced with the structure model through heat and mass transfer at structure surfaces. The neutronics portion provides nuclear heat sources based on the mass and energy distributions calculated by the other code models.

The user can choose to represent the system model either through one-dimensional or two-dimensional domains in cylindrical (RZ) or Cartesian (XZ) geometry.

5.2.1 SIMMER-III code nodalization of LIFUS5/Mod2 facility

The nodalization of LIFUS5/Mod2 is developed despite the limitation of the code (i.e. 2D axisymmetric representation). In view of this, THINS configuration of LIFUS5/Mod2 reaction vessel (S1) is axisymmetric. On the opposite, the other components, i.e. injection line and water storage tank (S2), are not coaxial with the vessel S1. This implies that the user effect and the modeling choices are more relevant.

Figure 5.21 depicts LIFUS5/Mod2 model by SIMMER-III code, as it is set up to simulate the Test A1.2_2 [31]. Colors distinguish the different fluids, as they are set at beginning of the transient ($t=0$ s).

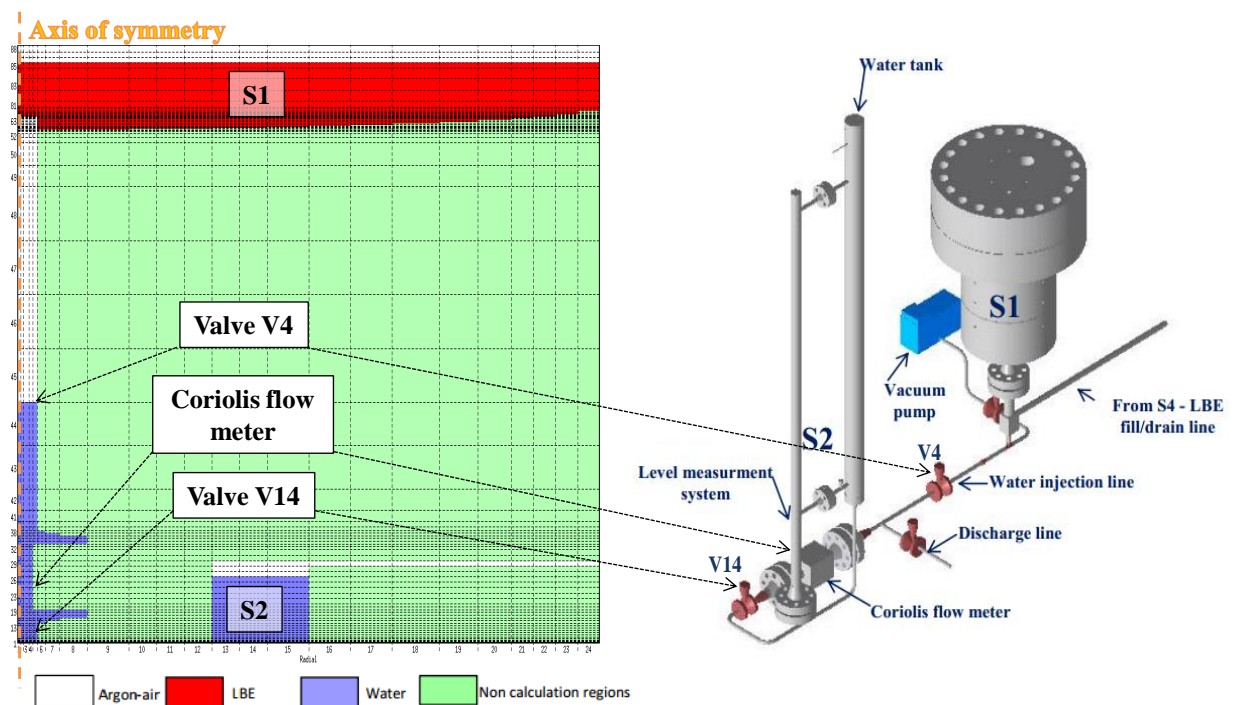


Figure 5.21 – LIFUS5/Mod2 modeling

The geometrical domain is obtained by 24 radial and 88 axial subdivisions. The LBE is represented in red, the water in blue, the argon (cover gas) in white and the non-calculation regions in light green. The reaction vessel S1 is partially filled by LBE and the cover gas

volume is coherent with the scheduled boundary conditions. The injection line is horizontally installed and cannot be coherently modeled in an axisymmetric domain. Therefore, to preserve the cylindrical shape of the injection tube, it is positioned vertically and coaxially with the model. This simplification does not respected the real geometry. It introduces distortion in pressure drops due to gravity, by entailing about 0.4 bar of gravity head not existing in the experiment. This approximation may be considered negligible if compared with the initial pressure of the water in S2 in test THINS A1.2_2, which equal to 40 bar.

The Coriolis flow meter is also modeled (Figure 5.21). As stated in section 5.1.3, the Coriolis flow meter is composed by two parallel tubes. SIMMER-III models this component with a single tube with having equivalent diameter. The vertical part of the injection line ($\frac{1}{2}$ " diameter) penetrates 120 mm into vessel S1. It has also an orifice of 4 mm at the top, just below the injector cap. The breakage of injector cap is simulated by means of virtual walls, which can be removed according with the user choices. Same approach is applied to simulate the operation of valves. Water tank S2 has an annular shape, according with the SIMMER-III modeling constraints. The volume and the height of S2 tank are preserved and the tank is connected to the injection line, horizontally. In SIMMER-III model, S2 cover gas is controlled through proper boundary conditions imposed according with the experimental data of the test.

The overall volume of the model is obtained, rotating the 2D SIMMER domain along the axis of symmetry (orange dot-dashed line in Figure 5.21). Concentrated pressure drops are set according with the outcomes of RELAP5/MOD3.3 analysis discussed in section 5.1 considering the "case_q" as reference. Analogous approach is for the friction losses. This required to inhibit the calculation of distributed pressure drop from SIMMER-III model. Then, based on the average velocity calculated at each junction in RELAP5, the Reynolds number is evaluated, and therefore the friction factor using the Moody diagram. The equivalent pressure drops are implanted the input deck as concentrated pressure drops. The limitation of this approach is that the equivalence is evaluated for single phase liquid. Thus, Lockart-Martinelli coefficients used in RELAP5 for two phase pressure drops are neglected.

5.2.2 Analysis of Test A1.2_2

The calculated results and experimental data of pressure in injection line and in S1 are shown in Figure 5.22. Time equal to 0 s corresponds the opening of the injection valve. The pressure calculated in S1 after the initial peak increases up to about 37 bar with a constant slope. Two main differences are observed with the experimental data.

Observing the experimental data trends, a two-phase mixture is injected up to 1 second. It is connected with the lower slope and the jagged trend of S1 pressure trend. On the opposite, the simulation (see Figure 5.23) predicts the injection line full of water at 0.5 seconds. The pressure trend is, therefore, stepper and an underestimation of two-phase pressure drop in this phase is expected, considering the modeling approach discussed in section 5.2.1.

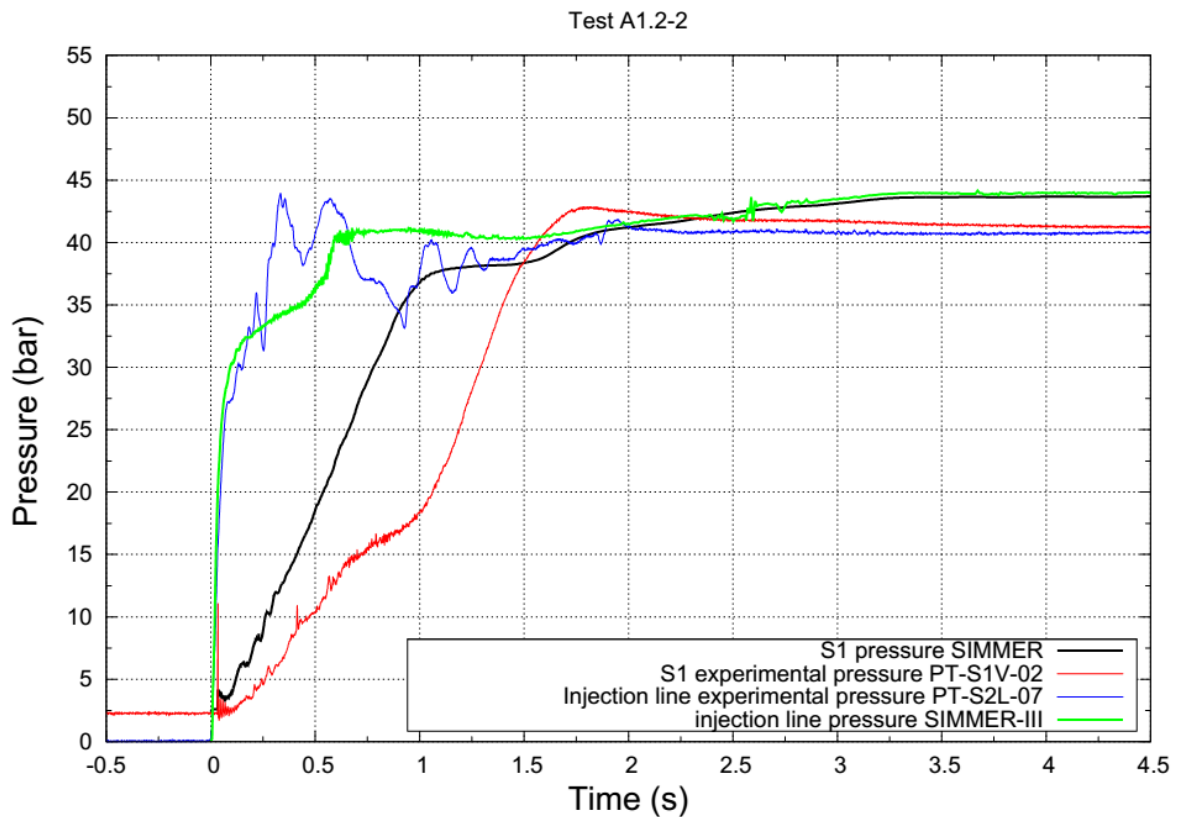


Figure 5.22 – experimental pressure trends for Test A1.2_2 compared with the SIMMER-III one

After 1 second the experimental pressure increases at the same rate as the core simulation, confirming analysis of the first part of the transient. The pressure trend predicted by the code in the injection line is in agreement with the experimental data during the overall transient, up to the equalization.

After reaching a peak of about 43 bar, the experimental trend settles with the pressure of the injection line. At the end of the transient the code predicts a pressure 2 bar higher than

the experiment: 41 bar versus 43 bar. This may be connected with a larger water injection predicted in the code simulation. The error should be accumulated during the first part of the transient, when the code predicts liquid phase injection.

Figure 5.24 shows the comparisons between the mass flow rate calculated by SIMMER-III (in red) and the RELAP5/MOD3.3 (in black) codes. The results are similar. SIMMER-III results have a larger initial peak (1.2 kg/s versus 0.9 kg/s). After, the mass flow rate shows a plateau, as for the pressure in S1. Finally, it decreases when the pressure difference between the injection line and S1, disappears. Differences are connected with the modeling: in SIMMER-III the pressure downstream the injection device is calculated by the code, whereas it is imposed as boundary condition in REALP5 calculation. This implies, that it is equal to the experimental data recorded. The total amount of water injected in both simulations is comparable. It is equal to 0.71 kg in RELAP5/MOD3.3 simulation and 0.77 kg in SIMMER-III. The overall mass of water injection measured by the Coriolis flow meter is 0.45 kg. According with these results, it is postulated that the Coriolis flow meter may underestimate the total amount of water injected.

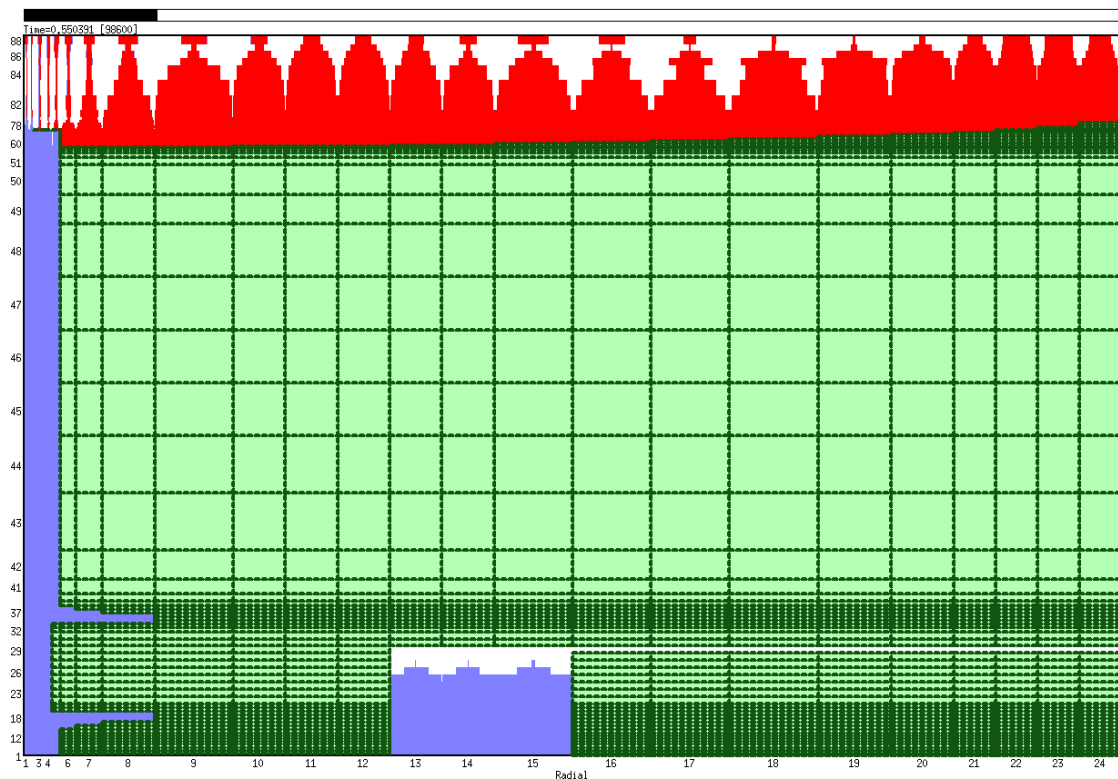


Figure 5.23 – Test A1.2_2 situation at $t=0.5$ s

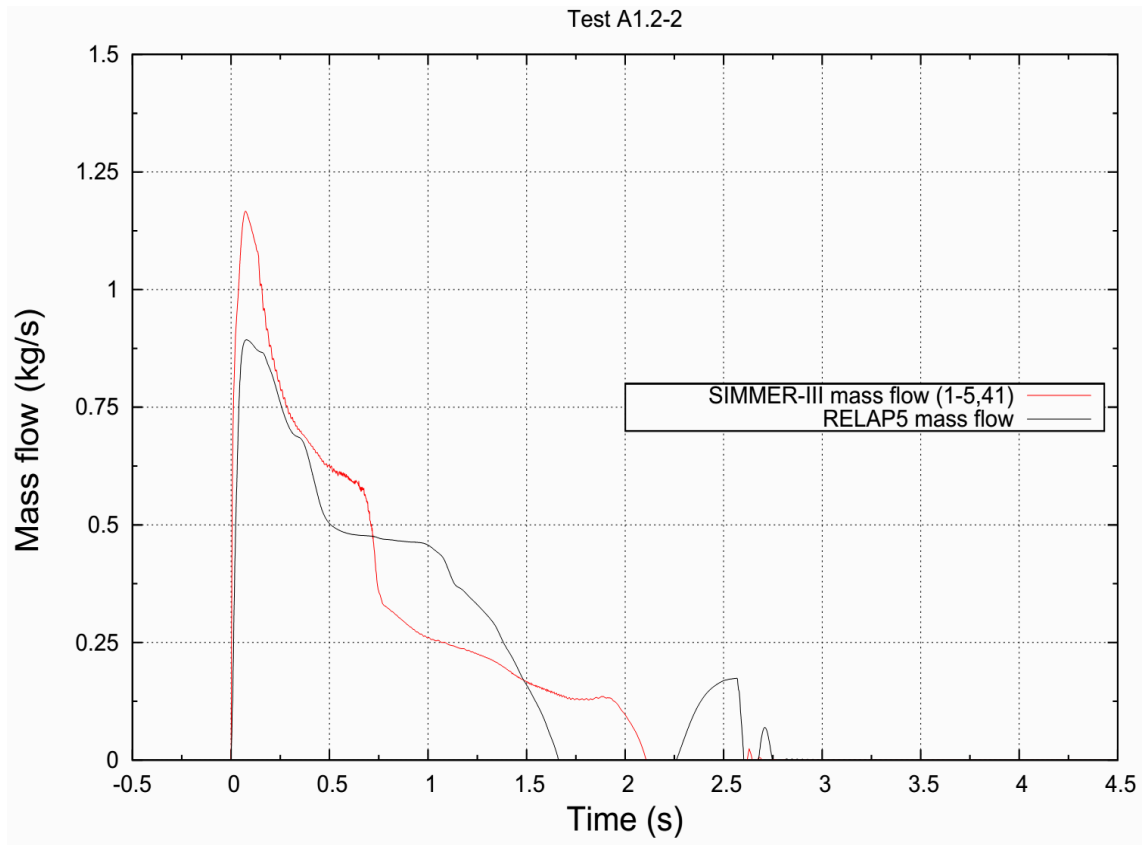


Figure 5.24 – mass flow rate RELAP5 vs SIMMER-III

6 LEADER experimental campaign

The main objective of LEADER experimental campaign is to investigate and assess the damping of pressure waves by SGTR event. In connection with this, the expected outcomes of the tests are:

- the generation of detailed and reliable experimental data;
- the improvement of the knowledge of physical behavior and of understanding of the phenomenon;
- the investigation of the dynamic effects of energy release on the structures; and
- the enlargement of the database for code validation.

Present section presents the first three experiments planned in LEADER project (B series). The project specifications plans 3 type of tests, having the same facility configuration, the same initial conditions and 3 different orifices diameter sizes: about 4mm, 8mm, and 13mm.

Table 6.1 summarized the main parameters of the tests. In Test B1.1 the injection time is not reported because the injection cap was broken when the injection valve was already closed. Therefore, injection time is not a parameter affecting the transient.

T# B1.--	Interaction system	LBE temperature [°C]	Water pressure [bar]	Water temperature [°C]	Test section tubes pressure [bar]	injection time [s]	Injector orifice diameter [mm]
1	S1	400	180	260	180	2	4
2	S1	400	180	270	180	2	4
3	S1	400	180	270	180	2	4

Table 6.1 – LEADER project tests matrix

6.1 Test B1.1

The test was carried out on the morning of 11 September 2014. Besides, the test objectives mentioned above, it has been a shake-down test giving feedbacks on test procedures; on behavior of power system; control and measurement system; as well as acquisition system.

6.1.1 Test configuration

The commissioning phase of the LIFUS5/Mod2 facility for the test lasts one day. This time is needed to heated up the facility and the LBE at 400°C through the heating cables. During this phase the set points are: the temperature increase rates and the final

temperatures. Parameters set for Test B1.1 are reported in Table 6.2. The initial water temperature is set to 260°C, about 90°C of sub-cooling. Heating cables (see Figure 6.1) installed in S2 and in the water injection line are set to 260°C except the vertical pipe connected with S1 (CS-S2-05). Although the LBE temperature in the test specification is 400°C, the thermal structure of S1 are heated up to 370°C. This is done to detect, using the thermocouples, the LBE flowing from the storage tank during the loading phase and to stop the loading procedure when the right level in S1 is reached (+0 cm in Figure 4.21).

Loading procedure starts with S4 pressurization at about 3.5. The overpressure overcomes the initial pressure in S1, the gravity head due to different elevation of the path and systems, the friction and pressure drops.

Valve V11 (Figure 6.1) in the pipeline connecting S1 and S4, is closed when the loading procedure is completed, and the melt in the pipeline is frozen to ensure that pressure wave propagation and pressurization in S4 during the experiment.

The conditioning phase is completed with the pressurization of S2 and the connection with the gas tank. The reference injection pressure in LEADER tests is 180 bar. Then, the injection procedure starts.

#	LIFUS5/Mod2	Project FP7 LEADER			Test B1.1		Date 11-09-2014
		Parameter	ID	Unit	Design	Actual	
SYSTEM S1							
S1-1	P @ SoT	--	bar	1	3.1	--	
S1-2	T _{LBE} @ SoT	--	°C	400	402	--	
S1-3	LBE LVL (from test section top flange)	--	mm	0	10	<i>max + 20 mm</i>	
S1-4	Set temperature heating cable	CS-S1-01	°C	400	400	--	
S1-5	Set temperature heating cable	CS-S1-02	°C	400	400	--	
S1-6	Set temperature heating cable	CS-S1-03	°C	400	400	--	
S1-7	Set temperature heating cable	CS-S1-04	°C	400	400	--	
S1-8	Set temperature heating cable	CS-S1-05	°C	400	400	--	
S1-9	Set temperature heating cable	CS-S1-06	°C	400	400	--	
S1-10	Set temperature heating cable	CS-S1-07	°C	370	370	--	
S1-11	Set temperature heating cable	CS-S1-08	°C	220	220	--	
S1-12	P @ SoT test section tubes	--	bar	180	180	--	
SYSTEM S2							
S2-1	P in gas line @ SoT	--	bar	180	174	--	
S2-2	P @ SoT	--	bar	180	174	--	
S2-3	T @ SoT	--	°C	260	262	--	
S2-4	LVL @ SoT	--	mm	--	1133	--	
S2-5	Charged water vol.	--	l	8	7.8	--	
S2-6	Set temperature heating cable	CS-S2-01	°C	260	260	--	
S2-7	Set temperature heating cable	CS-S2-02	°C	260	260	--	
S2-8	Set temperature heating cable	CS-S2-03	°C	260	260	--	
S2-9	Set temperature heating cable	CS-S2-04	°C	260	260	--	
S2-10	Set temperature heating cable	CS-S2-05	°C	300	300	--	
S2-11	Set temperature heating cable	CS-S2-06	°C	260	260	--	
INJECTION SYSTEM							
O-1	Injection valve	--	--	V4	V4	--	
O-2	Injection time	--	s	2	2.25	--	
O-3	Injector nozzle orifice	--	mm	4	4	--	
O-4	Injection Nozzle ID	5	--	--	--	--	
SYSTEM S3							
S3-1	P @ SoT	--	bar	1	3.1	--	
S3-2	T @ SoT	--	°C	150	146	--	
S2-3	Set temperature heating cable	CS-S3-01	°C	250	250	--	
S2-4	Set temperature heating cable	CS-S3-02	°C	220	220	--	
S2-5	Set temperature heating cable	CS-S3-03	°C	220	220	--	

Table 6.2 – Test B1.1 parameters

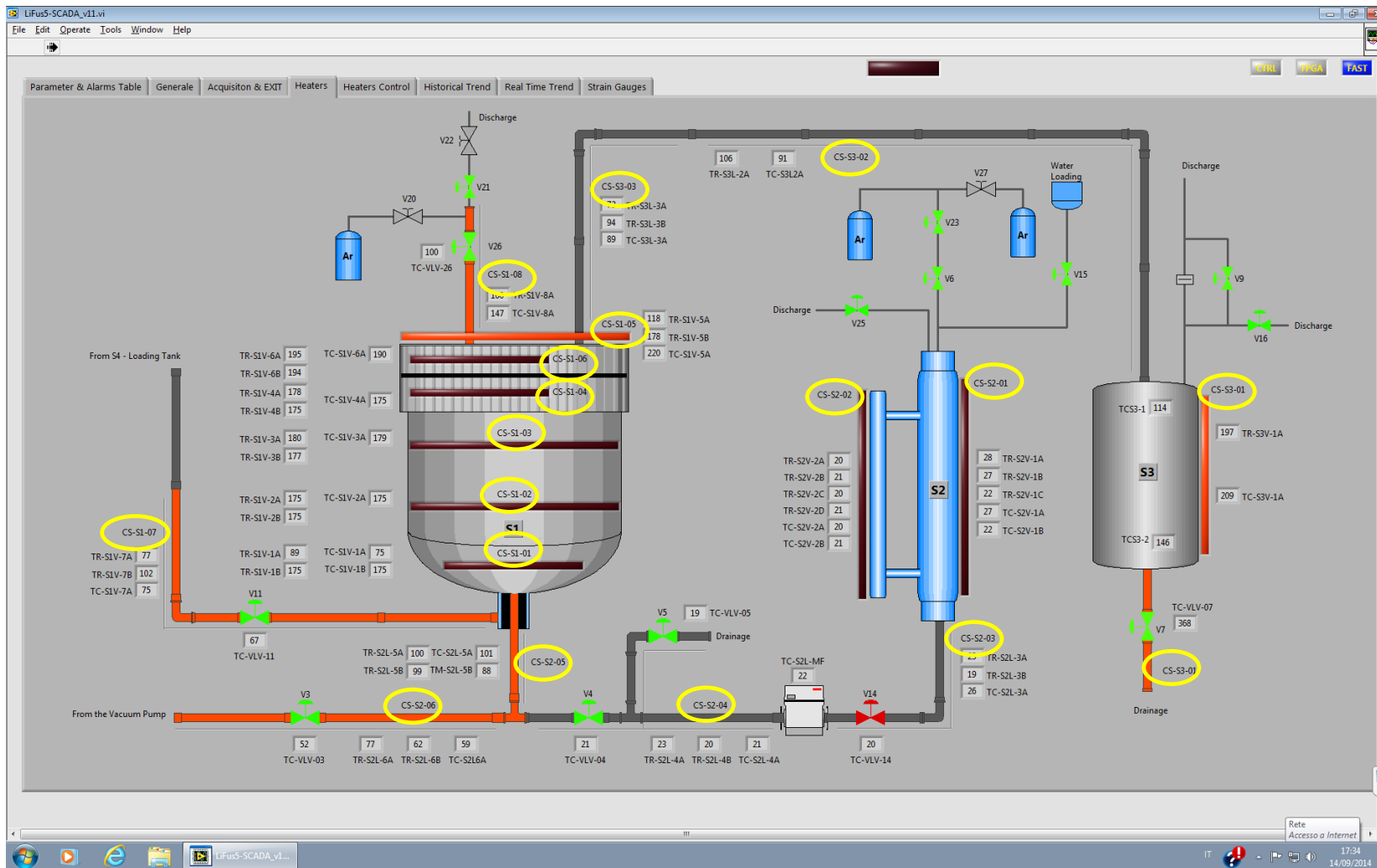


Figure 6.1 – LIFUS5/Mod2 synoptic with heating cable highlighted

6.1.2 Execution of the test

The injection procedure starts with a check of the test parameters and of the valves' status. The test parameters are defined in the specifications and the control system checks the correctness of their values (see Table 6.2 reporting the parameters measured at the beginning of the injection procedure during the execution of Test B1.1). The injection time is set (2 seconds in Test B1.1) in the control system. At the beginning of the injection procedure, the valves shall be closed, with the exceptions of those in the line connecting the Argon cylinder and S2 (V6 and V23 in Figure 6.2). The vacuum pump is activated and the valves V3, V19 and V4 are opened, thus the air is removed from the injection line. Once the pressure is below 10 mbar, the valves are closed again

Closed the valves V19, V3 and V4, the valve V14 is opened to flood the injection line up to valve V4. Acquisition system is in stand-by, waiting for the injection signal. This signal is activated by the operator. Then, the acquisition system starts to record the data, the valve V4 is opened, and it remains stand up the closure signal occurs (2 seconds in Test B1.1), actuating the valves V4, V14, V6 and V23. The acquisition system continues to record data for 30 seconds from the injection signal.

The test is executed and the facility shall be cooled and shut down. Therefore, LBE is drained back into the S4; the systems S1, S2 and S3 are depressurized and cooled for about two days, when the power is switched off. Finally, the tank S2 is emptied from residual water (7 l in Test B1.1) and the LBE transported in S3 because the interaction with water in S1 is removed (about 15 kg in Test B1.1).

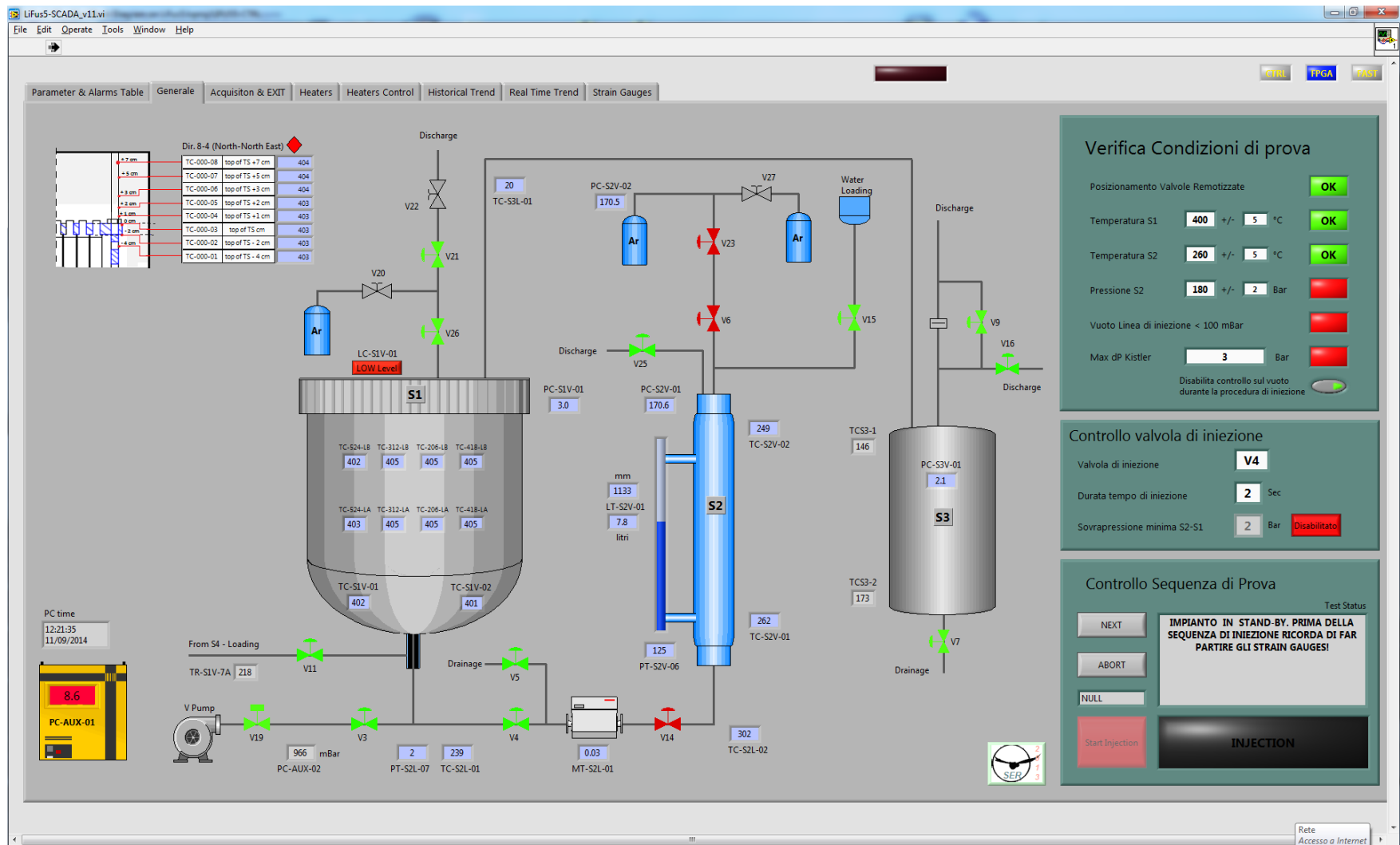


Figure 6.2 – condition of LIFUS5/Mod2 synoptic for Test B1.1

6.1.3 Data analysis and interpretation

The test execution did not follow the plan of the experiment. Indeed, following the commissioning tests (section 4.4), the protective cap should be broken immediately. On the opposite, rupture occurred with 16 seconds of delay. The following reasons might have an impact on this delay: 1) the gas cylinder tank had a pressure lower than the test specifications (174 bar against 180 bar planned), 2) the conditions of the experiments increase the ductility of the protective cap, which breaks but after some seconds of delay (phenomena observed in tests B1.2 and B1.3 [42]).

In case of Test B1.1 the injection procedure envisaged 2 seconds. Therefore, the injection valve closed before the cap was broken. This implied that the injection device at 400°C because in equilibrium with the melt in S1 heated the water in the injection line. Following the valve closure, the pressure rose because of the heating up to the rupture of the cap. This is demonstrated by the experimental data trends and by code simulations (in the following sections).

In detail, Test B1.1 can be divided into 3 main phases:

- I. Water injection phase;
 - II. Pressure increase in injection line due to heating;
 - III. LBE-water interaction phase.
- I. Water injection phase [0 to 2.2595 s] *from valve V4 opening to valve V4 closing.* Once valve V4 is opened, water fills injection line between the V4 and V3 and up to the cap. The pressure of S2, decreases slightly see trends of transducer PC-S2V-01 and PT-S2V-06 (see Figure 6.4). The injection has a duration of approximately 2.25 seconds, up to the complete closure of the valve, as shown in Figure 6.3. Indeed, the total opening time of the valve lasts approximately 250 ms and the signal of valve opened is set about 125 ms after the stem starts to move, according with the analysis of THINS tests in section 5. The rupture of the cap does not occur as quickly as expected. This implies that the total amount of water injected has a volume equivalent to the volume of the injection line downstream valve V4. Therefore, the total mass of water injected is 250 g, which is evaluated considering the volume and the density of water at time of valve closure. The pressure trend in the injection line is recorded by the pressure transducer PT-S2L-07 at a frequency of 10kHz, see Figure 6.4. The pressure in the injection line rises

rapidly, reaching an initial peak of about 210 bar, full scale of the dynamic transducer and, then, begins to oscillate. The high initial peak and the subsequent oscillations are probably due to phenomena of flashing and condensation inside the closed injection tube. Figure 6.5 reports the pressure in the injection line, and the water temperature downstream of the injection valve V4 (TC-S2L-02). It also shows the trend of saturation temperature calculated on the basis of pressure trend. During phase I the water temperature is below the saturation. At time 0 s, the water temperature measured in the injection line has a value of 222°C, despite S2 water temperature is set to 260°C. This is because the water entering in the line flashes, cooling the thermocouple installed in the line. On the opposite, the heating cables correctly heat the tube structure at 260°C.

Figure 6.6 shows the level trend in S2 and the mass flow rate measured by the Coriolis flow meter. The level trend is in agreement with the opening and closure of the injection valve.

- II. Pressure increase in injection line due to heating phase [2.2595 s to 16.05 s] *from valve V4 closing to cap rupture*. In this phase, the water trapped between the valve V4 and the cap is heated due to the contact with the injector surface at 400°C. The pressure (Figure 6.4) increases until it reaches the full scale of the instrument. Hence, the final value of the pressure reached at rupture of the cap is not measured. RELAP5 was employed to simulate this phase and to calculate the water pressure trend beyond the measurement transducer capability, see section 6.1.4. The difference in time between the temperature measured in the injection line and the pressure, is connected with the position of the thermocouple (TC-S2L-01) in the line and the occurrence of stratified conditions. The thermo-dynamic conditions evaluated of water at time of cap rupture are close to critical point (i.e. $P_{crit} = 221$ bar).
- III. LBE-water interaction phase [16.05 to EoT] *from cap rupture to end of transient*. When the cap breaks, the pressure in the injection line decreases rapidly up to about 50 bar (Figure 6.4). At the same time, the pressure in S1 rises rapidly from 3.1 bar, reaching a maximum pressure peak of about 30 bar (PT-S1V-04). Figure 6.7 reports the trends of dynamic pressure (PT) and absolute pressure (PC) transducers installed in S1 and the absolute pressure transducer of S3. Figure 6.8 highlights the pressure peak and the extreme velocity of the pressure wave propagation, thanks the

high frequency of the acquisition system 1 point each 0.1 ms. The results of the Test B1.1 demonstrate that different measured pressure peaks measured in THINS tests is due to undersampling of the pressure signal. The pressure peaks are connected with the propagation of waves in LBE, that is the reason why they are not detected by PT-S1V-08 and PT-S1V-05 (see section 4). When pressure in the injection line is about 50 bar (see Figure 6.4), the pressure decrease slowed down for a while, because evaporation of liquid water in the pipeline. Two peaks are observed during the injection in S1. The first peak recorded in S1 is due to the pressure wave that propagates inside the vessel. The second is due to the expansion of water and steam in S1 (see Figure 6.7). It is interesting to observe that the measured temperature of the two-phase mixture in the injection line deviates again from the saturated temperature at about 18.75 s (see Figure 6.5). This “temperature decrease”, is due to evaporation itself, which cools the thermocouple. At end of transient, the pressures measured in S1 and S3 are stabilized at about 3.6 bar. Figure 6.9 shows the trends of temperatures installed on the test section. Each figure reports the temperature trends of thermocouples installed in the same rank of the test section (rank 2 is the closest and rank 8 is the farthest). The thermocouples welded on the lateral surface of the test section (PP) are also reported. The initial temperature of the melt is 402°C. However, the temperature trends of ranks 2 and 3 highlight have recorded a perturbation before the cap is broken. A possible reason is a small loss of water due to a microcrack, which might explain the delayed rupture of the injector’s cap. When water enters in S1, there is an abrupt decrease of temperature which is damped moving away from the center of the test section. At the end of the transient all thermocouples settle to the starting value of about 402°C. It should be mentioned that during the Test B1.1, 4 thermocouples surrounding the injector have been damaged. The inspection will be done after the experimental campaign.

The trends of the strain measured by the strain gauges is shown in the Figure 6.10. Even in this case, figures are organized starting from the two strain gauges closest to the cap (SG-201 and SG-204), up to the strain gauge installed in the seventh rank (SG-710), plus the two on the outer surface (SG-PP1 and SG-PP2). The measured strain is lower moving away from the center of the test section, in radius direction, from about 500 $\mu\text{m}/\text{m}$ up to values of about 250 $\mu\text{m}/\text{m}$, measured in the seventh rank. The strain gauges installed on the second rank in fact

show the highest peaks (the maximum is recorded by the SG-204, about 535 $\mu\text{m}/\text{m}$). The measurement SG-201 is the only one having positive value. This suggests an incorrect orientation of the strain gauge itself. The two strain gauges installed on the lateral surface of perforated plate, measure a deflection equal to about 41 $\mu\text{m}/\text{m}$.

For completeness are also reported temperature trends (see Figure 6.11) of the inner surface of S1, not affected by water injection, and the trends of the strain (see Figure 6.12) measured by strain gauges in S1. This last still shows a residual strain value equal to about 20 $\mu\text{m}/\text{m}$ (see Figure 6.13). In the old tests THINS [31], which had a maximum injection pressure value equal to 40 bar, the peak of strain measured on the internal surface of S1 is equal to 10 $\mu\text{m}/\text{m}$. Whereas the highest injection pressure set for the LEADER tests, such a low strain values measured on the inner surface of S1 is comparable with the values achieved in THINS tests. This indicates a possible dumping of pressure waves by the “ tubes tangle ” and by perforated plate of the test section. This observation, will be further investigated, and it may be relevant to carry out evaluation of structures outside SG shell during a SGTR event. Another outcome is the structural integrity of pressurized tubes surrounding the injector, as demonstrated by their internal pressure at end of the test (180 bar).

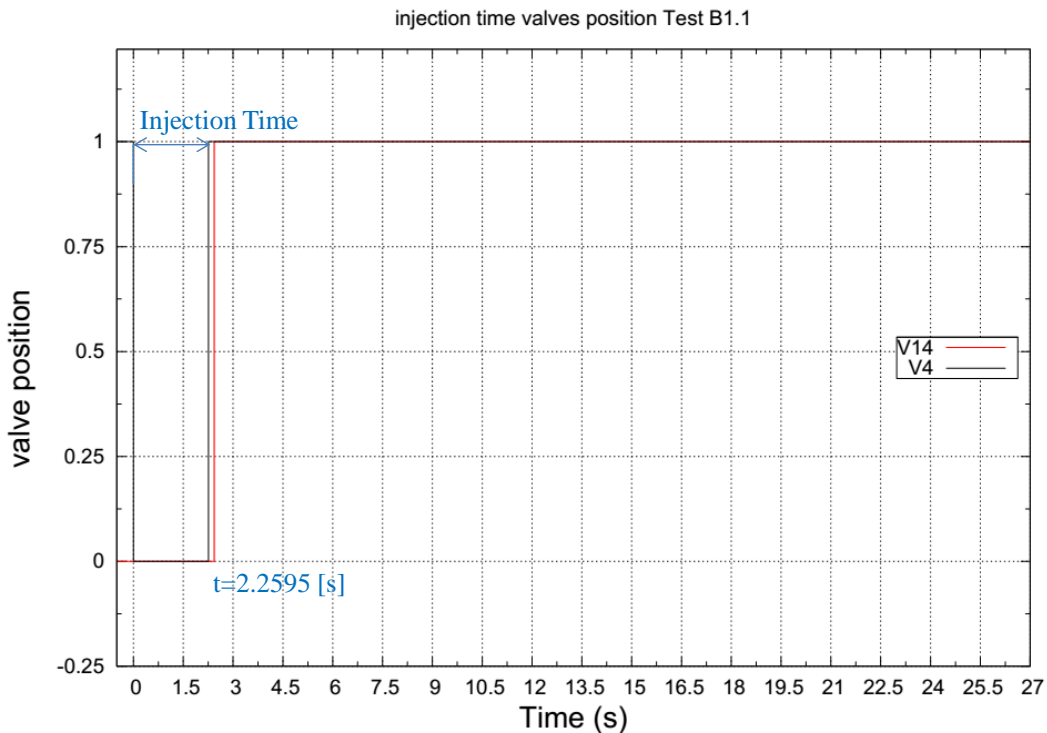


Figure 6.3 – Test B1.1 valves V4 and V14 position

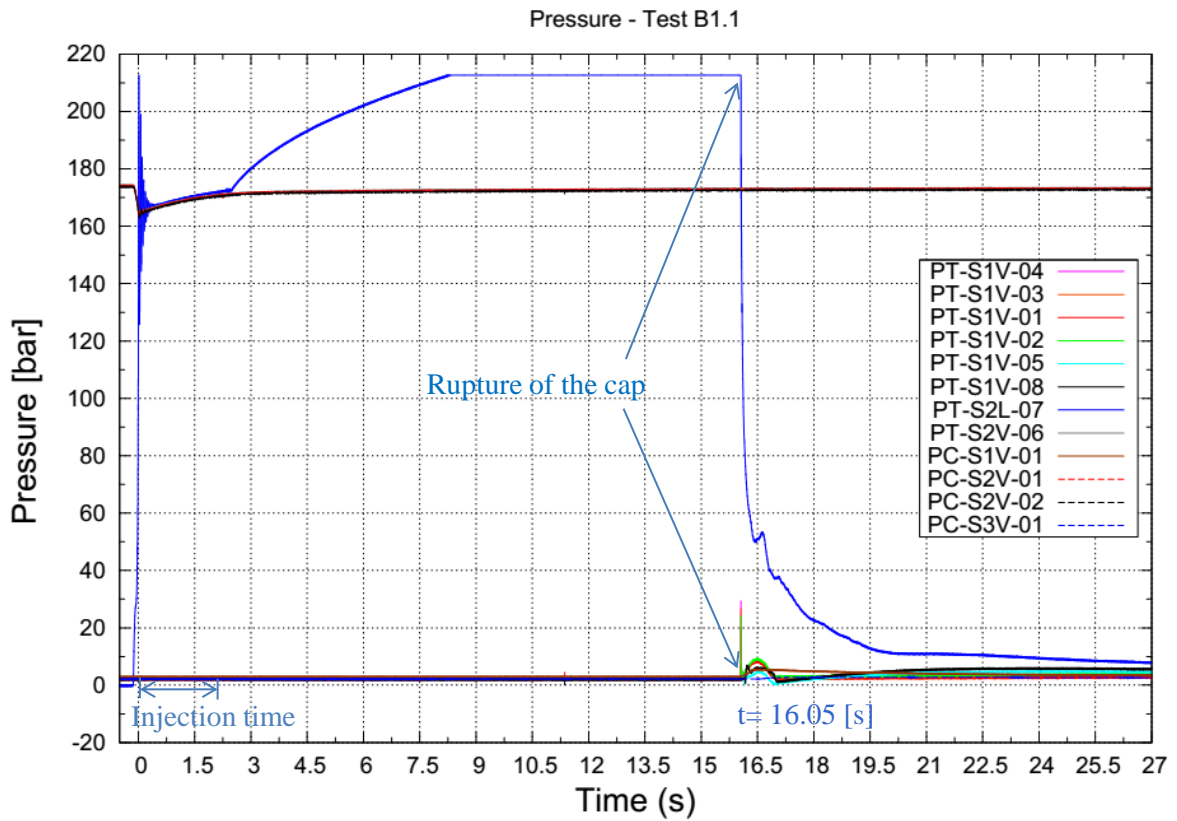


Figure 6.4 – Test B1.1 pressure trends in injection line, S1 and S3

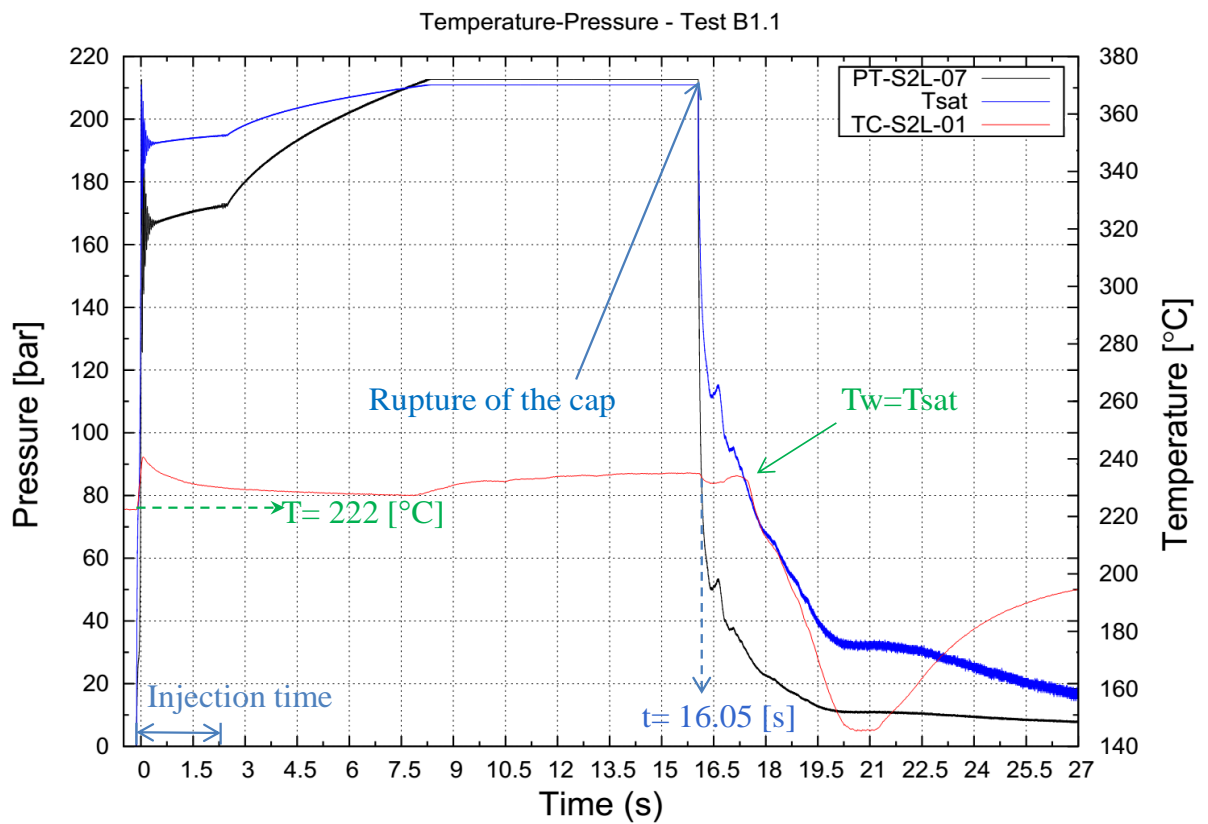


Figure 6.5 – Test B1.1 pressure and temperature trends in injection line

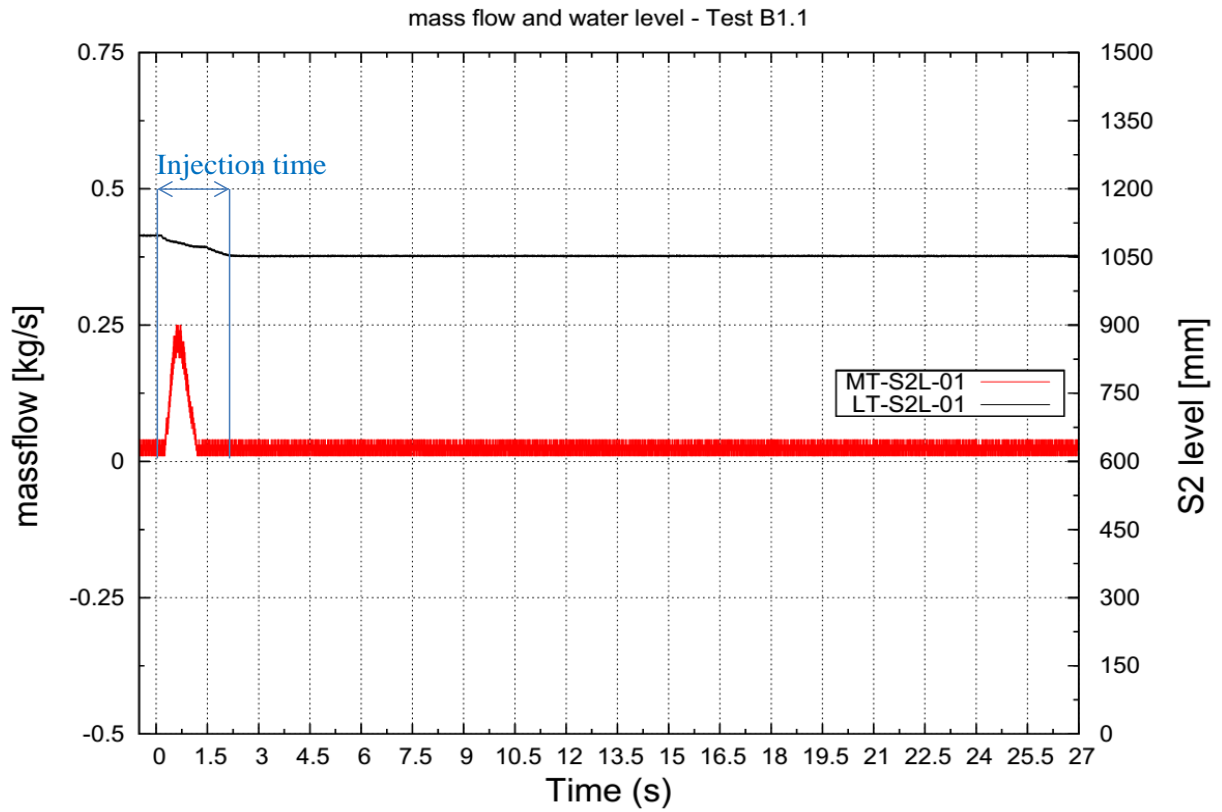


Figure 6.6 – Test B1.1 S2 level measurement and mass flow trends

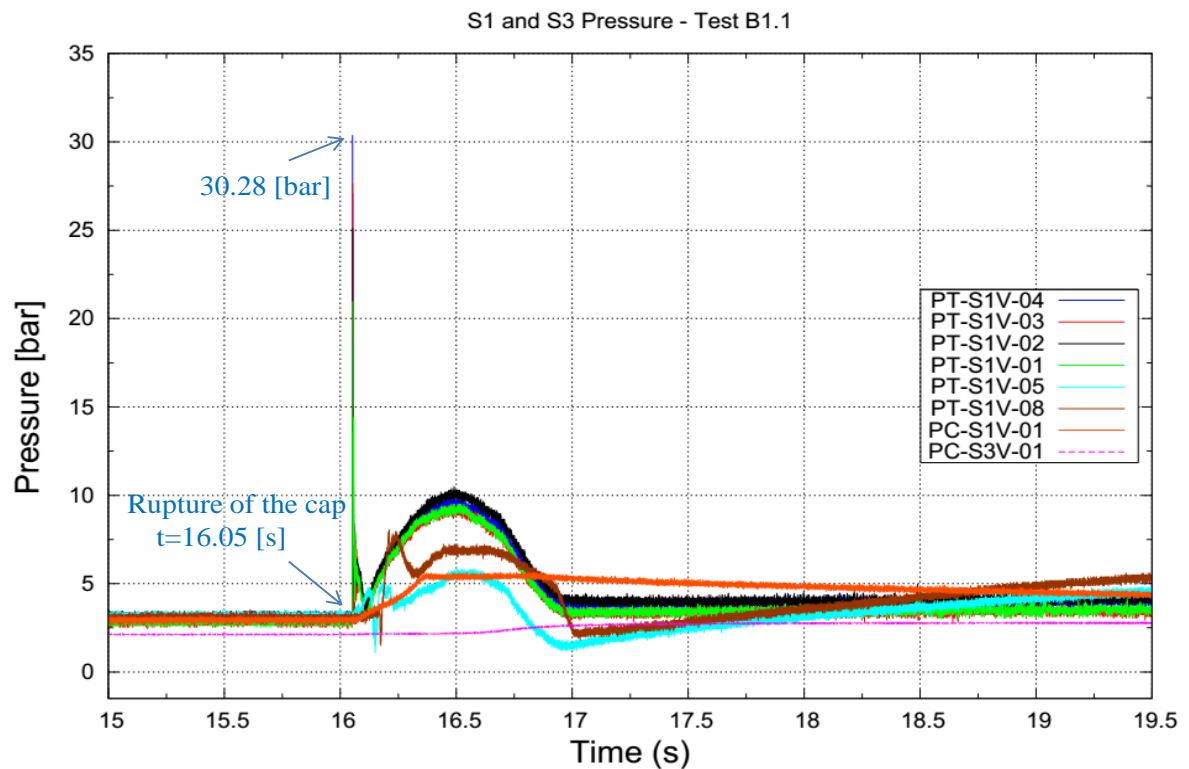


Figure 6.7 – Test B1.1 pressure trends in S1 and S3

S1 PT zoom - Test B1.1

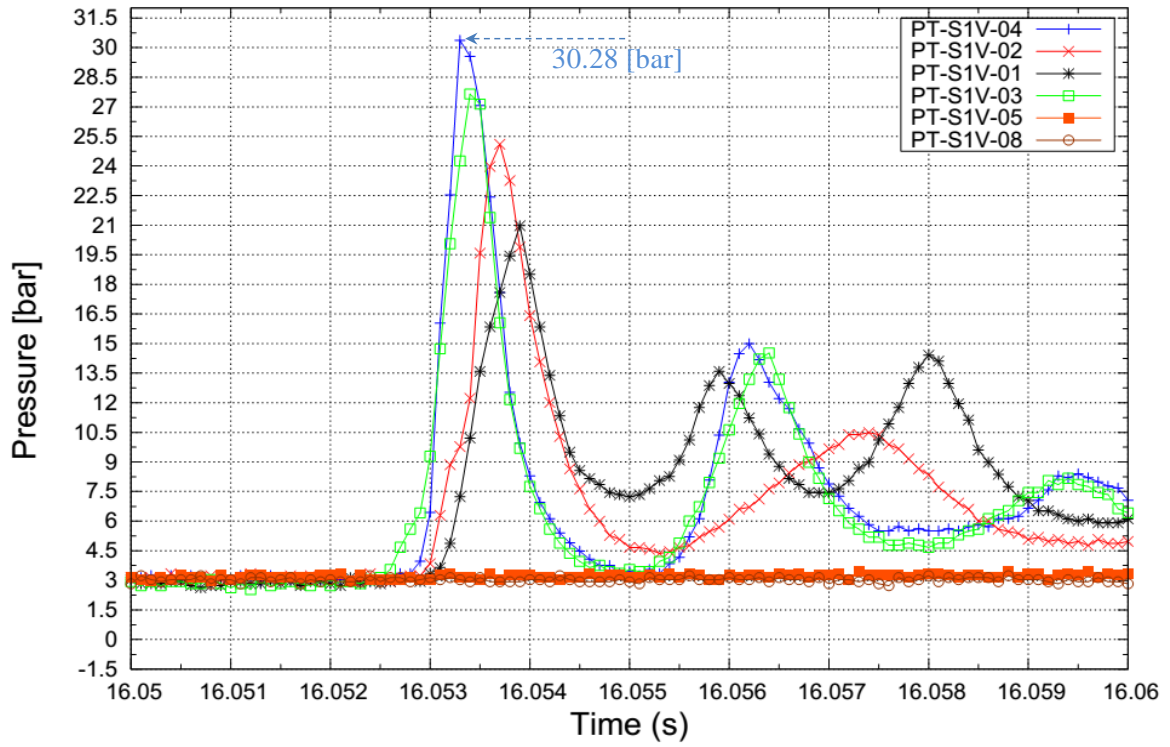
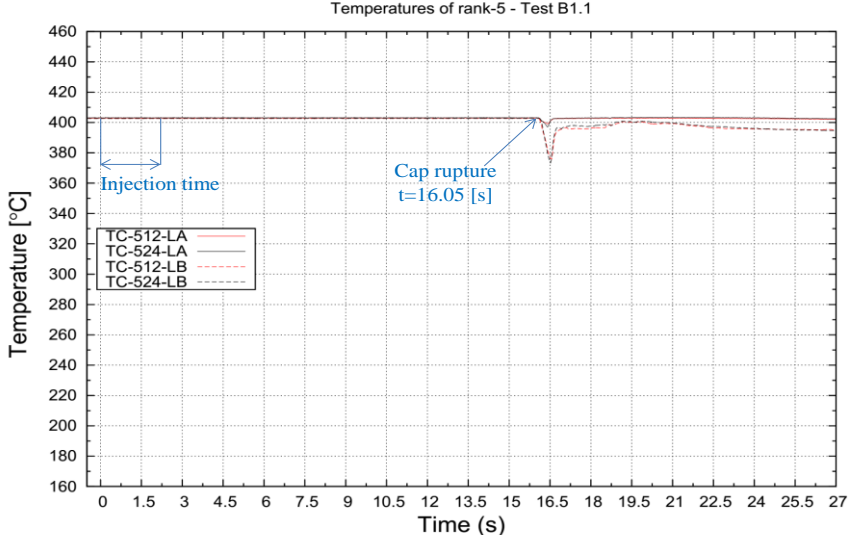
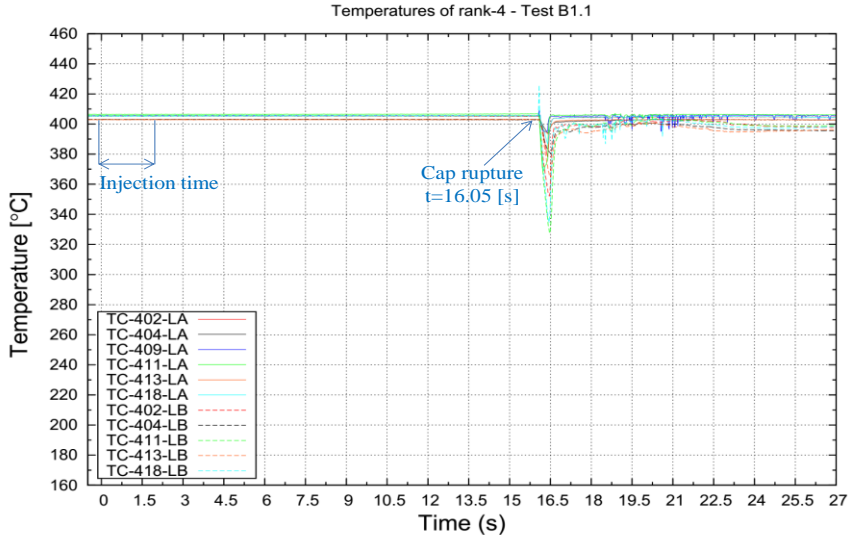
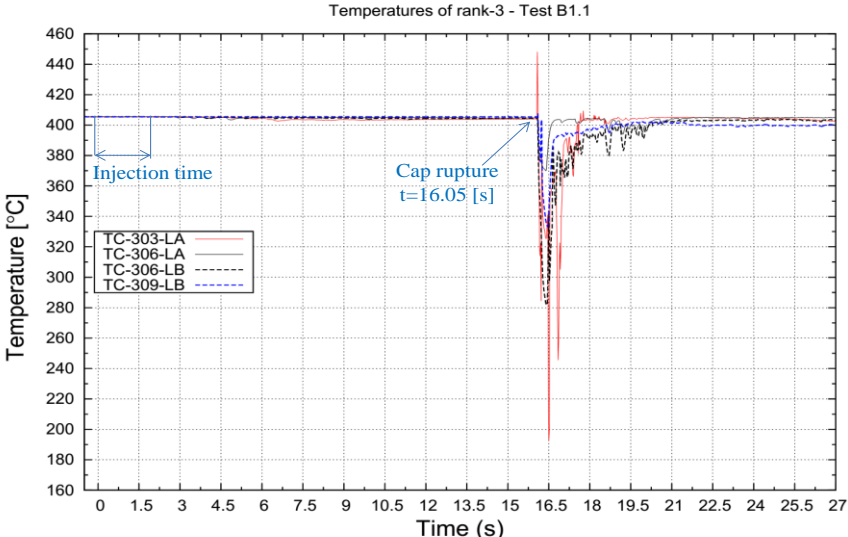
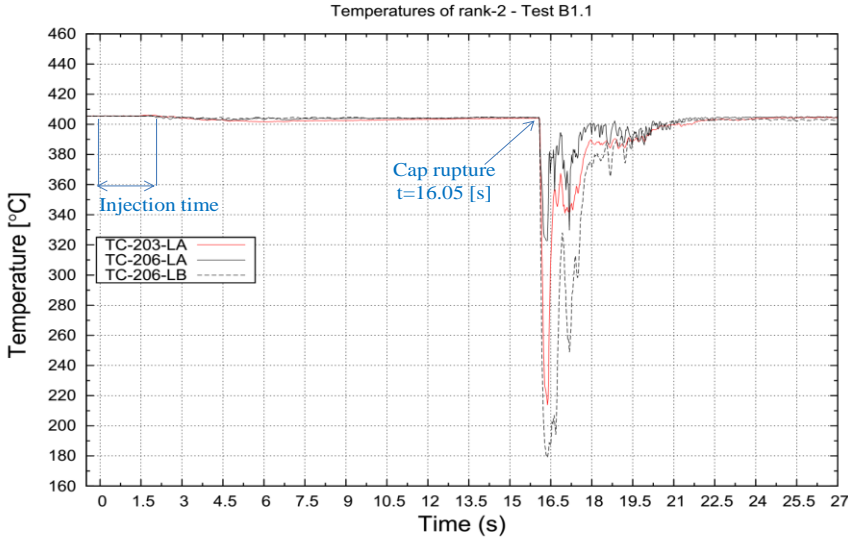


Figure 6.8 – Test B1.1 zoom of pressure peak in S1

Temperature trends



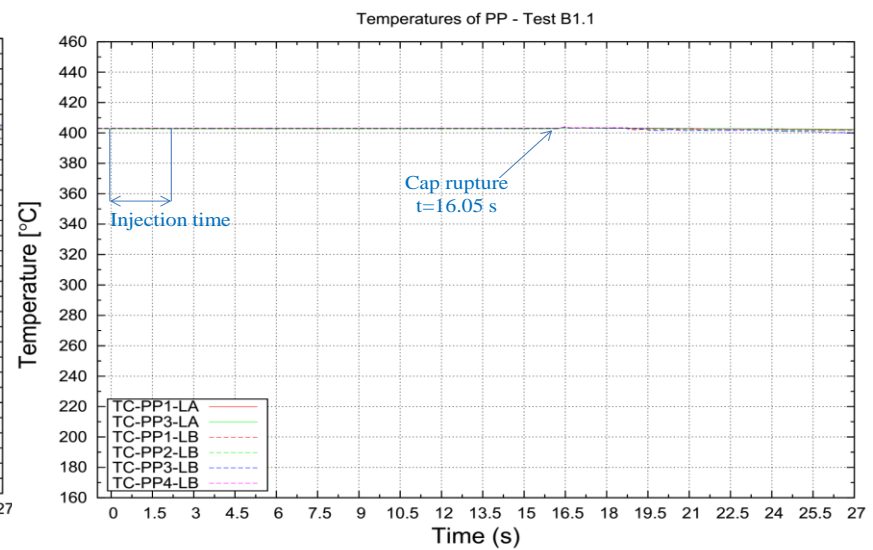
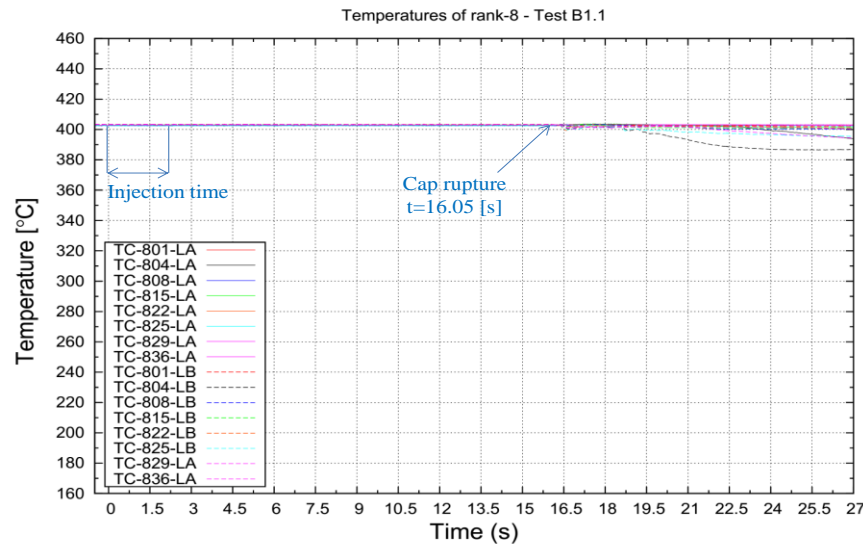
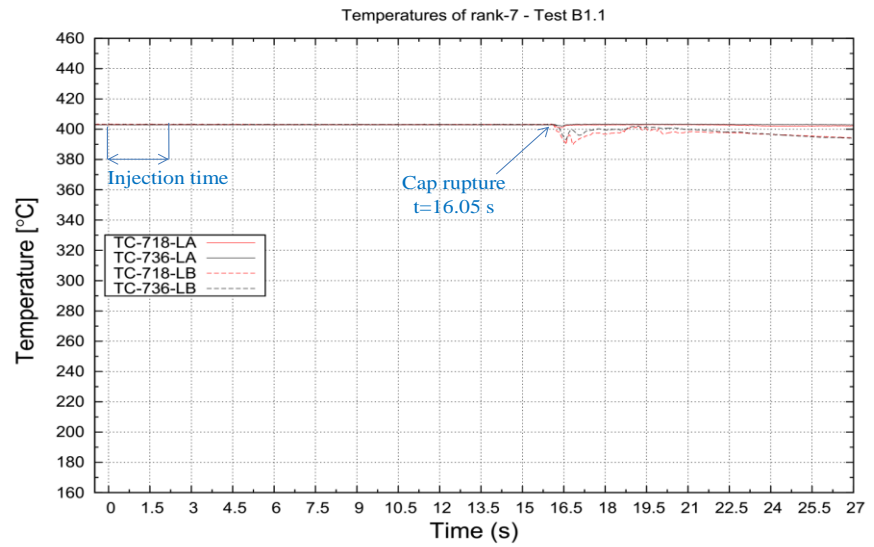
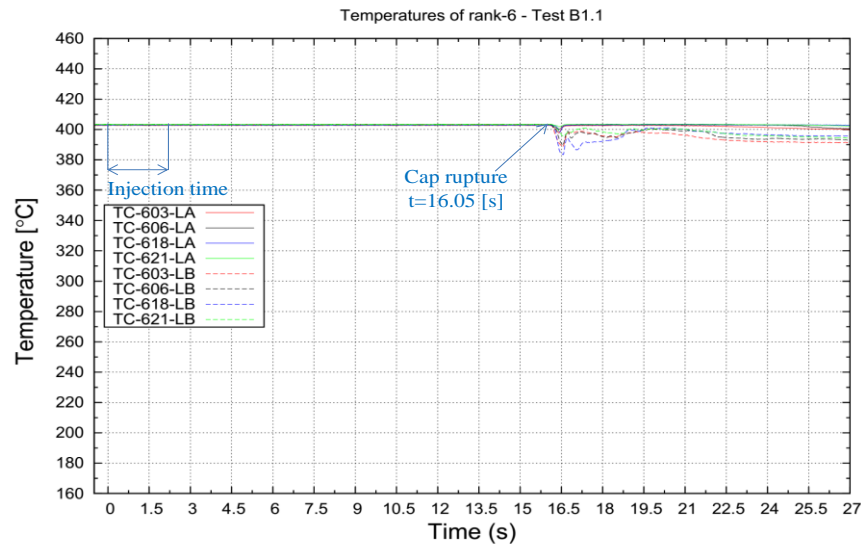
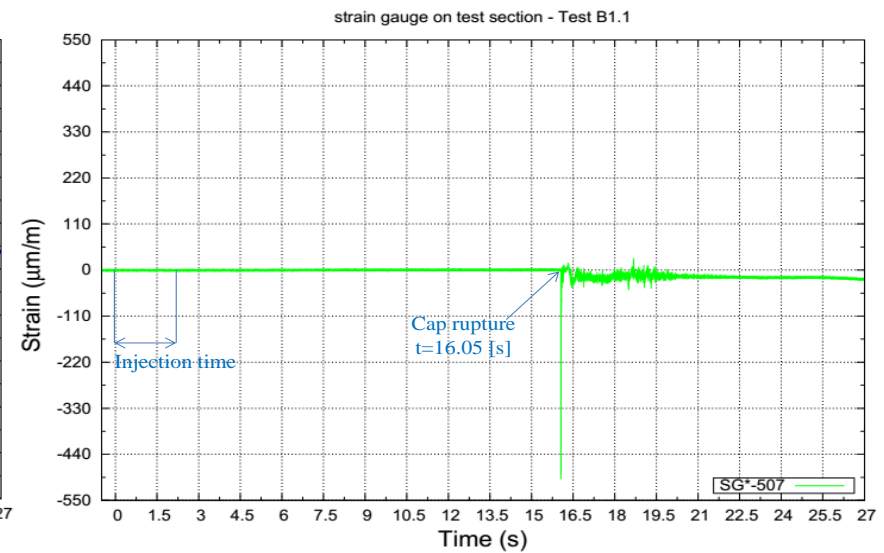
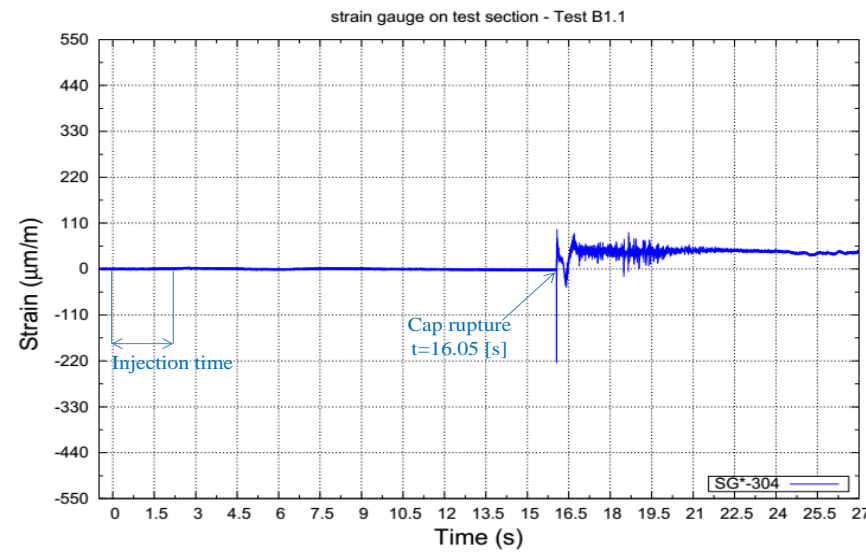
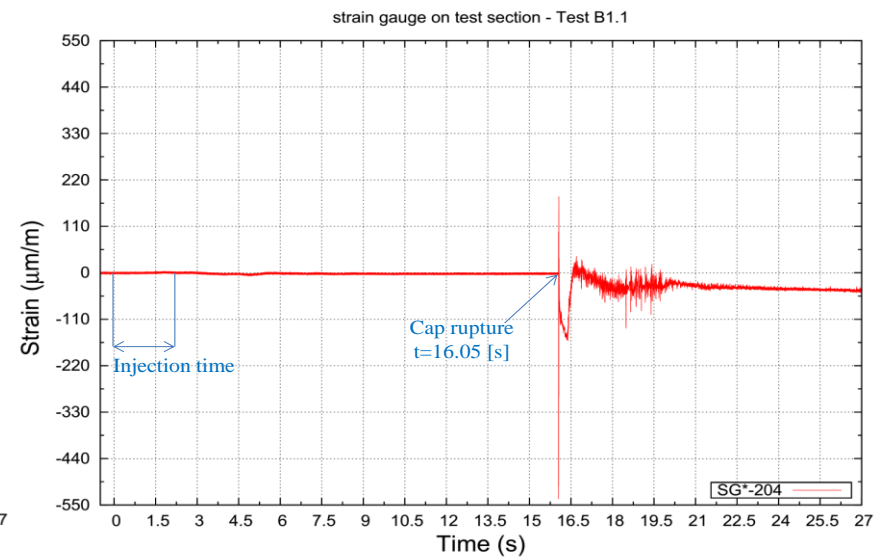
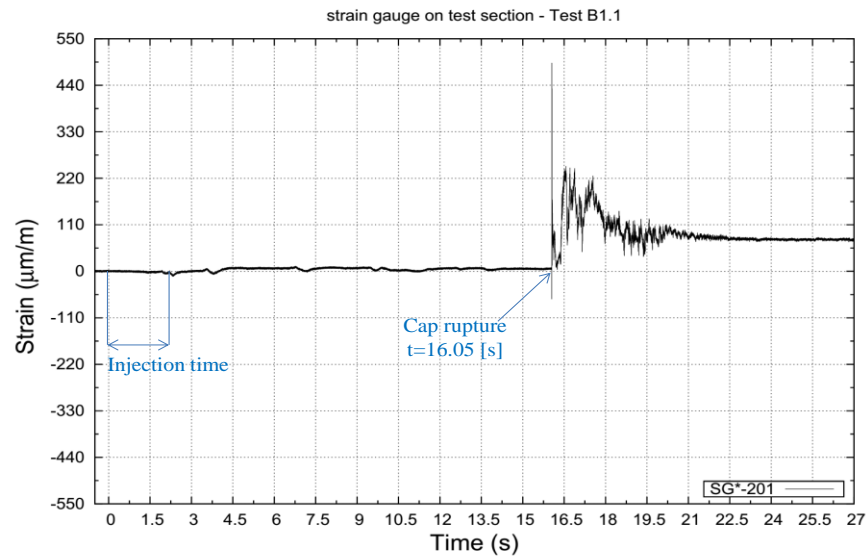


Figure 6.9 – Test B1.1 temperature trends of the ranks and internal surface of LEADER test section

Strain trends



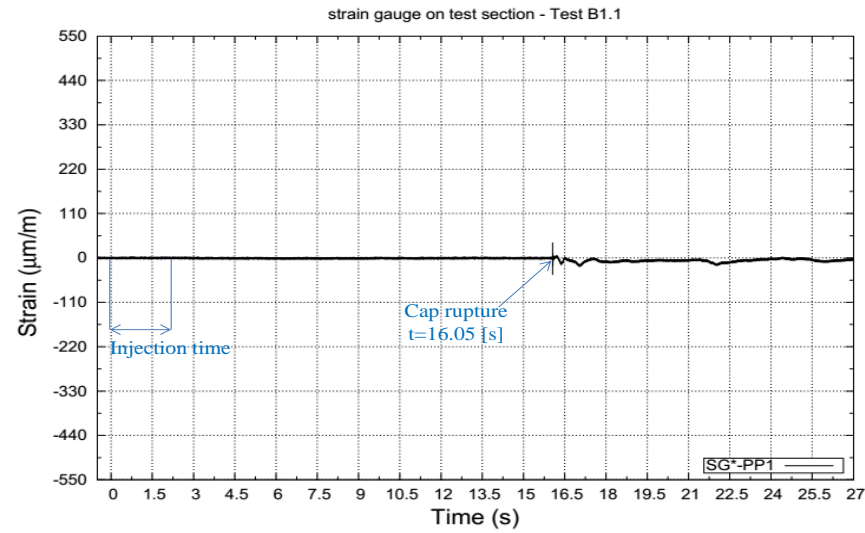
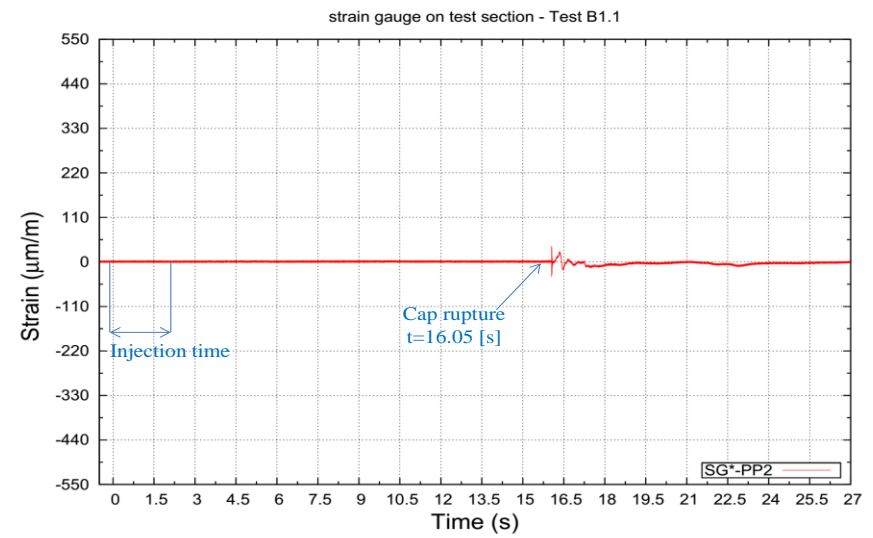
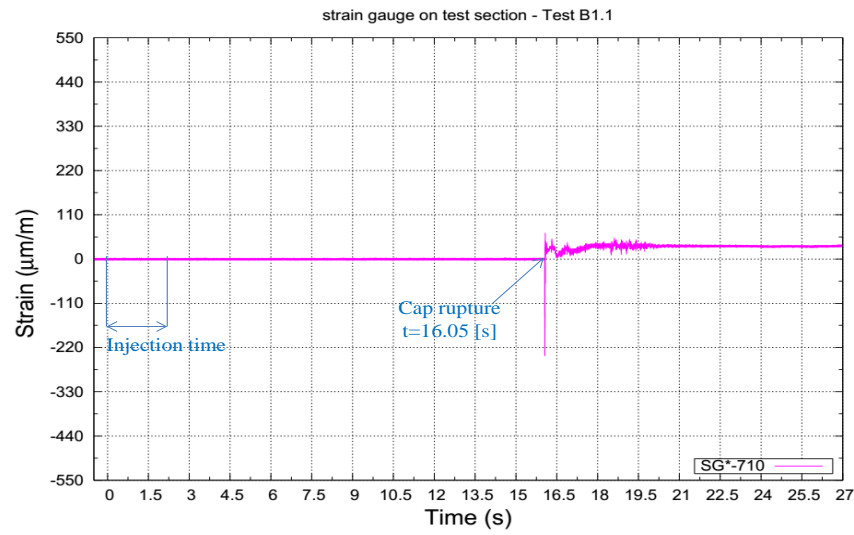


Figure 6.10 – Test B1.1 LEADER test section strain gauges strain trends

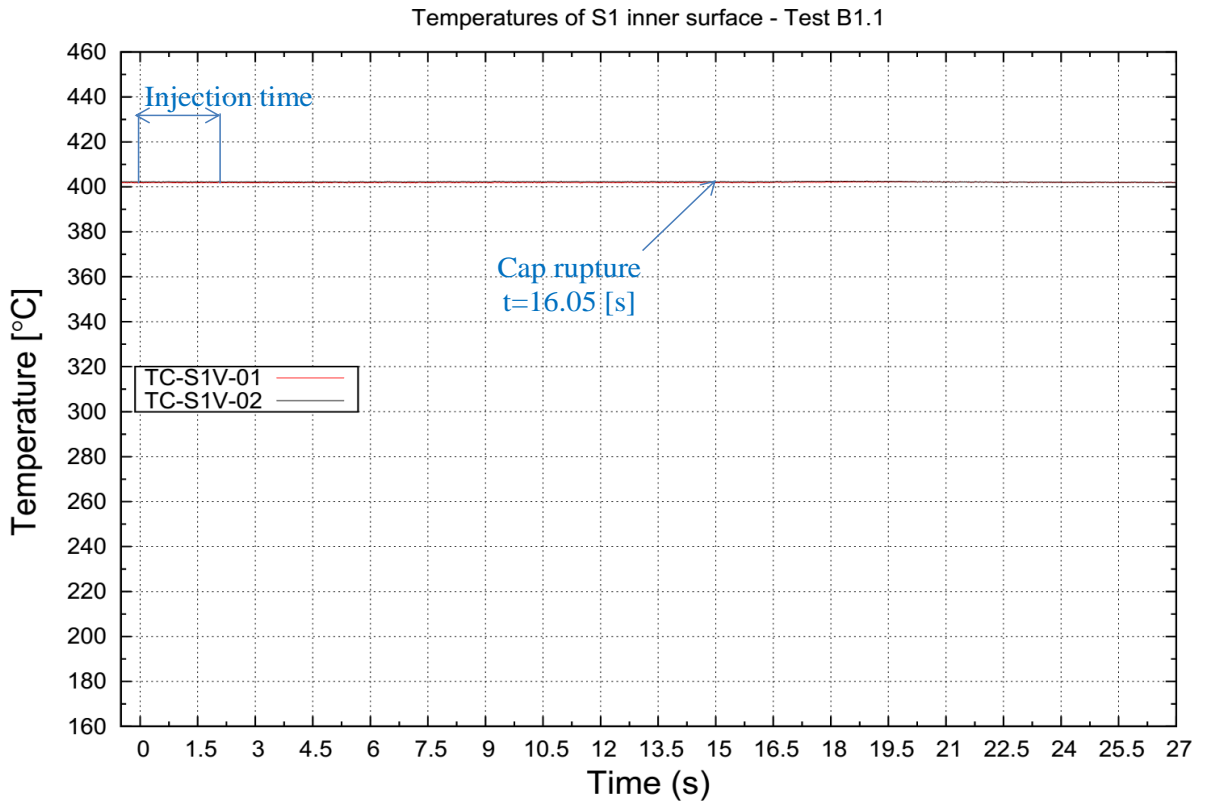


Figure 6.11 – Test B1.1 S1 internal surface temperature trends

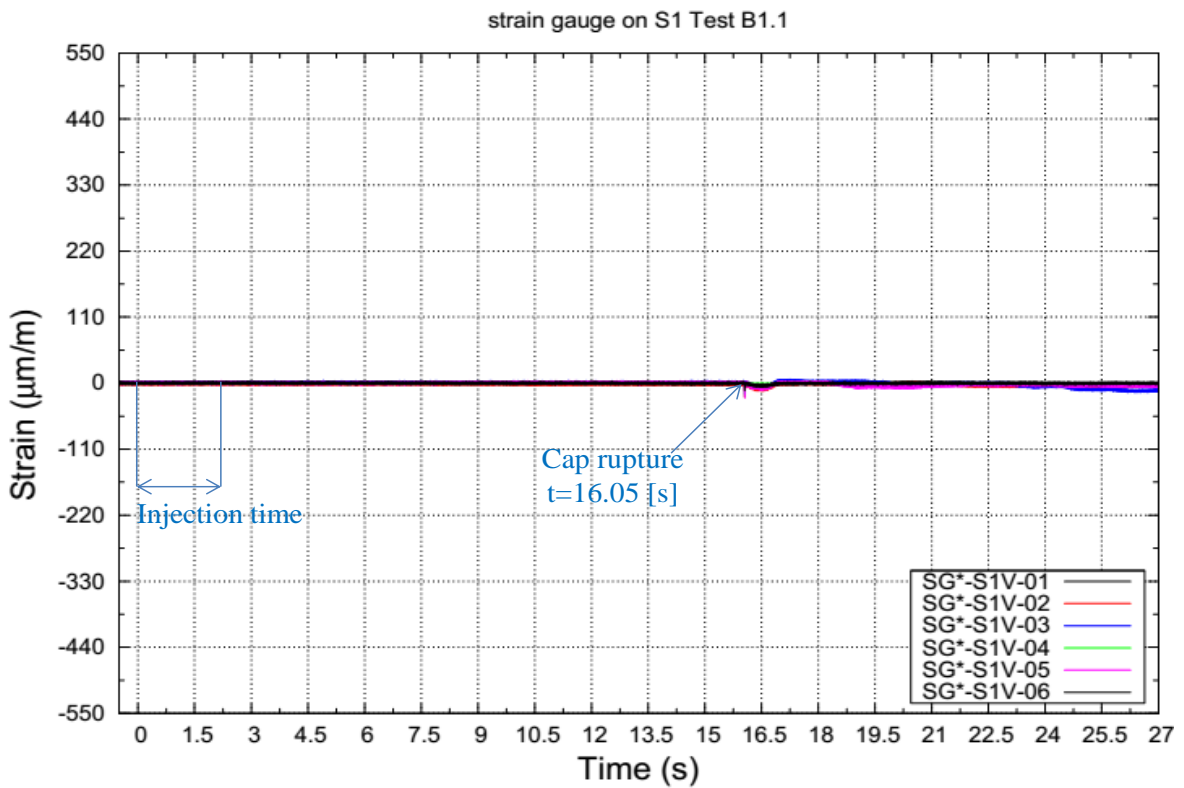


Figure 6.12 – Test B1.1 S1 internal surface strain trends

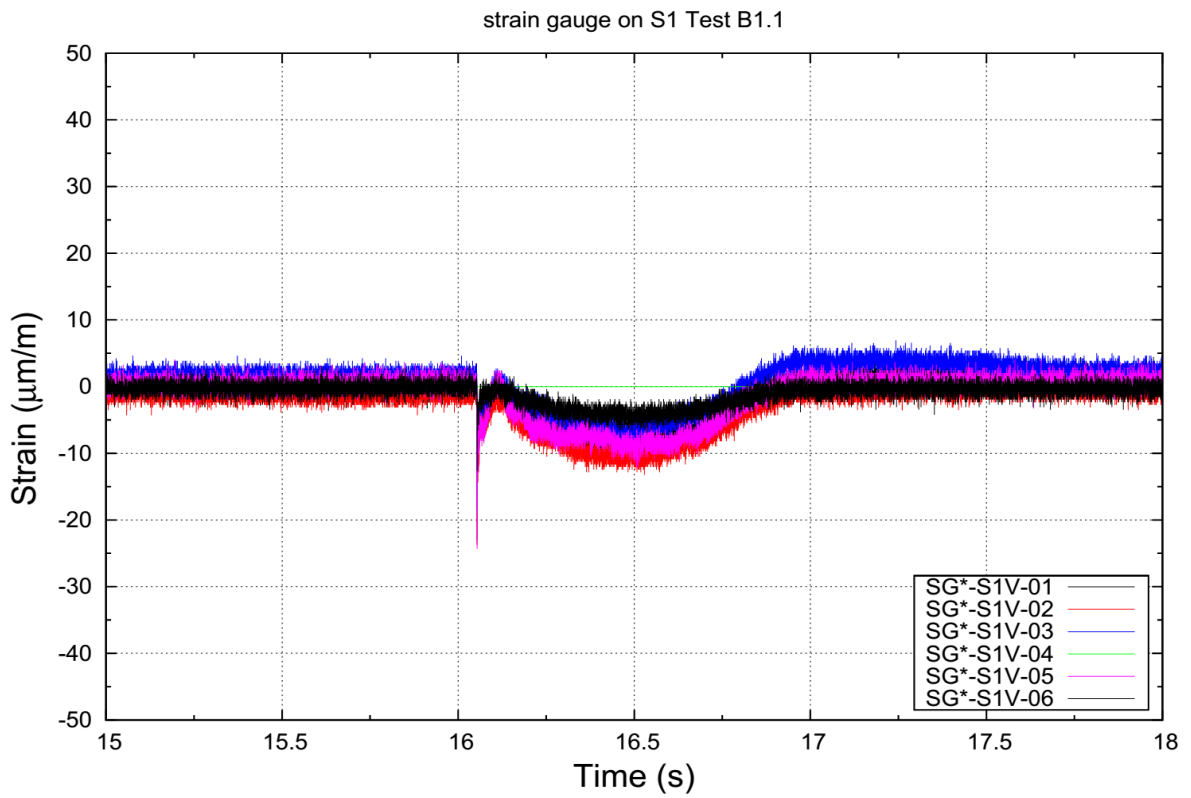


Figure 6.13 – Test B1.1 S1 internal surface strain trends zoom

6.1.4 Relap5 simulation of water injection line

The objective of the analysis is to investigate the water injection line during injection and to know the conditions of injected water during the test B1.1. The pressure transducer during the test reached, for two times, limit value and it remains for about 10 seconds in this condition before the break of the cap.

RELAP5/MOD3.3 input discussed in section 5.1 has been implemented with thermal structures at a constant temperature equal to 400°C to simulate the injection device and the heat exchange between LBE and water. The injector device was also modified according with the new LEADER design. Figure 6.14 reports a simplified scheme of the model with focus on the implemented modeling changes. Boundary and initial conditions were implemented according with the available experimental data: the pressure in S2 measured by PC-S2V-01, time of opening and closure of valves. The results obtained are compared with the experimental data in Figure 6.15. The pressure calculated by RELAP5/MOD3.3 is slightly overestimated in the first stage during the increase caused by the closure of injection valve. A slight underestimation is observed in the final part. The trend obtained by the simulation confirmed however the correct operation of the pressure transducer. It may be argue that the final pressure value in the experiment is higher than 212 bar calculated by RELAP5/MOD3.3 accordingly with the pressure measurement.

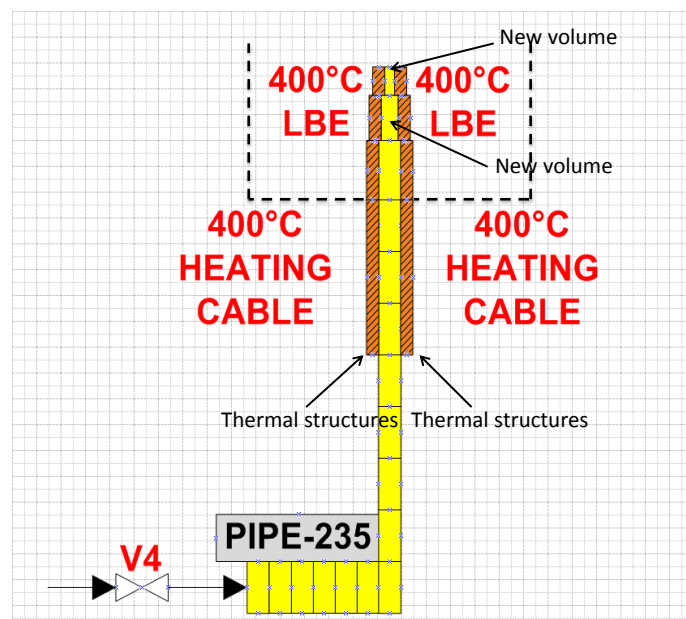


Figure 6.14–RELAP5 input implementation for testing pressure increase in water injection line of LIFUS5/Mod2 facility in Test B1.1

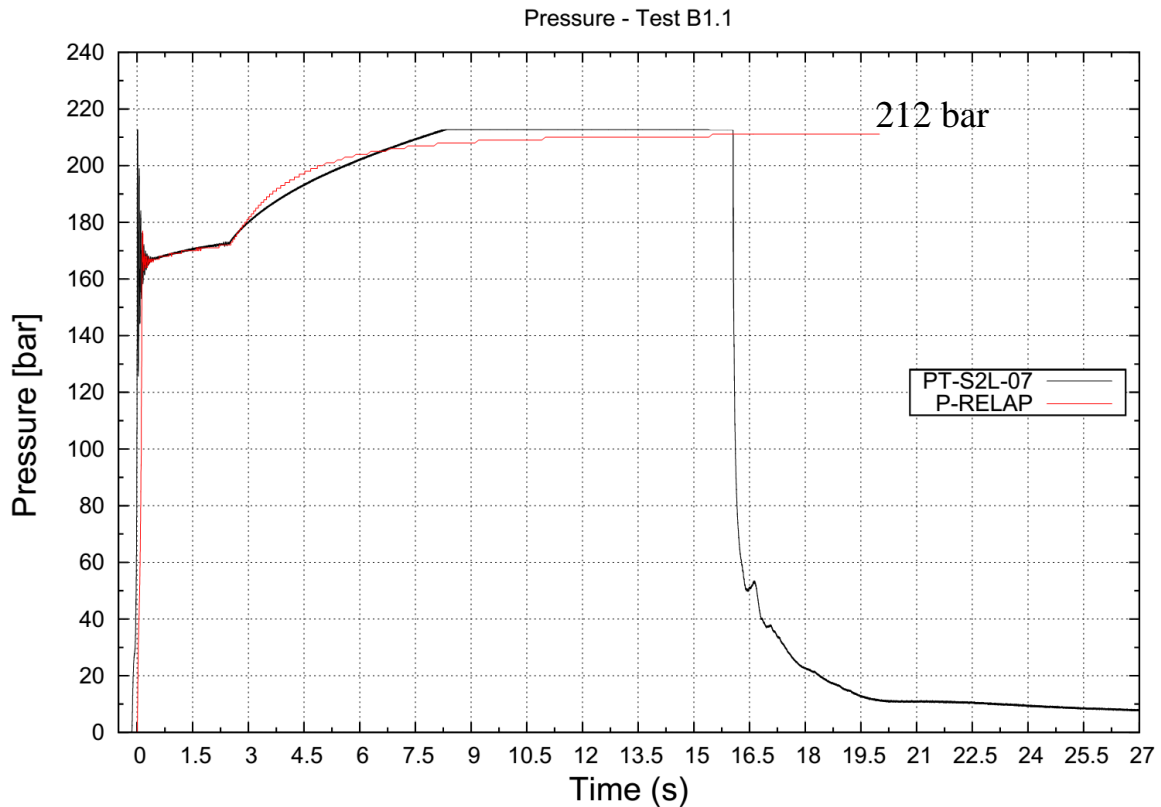


Figure 6.15 – RELAP5 and experimental water injection line pressure trends in Test B1.1

6.1.5 Post-test analysis of Test B1.1 by SIMMER-III code

The model developed of the entire LIFUS5/Mod2 facility in the LEADER configuration by means of SIMMER-III code and the simulation of Test B1.1 are described in this section.

6.1.5.1 Nodalization description

The model of LFUS5/Mod2 facility with the LEADER test section is developed starting from the model THINS used for the analysis of Test A1.2_2 (section 5.2). The updated model consists in a domain of 20 radial and 76 axial cells (Figure 6.16). LBE is represented in red, the water in blue, the argon and air (cover gas) in white and the non-calculation regions in light green. The color black is added to identify the metallic structures of LEADER test section and the thermal structures (can wall) implemented to simulate the heat exchange between the hot tubes surface and the water in the water injection line before the breaking of the cap. This is modeled by a segment 320 mm long with the same radius of the injection line. The heat exchange between the thermal structure of the injector are simplified. These structures are implemented at a constant temperature of 400°C. The water systems (S2 and the water injection line) are maintained as in THINS configuration.

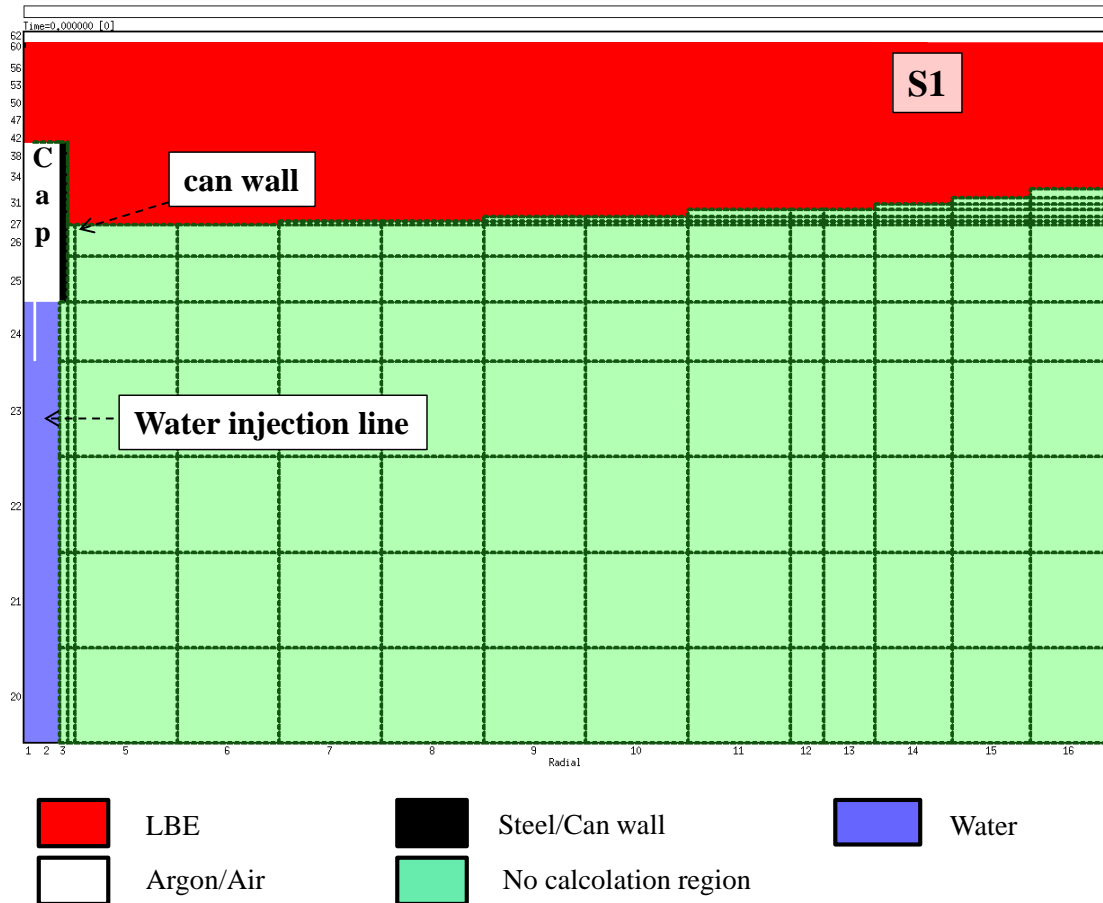


Figure 6.16 – cap and can wall modeling

The model of the test section has a complex structure. The rationale of the model is shown in Figure 6.17 and Figure 6.18. This is based on concentric circumferences. To simulate the various ranks of tubes, identified by regular hexagons, a pairs of circumferences (indicated in blue color in the Figure 6.18) form toroidal cells with a thickness equal to the pitch of the lattice. Each toroidal cell includes a volume fraction of steel pin (SIMMER-III code structural component used to simulate the nuclear fuel). In this way, the obstacles (tube) of the test section are simulated. The ninth rank of tubes is considered in previous ranks to avoid interference between the structures caused by geometric approximations made.

The holes of the perforated shell (see in Figure 6.17) are simulated considering ten toroidal cells of LBE, positioned at the same heights of the ten rows of holes and preserving the reference flow area of the test section.

The pipe 3” sch 160, connecting S1 with S3 is simulated with an inner radius slightly reduced due to the constraints imposed by the dimensions of the grid. This approximation causes an error in modeling the flow area of about 20%.

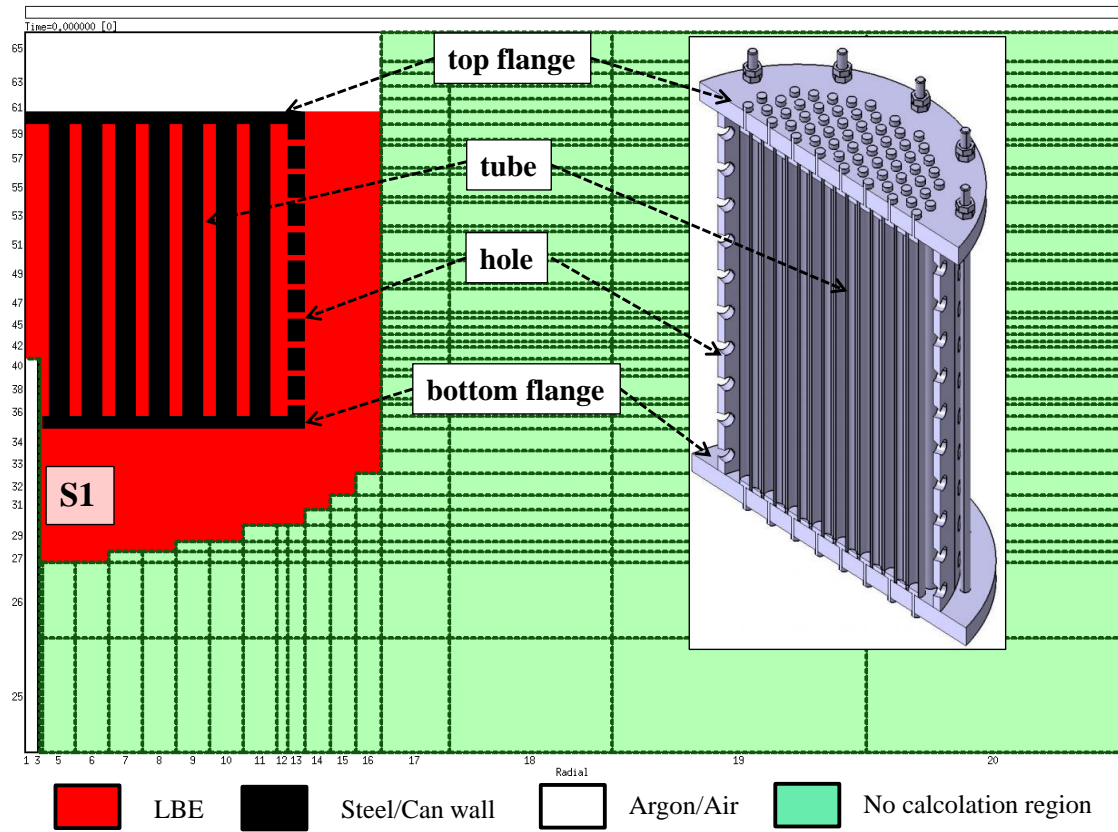


Figure 6.17 – LEADER test section modeling

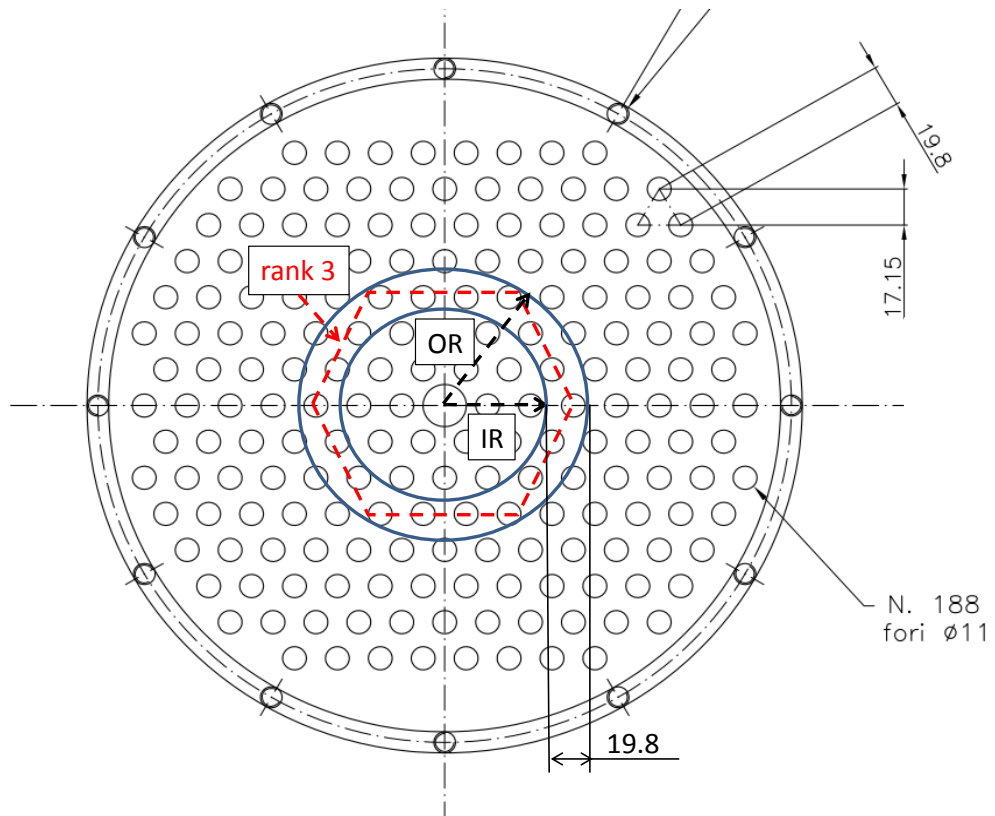


Figure 6.18 – example of rank 3 simulation procedure

The height of the connecting tube is preserved, but the horizontal part is not simulated because it would origin distortions in the dynamic of the transient due to modeling constraints imposed by the limit of the code to work in axisymmetric. The modeling is therefore based on imposing equivalent concentrated pressure drop of all tubing in the vertical section. S3 is implemented preserving the volume, but changing the area and height.

The sketch of SIMMER-III model is shown in Figure 6.19.

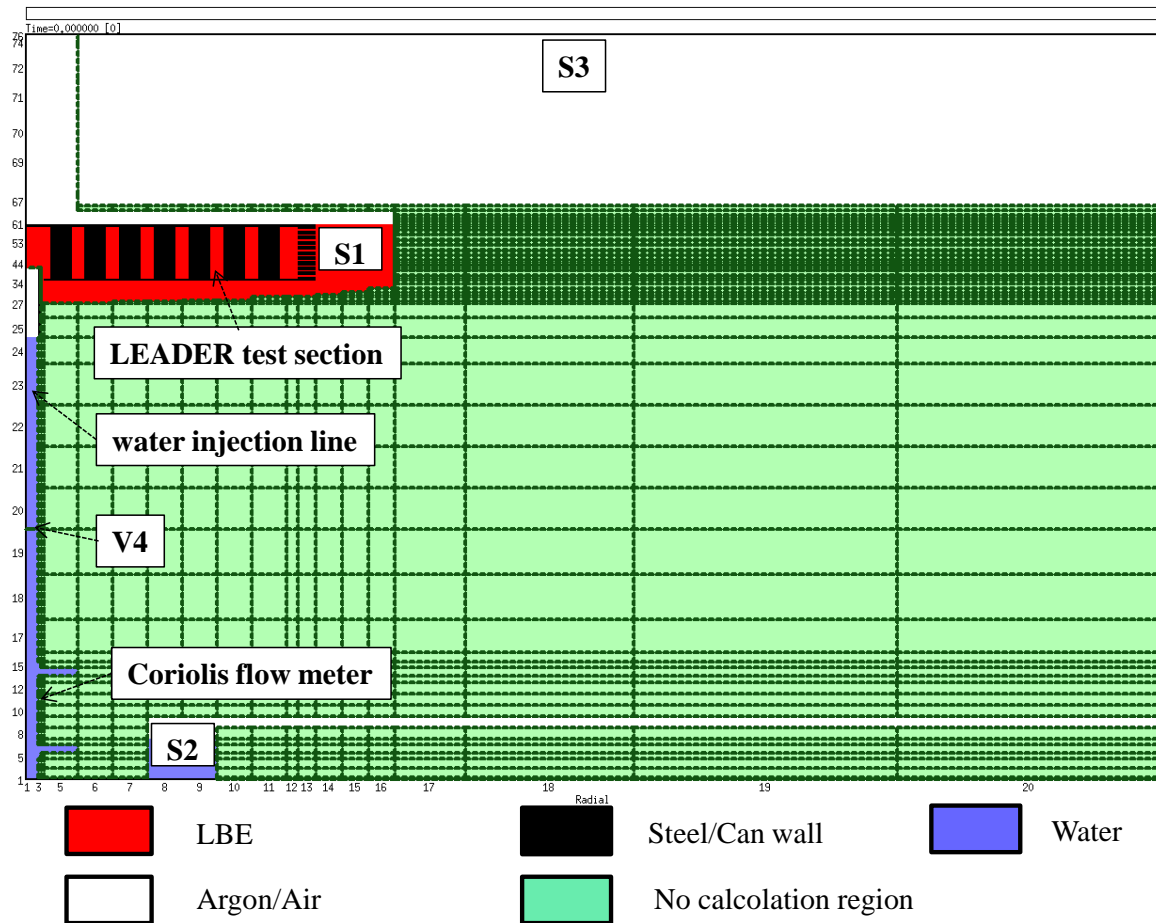


Figure 6.19 – LUFUS5/Mod2 with LEADER test section model

6.1.5.2 Calculation set up and results

The simulation of Test B1.1 is performed thanks to the support of RELAP5/Mod3.3 code. Indeed, the duration of the test would imply an excessive computational time. Therefore, the initial TH conditions are calculated with RELAP5/Mod3.3 (section 6.1.4) and implemented in SIMMER-III model. SIMMER-III simulation starts with the rupture of injector cap.

The section of water injection line between valve V4 and the cap is divided into four regions (see Figure 6.20) having the following thermo-hydraulic conditions:

- I. Single phase water at 210.5 bar and 260°C;
- II. Single phase water at 210.5 bar and 307°C;
- III. Two phase mixture at 210.5 bar with a title value of 85% and
 - a. Single phase water at 352°C;
 - b. Single phase vapour at 402°C.
- IV. Single phase vapour at 210.5 bar and 402°C..

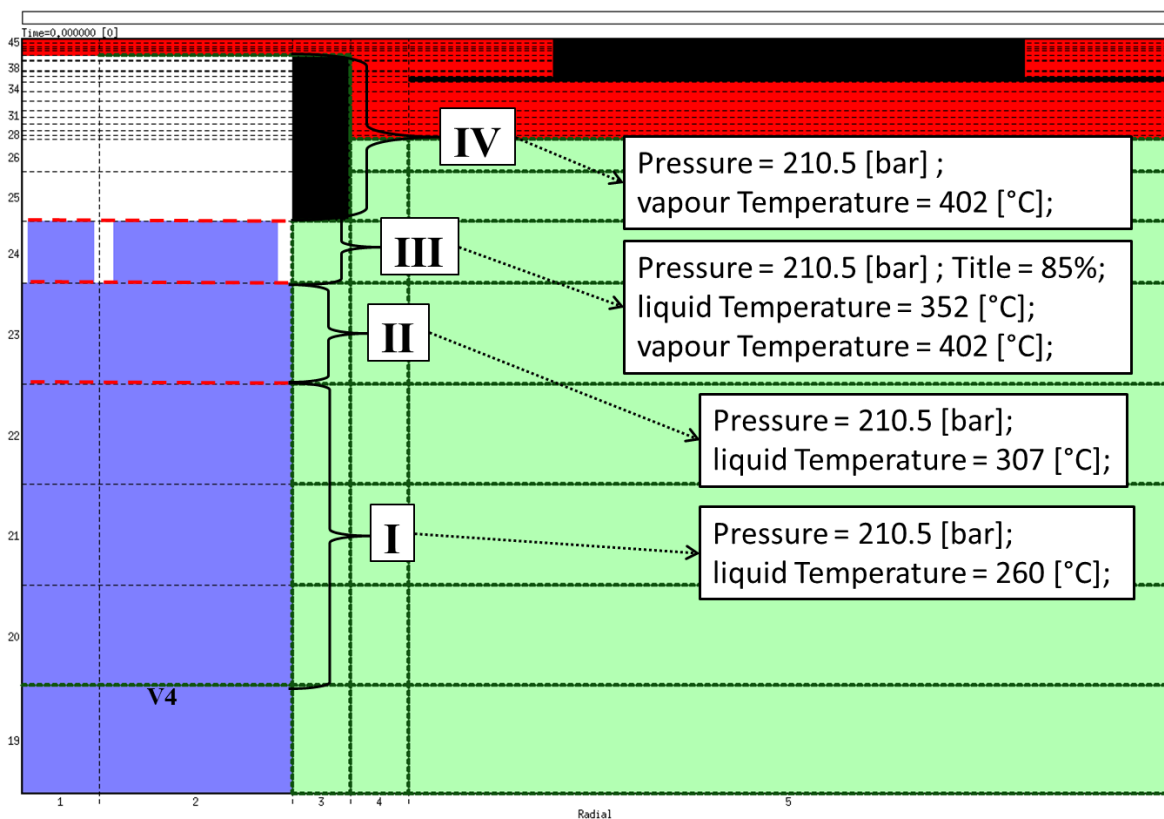


Figure 6.20 – Test B1.1 water injection line conditions before cap rupture

The transient starts when the injection cap is broken with the valve V4 closed. The injection orifice has a diameter equal to 4 mm, simulated with the opening of a virtual wall of the same size.

The simulation is focused on the pressure trend in S1. The propagation of the pressure wave and the rapid evaporation, is the parameter that might affect the integrity of surrounding structures and therefore of interest from safety point of view. The achieved result is in Figure 6.21.

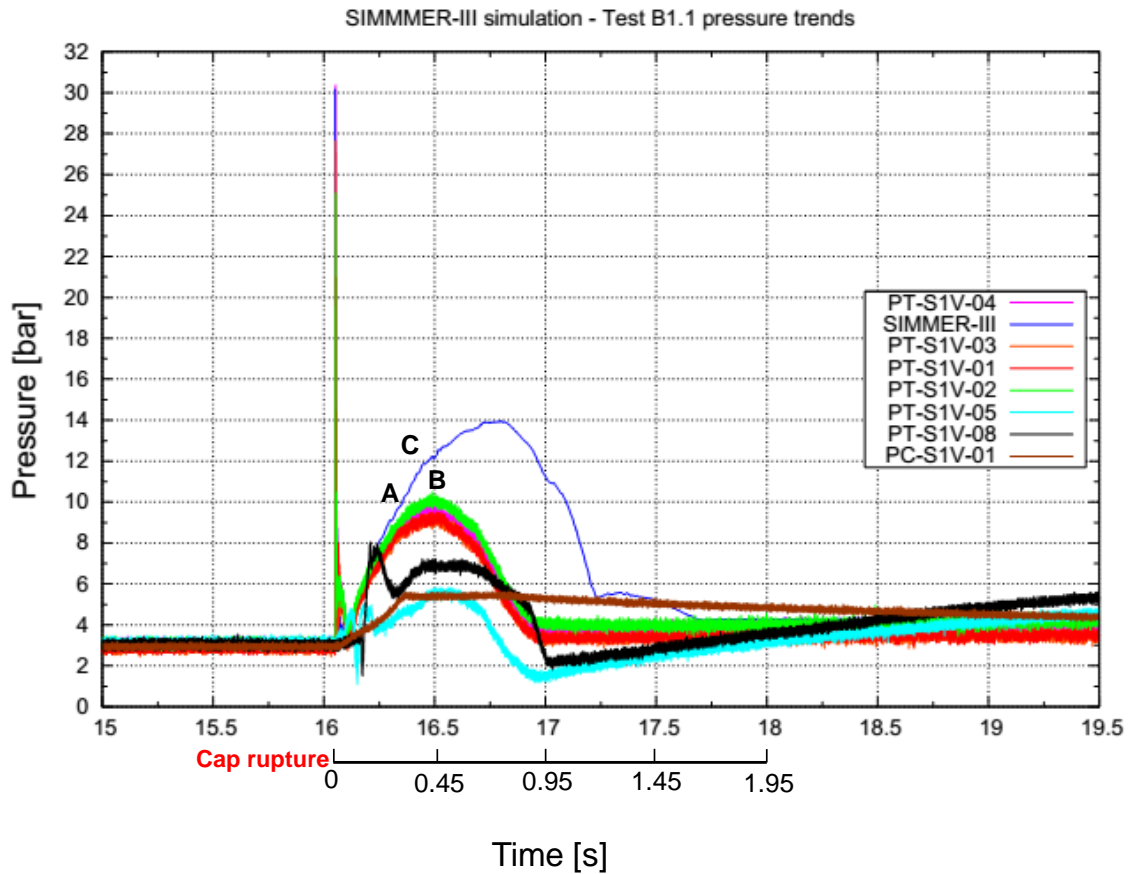


Figure 6.21 – Test B1.1 SIMMER-III/experimental pressure trends comparison

The pressure trend is calculated in S1, at the level where 3 out of 4 pressure transducers are installed (see the blue point in Figure 6.22).

The transient starts with an abrupt pressure spike in LBE due to injection. The code simulates the first measured pressure peak with an excellent accuracy (see Figure 6.23). This is an encouraging results considering that the initial and boundary conditions of this test are better defined than in any other LIFUS5 test.

Then, the liquid water evaporates causing a second pressure increase and pushing the LBE toward the dumping tank S3. The simulation shows a good agreement with the experimental data up to 0.3 seconds (point A in Figure 6.21). Indeed, the calculated pressure continues to increase, while the experimental data reach the maximum value of about 10 bar at 0.45 seconds from the beginning of the transient (point B in Figure 6.21). The experimental pressure measured at the end of the transient is stabilized at 3.6 bar. On the contrary the maximum pressure simulated by SIMMER-III is 14 bar achieved in delay, whereas the final pressure is about 4.1 bar.

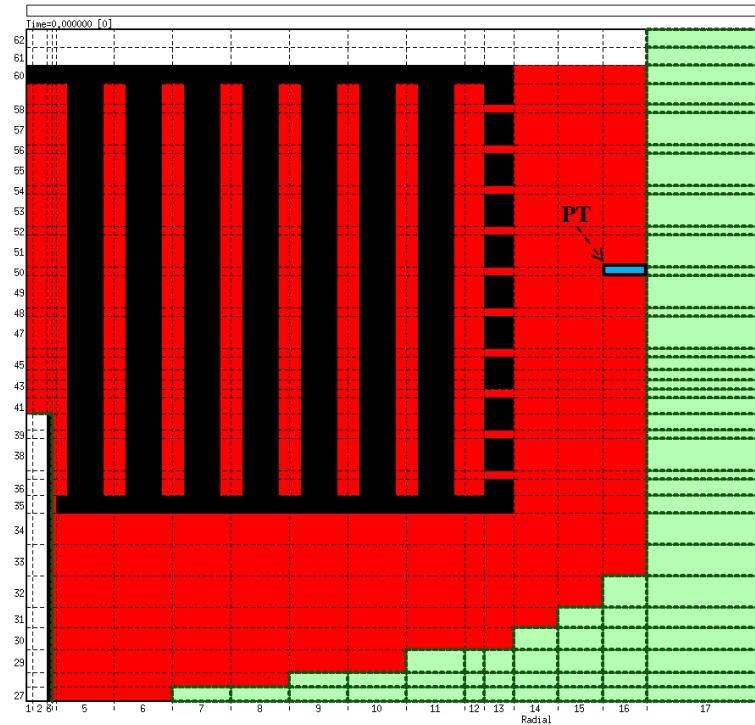


Figure 6.22 – measurement point in the code SIMMER-III

The different pressure trends are explained with the following two main reasons: 1) modeling performances (i.e. overestimation of pressure drop) of pipe connecting S1 with S3, as already discussed, and above all to the presence of stopper of LBE in the line and between the top flange of the test section and the main vessel S1 (see Figure 6.24 and Figure 6.25); 2) larger mass inventory of water entrapped in the injection line before the rupture of the cap. The second reason might be connected with the presence of few non-condensable gases in the injection line and with the higher average temperature of water at beginning of the transient.

The calculated pressure trend, before the stabilization lasts about 0.5 seconds more than in the experiment.

Regarding the quantity of LBE dragged in S3, the code overestimates this value (100 kg instead of 25 kg in the experiment). The difference might be connected mainly with modeling choices: the absence of the horizontal pipe between S1 and S3 in SIMMER-III. Other possible explanation is connected with the interfacial area and interfacial drag between the two fluids, two phases. This last hypothesis is based also on the observation that the speeds of the fluids (i.e. liquid LBE and water steam) are comparable. In principle, higher speed of vapor should be expected.

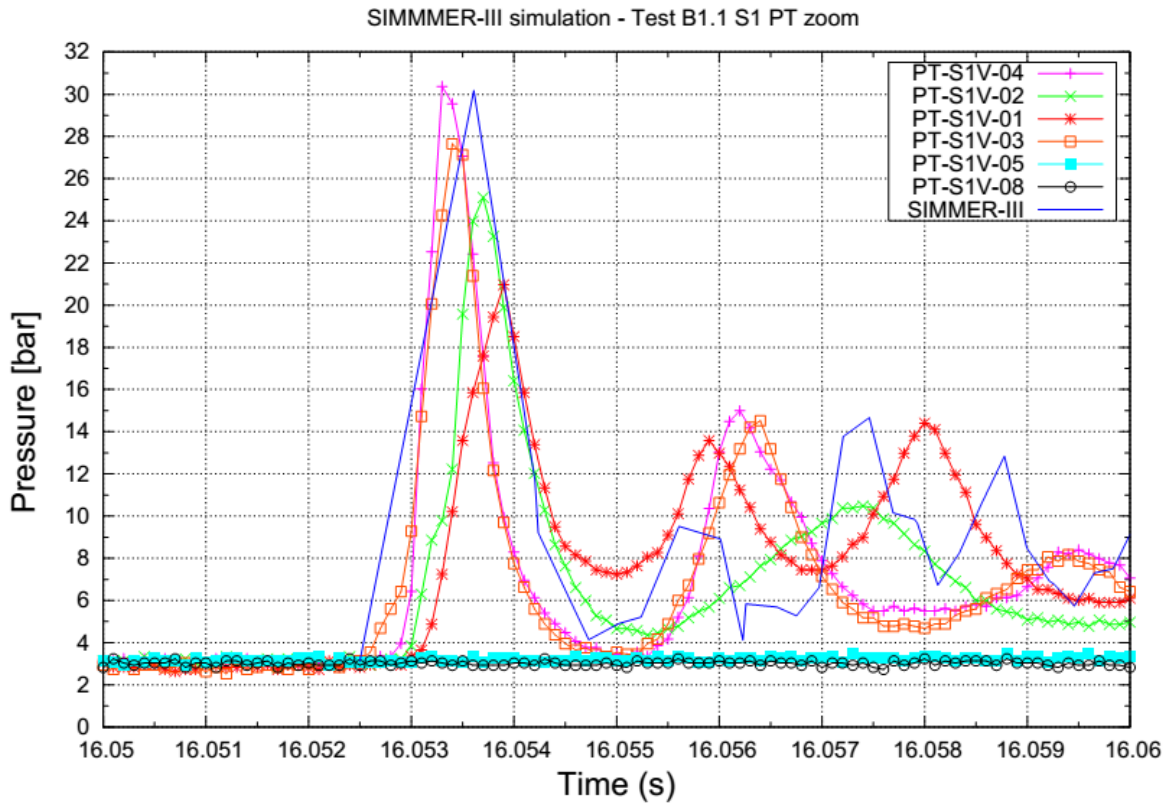


Figure 6.23 – Test B1.1 initial peak zoom

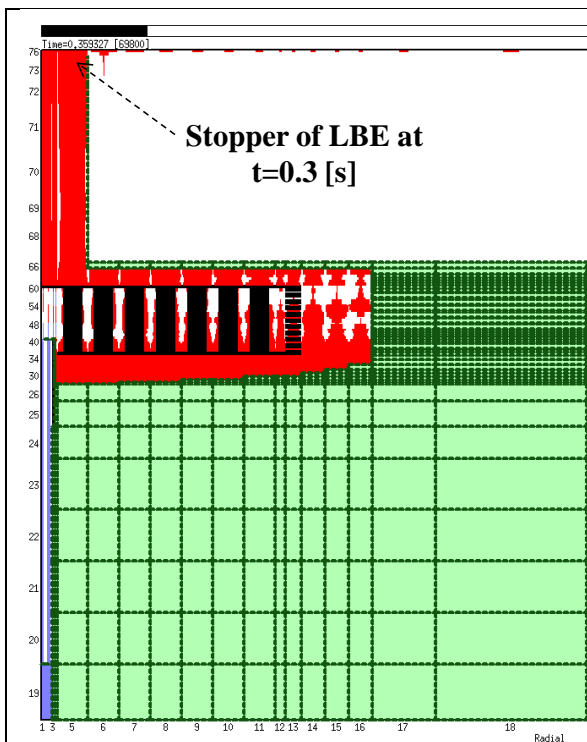


Figure 6.24 – situation at $t=0.3$ seconds

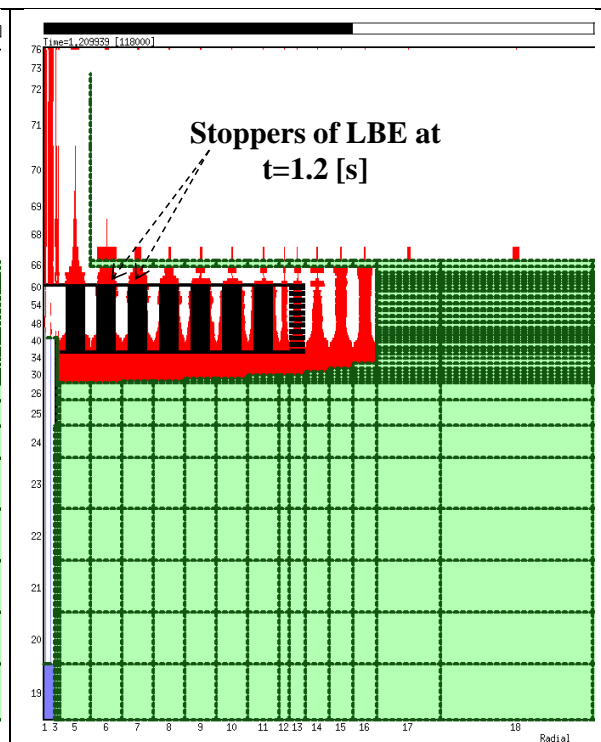


Figure 6.25 – situation at $t=1.2$ seconds

6.2 Test B1.2

The Test B1.2 is the second test effectuated on LIFUS5/Mod2 facility in the frame of LEADER project. The test is carried out in the morning of 14 November 2014. Compared to the previous Test B1.1 is provided a new injection water procedure, in order to guarantee the injection of a greater quantity of water respect to the previous test.

6.2.1 Test configuration

The test, is configured in a similar manner to the previous one (see section 6.1.1).

The relevant differences are:

- the water temperature is set to 270°C, compared to 260°C of Test B1.1;
- the heating cable CS-S2-06 is not activated due to a failure of the cable itself;
- the level reached by LBE above the test section during loading is equal to +20 mm compared to +10 mm of the previous test.

In Table 6.2 the set of initial conditions of Test B1.2 is shown.

6.2.2 Execution of the test

Regarding the execution of the test (see section 6.1.2) a single but significant change is implemented. In order to avoid the possibility of the injection of a small amount of water due to the delay in the rupture of the cap, after the V4 closure, a new control signal of the injection valve closure is chosen. It is correlated to the water level in S2 tank. When the water level decreases below a set value, which is required to the operator through synoptic before starting the injection procedure, the valve closes.

In Table 6.3, in the column called “actual” the real initial values of Test B1.2 are listed.

At the end of the test, as for the previous one, the tank S2 is emptied from residual water (0.5 l in Test B1.2) and the LBE transported in S3 because the interaction with water in S1 is removed (about 100 kg in Test B1.1).

#	LIFUS5/Mod2	Project FP7 LEADER			Test B1.1		Date 14-09-2014
		Parameter	ID	Unit	Design	Actual	
SYSTEM S1							
S1-1	P @ SoT	--	bar	1	1.2	--	
S1-2	T _{LBE} @ SoT	--	°C	400	402	--	
S1-3	LBE LVL (from test section top flange)	--	mm	0	20	<i>max + 20 mm</i>	
S1-4	Set temperature heating cable	CS-S1-01	°C	400	400	--	
S1-5	Set temperature heating cable	CS-S1-02	°C	400	400	--	
S1-6	Set temperature heating cable	CS-S1-03	°C	400	400	--	
S1-7	Set temperature heating cable	CS-S1-04	°C	400	400	--	
S1-8	Set temperature heating cable	CS-S1-05	°C	400	400	--	
S1-9	Set temperature heating cable	CS-S1-06	°C	400	400	--	
S1-10	Set temperature heating cable	CS-S1-07	°C	370	370	--	
S1-11	Set temperature heating cable	CS-S1-08	°C	220	220	--	
S1-12	P @ SoT test section tubes	--	bar	180	180	--	
SYSTEM S2							
S2-1	P in gas line @ SoT	--	bar	180	174	--	
S2-2	P @ SoT	--	bar	180	174	--	
S2-3	T @ SoT	--	°C	270	262	--	
S2-4	LVL @ SoT	--	mm	--	1128	--	
S2-5	Charged water vol.	--	l	8	8.6	--	
S2-6	Set temperature heating cable	CS-S2-01	°C	270	270	--	
S2-7	Set temperature heating cable	CS-S2-02	°C	270	270	--	
S2-8	Set temperature heating cable	CS-S2-03	°C	270	270	--	
S2-9	Set temperature heating cable	CS-S2-04	°C	270	270	--	
S2-10	Set temperature heating cable	CS-S2-05	°C	300	300	--	
S2-11	Set temperature heating cable	CS-S2-06	°C	broken	broken	--	
INJECTION SYSTEM							
O-1	Injection valve	--	--	V4	V4	--	
O-2	Injection time	--	s	--	5	--	
O-3	Injector nozzle orifice	--	mm	4	4	--	
O-4	Injection Nozzle ID	6	--	--	--	--	
SYSTEM S3							
S3-1	P @ SoT	--	bar	1	1.2	--	
S3-2	T @ SoT	--	°C	150	146	--	
S2-3	Set temperature heating cable	CS-S3-01	°C	220	250	--	
S2-4	Set temperature heating cable	CS-S3-02	°C	220	220	--	
S2-5	Set temperature heating cable	CS-S3-03	°C	220	220	--	

Table 6.3 – Test B1.2 parameters

6.2.3 Data analysis and interpretation

The new procedure for regulating the injection valve aims to obtain data from a large scale evaporation phenomenon.

To correlate the two tests, the same division in three phases is chosen:

- I. Water injection phase;
- II. Pressure increase in injection line due to heating;
- III. LBE-water interaction phase.

Because of the new regulation of the injection valve, the first two phases can be considered together.

I and II Water injection phase and Pressure increase in injection line due to heating [0 to 40.47 s] *from valve V4 opening to cap rupture*. Once valve V4 is opened, water fills injection line line between the V4 and V3 and up to the cap. Also in this test the rupture of the cap does not occur as quickly as expected. V4 valve remains open 45.5 s as shown in the Figure 6.26. By observing the trend of the pressure inside the injection line (PT-S2L-07) and in S2, shown in Figure 6.27, it can be noticed that the pressure in the line begins to increase with a slight advance respect to the instant $t=0$ s due to the delay with which the acquisition system notices the valve opening instant.

The pressure trend in the injection line is recorded by the pressure trasducer PT-S2L-07 at a frequency of 10 kHz, see Figure 6.27. The pressure in the injection line rises rapidly, reaching an initial peak of about 206 bar, full scale of the dynamic transducer and, then, begins to oscillate for the same reasons explained in the Test B1.1. Pressure, once settled, remains fixed to 176 bar until the cap rupture. The water trapped in the injection line is heated as in Test B1.1, in which instead the pressure in line rises. This difference is due to the fact that the valve V4 remains open in this test leaving a large expansion volume (S2 and argon cylinder) connected with the injection line.

Figure 6.28 reports the pressure in the injection line, and the water temperature downstream of the injection valve V4 (TC-S2L-02). It also shows the trend of saturation temperature calculated on the basis of pressure trend. During phase I the water temperature is below the saturation. At time 0 s, the water temperature measured in the injection line has a value of 175°C, despite S2 water temperature

is set to 270°C. This is because the water entering in the line flashes, cooling the thermocouple installed in the line. On the opposite, the heating cable correctly heat the tube structure at 270°C. Compared to the previous test water has cooled more despite it is 10°C warmer. This is due to the absence of the heating cable on the section where the TC-S2L-02 (CS-S2-06) is implemented, because it is broken.

Figure 6.29 shows the trend of the water level of S2 and the mass flow rate measured by the Coriolis flow meter. In this first phase, the level decreases by 54 mm corresponding to the amount of water required to fill the line. Once filled the level settles again. The Coriolis measures a first peak of mass flow with the same delay.

III. LBE-water interaction phase [40.47 to EoT] *from cap rupture to end of transient.*

When the cap breaks, the pressure in the injection line decreases rapidly up to about 112 bar (see Figure 6.27). At the same time, the pressure in S1 rises rapidly from 1.2 bar, reaching a maximum pressure peak of about 24.65 bar (PT-S1V-04). Figure 6.30 reports the trends of dynamic pressure (PT) and absolute pressure (PC) transducers installed in S1 and the absolute pressure transducer of S3. Figure 6.31 highlights the pressure peak and the extreme velocity of the pressure wave propagation, thanks the high frequency of the acquisition system 1 point each 0.1 ms. The pressure peaks are connected with the propagation of waves in LBE, that is the reason why they are not detected by PT-S1V-08 and PT-S1V-05 (see section 4).

When pressure in the injection line is about 112 bar, that coincides with the closing time of the injection valve, starts to decrease more rapidly. This is due to the instantaneous exclusion of S2 tank volume.

The first peak recorded in S1 (see Figure 6.30) is due to the pressure wave that propagates inside the vessel. The second is due to the expansion of water and steam in S1. The higher value, measured by the PC-S1V-01 (57.29 bar), is in disagreement with the other measured values, which have an average value equal to about 24 bar. Inside PC-S1V-01 at the end of the test a stopper of LBE that sealed the transducer was found. Therefore, the reliable maximum pressure value reached due to evaporation is 26.77 bar.

Compared to the previous test, it is interesting to note that the pressure peak reached after the rupture of the cap is less than the value measured in the Test B1.1. This difference is justified by lower pressure value reached in the line before cap rupture. Conversely, the pressure peak due to evaporation is higher in this test (27 against 10 bar) due to the big amount of water injected (6.8 liters).

In Figure 6.32 shows the trends of temperatures implemented on the test section. Each figure reports the temperature trends of thermocouples installed in the same rank of the test section (rank 2 is the closest and rank 8 is the farthest) starting from 35 seconds. The thermocouples welded on the lateral surface of the test section (PP) are also reported. The initial temperature of the melt is 402°C. When water enters in S1, there is an abrupt decrease of temperature which is damped moving away from the center of the test section. Subsequent a second reduction in temperature is observed. This is due to the evaporation of the injected water, which carries away heat from the surrounding LBE. The effect of the evaporation, which in the previous test was barely visible, has a high impact this test. At the end of the transient all the thermocouples settle to a value between 360°C and 380°C. It should be mentioned that during the Test B1.2, some thermocouples surrounding the injector have been damaged. The inspection will be done after the experimental campaign.

The trends of the strain measured by the strain gauges is shown in Figure.6.33. Even in this case, figures are organized starting from the two strain gauges closest to the cap (SG-201 and SG-204), up to the strain gauge installed in the seventh rank (SG-710), plus the two on the outer surface (SG-PP1 and SG-PP2). Observing the evolution of the deformation for the strain gauge 201 two distinct peaks can be identified. The first, narrower, is due to the pressure wave that propagates in LBE as result of the breaking of the cap. The second peak, is due to the evaporation of the injected water which generates a second pressure increase. This is wider because of the evaporation phenomenon is slower. The strain due to evaporation is minor despite the evaporation generates a pressure increase greater (as shown in Figure 6.30). The peak due to the evaporation is generated in a greater times compared to cap rupture peak. This implies that, even if the final pressure value reached is greater, the impulse that this has on the structures is smaller. A similar trend is seen in all strain gauges until the SG-507. In the outer strain gauges of the test section the peak due to evaporation seems completely

muffled. As for the previous test (B1.1) the measured strain is lower moving away from the center of the test section, in radius direction. Also the strain gauges set on S1 show two initial peaks. S1 is not only affected by the pressure waves generated, but also the effect of the overall pressurization reached inside. This observation motivates the increase of deformation recorded (see Figure 6.35), following the two initial peaks that are highlighted in Figure 6.36. This effect was much less marked in the previous Test B1.1, having injected a little water and consequently having reached a final pressure lower.

Whereas the highest injection pressure set for the LEADER tests, such a low strain values measured on the inner surface of S1 is comparable with the values achieved in THINS tests. This indicates a possible dumping of pressure waves by the “ tubes tangle ” and by perforated plate of the test section. This observation, will be further investigated, and it may be relevant to carry out evaluation of structures outside SG shell during a SGTR event. For completeness are also reported temperature trends (see Figure 6.34) of the inner surface of S1 that has recorded at the end of the transient a value of about 380°C.

Another outcome is the structural integrity of pressurized tubes surrounding the injector, as demonstrated by their internal pressure at end of the test (180 bar).

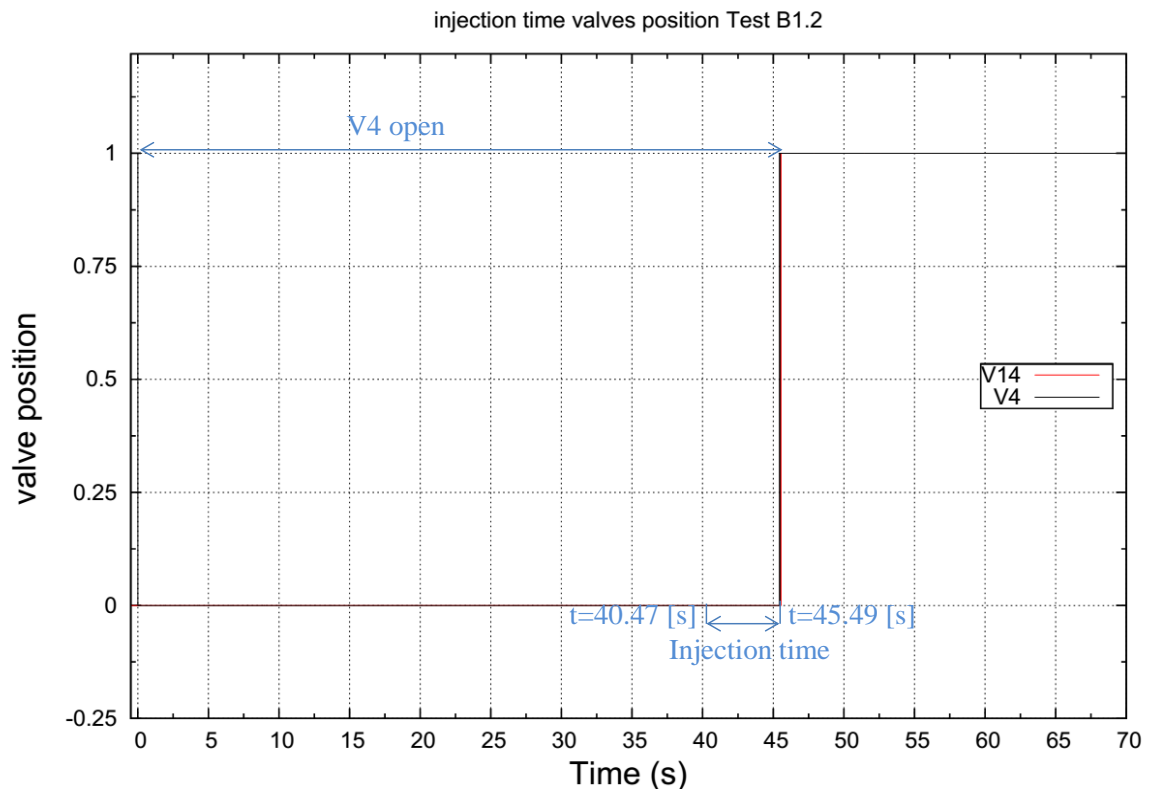


Figure 6.26 – Test B1.2 valves V4 and V14 position

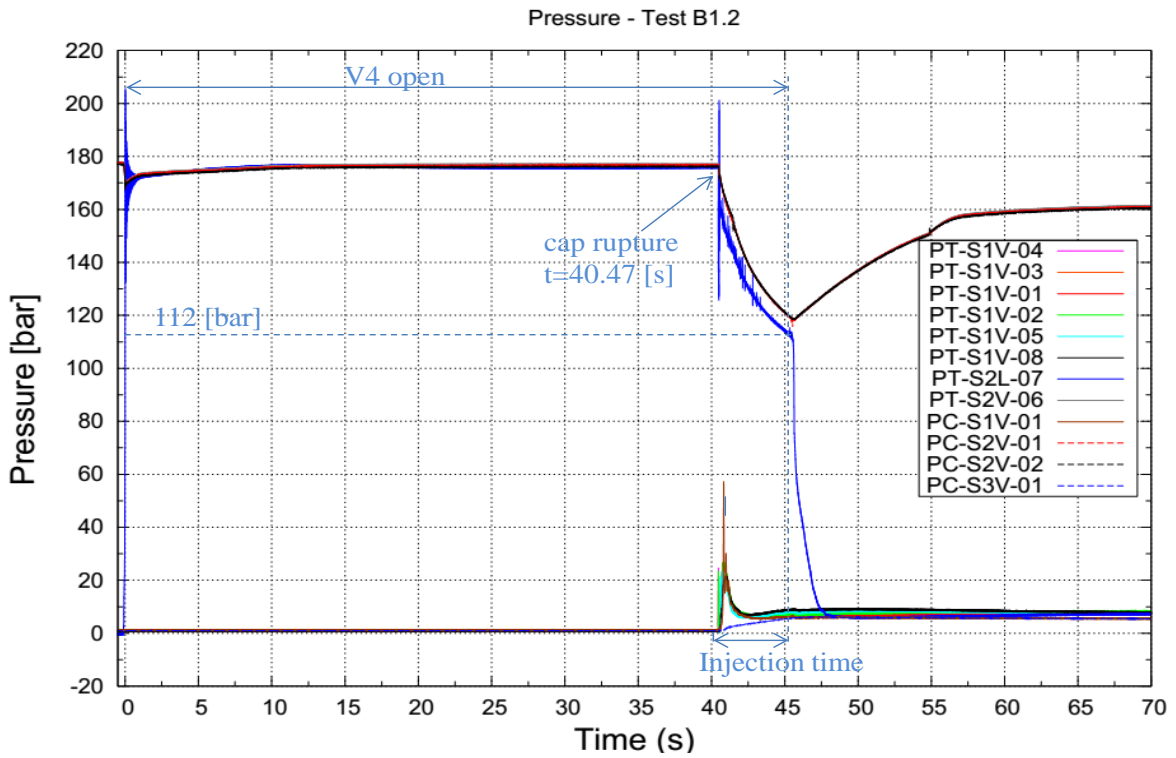


Figure 6.27 – Test B1.2 pressure trends in injection line, S1 and S3

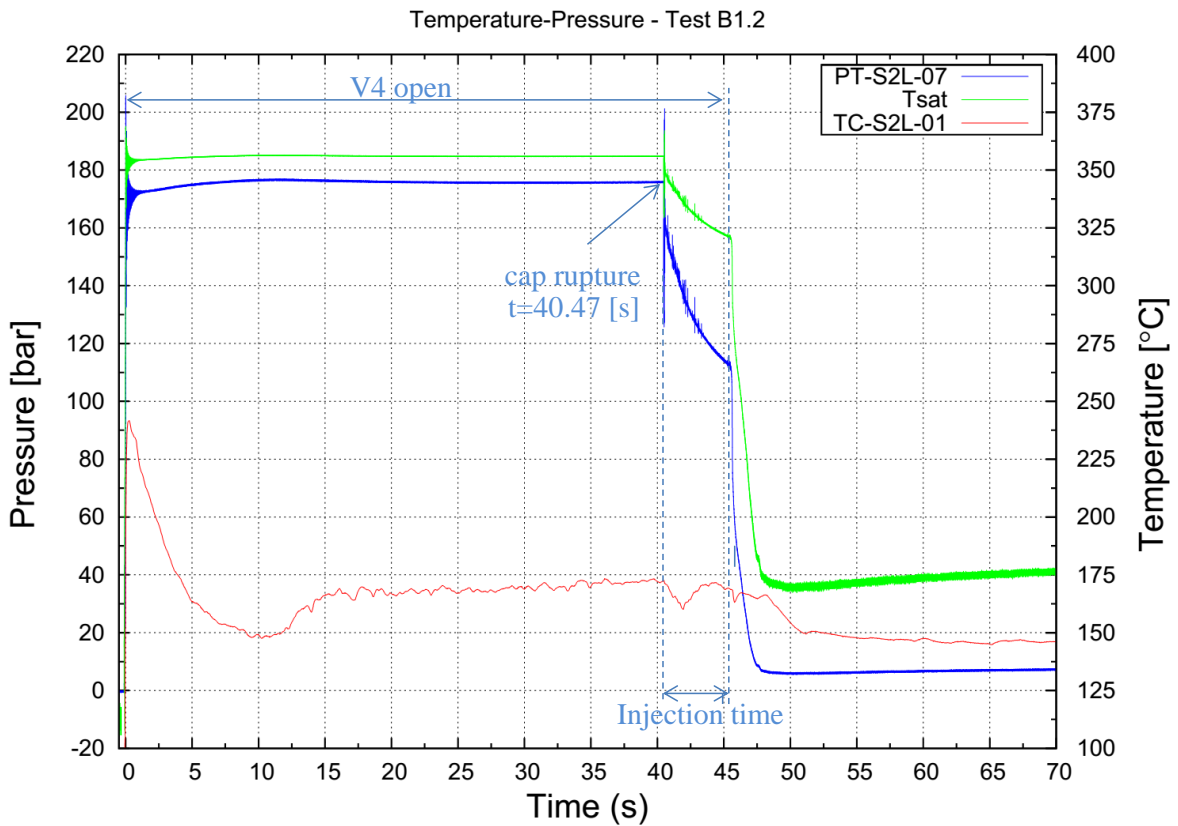


Figure 6.28 – Test B1.2 pressure and temperature trends in injection line

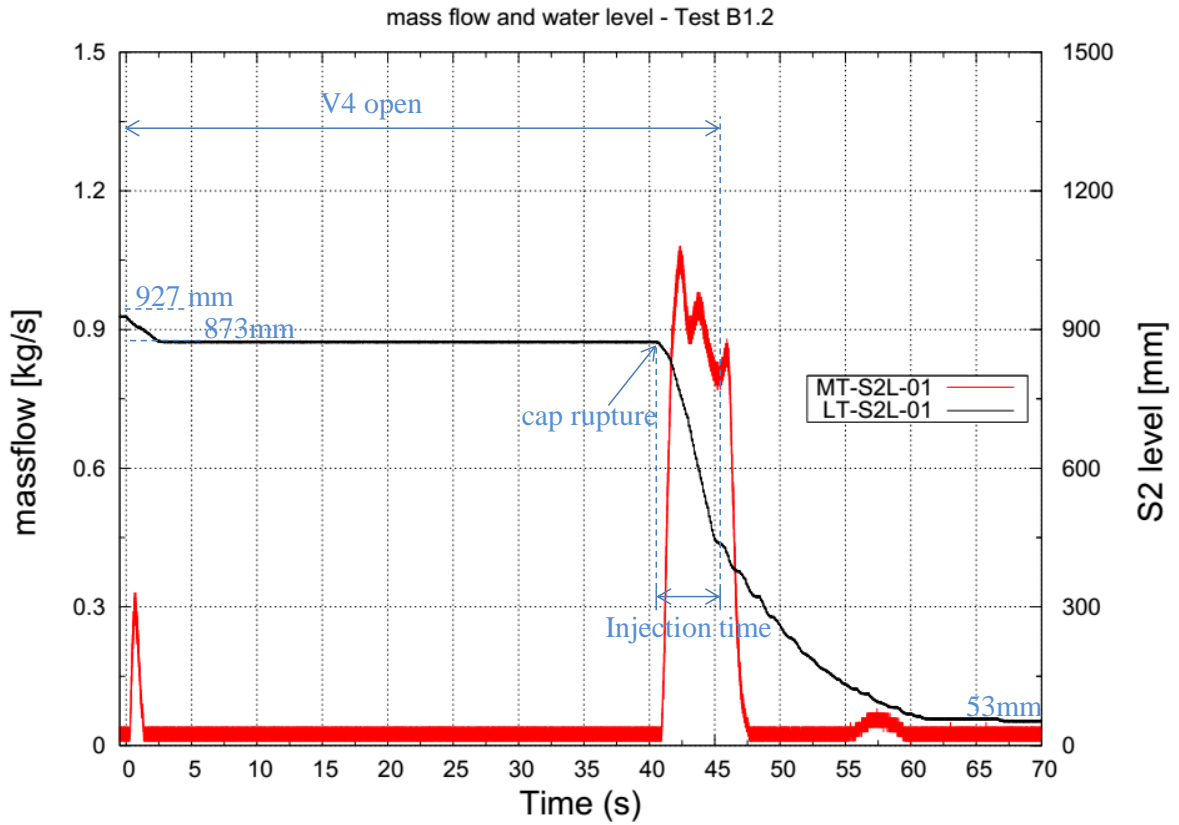


Figure 6.29 – Test B1.2 S2 level measurement and mass flow trends

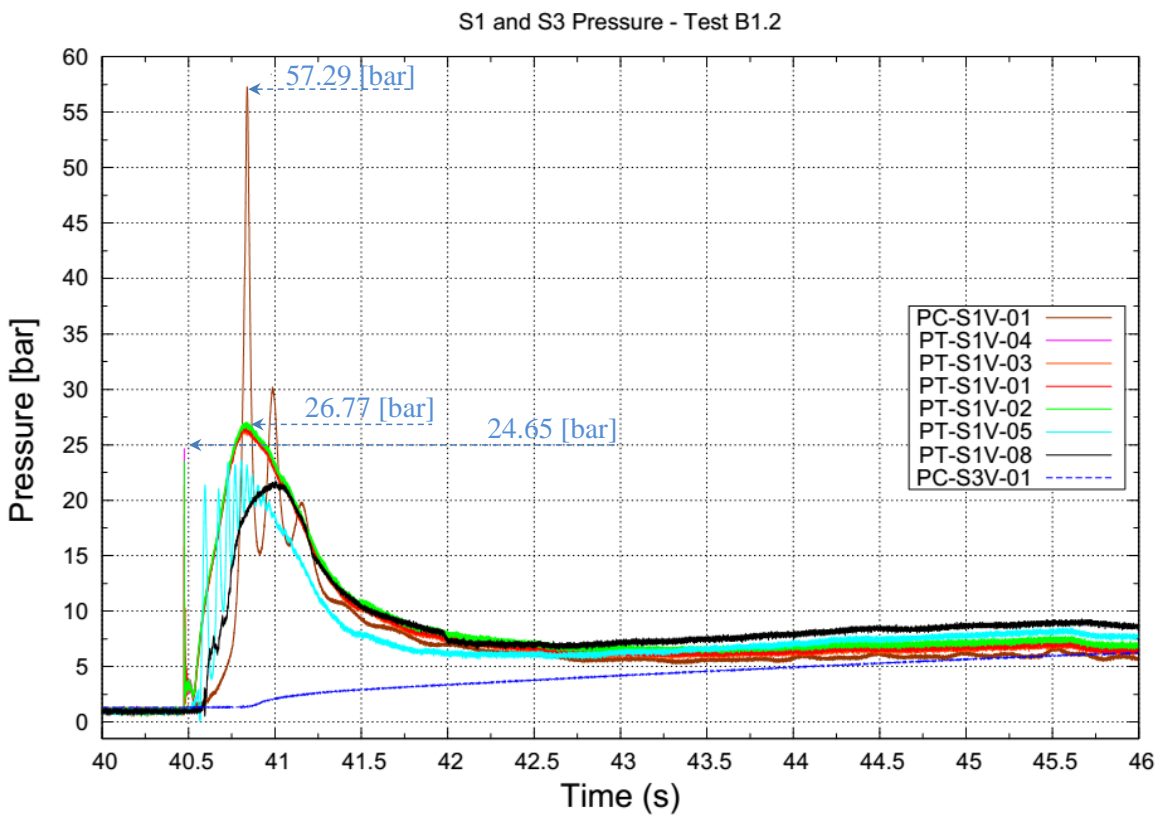


Figure 6.30 – Test B1.2 pressure trends in S1 and S3

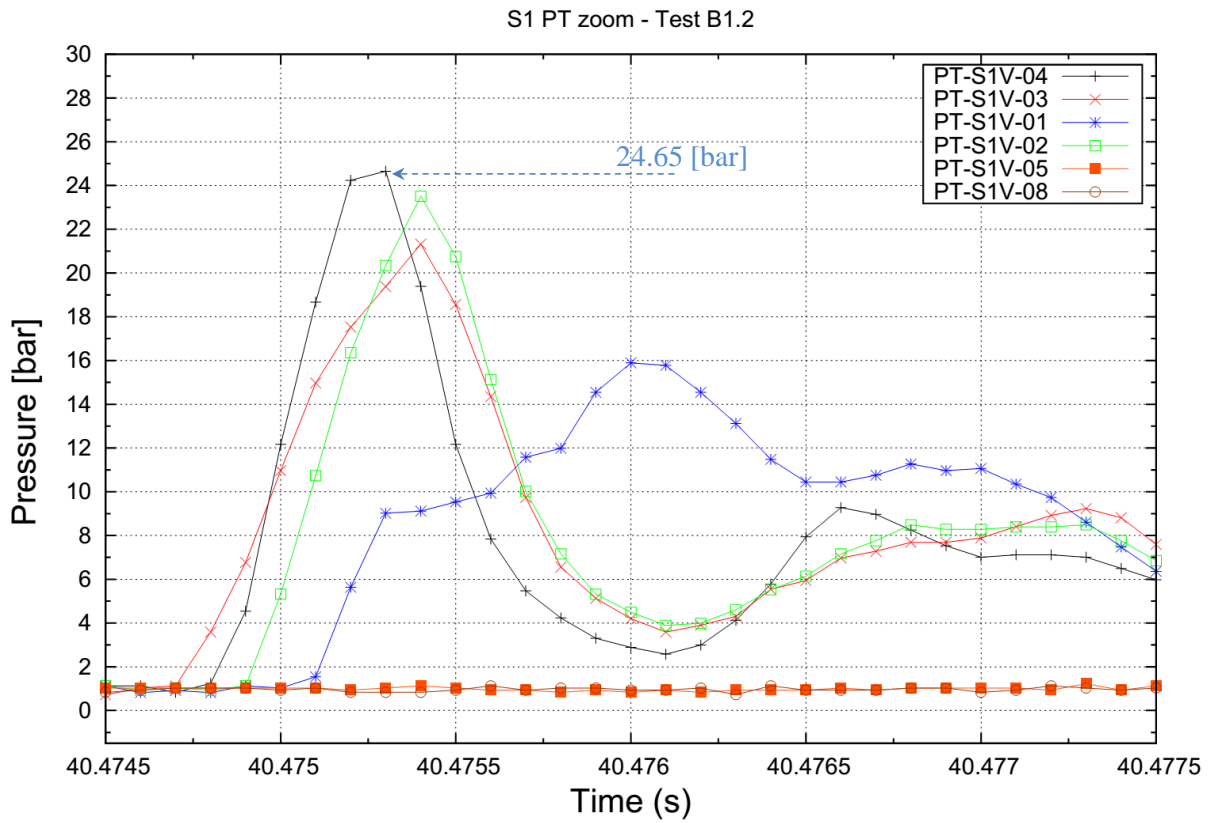
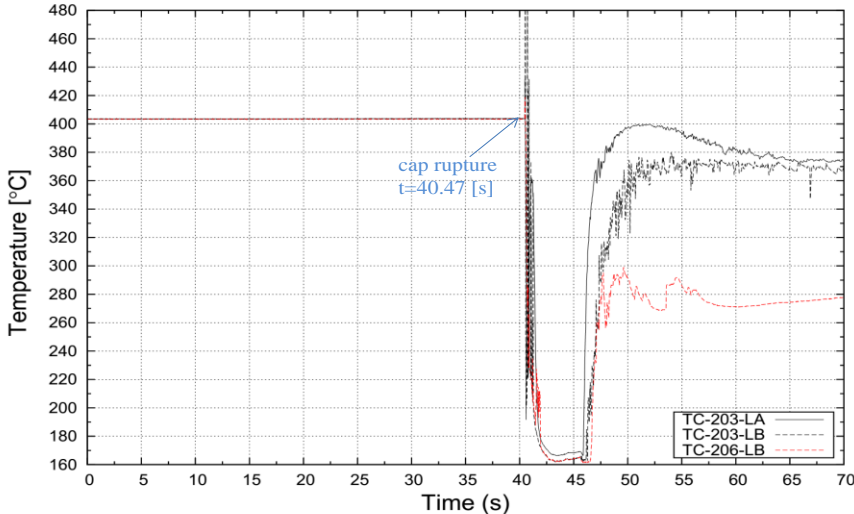


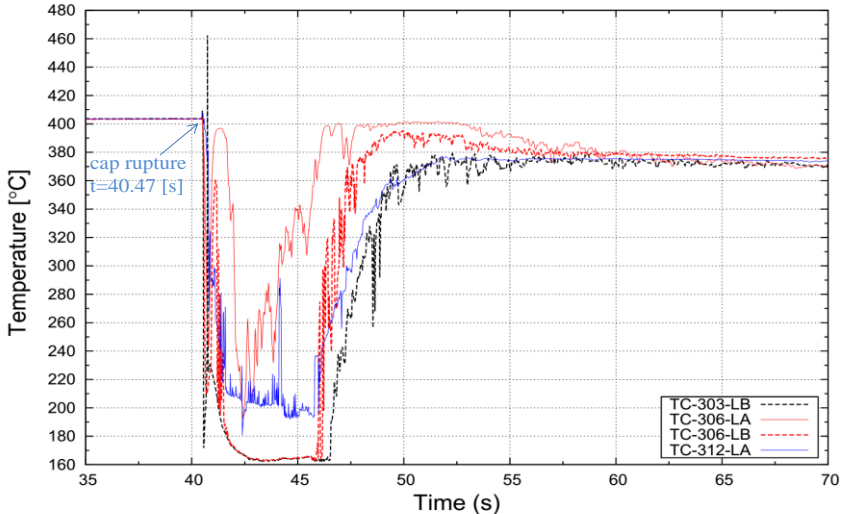
Figure 6.31 – Test B1.2 zoom of pressure peak in S1

Temperature trends

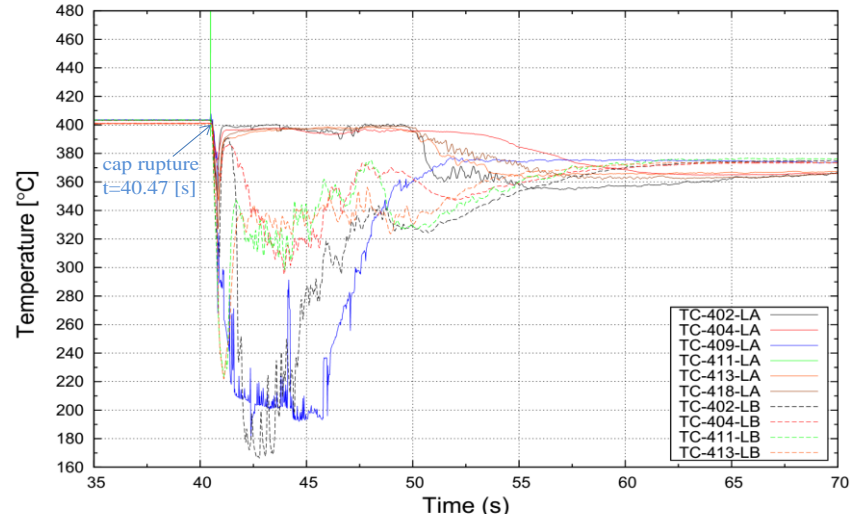
Temperatures of rank-2 - Test B1.2



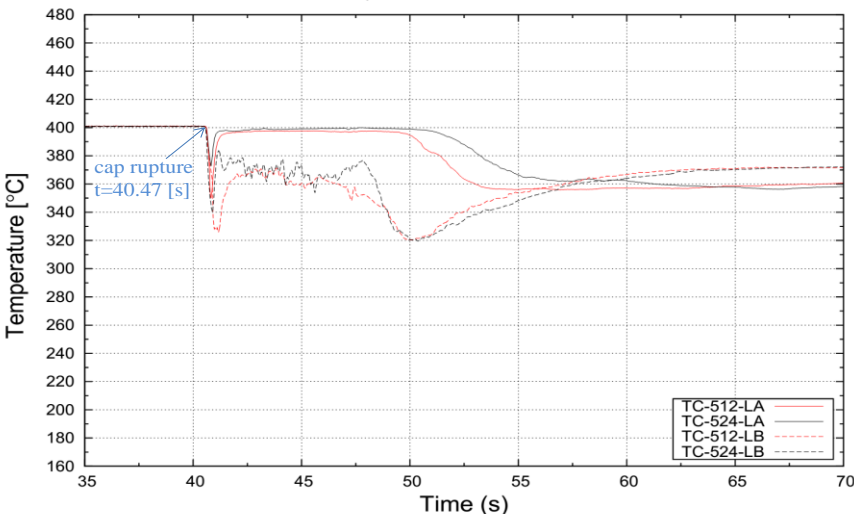
Temperatures of rank-3 - Test B1.2



Temperatures of rank-4 - Test B1.2



Temperatures of rank-5 - Test B1.2



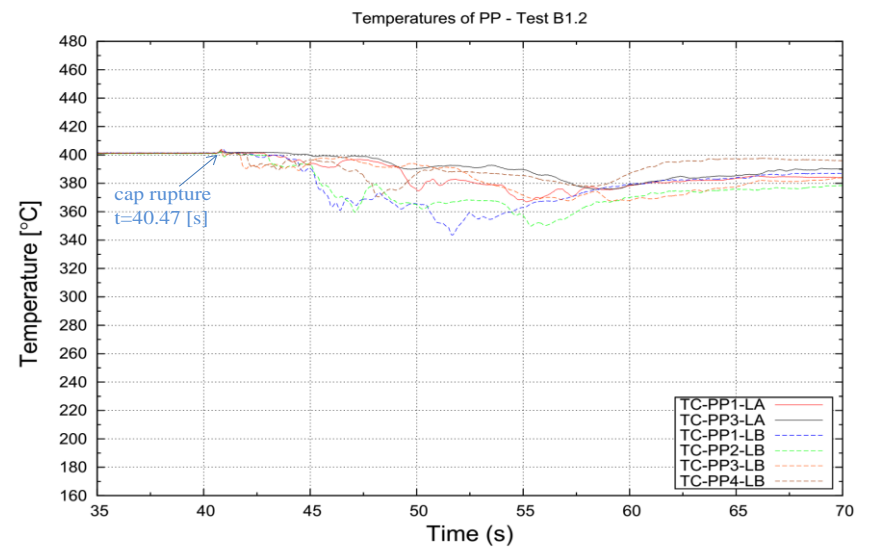
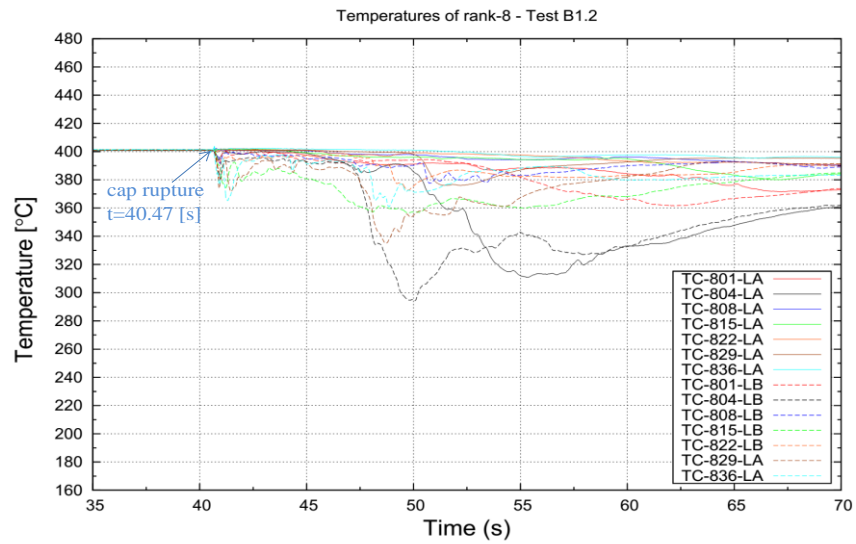
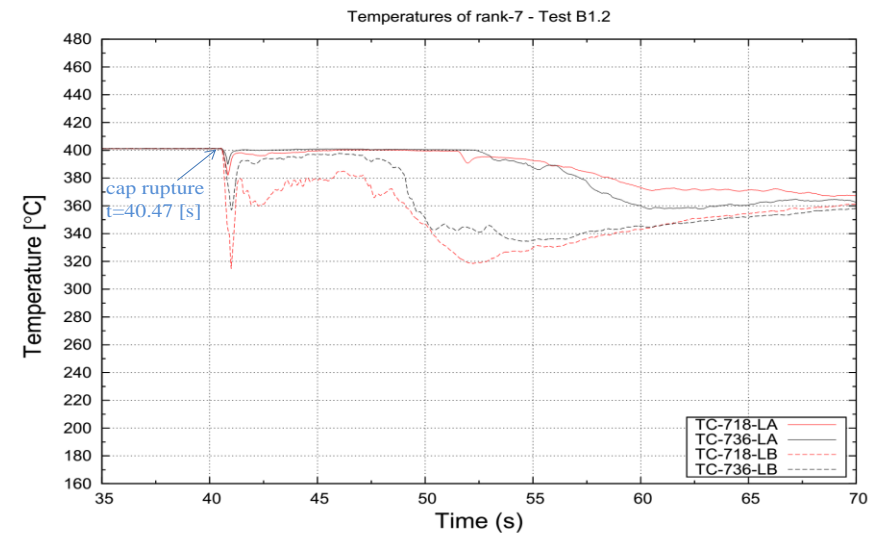
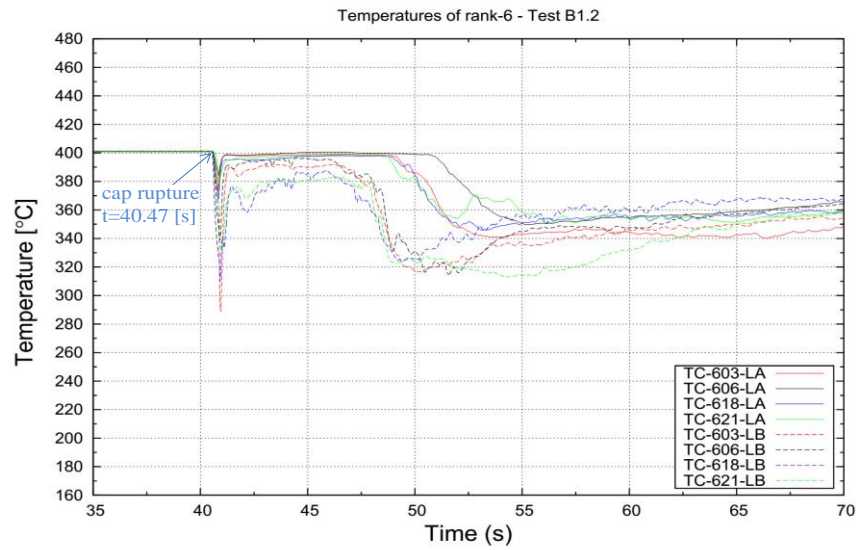
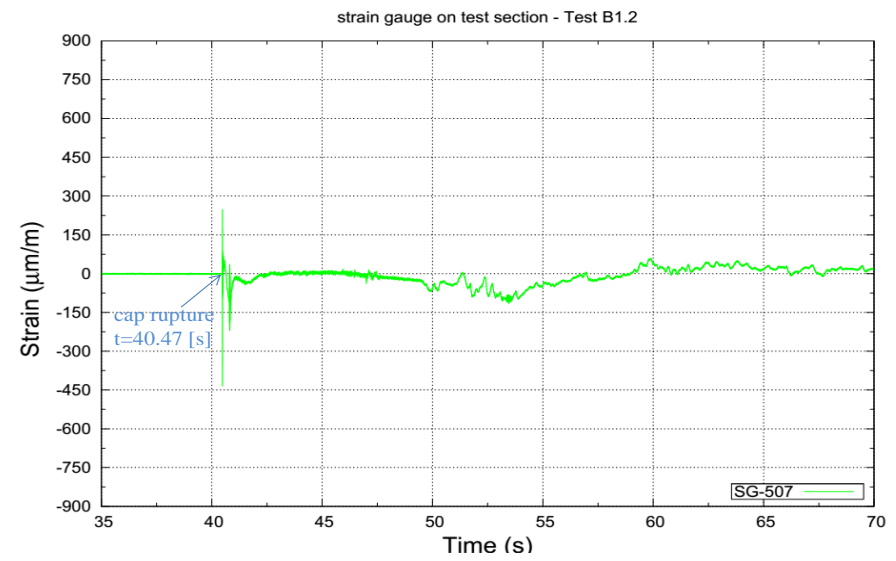
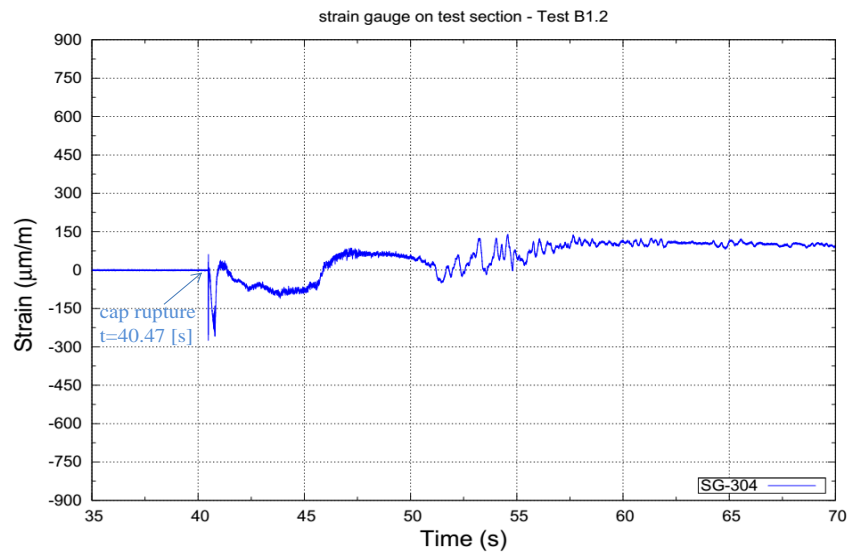
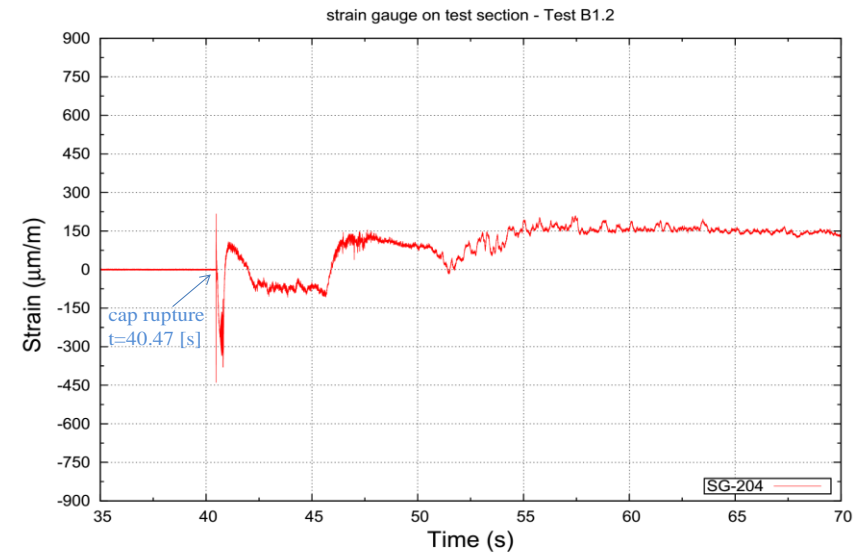
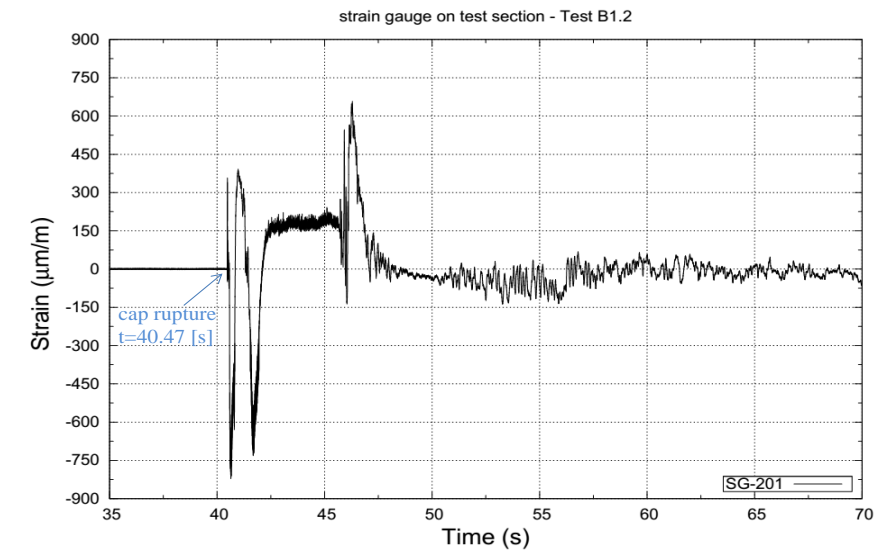


Figure 6.32 – Test B1.2 temperature trends of the ranks and internal surface of LEADER test section

Strain trends



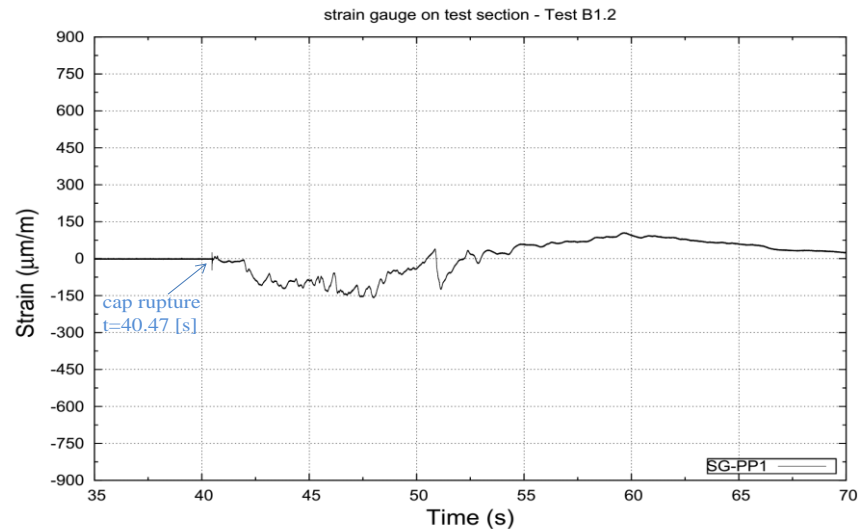
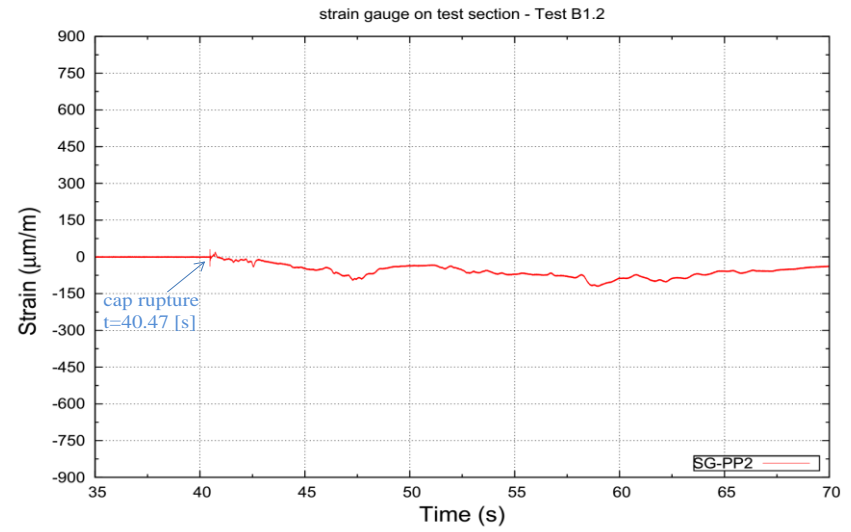
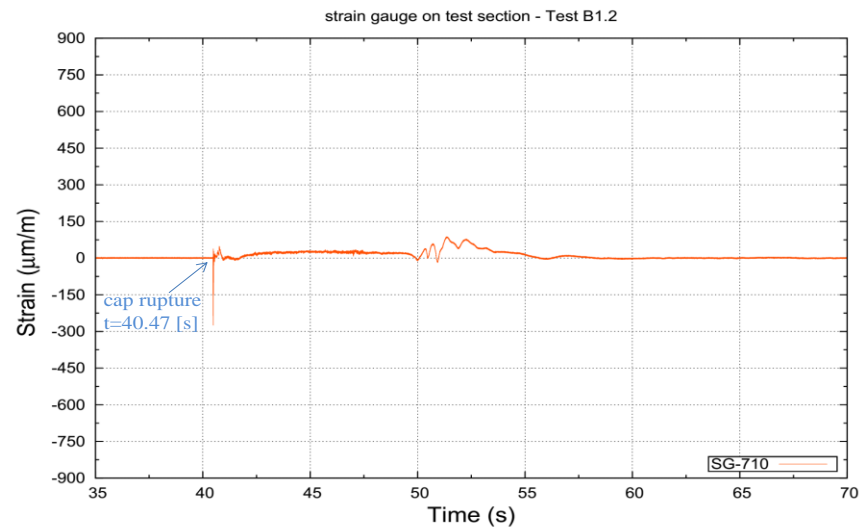


Figure.6.33 – Test B1.2 LEADER test section strain gauges strain trends

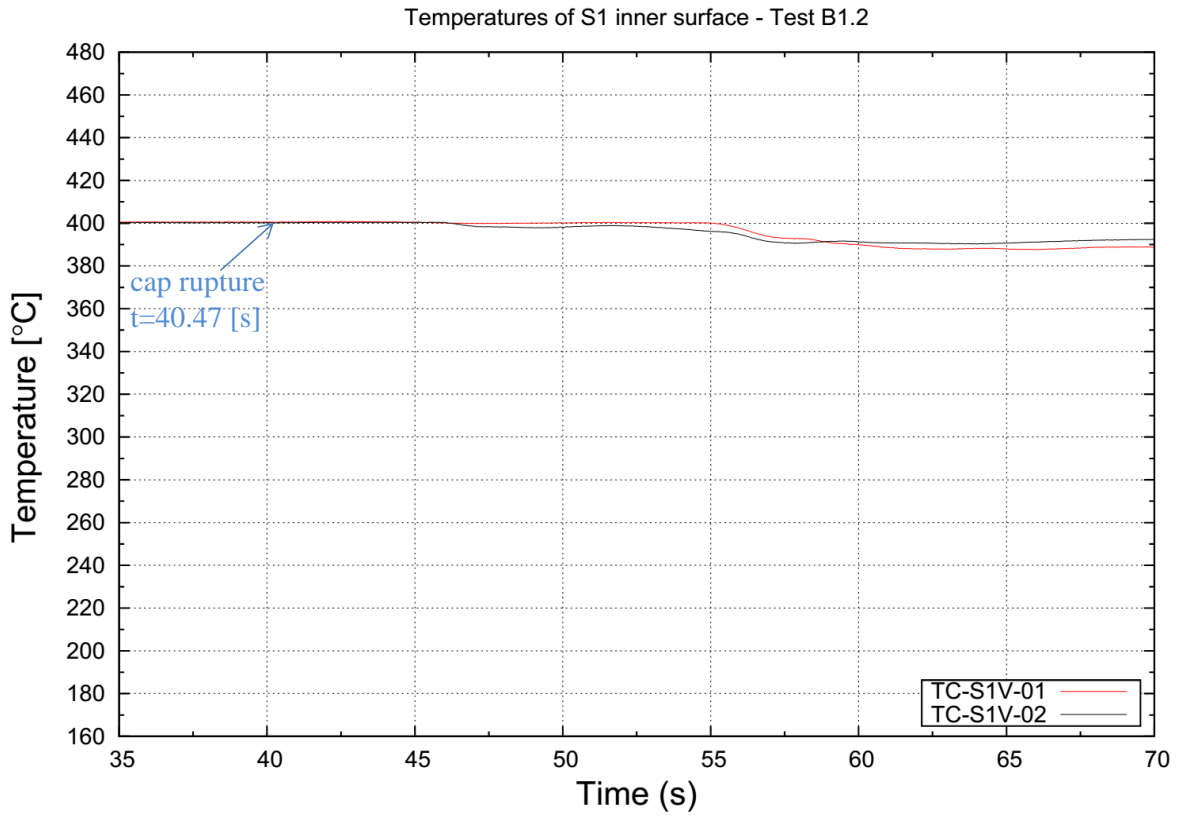


Figure 6.34 – Test B1.2 S1 internal surface temperature trends

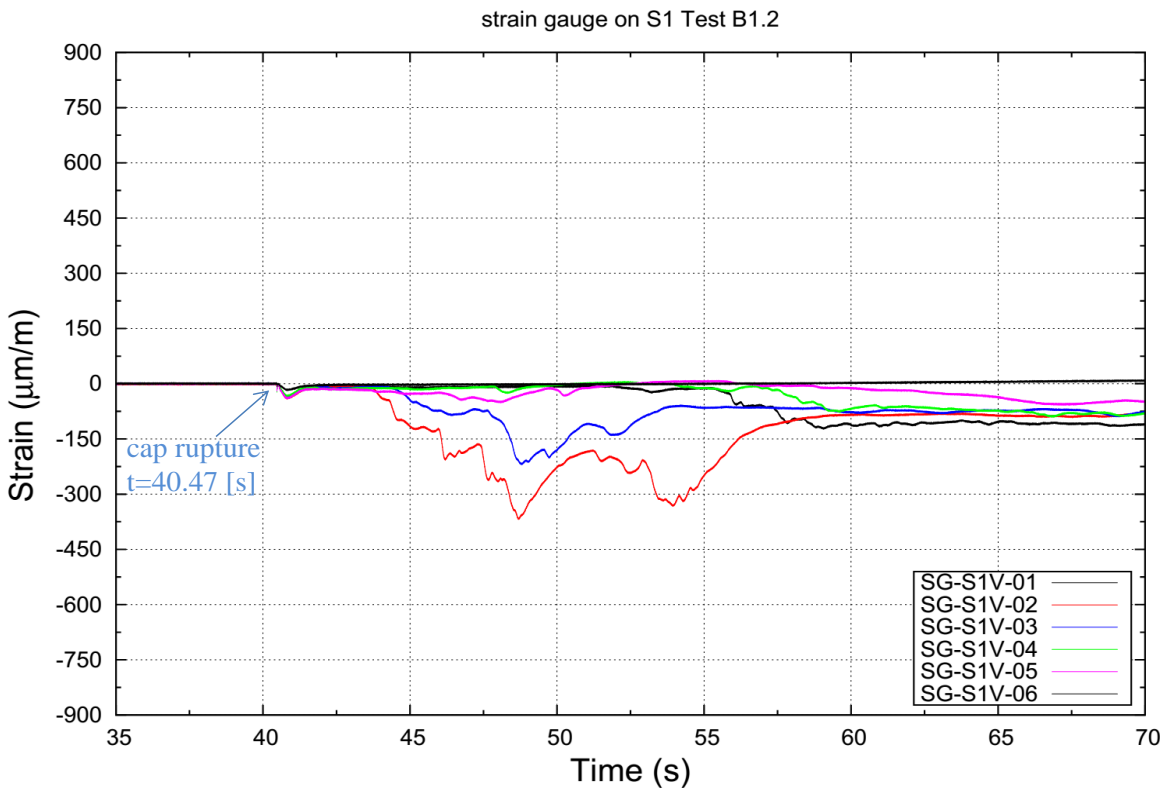


Figure 6.35 – Test B1.2 S1 internal surface strain trends

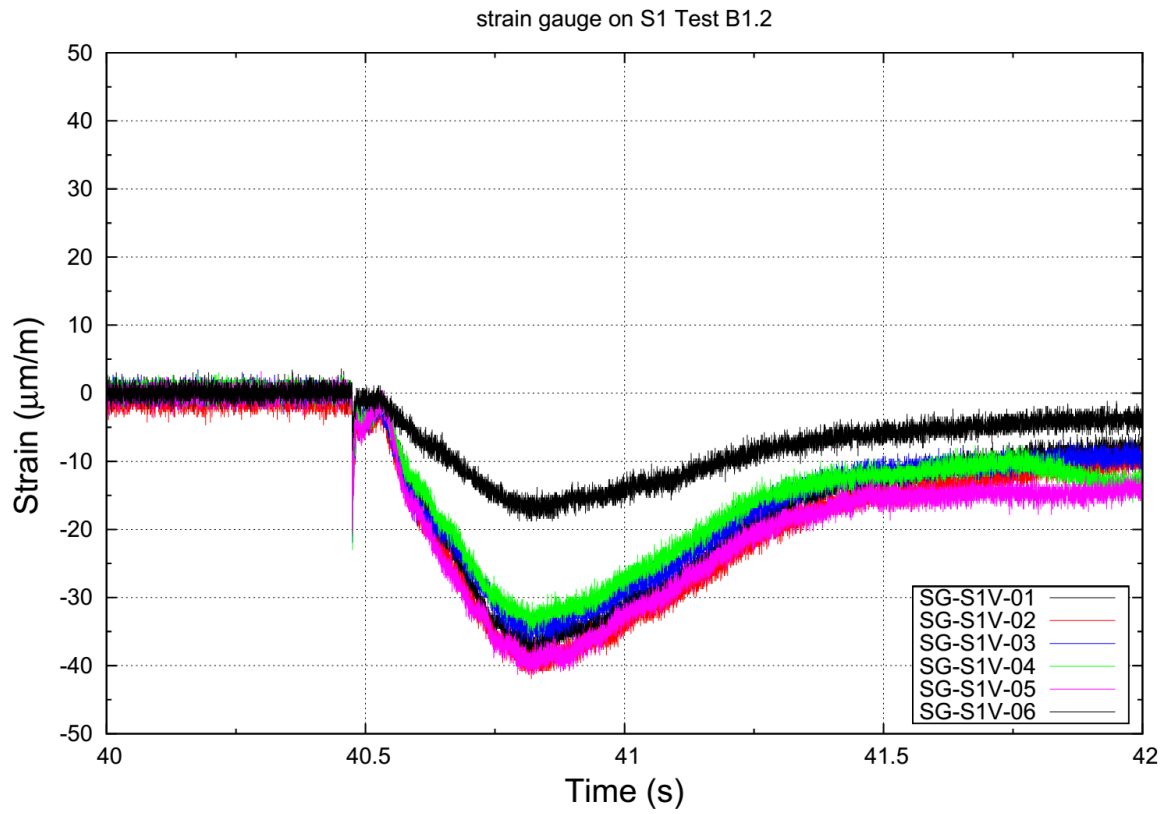


Figure 6.36 – Test B1.2 S1 internal surface strain trends zoom

7 Conclusions

The present thesis work has been carried out during an internship at ENEA Brasimone Research Centre (Italy). The technical activity was conducted in the framework of LEADER project (European Lead-cooled advanced Demonstration Reactor), launched from EURATOM under the 7th Framework Programme. This work contributes to the research and development activities focused on safety of Gen. IV reactors employing as primary coolant Heavy Liquid Metal (HLM).

The aim of the LEADER experimental campaign in LIFUS5/Mod2 facility is the study of the interaction between LBE and water following a postulated SGTR accident, having geometry and boundary conditions representative of ELSY fast reactor. The expected outcomes of these tests are: the generation of detailed and reliable experimental data; the improvement of the knowledge of physical behaviour and of understanding of the phenomena; the investigation of the dynamic effects of energy release on the structures; and the enlargement of the database for code validation.

The activity of the present work has the following objectives:

- the participation to the design and the assembling of the new LEADER experimental test section;
- the planning of tests, the definition of procedures, the set-up of initial and boundary conditions of tests;
- the participation in the execution of experiments;
- the generation and the analysis of detailed and reliable experimental data;
- the enlargement of the database for code validation;
- the acquisition of skills in using simulation codes such as RELAP5 and SIMMER-III;
- the simulation and preliminary assessment of the first test (B1.1) by SIMMER-III code.

Additional goals and experiences achieved are:

- the possibility to perform an internship at the ENEA Experimental Centre of Brasimone;

- the acquisition of practical skills related to welding procedures, to pressure fittings, to gaskets and to measurement instrumentation thanks the participation in the set-up and operation of the experimental facility;

The objectives were achieved through the following activities:

- studying peculiarities and features of Gen. IV HLM fast reactor, with particular focus on ELSY and its SG description;
- studying and summarizing a literature review about the HLM/water interaction;
- participating in the preparation of LIFUS5/Mod2 facility and LEADER test section;
- supporting the design and the execution of the experiments (two out of three are presented in the thesis);
- performing data analysis and interpretation of the tests B1.1 and B1.2;
- supporting the analysis of the experiments and the post-test analysis by SIMMER-III code, setting up a RELAP5/Mod3.3 input deck of LIFUS5 water injection line and studying two experimental tests (A1.2_1 and A1.2_2) of the previous THINS campaign;
- preparing a numerical model of LIFUS5 facility by SIMMER-III and performing the post-test analysis of test B1.1.

Main outcomes from the experimental and numerical activity apply.

- LIFUS5/Mod2 facility in LEADER configuration was completed and ready for the experimental activity. The documentation of the facility configuration and instrumentation, the execution of the preparatory (i.e. protective cap pressure tests) and commissioning (i.e. tests procedures and acquisition system) tests was also carried out.
- 3 tests were executed. Thanks the lesson learned from first Test B1.1 an updated injection procedure was set up to overcome the issue raised on the delayed rupture of the injector cap. The signal used to stop the injection (i.e. closure of valve V4) was connected with a pressure set point in S1 and S3.
- The availability of the experimental data of tests B1.1 and B1.2 demonstrated that the pressure peak generated was lower than 30 bar; the pressure wave propagation is largely damped, in both tests, by the “tubes tangle” present inside the test section

and by perforated plate of the test section. This damping is also confirmed by the strain by the strain gauges' measurements. Indeed, the strain trend on the tubes of the test section decreases from the center of the test section in the radial direction. Moreover, there is a residual deformation peak in the inner surface of S1 comparable with that of previous THINS tests. Finally, these experiments highlight that no leakages are observed in the pressurized tubes of the test section. This may implies a low probability of propagation of the tube rupture on surrounding tubes.

- The initial pressure peak are tracked by the improved acquisition frequency up to 10 kHz. This will imply a better interpretation of previous LIFUS5 experiments.
- A RELAP5 nodalization was developed to support the characterization of the water injection line, confirming the timing of opening and closure of the injection valve, the pressure drops in the injection line, the behavior during the THINS tests A1.2_1 and A1.2_2, and providing a more reliable quantification of the water injected, including considerations on the limits of the Coriolis flow meter. After the execution of the first Test B1.1, the RELAP5 model has been modified (i.e. implementation of thermal structures) to support the SIMMER-III simulations of Test B1.1 providing the conditions reached by water before being injected;
- A SIMMER-III nodalization of LIFUS5/Mod2 facility in LEADER configuration is developed and set-up. Preliminary qualification of the model is also achieved performing the post-test analysis of Test B1.1. The analysis of results demonstrates that the code is able to simulate the first pressure peak measured when the cap is broken. The code predicts the maximum pressure value (30 bar) and the timing of the phenomenon (10^{-3} s). The second pressure peak due to the steam expansion in S1 is also correctly simulated by the code, even though overestimated (4 bars higher). The deviation is probably correlated to a stopper that the LBE forms in the vertical section that connects S1 to S3 due to geometrical approximations of the model. The final experimental and simulated values of pressure in S1-S3 system are in agreement. This confirms that the amount of water and steam injected in the simulation is consistent with the experimental one. The final quantity of LBE dragged in S3 is higher in the simulation (100 kg against 25 kg experimental). This may be due to an overestimation in SIMMER-III of the drag coefficient between steam and LBE. Indeed, the code predicts comparable speeds of LBE and steam during the transient. In principle, higher speed of steam is expected.

The activity performed provided the availability of data of three experiments. These tests provided valuable experimental data for the assessment of SIMMER-III code. Moreover, the interpretation of strain data for improving the knowledge of the energy, deposited during the tube rupture on surrounded structures, could be used for future structural mechanics code assessment as well for fluid structure interaction analysis. Further experiments are planned using different injector orifices. The experiments carried out are related the case 0.1A of ELSY SG tube. B2 and B3 series will address the cases 0.6A and 1.0A.

(This page has been intentionally left blank)

REFERENCES

- [1] M. Ragheb “Fourth generation reactor concepts” chapter 6, November 2014.
- [2] Issued by the OECD Nuclear Energy Agency for the Generation IV International Forum “technology roadmap update for generation iv nuclear energy systems” january 2014.
- [3] <http://www.world-nuclear.org/info/Nuclear-Fuel-Cycle/Power-Reactors/Generation-IV-Nuclear-Reactors/>
- [4] IAEA, Technical Meeting on Fast Reactor Physics and Technology, Kalpakkam, India, 14 - 18 November 2011 Conference ID:41429 (TM-41429).
- [5] http://it.wikipedia.org/wiki/Reattore_nucleare_di_IV_generazione.
- [6] Handbook on Lead-bismuth Eutectic Alloy and Lead Properties, Materials Compatibility, Thermal-hydraulics and Technologies, OECD-NEA 6195, 2007.
- [7] D. Bernardi, A. Ciampichetti, N. Forgiione, Test parameters definition for SGTR experiments, Technical Report – Doc 57, Task 6.3 of ELSY project.
- [8] A. Ciampichetti, D. Bernardi, N. Forgiione, F.Poli, D. Pellini, T. Cadiou, Report on the results for the interaction of lead alloy with other coolant, EUROTRANS DEMETRA ET-S-R-006 Rev.0, April 2010.
- [9] Sergio Orlandi “Overview Reattori IV Generazione Parte III” Milano, 27 Maggio, 2009.
- [10] M. Tarantino “lead-cooled fast reactor (LFR) development gaps” Italian National Agency for New Technologies, Energy and Sustainable Economic Development, C.R. ENEA Brasimone.
- [11] Italy Cinotti L. “Spiral-Tube Steam Generators for compact integrated reactors”. “The ELSY project”, Technical Meeting on Innovative Heat Exchanger and Steam Generator Designs for Fast Reactors, Vienna December 21-22, 2011.
- [12] A. Alemberti “ Design, safety approach and safety characteristics ” technical meeting on “impact of fukushima event on current and future fast reactor designs ” 19 - 23 march 2012 helmholtz-zentrum dresden-rossendorf dresden, Germany.

- [13] S. J. Board and R.W. Hall “Recent advances in understanding large scale vapour explosion” Paper presented to the Third Specialist Meeting on Sodium Fuel Interactions in Fast Reactors, Tokyo, March 1976.
- [14] N. Forgione, W. Ambrosini et al., “Summary of previous applications and critical review on models and applications” for camping THINS, Pisa 2012.
- [15] Kurata, Y., “Summary of PbBi-water Interaction Experiments at CRIEPI in Japan”, presentation at MEGAPIE meeting, Mol, Belgium, 2004.
- [16] Sibamoto Y. et al., “Neutron radiography flow visualization of liquid metal injected into an empty vessel and a vessel containing saturated water”, Nuclear Technology, Vol. 133, 2001.
- [17] M.L. Corradini, B.J. Kim, M.D. Oh, “ Vapour explosion in light water reactors: a review of theory and modelling”, Progress in Nuclear Energy, vol.22, N°1, 1988.
- [18] S. Wang, M. Flad, W. Maschek, P. Agostini, D. Pellini, “Evaluation of a steam generator tube rupture accident in an accelerator driven system”, Progress in Nuclear Energy No. 50, 363-369, 2008.
- [19] G. Bandini, P. Meloni, M. Polidori, “ENEA activities on EFIT Safety Analysis”, (ENEA Report), WP5.1 Progress Meeting, Brussels.
- [20] Huhtiniemi I., Magallon D., “Insight into steam explosions with corium melts in KROTOS”, Nuclear Engineering and Design, Vol. 204, pp. 391-400, 2001.
- [21] Corradini M.L., Kim B.J., Oh M.D., “Vapor Explosions in Light Water Reactors: A Review of Theory and Modeling”, Progress in Nuclear Energy, Vol. 22, n. 1, pp. 1-117, 1988.
- [22] Zeldovich I.B., Kompaneets A.S., “Theory of Detonation”, Academic London, 1960.
- [23] Board S.J., Hall R.W., Hall R.S., “Detonation of a fuel coolant explosion”, Nature, Vol. 254, pp. 319–321, 1975.
- [24] T.C. Dinh, “Multiphase flow phenomena of steam generator tube rupture in a Lead-Cooled Reactor System: a scoping analysis”, Division of Nuclear Power Safety, Royal Institute of Technology (KTH), 2007.
- [25] http://en.wikipedia.org/wiki/Three_Mile_Island_accident

- [26] K.Morita, S.Kondo, Y. Tobita, “Applications of the SIMMER III Fast Reactor Safety Analysis Code to Thermal Interactions of Melts”, ICONE -7250,7th International Conference on Nuclear Engineering, Tokio, April 19-23,1999.
- [27] R.P. Taleyarkhan, “Vapor explosion studies for nuclear and non-nuclear industries”, Nuclear Engineering Design,2005.
- [28] X. Cao, Y. Tobita, S. Kondo, “A thermal fragmentation model induced by surface solidification”, Journal of nuclear science and technology, Vol.39, N° 6, 2002.
- [29] Ciampichetti A., Ricapito I., Aiello A., Benamati G., “Water large leaks into Pb–17Li: first experimental results on LIFUS 5 facility”, Fusion Engineering and Design Vol.69, pp.563–567, 2003.
- [30] Ciampichetti A., Mansani L., “Experimental test program and test set-up on the basis of the design needs of the LBE/water interaction”, ET-S-R-001, 12 May 2006.
- [31] A. Del Nevo et al. “LIFUS5/Mod2 facility Test A1.2_2 Experimental Data and Test Analysis Report”, RC ENEA 24 June 2014.
- [32] 7th FP of Euratom on Advanced nuclear systems for increased sustainability/ Fission 2009 2.2.1: Conceptual design of Lead and Gas cooled fast reactor systems, “Lead-cooled European Advanced DEMonstrator Reactor (LEADER) – Annex I – Description of Work” Grant agreement no.:FP7-249668, September 5, 2009.
- [33] A. Del Nevo, et. Al., LIFUS5/Mod2 facility – Test A1.2 – Experimental Data and Tests Analysis Report, Ref. L5-T-R-039, ENEA 26 July 2013.
- [34] <http://www.garlock.com/en/>
- [35] L. Cinotti et. Al., The potential of LFR and ELSY Project, Proceedings of ICAPP 2007, Nice, France, May 13-18, 2007.
- [36] L. Cinotti et. Al., Assessment of damping pressure wave inside the SG, definition of the experimental configuration, Technical Report – Doc 07, Task 3.2, EC LEADER project.
- [37] <http://office.microsoft.com/en-us/support/visio-2013-quick-start-guide-HA103673712.aspx>

- [38] Information Systems Laboratories, Inc. Rockville, Maryland, Idaho Falls, Idaho Nuclear Safety Analysis Division “ RELAP5/MOD3.3 CODE MANUAL VOLUME II:APPENDIX A INPUT REQUIREMENTS ”, June 2004.
- [39] Bohl W. R., et al., “SIMMER-II: A Computer Program for LMFBR Disrupted Core Analysis”, LA11415-MS, Los Alamos National Laboratory, June 1990.
- [40] Smith L. L., et al., “The SIMMER-II code and its applications”, Proc. Fast Reactor Safety Mtg., Knoxville, Tennessee, 21-25 April 1985.
- [41] A. Del Nevo et al. “ LIFUS5/MOD2 FACILITY – TEST A1.2_1 ”, Ref. L5-T-R-045, 19 August 2013.
- [42] Direct communication with Alessandro Del Nevo (ENEA).